The rational design and synthesis of novel antifreeze(glyco)protein biomimetics for biomedical applications

by

Ben Graham

A thesis submitted to the University of Warwick in partial fulfilment of the requirements for the degree of

Doctor of Philosophy

University of Warwick, Department of Chemistry

June 2019

Table of Contents

Chapters and Sections

Chapter 1

Chapter 2

Chapter 3

Photo-activatable ice recrystallisation inhibitors

Chapter 4

Rationally designed amphipathic glycopolymers for ice growth inhibition

Chapter 5

Chapter 6

Appendices

List of Figures

Chapter 1

Chapter 2

Chapter 3

Chapter 4

Chapter 5

Appendix A

List of Schemes

Chapter 3

Chapter 4

Chapter 5

List of Tables

Chapter 1

Chapter 2

Chapter 3

Chapter 4

Chapter 5

List of Equations

Chapter 1

Abbreviations

°C	Degrees Centigrade
µ	Micro ($\times 10^{-6}$)
Ac	Acetate
ACA	Anthracene Carboxylic Acid
AF(G)P	Antifreeze (Glyco)protein
AFP	Antifreeze Protein
Ala	Alanine
Asn	Asparagine
cm	Centimetre ($\times 10^{-2}$ meters)
Đ	Dispersity Index = M_w/M_n
Da	Daltons
DCM	Dichloromethane
DIS	Dynamic Ice Shaping
dm	Decimetre ($\times 10^{-1}$ meters)
DMAc	Dimethyl acetamide
DMF	Dimethyl formamide
DMSO	Dimethyl sulfoxide
DNA	Deoxyribonucleic acid
DP	Number average Degree of Polymerisation
ESI-MS	Electrospray Ionisation Mass Spectrometry
FDA	United States of America Food and Drug Administration
g	Gram
GPC	Gel Permeation Chromatography
[I]	Initiator concentration

IBS	Ice Binding Site
IR	Infrared Spectroscopy
IRI	Ice Recrystallisation Inhibition
kDa	kiloDaltons ($\times 10^3$ Daltons)
Lys	Lysine
m	Metre
[M]	Monomer concentration
MGA	Mean Grain Area/Size
mg	Milligram
min	Minute
mL	Millilitre
MLGS	Mean Largest Grain Size
mm	Millimetre ($\times 10^{-3}$ meters)
M_n	Number-Average Molecular Weight
Mol	Moles
M_w	Weight-Average Molecular Weight
nm	Nanometre ($\times 10^{-9}$ meters)
NCA	*N*-Carboxyanhydride
NPC	Nitrophenyl Chloroformate
NMR	Nuclear Magnetic Resonance
OH	Hydroxyl
PBS	Phosphate-Buffered Saline
PEG	Poly(ethylene glycol)
Pro	Proline
PVA	Poly(vinyl alcohol)

PVAc	Poly(vinyl acetate)
PVP	Poly(vinyl pyrrolidone)
RAFT	Reversible Addition-Fragmentation Transfer (Radical Polymerisation)
ROMP	Ring Opening Metathesis Polymerisation
ROP	Ring Opening Polymerisation
SAXS	Small-Angle X-Ray Scattering
SANS	Small-Angle Neutron Scattering
SEC	Size Exclusion Chromatography
TH	Thermal Hysteresis
THF	Tetrahydrofuran
Thr	Threonine
TPPO	Triphenylphosphine oxide
UV/Vis	Ultraviolet/Visible
WAXS	Wide-Angle X-Ray Scattering

Acknowledgements

First and foremost, my heartfelt thanks and appreciation go to Matt – for taking me on, for being an excellent supervisor (who was never short on encouragement or optimism), and for giving me the freedom to explore the field and to lead my own research. The past three and a half years have been a truly enjoyable experience and your support and mentorship, which will continue to make up the basis of my research career, has always been greatly received. The conference trips to Ghent, Tel Aviv, and Boston, amongst others, were fantastic experiences which won't be easily forgotten and have undoubtedly helped my development. Thank you!

Secondly, the Gibson Group. I couldn't have asked for a better team to work in. It was great (and well resourced!) fun. Specific thanks go to Alice, Alex, Caroline, and (other) Ben.

Next up, to the University of Warwick, the Department of Chemistry, and all the support, administrative, and technical staff. Thank you for the access to the resources, equipment, and services needed to get this far. Likewise, my thanks go to the European Research Council for my PhD funding, and to the Royal Society of Chemistry and the Society of Chemical Industry for their generous grants and career support/development over the years. Sincere thanks also go to my *alma matter*, the University of Reading – for an excellent undergraduate experience, for giving me the potential to succeed, and for making me who I am today.

To all my friends – but particularly Krissi, John, and Charlotte – thanks for always being there.

To Mum and Dad, for the financial and emotional support, for always believing in me, for spurring me forward, and for always telling me to 'reach for the stars'. I love you both. To my grandparents, Rose and the late Francis, whose support helped to make many things a reality.

Lastly – and by no means least – to Joe. The man to whom I owe everything, and who I'm nothing without. I love you. Your endless support, encouragement, and care over the years means this thesis is as much yours as it is mine, and it is only right that I dedicate it to you.

for Joe

“We are all in the gutter, but some of us are looking at the stars”

– Oscar Wilde, Lady Windermere's Fan

“I have broken the machine and touched the ghost of matter.”

– Sir. Ernest Rutherford

Declaration

This thesis is hereby submitted to the University of Warwick in partial fulfilment of the requirements for the degree of Doctor of Philosophy. The work reported herein was carried out in the laboratories of the Department of Chemistry, University of Warwick between October 2015 and March 2019. All reported work was carried out by the author alone unless otherwise stated, and no part of the reported work has been previously submitted in any shape or form for any other degree at any University.

Particular sections of this thesis have been published or submitted for publication, as follows:

- **Chapter 2**: B. Graham, T. L. Bailey, J. R. J. Healey, M. Marcellini, S. Deville, and M. I. Gibson, "Polyproline is a minimal antifreeze protein mimetic and enhances the cryopreservation of cell monolayers", *Angewandte Chemie Int. Ed.*, 2017, **56**, 15941 – 15944

- **Chapter 3**: B. Graham and M. I. Gibson, "Synthesis of anthracene-conjugates of truncated antifreeze protein sequences. Effect of end-group and photo-controlled dimerization on ice recrystallisation inhibition activity", *Submitted*

- **Chapter 4**: B. Graham, A. E. R. Fayter, J. E. Houston, R. C. Evans, and M. I. Gibson, "Facially amphipathic glycopolymers inhibit ice recrystallization", *Journal of the American Chemical Society*, 2018, **140**, 5682 – 5685

In line with the above declaration, the following sections contain contributions from colleagues:

- **Chapter 2**: Trisha L. Bailey: Performed the cell cryopreservation and cell toxicity assays and conducted the consequent data analysis.

  Dr. Joseph R. J. Healey: Provided the data of the modelled protein structures.

Dr. M. Marcellini and Dr. S. Deville: Performed the ice shaping experiments and conducted the consequent data analysis.

- **Chapter 3:** Dr. Steven Huband and Alice E. R. Fayter: Performed the SAXS and WAXS experiments, respectively, and conducted the consequent data analysis.

  Dr. Muhammad Hassan: Provided the AFP type I antifreeze protein data.

  Christopher D. Stubbs: Provided the poly(vinyl)acetate-*N*-hydroxysuccinimide.

- **Chapter 4:** Alice E. R. Fayter: Performed the sucrose sandwich/ice-shaping assay and provided the image files.

  Dr. Judith E. Houston/Dr. Rachel. C. Evans: Performed the SANS experiments and conducted the consequent data analysis.

Personal thanks go to all of the above named for their help, assistance, and involvement.

Abstract

The cryopreservation and storage of biological materials essential to biomedicine – such as blood, stem cells, and tissues – is hampered by poor cellular recoveries and viabilities. This is largely due to the formation of ice crystals during the freeze/thaw process, causing catastrophic ice induced damage to cell-based material. Without a reliable, reproducible, and effective cryopreservation method, it is not possible to maintain an on-demand, high quality, and ready supply of vital, life-saving biological products – impacting upon both lives and biomedical research and development. Strategies to inhibit this ice induced damage would therefore have wide application in biomedicine.

Many organisms inhabiting sub-zero environments are able to survive and thrive without issue. Shrubs, plants, insects, but particularly, marine life, have all demonstrated varying degrees of 'cold protection'. Antifreeze glycoproteins (AFGPs) found in cold water fish, are known to infer substantial protection on these cold-dwelling organisms, where surrounding water temperatures are typically –2 ºC, and yet, the fish don't freeze solid. AFGPs have been shown to prevent ice crystal growth, and whilst cytotoxic, mimics of AFGPs may have translational application in the cryopreservation of biological materials.

This thesis reports on a series of proof-of-concept studies, intending to replicate the fundamental cryoprotective properties of AFGPs on simple synthetic constructs, so that they may be applied to cryopreservation. This study intends to further elucidate the precise engineering required to incorporate potent ice growth inhibitory properties into a synthetic architecture. By establishing fundamental design rules, a 'blueprint' maybe prepared for the future development of potent ice recrystallisation inhibitors, with applications in improving biological storage. **Chapter 1** provides a comprehensive literature study of the pre-existing field, whilst **Chapter 2** reports on the development of poly(proline) as a potential ice growth inhibitor, mirroring the same solution structure and amphipathic balance as AFGP as core design motifs. **Chapter 3** outlines the synthesis of a photo-activatable ice growth inhibitors with potential applications in cryosurgery, representing a tuneable AFGP mimetic. Drawing further on the apparent design features and properties of AFGP, **Chapter 4** details the *de novo* design of a library of facially amphipathic and rigid AFGP mimetics, which are capable of potently inhibiting ice crystal growth. **Chapter 5** reports on the attempted development of a series of bile acid derivatives, featuring the core design motifs associated with AFGPs; domain rigidity/facial amphipathy, helicity, and flexibility.

CHAPTER 1

Introduction

The state of humanity's technological and scientific abilities can be best observed at the very forefront of biomedicine. From the first antibiotics of the early 20th Century to the CART-T treatments of the 21st, progress across medical science has in recent years exponentially soared above and beyond the capabilities of our predecessors. For the first time, we look to a future where the treatment of cancers, HIV/AIDS, and Alzheimer's may be routine. The effective application of stem cell therapies in particular, a biopharmaceutical market reputed to be worth $16bn US Dollars by 2025,[1] would mark a paradigm shift in modern medicine, allowing for the effective treatment of a myriad of currently untreatable conditions through the bioengineering of one's own immune system. Similarly, immunotherapies such as CAR-T are highly promising and have been shown to allow for the specific treatment of particular blood cancers by 'hijacking' the human immune system,[2,3,4] with a patient response rate of ~ 80% and a ~ 60% remission rate (12 months) for juvenile B-cell acute lymphoblastic leukaemia.[5] However, all these treatments fundamentally require, on demand, a ready and effective supply of medically important cell types or biological proteins.

This represents a significant logistical challenge. Given that many therapeutically important biological materials (cells, tissues, proteins etc.) have both poor stability and an intolerance towards extremes in temperature, how do you ensure a rapid and uncompromised supply of biomaterials when required? For the above treatments to be effective in the long-term, it is

essential we have a reliable process, giving us an effective methodology to get these species from ‘petri-dish to patient’, every time.

The natural assumption would be to freeze biological material in order to extend its shelf life. But whilst you can guard against exposure to heat (and its associated damage), freezing brings with it its own set of problems. Primarily, how do you ensure stability and viability of cell and tissue-based materials after being stored at low temperature?

The ‘Raspberry Problem’ is a prime example of this. If you freeze a raspberry, and thaw it, you lose the texture and the structural integrity. You get mush – Figure 1.1. The same is true of carrots, freeze then thaw a carrot, and you end up with a sodden, wringable sponge.

Figure 1.1 – Effect of the freeze/thaw process on biological material.

How do we prevent this same level of damage to a cell line? Or a blood bag?

Interestingly, many organisms (particularly extremophiles) are known to tolerate (and often thrive in) extremely cold temperatures. The atlantic cod survives in waters ~ 1.5 degrees Celsius below freezing, without freezing solid.[6,7] Likewise, tardigrades have been jettisoned into the cold vacuum of space, only to be recaptured and thawed, and found to still exhibit normal growth and signs of life.[8] Some insects have also been shown to have particular cold-tolerance, whilst certain classes of amphibians and reptiles have been found to have evolved to contain high levels of carbohydrates in their blood and tissues, allowing them to effectively ‘solidify’ without internal ice crystal formation, weathering their freezing winter environments

before thawing back to life in the spring.[9,10] In addition, numerous plants and shrubs have also been identified as possessing a disposition for severe climates.[11,12]

In order to begin to address the problems associated with ensuring effective cryoprotection during freezing, an understanding of these unusual effects in the natural world would seemingly be advantageous.

Once understood, we can then begin to ask the question – can we engineer our biological materials to withstand the harsh conditions of freezing?

1.1 – Antifreeze glycoproteins

Scholander and co-workers' first noted in 1957 the apparent ability of various arctic fish to thrive and survive in supercooled waters which were at least 0.7º C cooler than the freezing point of their blood serum (-0.9 to -1.0 ºC), without the fish freezing solid. This observation of an apparent freezing point depression – a thermal hysteresis effect – was claimed to be indicative of an inherent bloodborne 'antifreeze' quality, suggesting isotonicity with seawater and allowing the fish to survive in the 'Thermal Hysteresis (TH) Gap'. Figure 1.2.[13,7]

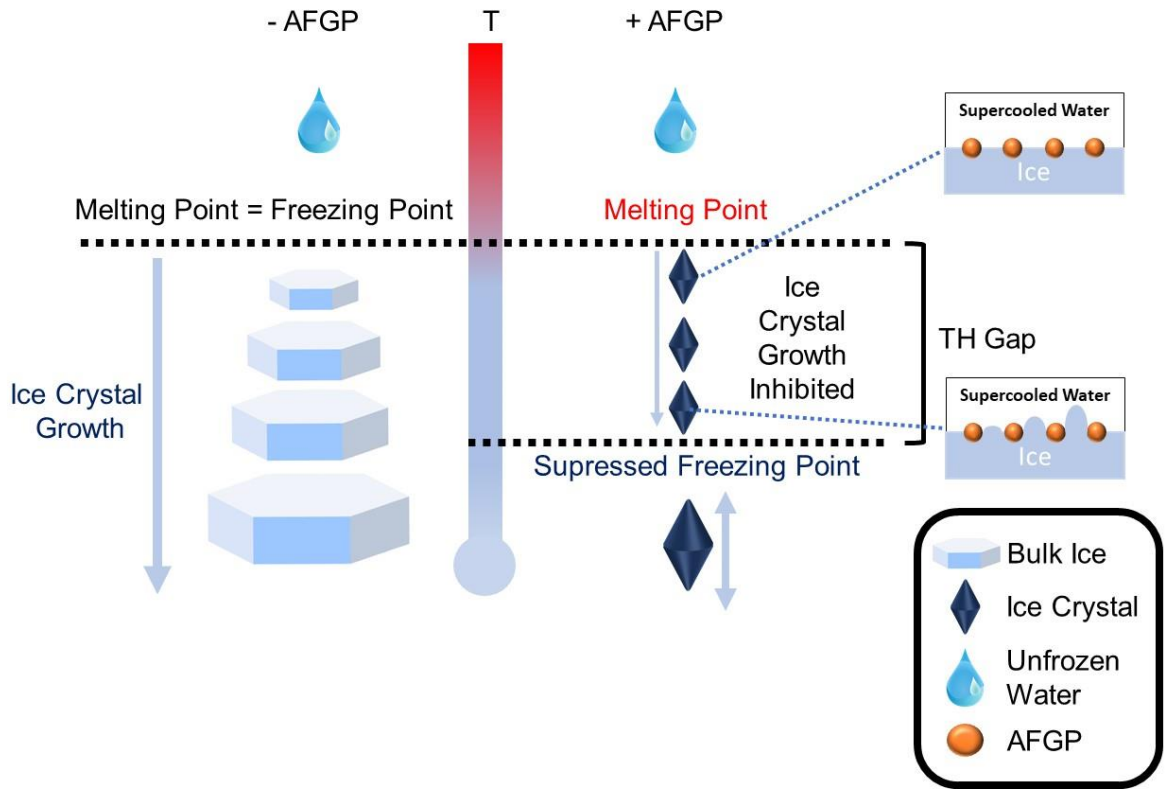

Figure 1.2 – Thermal Hysteresis effect of AF(G)Ps on ice crystal growth; In the presence of AFGP, the growth of the ice crystal is prevented (post nucleation) within the TH Gap due to inhibition of the primary prismatic plane by AFGP, with growth occuring only below the supressesed freezing point. Normal ice crystals in the absence of AFGP grow freely in all dimensions giving hexagonal ice, below the freezing point (0 ºC).

DeVries and Wohlschlang later reported (1969) on the isolation of a carbohydrate containing polypeptide from the blood of *Trematomus borchgrevinki* and *Dissostichus mawsoni*, which accounted for 30% of this observed freezing point depression. This represented a substantial freezing point depression, given the mix of low molecular weight amino acids, sugars, and salts contributing the remainder.[14] Importantly, whilst these glycosylated peptides are known to exhibit a maximum thermal hysteresis effect of 1.2 degrees at 40 $mg.mL^{-1}$,[15] they are found in the blood serum at concentrations as low as 5 $mg.mL^{-1}$,[16] at which they demonstrate a comparable freezing point suppression on a weight basis to sodium chloride. This ultimately represents a minimum x180 fold thermal hysteresis capacity relative to NaCl.[17] Subsequent studies by DeVries further elucidated the primary structure of this class of proteins, establishing them as freeze depressing (glyco)proteins or "FDGPs", and were found to contain threonine (16%), alanine (23%), D-galactose (28%), and *N*-acetyl-D-galactosamine (29%), and existing as a polydisperse mixture (2.6 – 33 kDa).[15] They were further identified as featuring an Ala-Ala-Thr (and rarely, a Pro/Arg-Ala-Thr) tri-mer repeat unit conjugated to an *O*-linked β-1,3-disaccharide (Gal/GalNAc) motif (Figure 1.3) and as having high water solubility.[17,18,19]

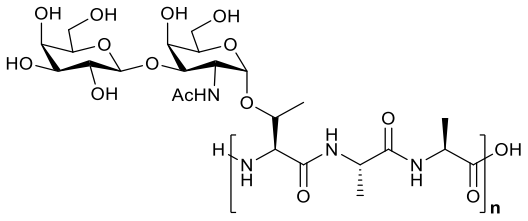

Figure 1.3 – AFGP repeat unit.

However, these FDGPs were quickly determined to possess two other potent cryogenic properties. The first of which was their ability to dynamically shape ice into spicular-like needles as a result of ice face binding, and the second, ice recrystallisation inhibition – the ability to retard ice crystal growth (Ostwald Ripening). The evolution of their initial

characterisation resulted in FDGPs being instead regarded as antifreeze glycoproteins or "AFGPs".[15]

Further analysis in recent years has enhanced our understanding of AFGP structure and function, although much remains unknown. Many isoforms of AFGP exist, with AFGP-8 as the shortest naturally occurring AFGP fraction found in extremophile fish, consisting of 4 repeat units and with a molecular weight of approximately Mw 2700 g/mol^{-1}.[20,21] The nature of AFGP's ice binding mechanism is contested, with some studies indicating it binds reversibly,[22] whilst others suggest irreversible binding occurs.[23] However, some key pieces of structural information which may shed light on these questions have been acquired. Due to its high degree of flexibility and the numerous conformers which AFGP is thought to be able to adopt in solution, no X-Ray crystal structure presently exists.[24] However, work by Matsumara and co-workers' has shown that AFGPs adopt a facially amphipathic structure by solution phase NMR (Figure 1.4A) – with the hydrophilic glycosyl units spatially segregated from the hydrophobic peptide backbone.[25]

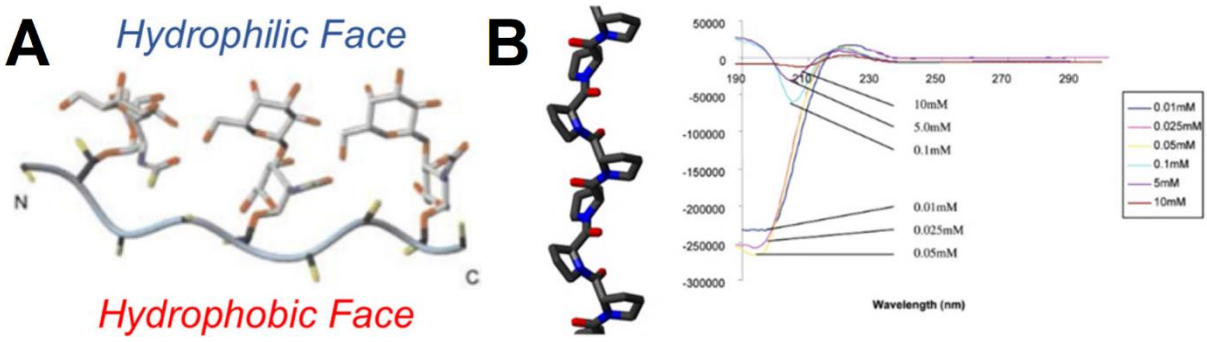

Figure 1.4 – A) Hydrophilic/phobic separation of AFGP.[24] B) Polyproline II Helix and Circular Dichroism analysis of AFGP.[21]

In addition, circular dichroism (Figure 1.4B) analysis has further indicated that this segregated domain structure occurs along a polyproline type II helix,[21] and also corroborates other NMR and simulation data which suggests that AFGP exists in solution as extended three-fold helices.[24]

1.2 – Antifreeze proteins

Whereas AFGPs are found only in Antarctic notothenioids and northern cods, antifreeze proteins – unglycosylated antifreeze proteins (AFPs) with similarly potent 'antifreeze' properties – are more widely spread in nature. Like AFGPs, AFPs developed in isolated species through convergent evolution.[26] However, whilst AFGPs exist as a highly conserved structure differing only by molecular weight and occasional amino acid substitution, AFPs possess substantially different structures and primary sequences depending upon their species of origin, and several 'classes' of AFPs exist. Table 1.1 and Figure 1.5.[27]

Table 1.1 – AFP Summary * One example of a myriad of plant AFPs.[24,28,29,30]

	Molecular Weight	Structure	Origin
Type I AFP	3.3 – 4.5 kDa	α-Helix, >70% Ala	Right eyed flounders, sculpins
Type II AFP	11 – 24 kDa	Disulphide Bonded Globule	Sea raven, herring, smelt
Type III AFP	6.5 kDa	β-Sandwich	Eel/ocean pout, wolfish
Type IV AFP	12.3 kDa	Helical Bundle	Longhorn sculpin
Insect AFP	50.2 kDa	β-Helical Bundle	Darkling beetle, spruce budworm moth, midge, fly
Plant AFP	27.6 kDa	β-Helical Bundle	Rye grass *

Antifreeze proteins are by and large better characterised than their AFGP counterpart. They are known to irreversibly bind to ice, and many X-Ray crystal structures exist, Figure 1.5. Similar

to AFGP, AFPs have been found to be intrinsically amphipathic with defined regions of hydrophobicity,[27] and exist as alpha helixes, beta-sheets, globules, and helical bundles. Unusually, many AFPs (such as Type I) contain high proportions of alanine in their structure, and yet are wholly water soluble.[30] Some AFPs – particularly plant AFPs, such as those extracted from the leaves of *Ammopiptanthus mongolicus* or the shoots of h*ippophae rhamnoides* – are glycosylated,[29,30] but represent a fundamentally different class of species and are not synonymous with AFGPs.

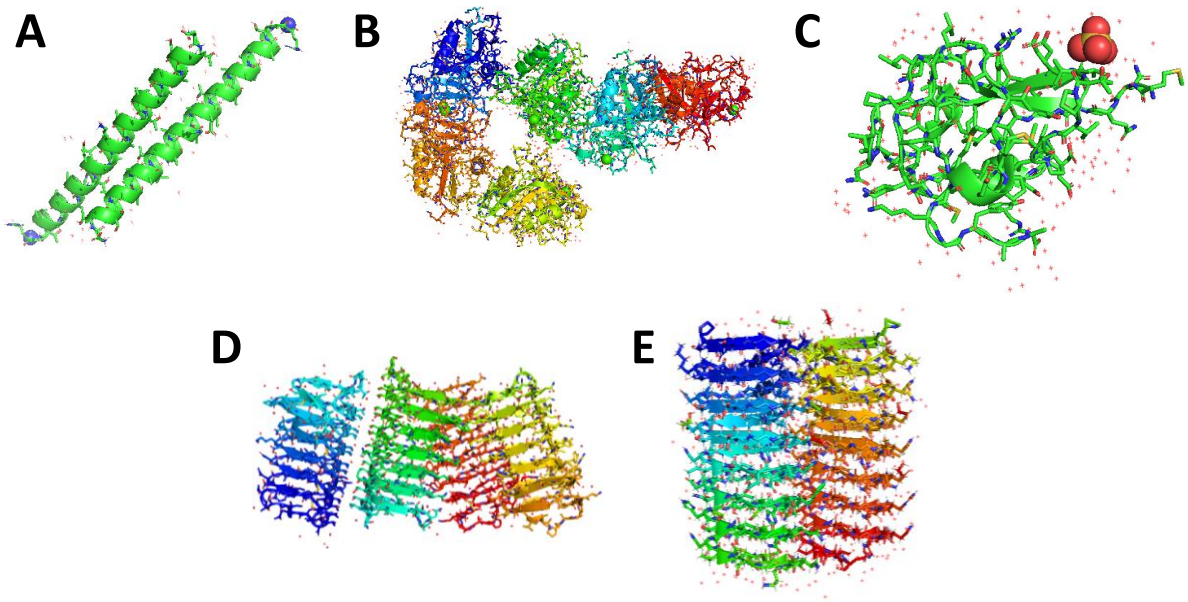

Figure 1.5 – Crystal Structures of A) AFP Type I – WFB1. B) AFP Type II – 2PY2. C) AFP Type III – 1HG7. D) Spruce budworm AFP – 1M8N. E) Perennial rye grass AFP – 3ULT.[31–35]

Whilst the thermal hysteresis effect is generally stronger for AFPs than AFGPs, this is further pronounced in the case of "Hyperactive AFPs" which have been reported in both cryophilic insects and bacteria. These species show substantially enhanced thermal hysteresis capacity relative to other AFPs, potentially due to basal face binding.[27]

1.3 – Mechanisms of action

The mechanism by which AF(G)Ps prevent ice crystal formation and growth, preventing ice induced cryoinjury, is fundamentally unknown. However numerous studies and hypotheses have been proposed in recent years.

Three properties are exhibited by AF(G)Ps:

I) Dynamic Ice Shaping (DIS)

II) Thermal Hysteresis (TH)

III) Ice Recrystallisation Inhibition (IRI)

Dynamic Ice Shaping

DIS is the most understood property of AF(G)Ps. It is thought that AF(G)Ps bind to specific planes of ice – usually the primary prismatic plane – preventing the addition of further water molecules to the ice crystal face, and so inhibiting the growth of the crystal along the bound axis. Figure 1.6.[36]

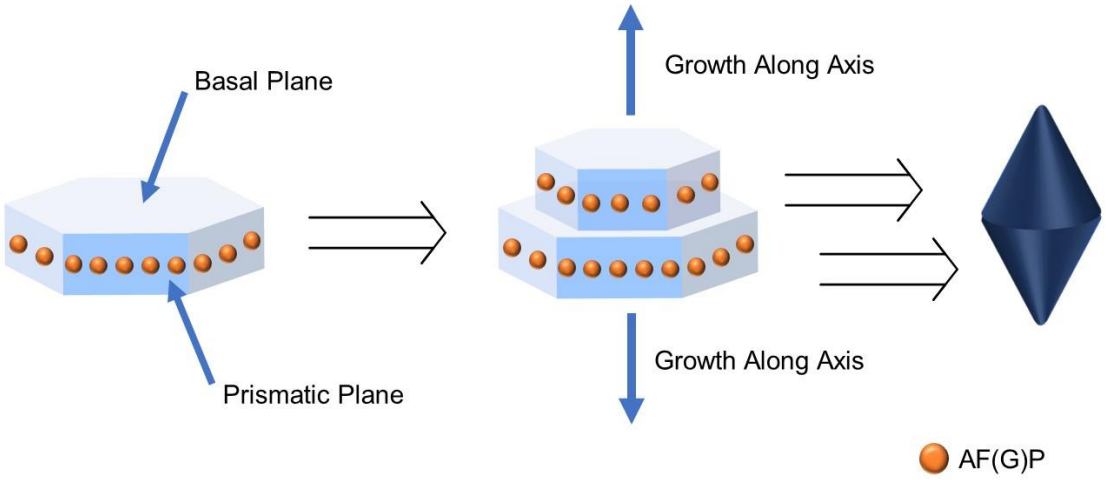

Figure 1.6 – AFGP primsatic face binding, leading to dynamic ice shaping / growth along the unbound axis.

Growth along the unbound axis results in the formation of long, spicular needles, which are able to cause catastrophic damage to biological matter on a cellular level – bursting and popping cells through effective 'puncturing'.[37] Dynamic ice shaping will however only occur below the TH Gap during ice crystal growth, and so this property is not detrimental to the marine life which utilise AFGPs for survival.[36,38]

Thermal Hysteresis

A non-colligative freezing point depression effect, thermal hysteresis (TH) acts to lower the freezing point of a solution whilst leaving the melting point fixed into place.[39] The addition of a solute (such as sodium chloride to water) will generally result in a colligative depression of the freezing and melting point of a solution – in the case of water, from 0 ºC to -6 ºC at 10% w/v NaCl.[40] This is proportionate to concentration and in-accordance with Gibbs' law of free energy.[39]

$$(T_m = T_f)_{Solution} > (T_m = T_f)_{Solution+Solute}.$$

Equation 1.1 – Thermal Hysteresis Gap.

However, the TH phenomenon results in the suppression of the freezing point of the solute containing solution further: $T_m > T_f$, – resulting in a 'TH Gap' between melting and freezing points, Figures 1.2 and 1.7.[39]

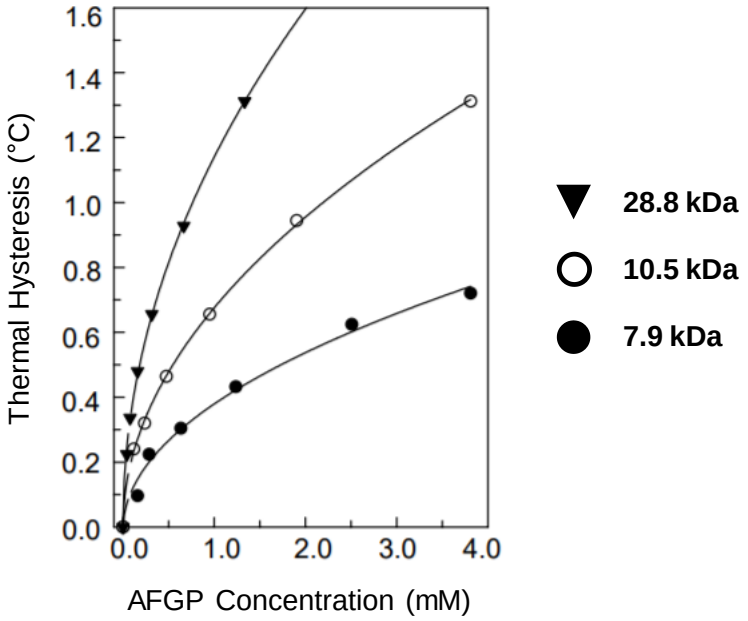

Figure 1.7 – Thermal Hysteresis effect of multiple AFGP molecular weight fractions. Adapted from [39].

Whilst the precise mechanism is unknown, and has been speculated on, TH is thought to occur through the binding of AF(G)P to the face of a seeded ice crystal which has spontaneously formed in supercooled solution, and then prevents it from expanding (or melting) within the TH Gap, with growth only occurring when the temperature drops below it. It is hypothesised that antifreeze proteins are capable of equilibrating vapour pressure at the concentrations within the TH range, so that 'molecular escape' is zero and the net on/off rate of water molecules to the ice crystal is equal. Crystal surfaces which are not bound to an AF(G)P however will exhibit 'budding' and slight growth along unhindered/uninhibited axis, a precursor to DIS. The TH effect is concentration dependent, with the greatest TH effect observed at higher concentrations.[39] Whilst some extremophile insect and plant AFPs are known to be 'hyperactive' – and able to supress freezing point to -30C – TH is problematic in the context of cryopreservation. Recent attempts to utilise the AFP *MpdAFP* to preserve horse sperm detrimentally impacted upon spermatozoa motility.[41]

Ice Recrystallisation Inhibition

Ice recrystallisation inhibition (IRI) is the observed effect by which the growth of ice crystals is impacted, slowed, or halted when solution freezing occurs in the presence of an AF(G)P or other synthetic mimic.[42] This is in comparison to an unadulterated solution, which will by comparison yield substantially and significantly larger crystals. Figure 1.8.

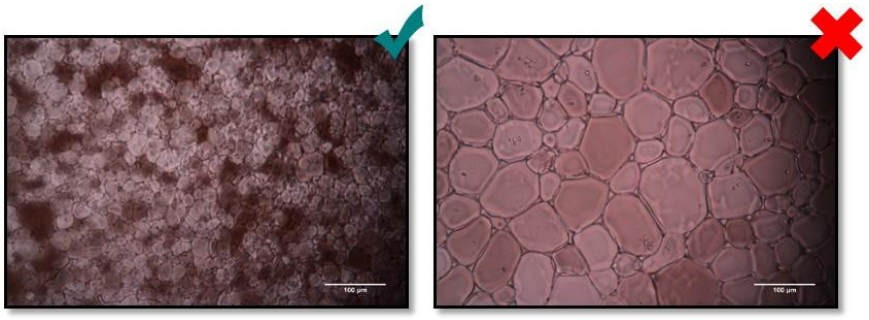

Figure 1.8 – 'Splat' Assay of AFGP in PBS (Left) and of PBS Alone (Right).

This phenomenon is a particular problem in the storage of biological samples (blood, tissues, cells of all types, organs etc.)[43] as Ostwald Ripening dictates that larger crystals will grow at the expense of smaller ones, especially during thawing.[44] As a result, large crystals are able to cause catastrophic ice induced cellular damage – squeezing and rupturing cells from the outside.[36,38,43] The smaller that ice crystals are allowed to grow, the less damage can result – which is of particular concern during thawing. A recent study by Gibson and co-workers' confirmed that cell recovery is directly linked to the restriction of ice crystal growth.[43]

The mechanism by which ice recrystallisation inhibition operates is unclear. Several competing arguments exist, and it is possible that different solutes function and infer IRI through different processes. It may even be the case that there is no 'one' unified or common mechanism of IRI. AF(G)Ps are all however thought to function through an adsorption-inhibition mechanism.

Jia and co-workers' have reported that many AFPs feature an "Ice Binding Site" (IBS) which is flat, rigid, and amphipathic, but with predominantly hydrophobic character.[45,46] An

established and accepted theory was subsequently postulated by Davies and co-workers', detailing how the IBS of a bacterial AFP (*Mp*AFP – 1.5 MDa) derived from *Marinomonas primoryensis* and displaying Ca^{2+} dependent hyperactivity, does not itself bind to ice, but instead orders local waters along the IBS which are a good 3D conformational match for the primary prismatic plane of ice.[47] These ordered waters then bind to the ice crystal face, co-ordinated in to place by the AFP to which they are hydrogen bonded, blocking bulk water addition and preventing crystal growth. Figure 1.9.

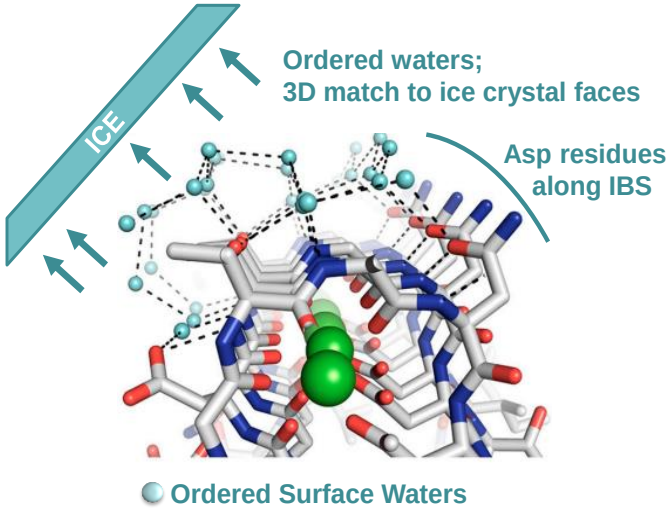

Figure 1.9 – AFP Clathrate water ordering postulated by Davies and co-workers' [47] on surface of *Mp*AFP. Figure Adapted.

Recent fluorescence/microfluidic studies have further indicated that this binding is irreversible in the case of AFPs.[48–50,51] Conversely, similar studies have indicated that some AFP binding is seemingly *reversible*,[52,53] whilst others have assumed reversibility of binding as a prerequisite for AFP function.[54,55] The phenomena is therefore not very well understood.

On the other hand, poly(vinyl) alcohol (PVA) has long been recognised as a potent IRI species and represents the most active synthetic mimetic of AF(G)P discovered to date. Koop and co-workers' – along with Molinero and co-workers' – have postulated that PVA binds to the ice crystal face through direct hydrogen bonding of the alcohol group.[44,56] It is believed that PVA

operates in a 'zipper-mechanism' like fashion. The precise spacing between PVA's alternating hydroxyl groups of 2.92Å and 7.46Å between every 2 groups, in addition to PVA's intrinsic flexibility, is believed to allow the polymer chain to 'explore' the ice crystal face, binding through every other 2 hydroxyl groups in a '2-on-1-off' approach. This is a good conformational match to the water molecules in the primary prismatic plane of ice at distances of 2.76Å and 7.35Å respectively. This site occupation again physically blocks-off the ice crystal from water addition, preventing growth, Figure 1.10.[44,56]

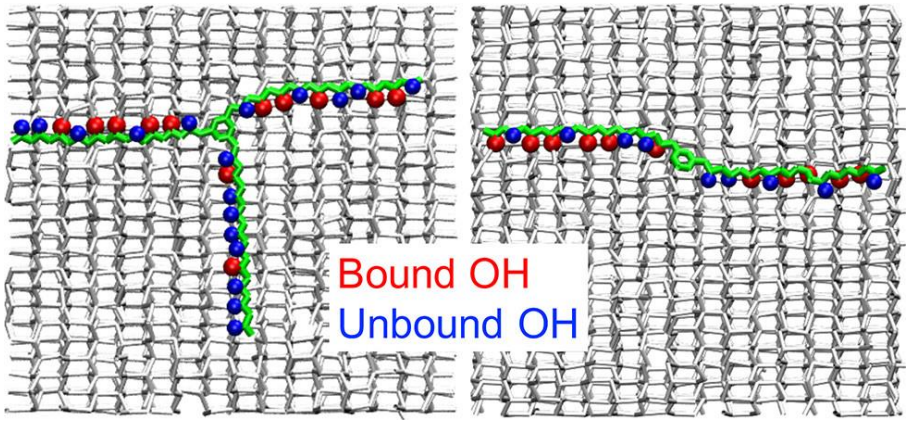

Figure 1.10 – Hydrogen bonding model postulated by Molinero and co-workers' [50] depicting the exploration by a single chain of PVA of the {10$\bar{1}$0} ice crystal face (primary prismatic plane).

The mechanism of AFGP's IRI activity is poorly understood and contested,[57] but is believed to be very different to that of AFP – described previously. A recent computational study by Molinero and co-workers' has suggested that the domain segregation AFGP is critical to IRI activity. It was hypothesised that the hydrophilic glycosyl units of the protein chain extend out into the non-frozen aqueous solution immediately surrounding the ice crystal and disrupt water ordering. Meanwhile, the hydrophobic units *reversibly* bind to the ice crystal face.[22] Given that the surface of ice has appreciable hydrophobic character (and has a reported water contact angle of 12 degrees)[58], the authors reported that the fatty methyl groups of the amino acids (Ala and Thr) in the backbone of the protein chain bind and 'rest' in the defects of the hydrophobic

crystal surface. The equilibrial occupation of these cracks, nooks, and cavities by AFGP then prevents crystal expansion. Figure 1.11.

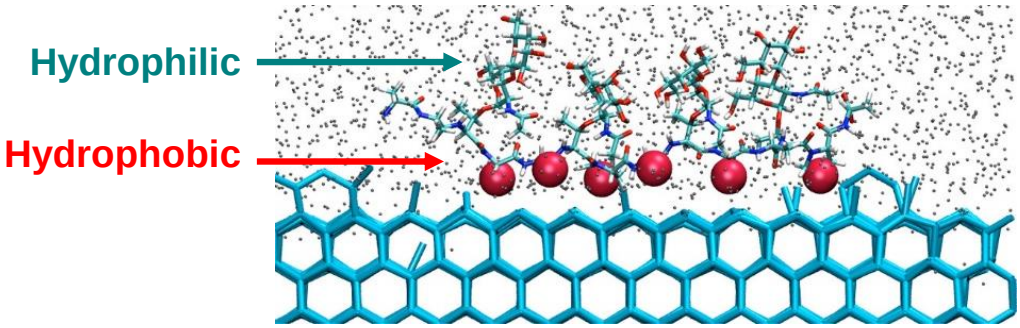

Figure 1.11 – Reversible AFGP face binding model postulated by Molinero and co-workers'.[22]

However, alternative theories have also been proposed. A further recent study by Drori and co-workers' has indicated that AFGPs in fact function through *irreversible* ice face binding, suggesting that their primary mechanism of action is *via* an adsorption-inhibition process, validating this hypothesis through microfluidic/AFGP fluorescence tagging experiments.[23] These studies corroborate the work of DeVries and co-workers', who has published extensively on the binding of glycans to ice.[59–61]

A recent model has also evolved in an effort to explain the ice recrystallisation inhibitory effect of synthetic mimics which display IRI properties in the absence of TH or DIS. It has been hypothesised that the presence of some AFGP mimetic solutes can disrupt bulk water ordering in the surrounding unfrozen solution.[62–64] This therefore energetically inhibits water transfer across a disordered water layer – an interstitial phase (~ 10Å thick) of neither frozen nor liquid water between the bulk water and an ice crystal face.[65] Whilst the mechanism has not been elucidated,[39,66] it is thought that this effect ultimately prevents/disrupts water molecule addition from the disordered layer to the ice crystal face, retarding crystal growth. Figure 1.12.

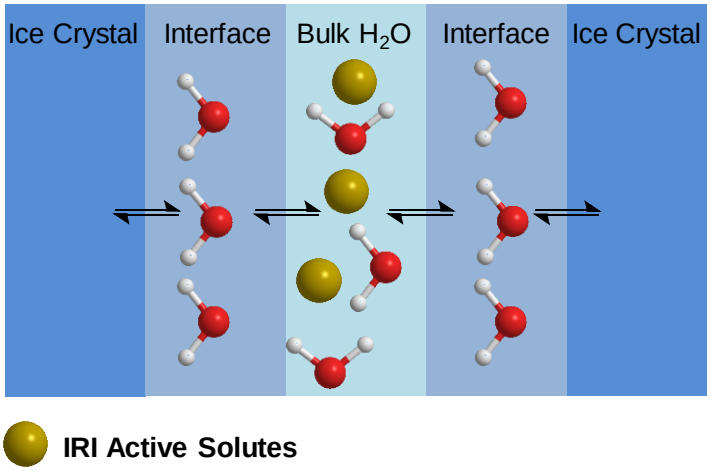

Figure 1.12 – Disordered Water Layer Hypothesis.

1.4 – Applications of AF(G)Ps

Tissue engineering, gene therapy, drug screening and emerging regenerative medicine therapies are fundamentally reliant on high-quality cell culture,[67] but current methods to cryopreserve cells typically result in extensive cell death, giving low yields and recoveries, especially in the case of adherent cell culture.[68,69] A similar problem is encountered with blood stocks and blood products, which are well known to suffer from a short shelf life. In conjunction with a shortage of donors, supplies are often stretched in some geographical areas, whilst discarded unused in others.[70] These issues are particularly pronounced when ensuring sufficient blood supplies of rare or essential blood groups, such as O Negative (the Universal Donor). The biobanking and storage of stem cells – which themselves represent a paradigm shift in biomedicine – and tissues is also a key problem, with low viabilities and recoveries again observed.[71]

A contributor to cell death during cryopreservation is ice recrystallisation. Ice recrystallisation occurs as a result of extracellular ice crystal formation (i.e. ice formation outside the cell) during freezing, which leads to mechanical damage and lysis as a result of repeat freeze-thaw cycles; where larger ice crystals grow at the expense of smaller ones through slow recrystallisation. This effect cannot be circumvented by rapid thawing, which is often difficult to achieve homogeneously.

However damage can also occurring during freezing and so the rate of freezing is significant. Very slow freezing results in the formation of extracellular ice, which no longer being liquid water, results in the flow of water out of the cell across the osmotic gradient to redress the equilibrium. As a result, the cell slowly dehydrates and dies. On the other hand, fast freezing at below -40 ºC hastens the formation of intracellular ice crystals, which can lead to cell lysis

by the expansion of trapped intracellular water and further cause catastrophic damage on thawing due to Ostwald Ripening.[72]

As such, an intermediate freezing rate is optimum, but extracellular ice crystal formation remains a problem – especially during thawing. Existing strategies to circumvent the damage induced by ice recrystallisation during the cryopreservation of cell and tissue biomaterials often involve the infusion of unsustainably large quantities of (typically cytotoxic) organic solvents such as DMSO, or alternatively, glycerol.[73]

Whilst IRI inactive – these penetrating cellular cryoprotectants act to prevent ice crystal growth in a colligative manner by freezing point suppression, and further modulate the concentration/increase in intracellular solutes during freezing.[74–76]

However, these techniques are non-ideal, and in the case of DMSO, often results in as little as 5% cellular recovery post-thaw in the case of adhered embryonic stem cells.[68,69] Furthermore, recent studies have indicated that despite common perception, DMSO's cytotoxicity profile [77] is a cause for concern and can lead to phenotypic changes and mutations in cell lines [78,79] – a fundamental problem in biomedicine where identical cell lines are required.

Clearly, engineering medically important cell and tissue types towards cold tolerance is key to pioneering new treatments and enhancing cellular storage, and by the elucidation of the mechanism of cold-tolerance exhibited by extremophile organisms, we may be able to incorporate freeze-tolerance properties, enhancing and facilitating cryopreservative techniques.

As such, additives which can inhibit recrystallisation have the potential to redefine cell storage and hence biomedicine, and antifreeze (glyco)proteins would seemingly have application herein. The total synthesis of AFGP and some modified derivatives has been reported several times – notably by Payne and co-workers' and Nishimura and co-workers'[80–82,83] Aside from

their suspected immunogenicity, the dynamic ice shaping effect of AFGPs in particular would pose a problem in cellular cryostorage.[84] As most biological samples are stored at -20, -80, or more commonly at -196 ºC – significantly below the TH gap – ice crystal growth (while IRI inhibited) would still result in the formation of spicular/needle like crystals, which are able to cause catastrophic mechanical damage and pierce cell membranes.

It is therefore clear that research towards a synthetic AF(G)P mimetic, which is capable of preventing ice induced damage above-and-without the use of organic solvents, would have clear application in biomedicine and cryostorage – and numerous studies have been reported in recent years.

1.5 – Synthetic AF(G)P Mimetics

Early attempts at preparing and identifying synthetic AF(G)P mimics were often unsystematic and disconnected, with individual studies investigating Thermal Hysteresis or Ice Recrystallisation Inhibition alone. Knight and co-workers' first identified the potential of synthetic polymers to act as potent ice recrystallisation inhibitors, emerging as a new paradigm for controlling ice crystal growth.[85]

Knight further developed the 'Splat' assay – a method of determining IRI activity by dropping a 10 µL sample (dissolved in PBS buffer – pH 7.4) onto a chilled glass coverslip. Upon hitting the coverslip, a frozen wafer forms instantaneously, the glass coverslip is then transferred to a cryostage and held at -6 to -8 ºC. Photographs are then obtained after a discreet interval and compared to a PBS negative control, allowing the size difference to be assessed and the IRI potency of the sample to be determined. The appropriate method for the reporting of data has become an arguable issue in recent years – initial experiments such as those performed by Knight (and perturbated in some recent studies) often presented micrographs of the ice crystal wafers in lieu of any mathematical or statistical analysis, and so acting as a simple visual comparison. More often, IRI activity has since been expressed as Mean Largest Grain Size (MLGS) – where the length of the 'n' largest crystals in the field of view are measured over three replicates and the average taken and given as a % relative to PBS. Similarly, Mean Grain Area or Size (MGA / MGS) has also been used, and has established its self as the predominant metric in recent literature. This measurement counts the number of crystals in the field of view, over three replicates, and is again expressed as a % of PBS. It is arguable that MLGS may represent a more appropriate figure, given that it would be the largest crystals that would induce the most damage upon biological material. However, it does not take into account that the

largest crystals in the sample may not be representative of the remaining field (where many small crystals may exist) – and so MGS is considered a better approximation.

In 1995, Knight first reported on the activities of *poly*(vinyl alcohol) (PVA) and *poly*(hydroxyproline), both demonstrating significant potency at 1 mg.mL^{-1}. On the other hand, a series of *poly*(histidine), *poly*(aspartic acid), *poly*(asparagine), *poly*(acryl acid), and *poly*(vinylpyrrolidone) all displayed weak-to-no activity.[85] These observations contributed to a long standing school of thought which suggested that hydroxyl group presence was ultimately required to incorporate IRI potency into synthetic architectures.

Poly(vinyl alcohol) is of particular interest and is the most studied (and potent) synthetic AF(G)P mimetic reported/identified to date. PVA is able to inhibit ice crystal growth to 10% of its original size (MLGS) at less than 0.1 mg.mL^{-1}, Figure 1.13,[86] and is notable for its ability to enhance the cryopreservation of cells in suspension.[86] Uniquely, PVA is IRI active over a large molecular weight range, and has recently been found by Gibson and co-workers' to 'become' IRI active at DP 14.[87]

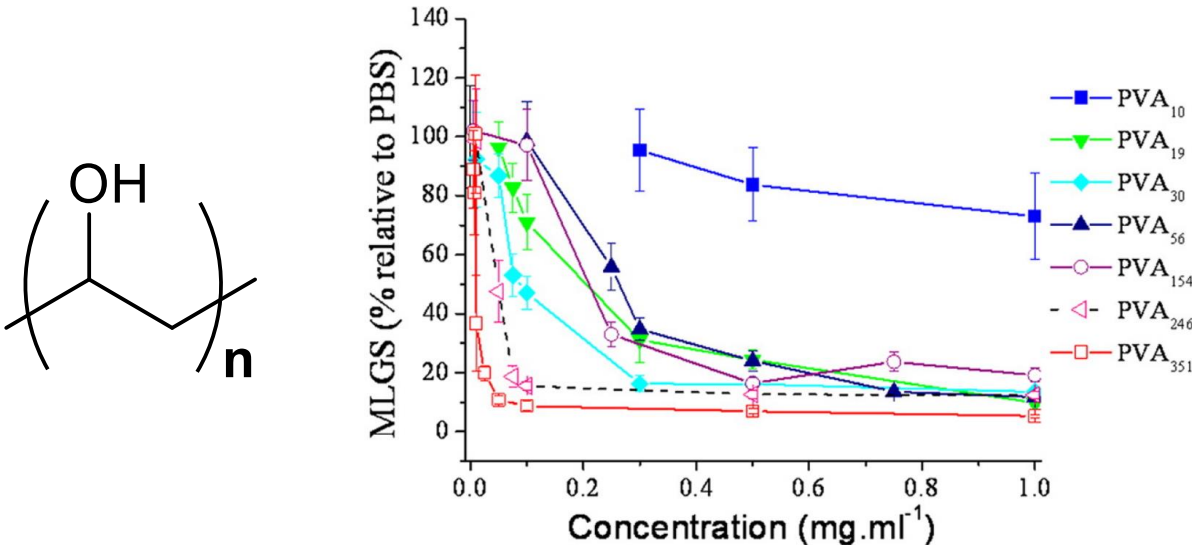

Figure 1.13 – IRI potency of *poly*(vinyl alcohol).[86]

However, in spite of PVAs IRI potency and biocompatibility/non-toxicity,[88,89] it's activity cannot be fine-tuned/optimised. It has been shown to dramatically lose activity when subjected to even slight structural modifications,[86,90] and consequently we do not know how it works. PVA may therefore not be applicable as a 'universal' ice recrystallisation inhibitor.

Ben and co-workers' first reported in 1999 on the development of a synthetic protocol for the preparation of a *C*-linked AFGP mimetic species, to act as probes in AFGP mechanistic studies. Figure 1.14.[91]

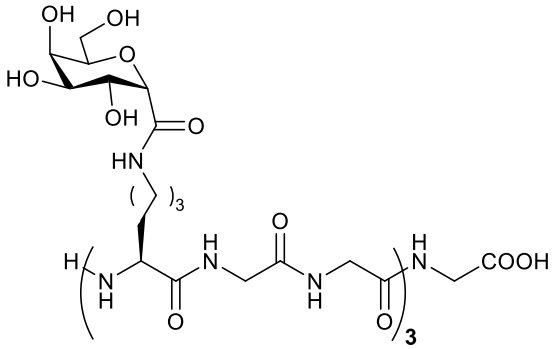

Figure 1.14 – Ben and co-workers' first generation *C*-linked AFGP mimetic probe.[91]

This low molecular weight, simplified species, featuring a monosaccharide motif attached to a lysine-glycine tri-repeat unit, eventually led to Ben's 2005 development of a series of galactosyl serine AFGP analogues (Figure 1.15),[92] following several precursor studies.[93–95]

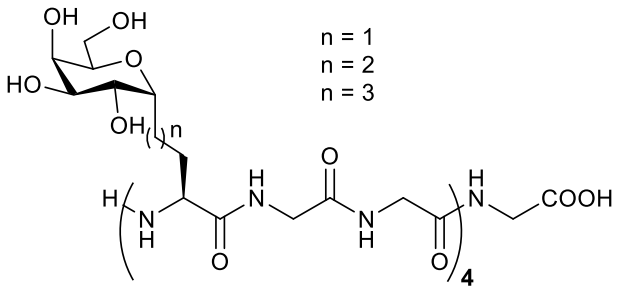

Figure 1.15 – Ben and co-workers' second generation *C*-linked AFGP mimetic probe.[92]

This study of the structure-activity relationship indicated the superior activity of the candidate where the number of carbon atom spacers between the sugar and peptide backbones was n=1.

Amazingly, this candidate was able to inhibit ice crystal growth to approximately 16% of their original size (MLGS) at 8.36 $mg.mL^{-1}$, relative to 14% of AFGP-8 at 14.3 $mg.mL^{-1}$, representing a new dimension of synthetic IRI potency. On the other hand, the longer side chain derivatives of n=2 and 3 rapidly lost activity – indicating that IRI activity is a highly tuned, sensitive property, and clearly intolerant to minor structural modification (as is also observed with PVA).

Similarly, Ben further reported that substitution of the galactose motif for other sugar residues impacted upon IRI potency.[64] A galactose derivative of the first generation probe – featuring an additional repeat unit to give a tetramer and one fewer carbon in the linker – had statistically similar activity at 27% MLGS at $mg.mL^{-1}$. A glucose derivative, however, exhibited just ~ 80% MLGS whilst substitution with mannose or talose reduced activity to effectively zero. Given that these derivatives are epimers and differ only by the stereochemical orientation of the hydroxyl group at the sugar C-4, Ben further speculated that molar hydration capacity influences IRI activity. Figure 1.16.

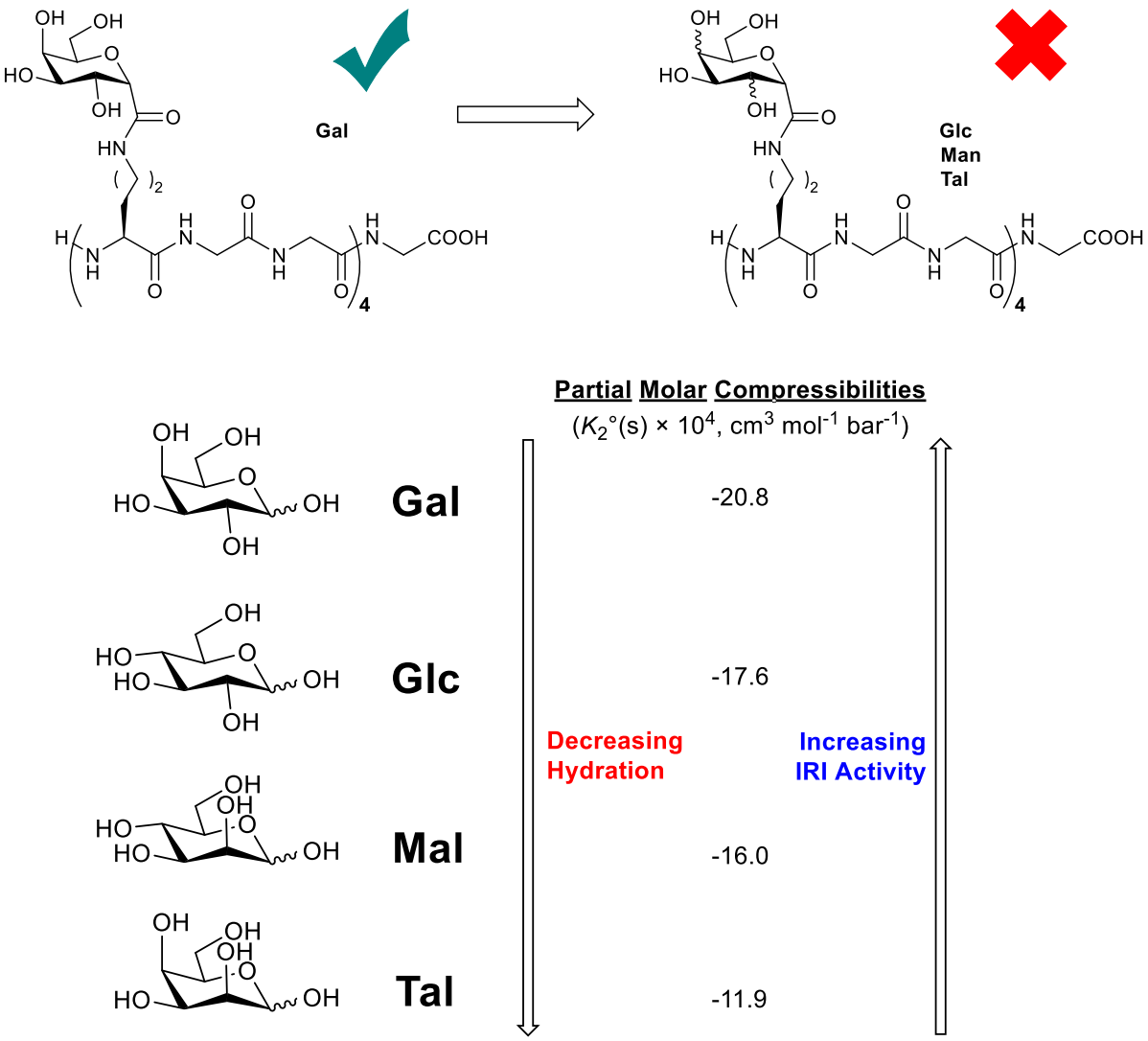

Figure 1.16 – IRI activity correlated to hydration potential of carbohydrates. Reproduced from Ben and co-workers'.[96,97]

This clear trend in IRI potency dependent upon the extent of sugar hydration would seemingly lend credence to the disordered water layer hypothesis – suggesting (as the authors claim) that the individual glycosyl's affinity towards and differing interactions with the hydrogen bonded network of supercooled water at the bulk/disordered water interface directly impacts upon the energetic transfer of water to the ice crystal face. Galactose clearly has a greater proclivity towards hydration, and therefore has a greater disruptive force on local hydrogen bonding, disrupting water transfer and imparting IRI activity.[62,64] This fundamentally disagrees with the mantra that 'hydroxyl groups = IRI activity'.

In addition, this observation would seemingly indicate the preference/selection for galactose and *N*-acetyl-galactosamine over other carbohydrate units in the natural product.

Further assessment of the primary candidate through *in vitro* cell assays indicated that whilst AFGP-8 exhibited intrinsic cytotoxicity to human liver (WRL 68) and kidney cells (HEK 293) – hypothesised to be as a result of rapid endocytosis promoting 3/7-capase activity – the synthetic analogue did not induce cell death and apoptosis. This was attributed to the ability of the mimic to on the other hand *supress* the 3/7-capase pathway when taken into the cell. Crucially, and unlike AFGP, the mimic exhibited no detrimental effect on cell viabilities after incubation (37 ºC) for 20 hrs at 5 $mg.mL^{-1}$.[98]

Interestingly, the first generation probe devised by Ben did not have any thermal hysteresis activity, despite being highly IRI active. Nishimura and co-workers' first reported the ability to separate out two of the three key effects of AF(G)Ps into discreet qualities, showing that it was possible to have a TH effect in the absence of DIS.[99] This is ultimately important, as this allows for the rational design of potent IRI inhibitors with the detrimental properties dispensed with.

Further studies by Ben and co-workers' have covered the synthesis of a sequentially modified derivative of the second generation probe, featuring a triazole linker in place of the *C*-linked amide, and was found to possess poor activity. This study again reinforces the structural sensitivity of AF(G)P mimetics, ultimately indicating the necessity of the amide unit.[100] Specifically, this may indicate that the comparatively increased structural rigidity of the triazole has impacted upon solution confirmation, affecting the ability of the candidate to disrupt water ordering.

Numerous studies investigating the preparation of AF(G)P mimetics with IRI potency have continued to focus on the development of polymers. This is however a non-trivial task and is

highly challenging, as it is often necessary to precisely engineer structures given that many polymers (such as PEG) show no IRI activity whatsoever, and minor modifications of potent species generally lead to a loss of activity. Whilst the design rules are unclear, it has been hypothesised that – due to the hydrophobic nature of ice – that the presence of hydrophobic groups in synthetic mimics is essential for IRI.

Cameron and co-workers' reported on the IRI inactivity of a series of glycopolymers and polypeptides derived through RAFT polymerisation and the ring opening of *N*-carboxyanhydrides. The polypeptides – including poly(lysine) and poly(glutamic acid) – did not show any meaningful activity.[101] However (and unusually) the range of flexible glycopolymers assayed showed next-to-no IRI activity at all molecular weights, despite the chain possessing carbohydrate motifs and a simplified polymer backbone, representative of AFGP. Figure 1.17.

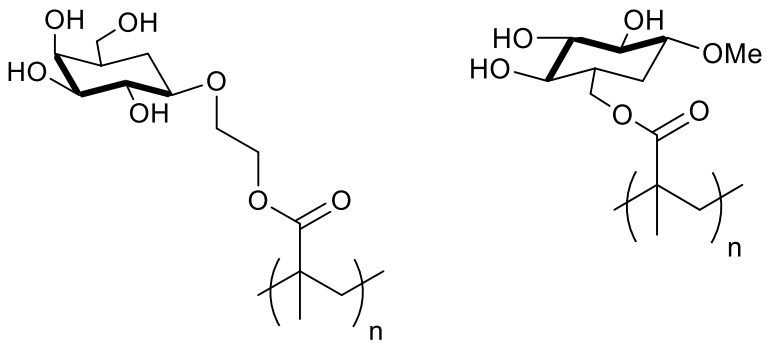

Figure 1.17 – Flexible glycopolymers prepared by Cameron and co-workers'.[101]

This disparity of non-hydroxylic polyampholytes showing potency, whereas hydroxylic glycopolymers are wholly inactive, has begun to suggest that the presence of hydroxyl groups in IRI inhibitors are not actually responsible for the incorporation of IRI activity. In association with this, Gibson and co-workers' have assayed a large range of small molecule mono, di, and polysaccharides, with none displaying any significant IRI properties at elevated concentration.[102] Ben and co-workers' have also assayed a number of synthetic mono and

disaccharides, again, observing little-to-no activity.[103] Given that Safranine O – a non-hydroxylic synthetic dyestuff – has been reported by Drori and co-workers' to be a potent ice recrystallisation inhibitor, this would indicate that hydroxyl groups in-and-of themselves are not essential for IRI.[104] Safranine O is believed to self-assemble in solution, forming an amphipathic, supramolecular structure, with defined regions of hydrophobicity and hydrophilicity – akin to AFGP. Figure 1.18.

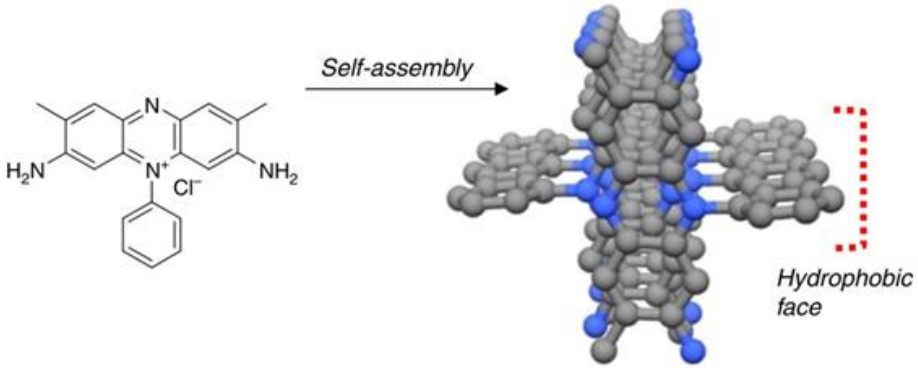

Figure 1.18 – Self-assembly of Safranine O, a potent IRI. Adapted from Drori and coworkers'.[104]

Likewise, a similar species – zirconium acetate – has been shown to adopt an amphipathic and polymer-like supramolecular architecture in solution, again showing particular potency.[105]

Unusually – Nisin A – a naturally occurring protein which is added to milk products as a preservative, has also been shown to be IRI active at low pH (~ 5) only (where it adopts an amphipathic structure in acetate buffer).[106]

Other small molecules have also shown unprecedented levels of activity. A water soluble synthetic metallorganic framework or 'metallohelix' reported by Scott and Gibson and co-workers', featuring an Fe^{2+} centre in the core of a stereochemical pure helix, has supressed ice crystal growth to approx. 15% MLGS at ~ 32 $mg.mL^{-1}$. Intriguingly, modelling of the surface electronic distribution has indicated that this species too adopts an amphipathic structure, Figure 1.19.[107]

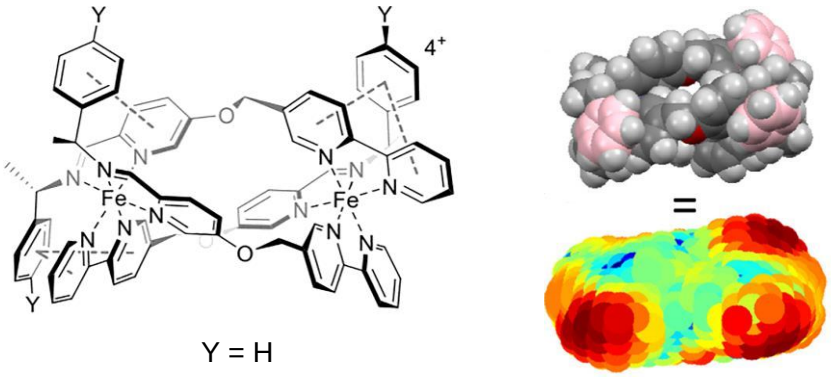

Figure 1.19 – Enantiomerically pure metallohelix reported by Gibson and Scott and co-workers' featuring an amphipathic surface.[107]

These combined studies begin to suggest that amphipathy maybe a core design motif, as opposed to hydroxyl group presentation. Specifically, this asks a greater mechanistic question too, as to whether ice face binding is actually required for 'isolated' IRI activity (in the absence of TH or DIS effects) or whether simple disruption of the supercooled water at the bulk/disordered water interface by an amphipath is sufficient to impart inhibition. Gibson previously surmised that long-range order was deemed to be inessential for IRI activity, whilst necessary for thermal hysteresis effects.[108] In terms of a mechanistic mode of action, disruption to give a bulk/disordered water interface would not require long range order, only efficient & effective local disruption to impart a long range effect.[109]

Ben and co-workers' have also reported on the development of small molecule mimetics of AF(G)P. Whilst it has been demonstrated that monosaccharides lack IRI potency, Ben has recently shown how a series of modified glycosides are however able to potently inhibit ice crystal growth. Figure 1.20.

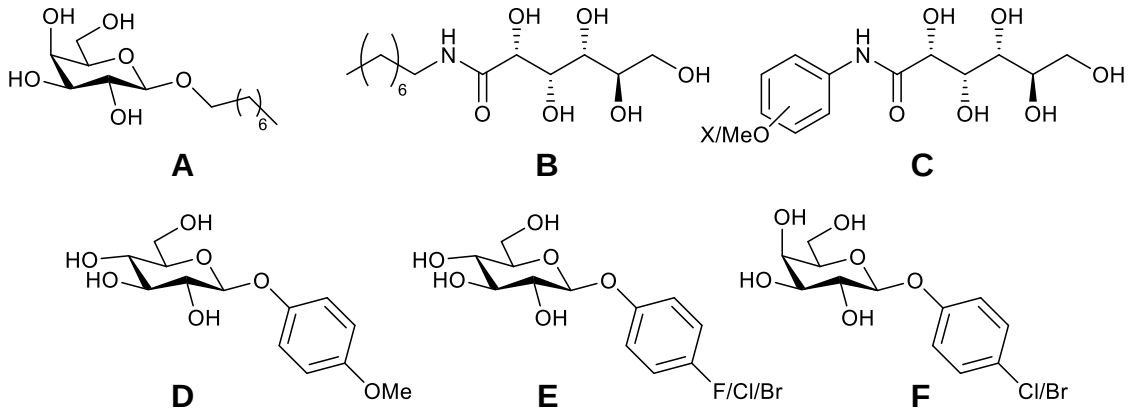

Figure 1.20 – Small molecule library of IRI active AFGP mimetics designed by Ben and co-workers'.[110-113]

Unexpectedly, an octyl galactose derivative (Figure 1.20A) is capable of potent inhibition of the order of < 10% MGA at 12.86 mg.mL^{-1}, signifying the importance of hydrophobic domain incorporation.[110] Unusually, aryl functionalisation of the galactose motif in place of the octyl chain (Figure 1.20F) inferred greater activity upon the unit. This is potentially due to the aromatic ring acting as a 'tighter' and more defined hydrophobic unit (with less intrinsic flexibility, and with fewer solution conformations available to it). Exceptional activity was however only present when the ring was halogenated in the *para* position with specifically bromine (5% MGA at 7.4 mg.mL^{-1}) and chlorine (20% MGA at 6.4 mg.mL^{-1}), with other derivatives displaying moderate-to-little activity.[111] Curiously, a glucose equivalent (Figures 1.20D and E) showed stronger activity with fluorine or methoxy in the same position (20% MGA in both instances versus 80% for Gal), in addition to bromine and chlorine (with very slight reductions in activity observed).[111,112] This is highly unusual, given Ben's earlier report that glucose derived species had no activity and were hypothesised to be IRI inactive due to weak hydration effects. The brominated glucose derivative was further found to be a highly effective cryoprotectant in red blood cell cryopreservation, with significant protective capacity above and beyond the rest of the series. A 15% glycerol solution (acting as a conventional cryoprotective mix, but lower than the industrially 'standard' 40%), supplemented with 30 mM

(10 mg.mL^{-1}) of this agent increased RBC integrity post-thaw by 40% and 20% (relative to no adulteration) for slow and fast freezing protocols, respectively. The equivalent bromo-galactose derivative exhibited comparable effects at 30 mM (fast freezing) and 55 mM (slow freezing).[111] The ability to lower the requisite concentration of glycerol is undoubtedly beneficial, reducing the complexity of protracted glycerol removal procedures.

The rationale for the substantially different activity profiles of this series is unclear. The authors note that electronic effects of the ring substituents seemingly have no correlation in terms of IRI activity, whilst the introduction of alpha-linkages (in place of beta) cause a substantive loss in potency. In the case of the glucose anisole derivative (representing the most potent IRI of this class), it was clear that the 'methoxy' group in particular was essential for activity, with substitution for a hydroxyl or methyl group leading to an immediate loss of activity. Likewise, other structural substitutions (such as for bromine) yielded a weaker IRI candidate. Further studies on synthetic disaccharides in this report again show the sensitivity and significance of the carbohydrate hydroxyl groups and epimeric confirmations upon IRI.[111] Collectively, these observations indicate that the ability to disrupt the ordering of water by small molecules is ultimately dependent upon very specific structural properties, conformations, and overall net polarity – with minor changes vastly impacting IRI ability.

Aldonamide species derived from sorbitol have also shown hyper potency, with a similar octyl functionalised derivative inhibiting ice growth to ~10% MGA at 0.15 mg.mL^{-1} (Figure 1.20B). Whilst no hydration parameters are available, this derivative is however known for its ability form micelles and increasing the solution concentration eventually led to the neutralisation of activity (> 10 mM).[110] This may be ultimately problematic in cryopreservative applications, where higher concentrations (above and beyond the candidates IRI potency range) maybe required. However, this observation has shown that micelle formation is not a structural factor in IRI activity. Interestingly, the amide group was found to be critical for IRI (as observed in

Ben's previous work where the amide was substituted for a triazole), with removal and substitution causing an unrecoverable loss of activity.[110] Functionalisation of this aldonamide with an aryl group in place of the octyl unit (Figure 1.20C), specifically either 2-F, 4-OMe, or 2,6-difluoro, displayed comparable IRI activity, but at elevated concentration (6.4 – 6.8 $mg.mL^{-1}$).[113] This is unusual, as other permutations of this structure (such as 2-Cl or 4-F), failed to infer any IRI properties. However, this study further confirmed that hydrogelation of these candidates had no bearing on IRI activity. Furthermore, when employed as a cellular cryoprotectant, the 2-F derivative at 1.45 $mg.mL^{-1}$ enhanced the total number of UCB/Progenitor CD34+ cell colonies post-thaw, up by approximately 10% - further showing that an IRI active compound has cryoprotective ability.[113]

As further discussed *vide infra* (Chapter 3), Ben and co-workers' have further detailed the development of 'photoswitchable' carbohydrate derived surfactants, which by virtue of an azo-benzene linker, are able to weakly modulate IRI activity upon irradiation.[114,115] Other stimuli-response IRI active species have also been reported, with Gibson and co-workers' detailing the development of a catechol-PVA system, which 'engaged' IRI activity in the presence of Fe^{3+} cations *via* aggregation, resulting in an increase in PVA molecular weight.[116]

Gibson and co-workers' have reported on the development of polyampholytes for IRI,[117] recently detailing the development of a zwitterionic alternating polymer which increased red blood cell recovery by around 40% post-thaw (with 100% cell viability up to 60 $mg.mL^{-1}$).[118]

Another recent polymer study by Gibson and co-workers' detailed the preparation of a panel of polyampholytes prepared *via* isopropyl acetate/maleic anhydride RAFT polymerisation – giving an expanded series of candidates at a range of molecular weights. Figure 1.21. One particular candidate, featuring an *N*,*N*-dimethylethylamine motif was found to possess superior activity (16% MGA or 55% MLGS) over the rest of the range at 20 $mg.mL^{-1}$ and DP 92. The

remaining candidates possessed comparable activity in the ~ 50% MGA range at the same concentration.[119]

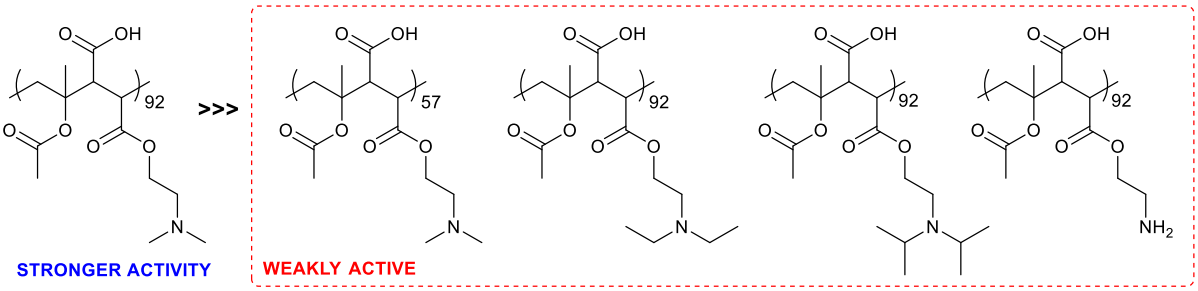

Figure 1.21 – Ampholyte polymer series prepared by Gibson and co-workers'.[119]

This data supports the concept that precise engineering of the hydrophilic/hydrophobic balance is essential for IRI, and that whilst itself essential, over-introducing 'hydrophobicity' does not necessarily infer greater activity. Similarly, this study also serves to demonstrate the perils of minor structural modification upon activity. As the prepared candidates did not feature any obvious ice binding motif or engineered ice binding face (and so have no inherent 3D 'match' for an ice crystal plane),[119] they potentially lend support to the hypothesised disordered water layer mechanism of inhibition.

Matsumura *et al*. have developed several libraries of polyampholytes which have shown cryoprotective qualities despite having only moderate IRI activity.[120] Two particular copolymeric species were able to inhibit crystal growth to around 5 – 10% MGA but only at very high concentration (100 mg.mL^{-1}).[121] A similar species lacking a third 'bloc' inhibited growth to 48% MGA.[120] This again effectively demonstrates the importance of precise engineering, and further shows that the introduction of a more pronounced hydrophobe (octyl *vs* methyl) does not enhance activity. Figure 1.22.

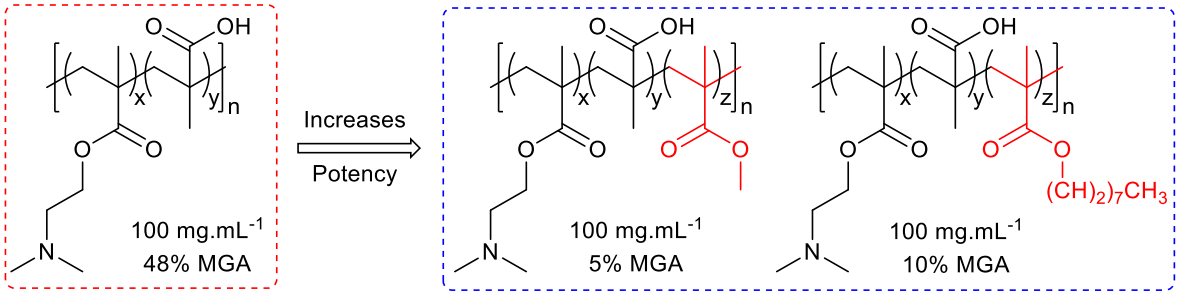

Figure 1.22 – Amphipathic polymer series prepared by Matsumura and co-workers'.[120]

These species effectively enhanced the cryopreservation of L929 cells, demonstrating (on average) > 50% cell viability with a polymer loading of 7.5%.[121] However, 100 mg.mL^{-1} is a prohibitively concentrated solution, and a cryoprotectant requiring such a large infusion would not normally be applicable for biomedical translation, equating to 10% w/v of the total volume. It does however show remarkable inhibitory properties, as colligative effects alone would not account for this extent of potency at this concentration.

Other species have also been shown to possess significant IRI potency. Wang *et al.* have demonstrated the significant IRI and cryoprotective activity of graphene oxide (GO), reducing ice crystal growth to around 20% MLGS at 5 mg.mL^{-1}.[41] The authors hypothesise that GO possesses such IRI potency due to the preference for the hydroxy groups on the GO basal plane to form hydrogen bonds with the ice crystal face over surrounding water, facilitated by the graphitic 'honeycomb' lattice. This preferred adsorption leads to a curved ice crystal surface, lowering the freezing point. The authors further demonstrate graphene oxide's application in the cryopreservation of horse sperm, increasing spermatozoa motility by nearly 50% in the presence of 0.01 wt % of graphene oxide, post-thaw.

Of the many IRI active species detailed herein, a major setback is that many are not necessarily biocompatible, biodegradable, nor bioresorbable and have not been applied to the significant challenge of cell monolayer storage. As per Figure 1.23, it is further apparent that – whilst a wide range of IRI active compounds exist – they all possess wildly different activities and have

disparate structures and functional properties. Furthermore, many may not be applicable to biomedical translation due to their intolerance to functional modification. Given the disparity between IRI active structures, it is entirely possible that there are multiple distinct mechanisms responsible for IRI activity. As such, it is necessary to probe the boundaries of the IRI structure-activity relationship, so that a blue-print for the rational design of better mimics maybe developed, which have real translatable application in biomedicine.

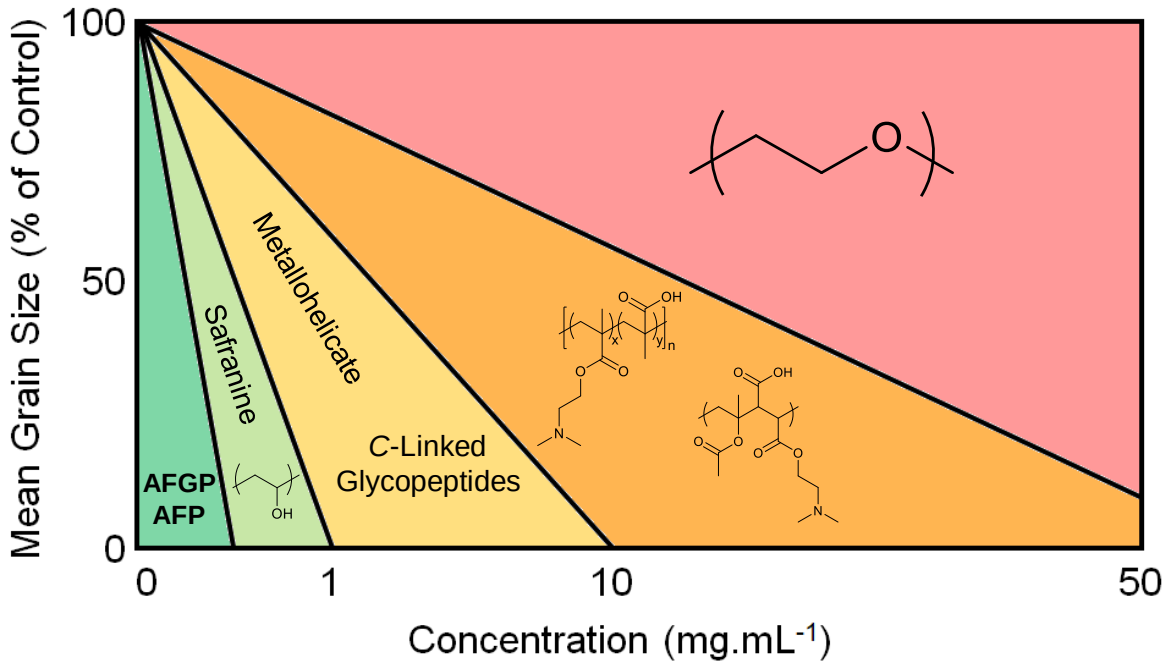

Figure 1.23 – Summary of IRI active substances prepared to date.

1.6 – Protein Mimics in Biomedicine

Numerous examples exist in the biochemical and pharmaceutical sciences of 'synthetically engineered' species capable of mimicking the effect and action of naturally occurring proteins and peptides.[122,123,124,125]

In particular, Tew and co-workers' have done extensive work on the development of antimicrobial polymers known as "SMAMPs" (Synthetic Mimics of Antimicrobial Peptides), which mimic the naturally occurring Antimicrobial Peptides (AMPS) used by bacterial species as a defence mechanism. Figure 1.24. AMPs are often highly potent and are of vital importance given the increasing rates of antimicrobial resistance in the modern world, potentially offering therapeutic benefits. However, they often possess poor biocompatibility and significant cytotoxicity towards mammalian cells, necessitating the development of mimetics.[126,127]

The ROMP methodology used in the development of SMAMPs by Tew has also been applied to the development of similar polymeric architectures for the purposes of controlled drug delivery. Figure 1.24. These derivatives are capable of mimicking protein transduction domains (PTDMs), acting as protein transporter molecules. Inspired by amphipathic peptides known to transport biologically active/functional proteins into cells (which usually possess poor membrane permeability – thereby limiting their biomedical applicability), the PTDMs developed were capable of transporting the EGFP protein into Jurkat T Cells.[128] This concept is of significant importance, as the shift in contemporary medicine moves towards biopharmaceuticals, effective therapeutic protein delivery is a primary concern in the viability of treatments.

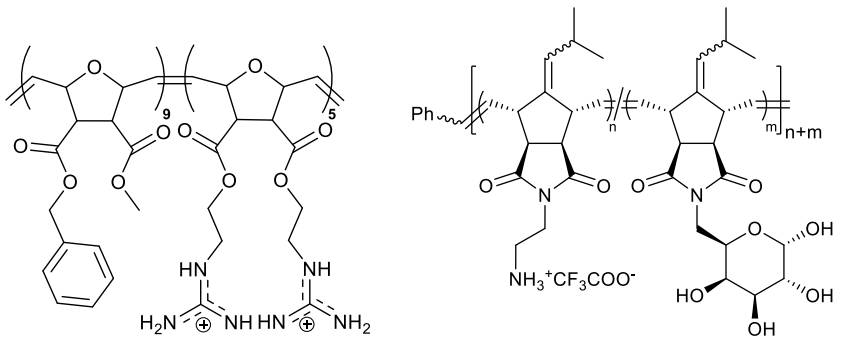

Figure 1.24 – Examples of protein biomimetic polymers from Tew and co-workers'.[128]

Examples of synthetic protein mimetics also exist in marine science. The biofouling of surfaces represents a major problem, and efforts have been deployed in the development of polymeric species which are capable of inhibiting attachment of species, debris, and the formation of biofilms on submerged surfaces.[129]

Similarly, zwitterionic polymers and small molecules inspired by this technology have also been developed to prevent the adhesion of bacteria, proteins, and other cellular and biological debris on implantable medical devices (such as arterial stents and catheters).[129,130]

Some marine species – such as mussels and barnacles – are known for their ability to produce a natural protein with pronounced adhesive qualities, allowing them to 'stick' to surfaces. These proteins would have particular application a number of heavy industries, but can not be isolated in significant quantities or easily synthesised. Synthetic mimics of these proteins have therefore been investigated and reported, with many replicating the naturally occurring DOPA unit, but on a simplified polymer chain, Figure 1.25.[131,132]

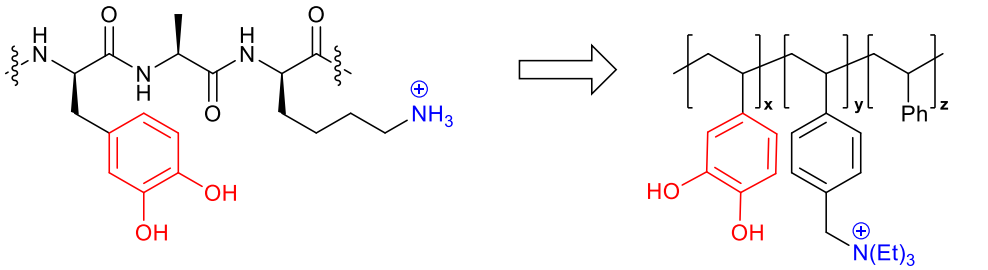

Figure 1.25 – Biomimetic adhesive polymers inspired by a molusc natural product (catechols and cations).[131,132]

The development of antifreeze glycoprotein mimetics therefore represents an exciting expansion to this field, and inspiration maybe drawn from the established literature in order to best facilitate the development of potent, IRI active, biomimetics.

1.7 – Summary

It is clear from the prevailing literature that the development of new, potent, IRI inhibitors with potential applications in cryostorage and biomedicine is slowed by the poor understanding of the root cause of IRI activity. The mechanism of action is unknown and the structural design rules governing the incorporation of IRI activity in to synthetic inhibitors are fundamentally unclear, and in some cases contradictory. This is further complicated by the probability of there being multiple mechanisms of action. At present, serendipitous discovery / trial-and-error is the beacon by which the field advances, but this is unsustainable, and it is essential that we have a defined series of design criteria to guide the development of adaptable, clinically useful and applicable ice recrystallisation inhibitors.

PVA represents the most potent synthetic AF(G)P mimic to date, but it is not wholly applicable for biomedical translation. Many synthetic mimics also suffer from this problem, generally due to suspected toxicity or intolerance to functionalisation. Natural AF(G)P products also have detrimental ice shaping and immunogenic properties.

Whilst a definitive structure-activity relationship does not yet exist, a number of recent studies have provided convincing evidence which may guide the rational design of IRI active AF(G)P mimics. Amphipathy (in conjunction with prominent hydrophobicity), over hydroxyl group presentation, may be the preeminent structural motif required for IRI potency. This warrants further investigation in the pursuit of a blueprint for the design of highly active materials with applications in biomedicine.

1.8 – Project Aims and Overview

Various small molecule, polymer, peptide, and protein-conjugates, containing specific structural motifs and chemical properties as observed in AFGPs, will be prepared through synthetic organic, carbohydrate, amino acid, and ROMP chemistries. Using these species (and some sequentially modified derivatives), we will probe the boundaries of IRI activity in order to enhance our understanding of the mechanistic mode of action of AF(G)P mimetics. It is envisioned that this improved understanding will represent a 'blueprint' for the better (and more rational) design of AF(G)P mimetics, with superior IRI potency, for application in biomedicine.

1.9 – Thesis Summary

Chapter 2 details the synthesis and activity assessment of poly(proline) – specifically, oligomeric stretches of homo-proline – which is known (and shown herein) to adopt a polyproline type II helix, akin to AFGP. The poly(proline) was shown to inhibit ice crystal growth to a significantly greater extent than poly(hydroxyproline), a previously identified IRI which is prepared from poly(proline) *via* a non-quantitative biotransformation. Poly(proline) (at as short as 20 residues) is therefore IRI active – in the absence of hydroxyl groups – due to its amphipathic domain presentation along a PPII helix, therefore demonstrating the unequivocal importance of amphipathy in IRI design. Cell recovery assays further indicated its potential as a synthetic cryoprotectant, increasing cellular recovery by over 30% post-thaw, without dynamic ice shaping.

Chapter 3 reports on the development of a stimuli-responsive, photo-activatable, small molecule IRI inhibitor prepared from anthracene and a short (IRI inactive) peptide stretch, but which was derived from a potent antifreeze protein primary sequence. Inactive as a monomeric unit in solution, this anthracene-peptide conjugate was capable of enhanced IRI inhibition when photo-irradiated, triggering covalent dimerisation through an on-water Diels-Alder cycloaddition, increasing the effective molecular weight (from a 22-mer to a 44-mer). This species possessed a 'reversed' sequence as a photodimer, indicating that a specific peptide sequence may not be required, and that activity is more 'functionally centred' around the presence of a 'good' hydrophobic/hydrophilic domain structure. This conjugate may represent a blueprint for the design of ice recrystallisation inhibitors with potential applications in cryosurgery. A panel of small molecule Simvastatin analogues were also assayed and found to have no activity.

Chapter 4 builds upon the work of Chapter 2 and deals with the *de novo* rational design of a potent AFGP mimetic. In order to replicate the structural rigidity observed in AFGP whilst maintaining hydrophobic/hydrophilic domain balance, a panel of monomers were prepared – featuring disparate head and tail groups (some hydrophobic, some uniformly hydrophilic) – and a series of (co)polymers derived from them *via* Grubbs' Metathesis (ROMP). These sequentially modified architectures were assayed and an optimum candidate identified – indicating that a rationally designed, structurally rigid, amphipathic candidate of a particular molecular weight could demonstrate IRI potency at the $\mu g.mL^{-1}$ level. This provides further evidence that amphipathy is a core design motif, and why some structurally flexible polymers – which can adopt many different conformations – do not have the same levels of IRI potency, due to their poorly segregated, domain structure.

Chapter 5 discusses the attempted preparation of an IRI mimic with the same fundamental structural properties as AFGP. Namely; polydispersity, structural rigidity, helicity, and amphipathy. These species, prepared from bile acids, did not display any IRI potency, despite meeting the hypothesised design criteria. This work may indicate an element of (essential) ice face binding in the IRI mechanism.

1.10 – References

1 Grand View Research, *Stem Cell Market Size Analysis Report By Product (Adult, hESC, Induced Pluripotent), By Application (Regenerative Medicine, Drug Discovery & Development), By Technology, By Therapy, And Segment Forecasts, 2019 - 2025*, San Francisco, 2019.

2 L. M. Whilding and J. Maher, *Mol. Oncol.*, 2015, **9**, 1994–2018.

3 M. H. Forsberg, A. Das, K. Saha and C. M. Capitini, *Ther. Clin. Risk Manag.*, 2018, 14, 1573–1584.

4 A. N. Miliotou and L. C. Papadopoulou, *Curr. Pharm. Biotechnol.*, 2018, **19**, 5–18.

5 C. E. Brown and C. L. Mackall, *Nat. Rev. Immunol.*, 2019, **19**, 73–74.

6 F. T. Dahlke, M. Butzin, J. Nahrgang, V. Puvanendran, A. Mortensen, H.-O. Pörtner and D. Storch, *Sci. Adv.*, 2018, **4**, eaas8821.

7 G. N. Somero and A. L. DeVries, *Science*, 1967, **156**, 257–258.

8 K. I. Jönsson, E. Rabbow, R. O. Schill, M. Harms-Ringdahl and P. Rettberg, *Curr. Biol.*, 2008, 18, R729–R731.

9 K. B. Storey, *Biochem. Cell Biol.*, 1990, **68**, 687–98.

10 A. A. Steiner, S. O. Petenusci, L. G. Brentegani and L. G. S. Branco, *Rev. Bras. Biol.*, 2005, **60**, 321–328.

11 M. Alberdi, L. A. Bravo, A. Gutiérrez, M. Gidekel and L. J. Corcuera, *Physiol. Plant.*, 2002, **115**, 479–486.

12 A. J. Middleton, C. B. Marshall, F. Faucher, M. Bar-Dolev, I. Braslavsky, R. L. Campbell, V. K. Walker and P. L. Davies, *J. Mol. Biol.*, 2012, **416**, 713–724.

13 P. F. Scholander, L. V. D. Dam, J. W. Kanwisher, H. T. Hammel and M. S. Gordon, *J. Cell. Comp. Physiol.*, 1957, **49**, 5–24.

14 D. E. Wohlschlag and A. L. Devries, *Science*, 1969, **163**, 273–274.

15 M. M. Harding, P. I. Anderberg and A. D. J. Haymet, *Eur. J. Biochem.*, 2003, **270**, 1381–1392.

16 Y. Jin and A. L. DeVries, *Comp. Biochem. Physiol. - B Biochem. Mol. Biol.*, 2006, **144**, 290–300.

17 E. Feeney, L. Devries and S. K. Komatsu, *J. Biol. Chem.*

18 A. L. DeVries, J. Vandenheede and R. E. Feenet, *J. Biol. Chem.*, 1970, **246**, 305–308.

19 A. L. Devries, *Adv. Sci.*, 1971, **172**, 1152–1155.

20 M. Urbańczyk, J. Góra, R. Latajka and N. Sewald, *Amino Acids*, 2017, 49, 209–222.

21 V. R. Bouvet, G. R. Lorello and R. N. Ben, *Biomacromolecules*, 2006, **7**, 565–571.

22 K. Mochizuki and V. Molinero, *J. Am. Chem. Soc.*, 2018, **140**, 4803–4811.

23 K. Meister, A. L. Devries, H. J. Bakker and R. Drori, *J. Am. Chem. Soc.*, 2018, **140**, 9365–9368.

24 I. K. Voets, *Soft Matter*, 2017, 13, 4808–4823.

25 M. Hasegawa, A. Suzuki, S. Matsumura and K. Toshima, *Sci. Technol. Adv. Mater.*, 2006, **7**, 169–174.

26 A. Nath, R. Chaube and K. Subbiah, *Comput. Biol. Med.*, 2013, **43**, 817–821.

27 P. L. Davies, J. Baardsnes, M. J. Kuiper, V. K. Walker, D. Hall, M. A. Marahiel, M. Smallwood, D. Smith, T. Haymet and C. Knight, in *Philosophical Transactions of the Royal Society B: Biological Sciences*, The Royal Society, 2002, vol. 357, pp. 927–935.

28 C. J. Capicciotti, M. Doshi and R. N. Ben, in *Recent Developments in the Study of Recrystallization*, ed. P. Wilson, InTech, 2013.

29 R. Gupta and R. Deswal, *J. Biosci.*, 2014, **39**, 931–944.

30 S. N. Patel and S. P. Graether, *Biochem. Cell Biol.*, 2010, **88**, 223–229.

31 Protein Data Bank, Entry WFB1, https://www.rcsb.org/.

32 Protein Data Bank, Entry 2PY2, https://www.rcsb.org/.

33 Protein Data Bank, Entry 1HG7, https://www.rcsb.org/.

34 Protein Data Bank, Entry 1MBN, https://www.rcsb.org/.

35 Protein Data Bank, Entry 3ULT, https://www.rcsb.org/.

36 M. I. Gibson, *Polym. Chem.*, 2010, 1, 1141–1152.

37 J. F. Carpenter and T. N. Hansen, *Proc. Natl. Acad. Sci. U. S. A.*, 1992, **89**, 8953–8957.

38 C. I. Biggs, T. L. Bailey, Ben Graham, C. Stubbs, A. Fayter and M. I. Gibson, *Nat. Commun.*, 2017, **8**, 1546.

39 E. Kristiansen and K. E. Zachariassen, *Cryobiology*, 2005, **51**, 262–280.

40 Georgia State University, Freezing Point Depression in Solutions, http://hyperphysics.phy-astr.gsu.edu/hbase/Chemical/meltpt.html, (accessed 5 April 2019).

41 H. Geng, X. Liu, G. Shi, G. Bai, J. Ma, J. Chen, Z. Wu, Y. Song, H. Fang and J. Wang, *Angew. Chem. Int. Ed.*, 2017, **56**, 997–1001.

42 S. Zalis, M. B. Dolev and I. Braslavsky, *Cryobiology*, 2013, **67**, 438.

43 D. E. Mitchell, J. R. Lovett, S. P. Armes and M. I. Gibson, *Angew. Chemie - Int. Ed.*, 2016, **55**, 2801–2804.

44 C. Budke and T. Koop, *ChemPhysChem*, 2006, **7**, 2601–2606.

45 C. S. Strom, X. Y. Liu and Z. Jia, *J. Biol. Chem.*, 2004, **279**, 32407–32417.

46 K. Meister, S. Lotze, L. L. C. Olijve, A. L. Devries, J. G. Duman, I. K. Voets and H. J. Bakker, *J. Phys. Chem. Lett.*, 2015, **6**, 1162–1167.

47 C. P. Garnham, R. L. Campbell and P. L. Davies, *Proc. Natl. Acad. Sci.*, 2011, **108**, 7363–7367.

48 R. Drori, Y. Celik, P. L. Davies and I. Braslavsky, *J. R. Soc. Interface*, 2014, **11**, 20140526–20140526.

49 R. Drori, P. L. Davies and I. Braslavsky, *Langmuir*, 2015, **31**, 5805–5811.

50 J. A. Raymond and A. L. DeVries, *Proc. Natl. Acad. Sci. U. S. A.*, 1977, **74**, 2589–93.

51 J. A. Raymond and A. L. DeVries, *Proc. Natl. Acad. Sci. U. S. A.*, 1977, **74**, 2589–93.

52 S. Zepeda, E. Yokoyama, Y. Uda, C. Katagiri and Y. Furukawa, *Cryst. Growth Des.*, 2008, **8**, 3666–3672.

53 Y. Ba, J. Wongskhaluang and J. Li, *J. Am. Chem. Soc.*, 2003, **125**, 330–331.

54 A. Jorov, B. S. Zhorov and D. S. C. Yang, *Protein Sci.*, 2004, **13**, 1524–1537.

55 S. Wang, N. Amornwittawat and X. Wen, *J. Chem. Thermodyn.*, 2012, **53**, 125–130.

56 P. M. Naullage, L. Lupi and V. Molinero, *J. Phys. Chem. C*, 2017, **121**, 26949–26957.

57 K. A. Sharp and J. M. Vanderkooi, *Acc. Chem. Res.*, 2010, **43**, 231–239.

58 C. A. Knight, *J. Colloid Interface Sci.*, 1967, **25**, 280–284.

59 C. A. Knight, E. Driggers and A. L. DeVries, *Biophys. J.*, 1993, **64**, 252–259.

60 R. Peltier, C. W. Evans, A. L. Devries, M. A. Brimble, A. J. Dingley and D. E. Williams, *Cryst. Growth Des.*, 2010, **10**, 5066–5077.

61 C. A. Knight and N. C. Knight, *Science*, 1989, **245**, 505–507.

62 R. Y. Tam, S. S. Ferreira, P. Czechura, R. N. Ben and J. L. Chaytor, *J. Am. Chem. Soc.*, 2008, **130**, 17494–17501.

63 R. Y. Tam, C. N. Rowley, I. Petrov, T. Zhang, N. A. Afagh, T. K. Woo and R. N. Ben, *J. Am. Chem. Soc.*, 2009, **131**, 15745–15753.

64 P. Czechura, R. Y. Tam, E. Dimitrijevic, A. V. Murphy and R. N. Ben, *J. Am. Chem. Soc.*, 2008, **130**, 2928–2929.

65 O. A. Karim and A. D. J. Haymet, *J. Chem. Phys.*, 1988, **89**, 6889–6896.

66 J. D. Madura, K. Baran and A. Wierzbicki, *J. Mol. Recognit.*, 2000, **13**, 101–113.

67 A. Fowler and M. Toner, *Ann. N. Y. Acad. Sci.*, 2005, **1066**, 119–135.

68 B. C. Heng, C. P. Ye, H. Liu, W. S. Toh, A. J. Rufaihah, Z. Yang, B. H. Bay, Z. Ge, H.

W. Ouyang, E. H. Lee and T. Cao, *J. Biomed. Sci.*, 2006, **13**, 433–445.

69 Q. Xu, W. J. Brecht, K. H. Weisgraber, R. W. Mahley and Y. Huang, *J. Biol. Chem.*, 2004, **279**, 25511–6.

70 R. M. Far, F. S. Rad, Z. Abdolazimi and M. M. D. Kohan, *Turkish J. Hematol.*, 2014, **31**, 161–167.

71 J. Kaindl, I. Meiser, J. Majer, A. Sommer, F. Krach, A. Katsen-Globa, J. Winkler, H. Zimmermann, J. C. Neubauer and B. Winner, *Stem Cells Transl. Med.*, 2019, **8**, 247–259.

72 L. H. Campbell and K. G. M. Brockbank, in *Recent Advances in Cryopreservation*, ed. H. Yamashiro, InTech, 2014.

73 D. E. Pegg, in *Cryopreservation and Freeze-Drying Protocols*, eds. J. G. Day and G. N. Stacey, Humana Press, Totowa, New Jersey, 2nd edn., 2007, pp. 39–57.

74 P. Mazur, *Science*, 1970, **168**, 939–49.

75 P. Mazur, J. Farrant, S. P. Leibo and E. H. Chu, *Cryobiology*, 1969, **6**, 1–9.

76 X. Stéphenne, M. Najimi and E. M. Sokal, *World J. Gastroenterol.*, 2010, **16**, 1–14.

77 K. Brockbank and M. Taylor, *Adv. biopreservation*, 2007, **5**, 157–196.

78 M. Iwatani, K. Ikegami, Y. Kremenska, N. Hattori, S. Tanaka, S. Yagi and K. Shiota, *Stem Cells*, 2006, **24**, 2549–2556.

79 K. Kawai, Y.-S. Li, M.-F. Song and H. Kasai, *Bioorg. Med. Chem. Lett.*, 2010, **20**, 260–5.

80 B. L. Wilkinson, R. S. Stone, C. J. Capicciotti, M. Thaysen-Andersen, J. M. Matthews, N. H. Packer, R. N. Ben and R. J. Payne, *Angew. Chemie - Int. Ed.*, 2012, **51**, 3606–3610.

81 R. Orii, N. Sakamoto, D. Fukami, S. Tsuda, M. Izumi, Y. Kajihara and R. Okamoto, *Chem. - A Eur. J.*, 2017, **23**, 9253–9257.

82 T. Tsuda and S. I. Nishimura, *Chem. Commun.*, 1996, 2779–2780.

83 R. Peltier, M. A. Brimble, J. M. Wojnar, D. E. Williams, C. W. Evans and A. L. Devries, *Chem. Sci.*, 2010, 1, 538–551.

84 H. Chao, P. L. Davies and J. F. Carpenter, *J. Exp. Biol.*, 1996, **199**, 2071–2076.

85 C. A. Knight, D. Wen and R. A. Laursen, *Cryobiology*, 1995, 32, 23–34.

86 T. Congdon, R. Notman and M. I. Gibson, *Biomacromolecules*, 2013, **14**, 1578–1586.

87 N. S. Vail, C. Stubbs, C. I. Biggs and M. I. Gibson, *ACS Macro Lett.*, 2017, **6**, 1001–1004.

88 C. C. DeMerlis and D. R. Schoneker, *Food Chem. Toxicol.*, 2003, 41, 319–326.

89 G. Paradossi, F. Cavalieri, E. Chiessi, C. Spagnoli and M. K. Cowman, in *Journal of Materials Science: Materials in Medicine*, Kluwer Academic Publishers, 2003, vol. 14, pp. 687–691.

90 T. R. Congdon, R. Notman and M. I. Gibson, *Biomacromolecules*, 2016, **17**, 3033–3039.

91 R. N. Ben, A. a. Eniade and L. Hauer, *Org. Lett.*, 1999, **1**, 1759–1762.

92 S. Liu and R. N. Ben, *Org. Lett.*, 2005, **7**, 2385–2388.

93 A. Eniade, M. Purushotham, R. N. Ben, J. B. Wang and K. Horwath, *Cell Biochem. Biophys.*, 2003, **38**, 115–124.

94 A. Eniade and R. N. Ben, *Biomacromolecules*, 2001, **2**, 557–561.

95 A. Eniade, A. V. Murphy, G. Landreau and R. N. Ben, *Bioconjug. Chem.*, 2001, **12**, 817–823.

96 P. Czechura, R. Y. Tam, E. Dimitrijevic, A. V. Murphy and R. N. Ben, *J. Am. Chem. Soc.*, 2008, **130**, 2928–2929.

97 R. Y. Tam, S. S. Ferreira, P. Czechura, J. L. Chaytor and R. N. Ben, *Electrochemistry*, 2008, 17494–17501.

98 S. Lui, W. Wang, E. von Moos, J. Jackman, G. Mealing, R. Monette and R. N. Ben, *Biomacromolecules*, 2007, **8**, 1456–1462.

99 Y. Tachibana, G. L. Fletcher, N. Fujitani, S. Tsuda, K. Monde and S. I. Nishimura, *Angew. Chemie - Int. Ed.*, 2004, **43**, 856–862.

100 C. J. Capicciotti, J. F. Trant, M. Leclère and R. N. Ben, *Bioconjug. Chem.*, 2011, **22**, 605–616.

101 M. I. Gibson, C. A. Barker, S. G. Spain, L. Albertin and N. R. Cameron, *Biomacromolecules*, 2009, **10**, 328–333.

102 R. C. Deller, T. Congdon, M. A. Sahid, M. Morgan, M. Vatish, D. A. Mitchell, R. Notman, M. I. Gibson, C. S. Findlay, D. S. Allan and R. N. Ben, *Biomater. Sci.*, 2013, **1**, 478.

103 A. K. Balcerzak, S. S. Ferreira, J. F. Trant and R. N. Ben, *Bioorganic Med. Chem. Lett.*, 2012, **22**, 1719–1721.

104 R. Drori, C. Li, C. Hu, P. Raiteri, A. L. Rohl, M. D. Ward and B. Kahr, *J. Am. Chem. Soc.*, 2016, **138**, 13396–13401.

105 O. Mizrahy, M. Bar-Dolev, S. Guy and I. Braslavsky, *PLoS One*, , DOI:10.1371/journal.pone.0059540.

106 D. E. Mitchell and M. I. Gibson, *Biomacromolecules*, 2015, **16**, 3411–3416.

107 D. E. Mitchell, G. Clarkson, D. J. Fox, R. A. Vipond, P. Scott and M. I. Gibson, *J. Am. Chem. Soc.*, 2017, **139**, 9835–9838.

108 M. I. Gibson, *Polym. Chem.*, 2010, **1**, 1141.

109 S. Ebbinghaus, K. Meister, B. Born, A. L. Devries, M. Gruebele and M. Havenith, *J. Am. Chem. Soc.*, 2010, **132**, 12210–12211.

110 C. J. Capicciotti, M. Leclere, F. A. Perras, D. L. Bryce, H. Paulin, J. Harden, Y. Liu and R. N. Ben, *Chem. Sci.*, 2012, **3**, 1408–1416.

111 C. J. Capicciotti, R. S. Mancini, T. R. Turner, T. Koyama, M. G. Alteen, M. Doshi, T. Inada, J. P. Acker and R. N. Ben, *ACS Omega*, 2016, **1**, 656–662.

112 C. J. Capicciotti, J. D. R. Kurach, T. R. Turner, R. S. Mancini, J. P. Acker and R. N. Ben, *Sci. Rep.*, 2015, **5**, 9692.

113 J. G. Briard, S. Jahan, P. Chandran, D. Allan, N. Pineault and R. N. Ben, *ACS Omega*, 2016, **1**, 1010–1018.

114 M. K. Adam, J. S. Poisson, Y. Hu, G. Prasannakumar, M. J. Pottage, N. Ben and B. L. Wilkinson, *RSC Adv.*, 2016, **6**, 39240–39244.

115 M. K. Adam, Y. Hu, J. S. Poisson, M. J. Pottage, R. N. Ben and B. L. Wilkinson, *Carbohydr. Res.*, 2017, **439**, 1–8.

116 D. J. Phillips, T. R. Congdon and M. I. Gibson, *Polym. Chem.*, 2016, **7**, 1701–1704.

117 D. E. Mitchell, M. Lilliman, S. G. Spain and M. I. Gibson, *Biomater. Sci.*, 2014, **2**, 1787–1795.

118 D. E. Mitchell, N. R. Cameron and M. I. Gibson, *Chem. Commun.*, 2015, **51**, 12977–80.

119 C. Stubbs, J. Lipecki and M. I. Gibson, *Biomacromolecules*, 2017, **18**, 295–302.

120 R. Rajan, M. Jain and K. Matsumura, *J. Biomater. Sci. Polym. Ed.*, 2013, **24**, 1767–80.

121 R. Rajan, F. Hayashi, T. Nagashima and K. Matsumura, *Biomacromolecules*, 2016, **17**, 1882–1893.

122 R. W. Scott and G. N. Tew, *Curr. Top. Med. Chem.*, 2016, **17**, 576–589.

123 G. N. Tew, R. W. Scott, M. L. Klein and W. F. Degrado, *Acc. Chem. Res.*, 2010, **43**, 30–39.

124 A. E. Barron and R. N. Zuckerman, *Curr. Opin. Chem. Biol.*, 1999, 3, 681–687.

125 K. Kirshenbaum, R. N. Zuckermann and K. A. Dill, *Curr. Opin. Struct. Biol.*, 1999, **9**, 530–535.

126 S. Colak, C. F. Nelson, K. Nusslein and G. N. Tew, *Biomacromolecules*, 2009, **10**, 353–359.

127 H. D. Thaker, A. Cankaya, R. W. Scott and G. N. Tew, *ACS Med. Chem. Lett.*, 2013, **4**, 481–485.

128 A. Ö. Tezgel, P. Jacobs, C. M. Backlund, J. C. Telfer and G. N. Tew, *Biomacromolecules*, 2017, **18**, 819–825.

129 V. B. Damodaran and S. N. Murthy, *Biomater. Res.*, 2016, **20**, 1–11.

130 K. Hirota, K. Murakami, K. Nemoto and Y. Miyake, *FEMS Microbiol. Lett.*, 2005, **248**, 37–45.

131 G. Westwood, T. N. Horton and J. J. Wilker, *Macromolecules*, 2007, **40**, 3960–3964.

132 J. D. White and J. J. Wilker, *Macromolecules*, 2011, **44**, 5085–5088.

CHAPTER 2

Polyproline – Amphipathy and the polyproline II helix in ice inhibitor design

---

2.1 – Chapter Abstract

This chapter describes a study in to the core structural motifs responsible for incorporating ice recrystallisation inhibition (IRI) activity into synthetic proteins, as a means to guide rational AF(G)P mimetic design. A brief review of the literature is presented, which highlights facial amphipathy as a necessary structural motif. Like, poly(vinyl alcohol) (PVA)[1,2,3], the IRI activity of poly(L-hydroxy proline) has previously been considered to stem from the presence of hydroxyl groups directly binding to ice (hydrogen bonding)[4,5]; Indeed, it has been proposed that AF(G)Ps themselves may function the same way.[6] Recently however, there have been many literature assertions of structural amphipathy as a driver for IRI activity in synthetic AF(G)P mimetics, with hydrophobic binding dominating.[7,8] In order to resolve this contradiction and clearly establish a structure-activity relationship for IRI, we aimed to prepare the structural analogue poly(L-proline) at a series of molecular weights, and to investigate its IRI activity. An optimised synthetic route – using *in situ N*-carboxyanhydride chemistry – for the preparation of low molecular weight poly(proline) is also discussed. The IRI activities of the prepared poly(L-proline) molecular weight series were subsequently determined by 'Splat' assay, the results of which indicate that poly(L-proline) is a superior IRI inhibitor to poly(L-hydroxy proline), exhibiting a 30% increase in IRI at 20 mg.mL^{-}1. This suggests that the

presence of repetitive hydroxyl units are not essential for IRI activity, and that an amphipathic surface structure is a key factor in synthetic (non-PVA) species exhibiting ice recrystallisation inhibition. Poly(L-hydroxy proline)'s biotransformative preparation from poly(L-proline), which is often incomplete,[9] distorts the potency of poly(L-proline) whilst leaving some stretches intact, therefore explaining its residual (albeit weaker) activity. Poly(proline) is shown to be an excellent additive for the cryopreservation of adherent cell culture. It is accessible by both solution and recombinant methods, it does not dynamically shape ice, and is haemolytically compatible, and so maybe suitable for biomedical translation.

2.2 – Chapter Introduction

In recent years, the number of studies concerning the IRI activity of synthetic macromolecules has steadily increased.[10] Poly(vinyl alcohol) (PVA) in particular has been the core focus of a number of research projects, representing the most potent synthetic IRI inhibitor discovered to date.[11,12] Its potential mechanisms of action have been explored and is widely believed to function through hydrogen bonding by binding to the prismatic ice crystal face.[1] Molinero and co-workers have computationally hypothesised that PVA binds in this way to the prismatic faces of ice *via* a 'zipper'-like mechanism,[2] whilst Koop and co-workers has suggested PVA's attuned repeat spacing allow it to engage in a '2-on-1-off' binding strategy, preventing ice crystal growth.[1] The mechanism of PVA's activity may well be unique among IR inhibitors, however, and considerable effort has also been applied to elucidating the mode of action for the naturally occurring IRI active species – AFPs and AFGPs. The lack of a crystal structure naturally makes assessment of the AFGP mechanism of action difficult, but many hypotheses have still been offered (Chapter 1).

Davies and co-workers in conjunction with Sonnischen, have however extensively analysed the "ice binding site" (IBS) of numerous AFPs, of which several crystal structures have been obtained. As is hypothesised for AFGPs, AFPs are known to be intrinsically amphipathic, and these ice binding sites are not thought to directly bind to ice, but are thought to order local clathrate waters, which themselves providing a good 3D conformational match to the primary prismatic ice crystal face.[13] Binding through these ordered waters then impedes ice crystal growth. The ice binding site itself is believed to be relatively flat and rigid, and largely hydrophobic, but with a degree of amphipathic character.[13,14] This common structural property of AF(G)Ps is of particular importance and interest, as many species which exhibit IRI activity

other than the natural AF(G)Ps also appear to have surface amphipathy as a core structural motif (Figure 2.1).

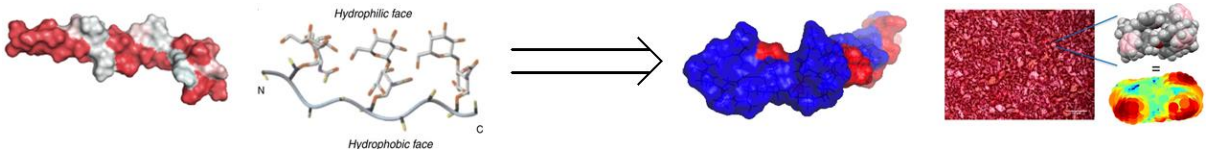

Figure 2.1 – Structural comparisons of Sculpin Type I AFP, AFGP, Nisin A, and Metallohelices.

Nisin A, a natural product and antimicrobial protein often added to milk products, has been shown to possess IRI activity when protonated at pH ~4, where it adopts an amphipathic structure.[8] Interestingly, enantiomerically pure amphipathic metallohelices, featuring a Fe^{3+} centre in a metal-organic framework, have also been shown to possess highly potent IRI activity at micromolar concentrations.[7] This particular class of species is however unusual, in that they do not possess any obvious H-bond donors, nor do they possess hydroxyl groups, which have previously been held responsible for the inference of IRI activity. In addition, some structurally simplified glycopolymers (representative of the more complex AFGP) have been shown to have little to no activity whatsoever, despite possessing high degrees of structural similarity.[5] It is apparent from this that simply possessing a high proportion/density of hydroxyl groups may not be sufficient (or they key) to instilling potency in IRI species other than (the structurally unique) PVA.

Furthermore, many of the IRI active species reported to date often have limited potencies, and few examples exist amongst them of biomedically translatable materials – with cytotoxicity [15,16] and intolerance to functionalisation [17] preventing application.

What is clear, is that in order to access new highly potent IRI active species which have real biomedical application, a rational design blueprint is required to highlight the key structural motifs necessary to engineer in IRI potency into synthetic architectures which may be functionalised as necessary for biocompatibility, and biomedical translation.

In pursuit of this, we were interested in establishing the role of amphipathy in IRI design. AFGP is thought to adopt a polyproline type II like-helix, as confirmed by CD spectroscopy,[18] which is believed to be fundamental in the presentation of the amphipathic surface structure.[19] Curiously, poly(L-hydroxy proline) has been observed to have IRI activity and was first reported by Knight and co-workers in 1995.[11] This activity has long been attributed to the presence of a hydroxyl group in the 3' position of the cyclic proline ring. However, poly(L-proline), like poly(L-hydroxy proline), also adopts a polyproline type II helix in aqueous solution. Poly(L-proline), however, has not been previously investigated. It contains a spatially separated secondary amide (hydrophilic and only H-bond accepting, preventing intramolecular H-bonding) distinct from a hydrophobic ring, giving a relatively open and solvent accessible structure, resulting in significant water solubility (similar to AFPI, which is 70% alanine – a hydrophobic amino acid). We therefore hypothesised that poly(proline) could be a minimal AF(G)P mimic and may possess sufficient surface amphipathy that it can act as an effective IR inhibitor. Homo-polypeptides are appealing targets compared to vinyl polymers as they can be prepared *via* solid phase synthesis,[20] solution phase polymerization[21] or by recombinant methods,[22] proving vast (bio)synthetic space. If correct, this would facilitate the synthesis of and provide a new, versatile and easy to access IRI active polymer. As such, we aimed to investigate as to the necessity of this ring hydroxyl in poly(L-hydroxy proline) and determine the IRI activity of poly(L-proline) through the preparation of a molecular weight series. Crucially, this study will indicate as to the supremacy of amphipathy over hydroxyl group presentation, contributing to the understanding of necessary structural motifs in rational IRI design.

2.3 – Results and Discussion

2.3i – Synthesis of oligo- and poly-prolines

Initial attempts to prepare poly-L-proline for IRI activity assessment were made through the attempted synthesis of the *N*-carboxyanhydride (NCA) of proline, which was to be subsequently polymerised through Ring Opening Polymerisation (ROP), Figure 2.2.

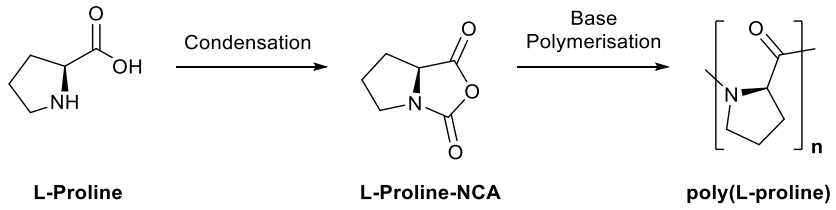

Figure 2.2 – Proposed preparation of poly(L-proline) from the *N*-carboxyanhydride of L-proline.

However whilst many literature examples exist describing the preparation of *N*-carboxyanhydrides from amino acids in general,[23] which are widely exploited in polypeptide chemistry, the preparation of polyproline and the synthesis of its Proline-NCA precursor is often a non-trivial task. [24,25,26] The classical 'Leuchs Method' for the synthesis of amino acid derived *N*-carboxyanhydrides involves a one-pot reaction of phosgene or triphosgene and the relevant amino acid in THF at elevated temperature (50 – 60ºC), Figure 2.3A. Boc protection of the starting amino acid (Figure 2.3B) often improves yield and supresses the formation of Diketopiperazine (DKP) by-products, although DKP product formation is generally of limited issue for non-proline amino acids. Boc protection is the preferred methodology for preparing proline-NCA. Specifically, due to prolines unique status amongst the canonical amino acids, featuring a cyclic secondary amine at its α-carbon, exploitation of the classical Leuchs Method is often not possible, as the carbamoyl chloride intermediate does not spontaneously cyclise (in the absence of a tertiary base) due to its restricted conformation (Figure 2.3C). However, the presence of bases such as triethylamine often exacerbate the production of the DKP by-

products (by increasing the nucleophilicity of the carboxylic acid). Even if successfully prepared, removal of residual quantities of base, salts, and DKP have been previously reported as problematic. Proline-NCA is particular sensitivity to heat, moisture (and therefore, air) as a result of its unfavourable conformational strain promoting rapid hydrolysis, complicating isolation.

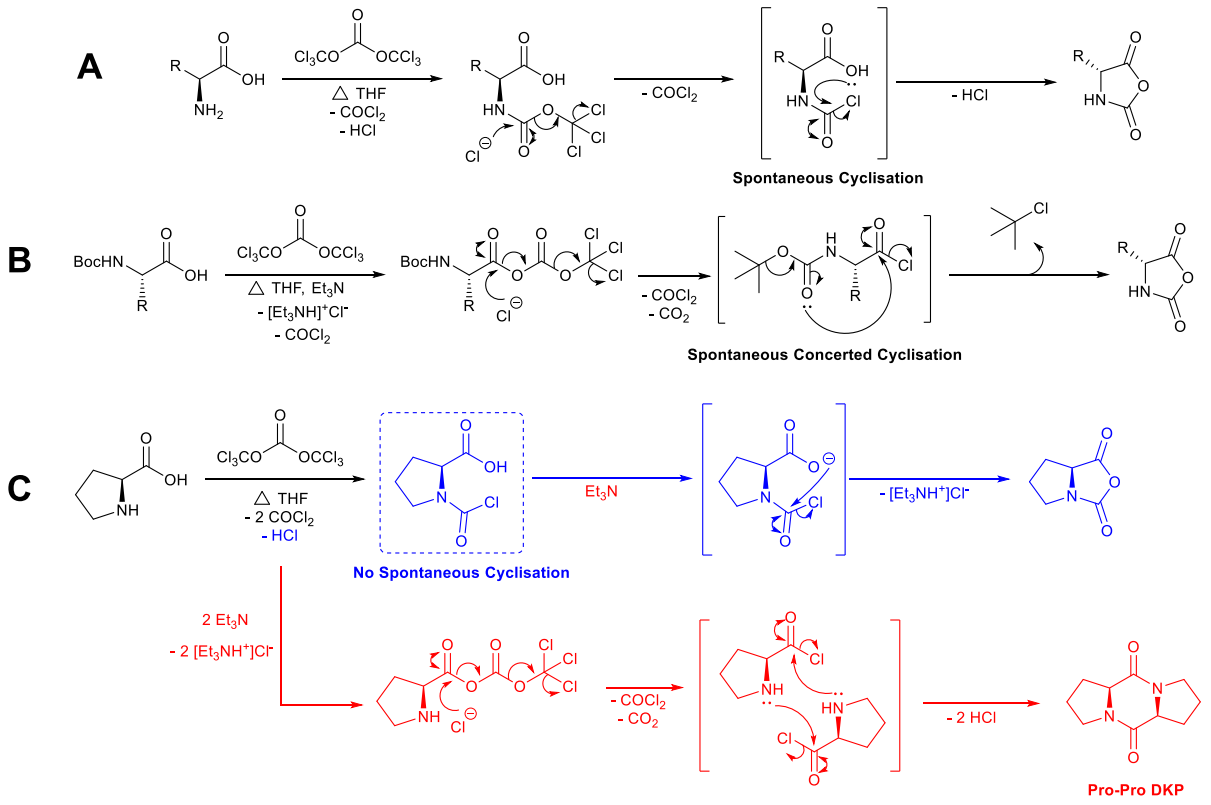

Figure 2.3 – Preparatory routes of *N*-carboxyanhydrides.

In light of this, initial inspiration was taken from work previously conducted by Giralt and co-workers,[24] who pioneered the use of a polymer-bound tertiary amine (*N*,*N*-diethanolaminomethyl polystyrene – DEAM-PS) in the Leuchs method (Figure 2.3C), in place of TEA, in 3x excess. This route reportedly overcame the noted problems of triethyl ammonium salt and Pro-Pro DKP by-product contamination, in the absence of Boc protection, Table 2.1. However this initial attempt to prepare Pro-NCA was not fruitful, with ^{1}H NMR indicating the absence of the anticipated NCA triplet at 4.34 ppm. As ethyl acetate was used as the solvent in

place of the THF due to its properties as a non-hygroscopic dry medium, we hypothesised that it likely failed to swell the DEAM-PS resin to a sufficient extent. A dry atmosphere (nitrogen) was introduced in conjunction with dry THF, and *N*-Boc-protected proline was substituted for the free amino acid.

	Starting Material	**Base (Excess)**	**% Yield**
Free Amino Acid Method	L-Proline *	PS-DEAM (3 eqv)	0%
N-Boc Protected Method	*N*-Boc-L-Proline	PS-DEAM (3 eqv)	53%
Modified *N*-Boc Protected Method	*N*-Boc-L-Proline	Triethylamine (1 eqv)	0%

Table 2.1 – Attempted syntheses of Proline-NCA in the presence of Triphosgene, Base, at 0ºC in dry THF under N_2. * Solvated in dry EtOAc, in air.

Pro-NCA was successfully obtained in reasonable yield *via* this revised route and confirmed as present by GC/MS (Figure 2.4), with peaks observed at 70 and 114 m/z – characteristic of Pro-NCA fragmentation products. Likewise, IR signals in the C=O region followed the general morphology of the anticipated NCA peaks (Appendix A).

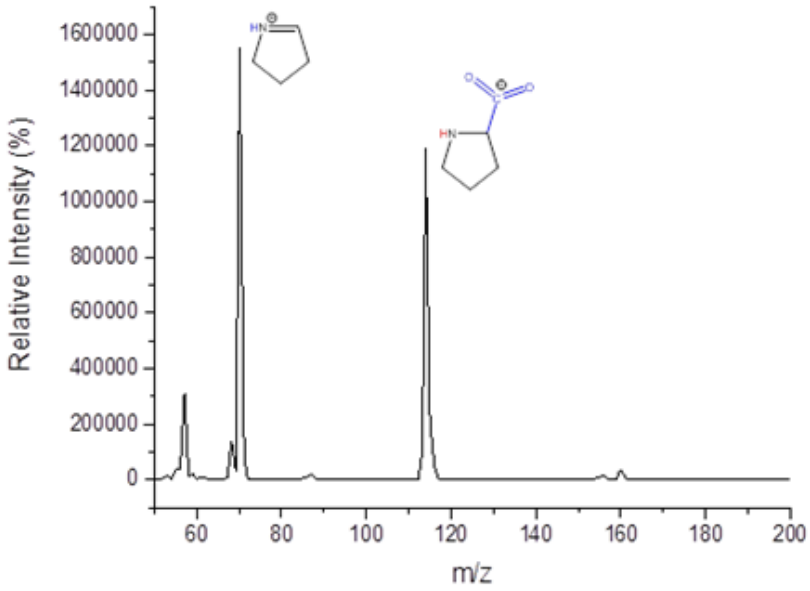

Figure 2.4 – Mass Spectrum of Pro-NCA (GC/MS). Corroborative of Gkikas and co-workers.[25]

The use of PS-DEAM resin was more efficient, as attempts to prepare Pro-NCA utilising triethylamine (as per Figure 2.3B), showed no success. Ring opening polymerisation (ROP) of the NCA would be expected to proceed through the normal amine mechanism (NAM), initiated by a primary amine (Figure 2.5). Usually, an amino acid NCA is capable of proceeding through both NAM and the activated monomer mechanism (AMM), with both mechanisms actively competing with one another to give the polypeptide. Proline's unique status as containing a secondary α-amine, however, prevents the AMM pathway from being pursued, due to the lack of an abstractable hydrogen.

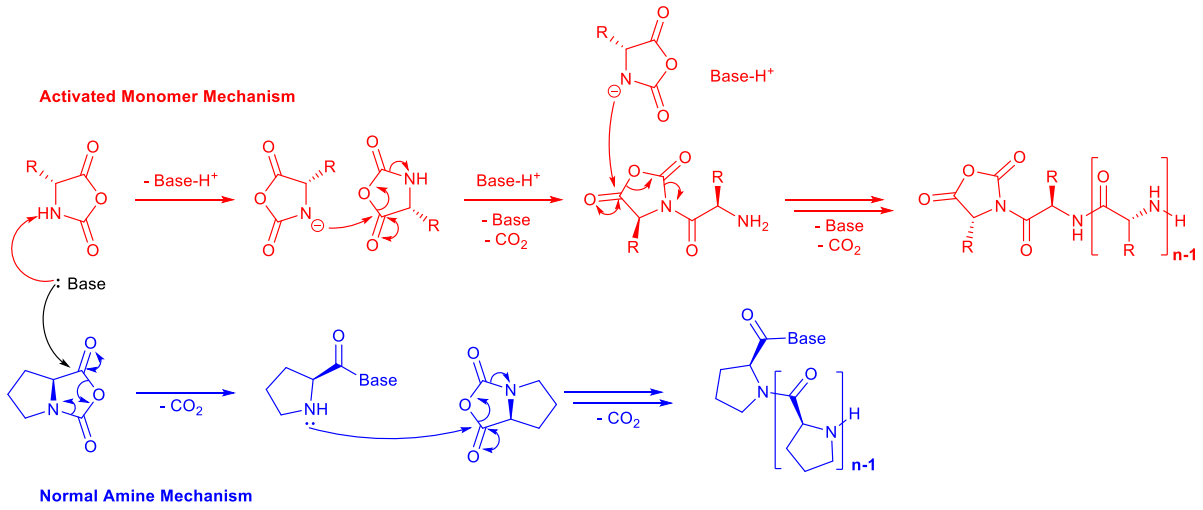

Figure 2.5 – Ring Opening Polymerization of Proline-NCA proceeding through the Normal Amine Mechanism (NAM) only, facilitated by a primary amine base.

Isolation of the NCA proved complex, however, and attempts to polymerise the obtained Pro-NCA gave no polymer product. This likely indicates degradation, supported by the presence of carboxylic acid proton signals in the ^{1}H NMR of the crude – suggesting hydrolysis of the anhydride ring due to the poor stability of Pro-NCA towards heat and principally, water. Being highly hygroscopic, the moisture content of anhydrous THF is likely a significant factor promoting hydrolysis, despite the use of air-free techniques, with literature precedents suggesting that Pro-NCA synthesis may be better suited to a glove box.

Due to the difficulty encountered in preparing polyproline by NCA methods, condensation polymerisation was used.

A molecular weight series of L, D, and D/L (racemic) polyproline were synthesized by condensation polymerization using 1-ethyl-3-(3-dimethylaminopropyl) carbodiimide, EDCI, Figure 2.6 (alongside several commercial samples). Following dialysis, unexpected narrow dispersity was observed (due to fractionation), the polymers were characterized by SEC (size exclusion chromatography), Table 2.2.

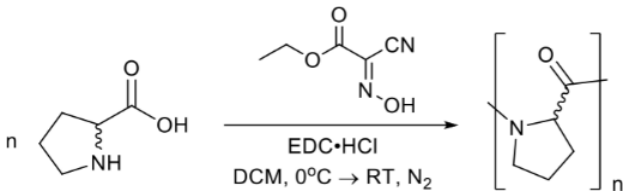

Figure 2.6 – Condensation polymerization of proline. Materials are stereo-pure, but both L and D isomers used, hence no stereo centre shown.

	M_n, (g.mol^{-1})	$Đ$, SEC [a] (-)	DP (-)	Secondary Structure
$PPro_{11}$	1300 [a]	1.03	11	
$PPro_{15}$	1700 [a]	2.12	15	PPII
$PPro_{19}$	2100 [a]	1.50	19	
$P(D)Pro_{15}$	1700 [a]	1.01	15	Enantiomeric PPII
$P(DL)Pro_{21}$	2400 [a]	1.01	21	-
$PPro_{10\text{-}100}$	1 – 10000 [b]	-	10-100	PPII [e]
$PPro_{10}$	900 [c]	[d]	10	PPII [e]
$PPro_{20}$	2000 [c]	[d]	20	PPII [e]

Table 2.2 – Polyproline Characterisation [a] Determined by SEC; [b] Value from supplier; [c] Mass Spectrometry provided by commercial supplier; [d] Single species [e] From Literature.[27,28,29]

Circular dichroism spectroscopy (CD) further confirmed that $PPro_{15}$ adopted a PPII helix (Figure 2.7A and Appendix)[30] with characteristic signals present at 207 and 228 nm, whilst a random coil would exhibit slight peak shifting, with signals absent in the 220 nm region.[31] $P(D)Pro_{15}$ gave the mirror spectrum whilst the D/L racemic mixture showed no secondary structure.

2.3ii – The IRI activity of oligo- and poly-prolines

This series of peptides were subsequently tested for IRI activity using a SPLAT assay.[12] This involves seeding a large number of small ice crystals, which are annealed for 30 minutes at –8 ºC, before being photographed. The average crystal size is measured, relative to a PBS control, with smaller values indicating more IRI activity, Figure 2.7B/C.

All polyprolines were found to display dose-dependent IRI activity but weak molecular weight dependence in the range tested. The shortest peptide ($PPro_{10}$) lost activity below 10 $mg.mL^{-1}$, but the longer species retained activity at 5 $mg.mL^{-1}$. The magnitude of activity is significantly less than AF(G)Ps which function at concentrations as low as 0.14 $\mu g.mL^{-1}$,[32] but comparable to polyampholytes.[33,34]

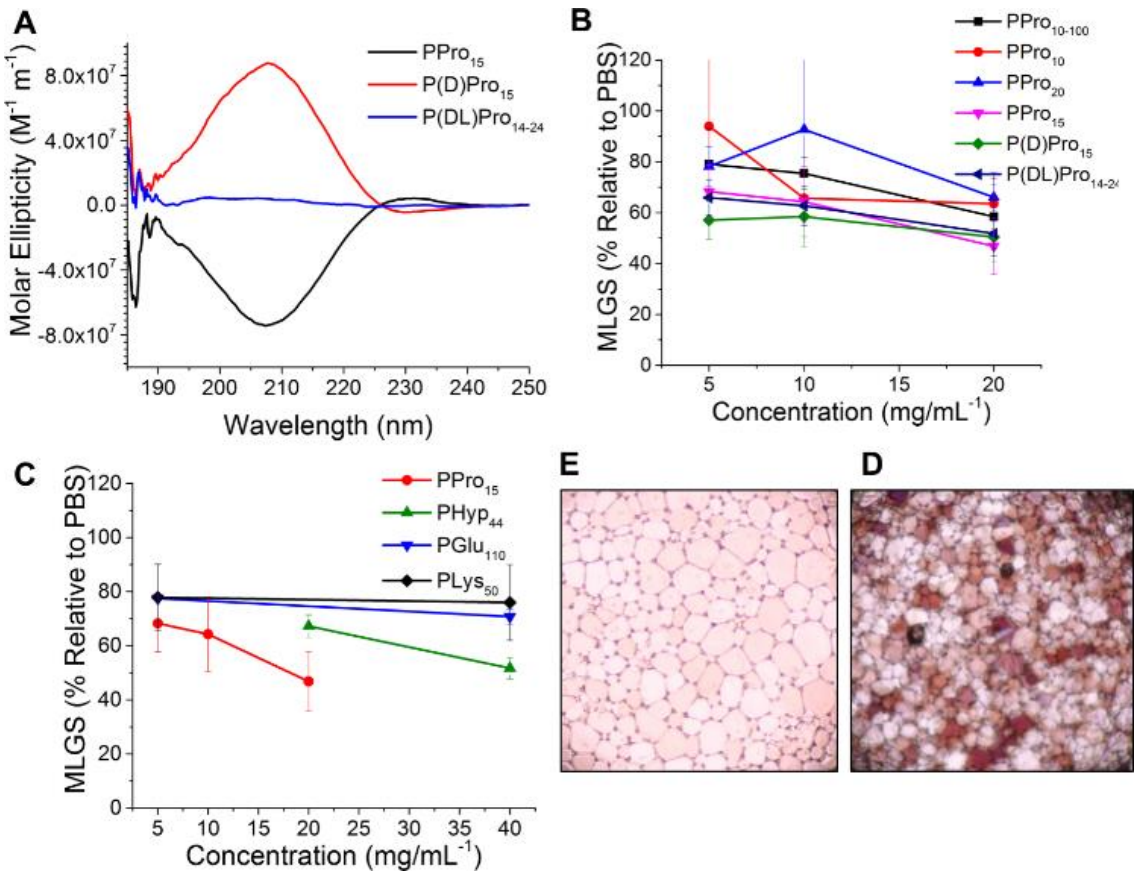

Figure 2.7 – A) Circular dichroism spectra; B) IRI activity of polyproline series, measured as a function of solute concentration; C) IRI activity compared to other homo-polypeptides; D) Cryomicrograph of a PBS negative control; E) Cryomicrograph of 20 mg.mL^{-1} poly(proline). Photos taken after 30 mins at –8 °C. Error bars represent the ± standard deviation from three independent measurements. Images shown are 1.2 mm across. MLGS = Mean largest grain size relative to a PBS control, expressed as %.

Knight has observed that poly(hydroxy-L-proline) has IRI activity, which was assumed to be due to the regularly spaced hydroxyl groups along the backbone.[11] However, the observations made here suggest that the PPII helix, rather than hydroxyl groups, are what gives rise to the observed activity. Figure 2.7C compares IRI activity of poly(hydroxyl proline) with $PPro_{15}$ and, two α-helical poly(amino acids).[35] Poly(lysine) ($PLys_{50}$) and poly(glutamic acid) ($PGlu_{110}$), show no IRI, similar to the negative control. $PPro_{15}$ was found to be more active than poly(hydroxyl proline) of higher molecular weight. This confirms that hydroxyl groups are not essential for activity in IRI active compounds. $P(D)Pro_{15}$ and $P(DL)Pro_{21}$ had

statistically identical activity to $PPro_{15}$ suggesting local rather than long range order is crucial for activity. Specifically, we hypothesise that IRI activity requires segregated hydrophilic and hydrophobic domains (amphipathy).[8,36] As per Figure 2.8, $PPro_{10}$ was compared to a non-glycosylated Type I sculpin AFP[37] and also against $PGlu_{10}$, by mapping their hydrophobic/hydrophilic domains. Type I sculpin AFP (Figure 2.8A) possess 'patches' of hydrophobic/hydrophilic groups, and likewise, $PPro_{10}$ (Figure 2.8B) also possesses this facial amphiphilicity. The intrinsically amphipathic nature of poly(proline) and therefore, of the polyproline type II helix, in the absence of hydroxyl groups – can be attributed to as responsible for the observed IRI activity. In comparison, $PGlu_{10}$ (no IRI activity) has charged groups around the core of the helix, which prevents the presentation of the central hydrophobic domains. This agrees with a previous study by Gibson and co-workers on Nisin A, which has IRI activity associated with segregated domains[8] and also of amphiphiles developed by Ben *et al*., which only function below the critical micelle concentration.[36]

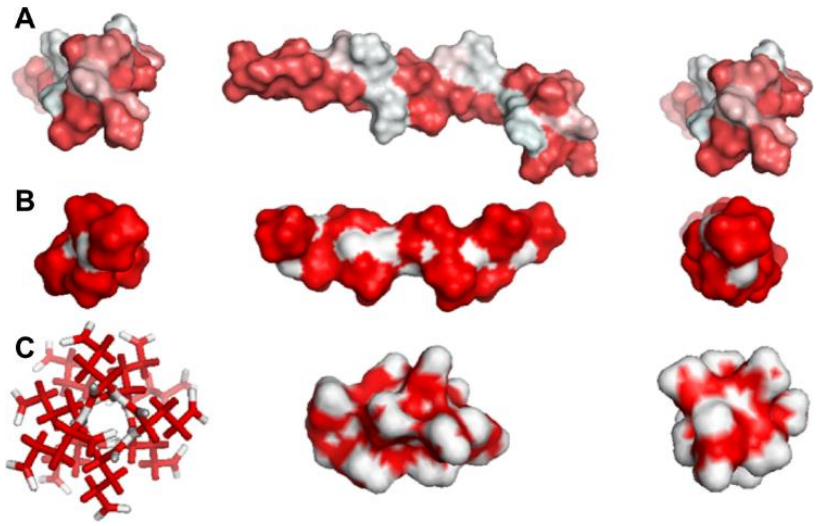

Figure 2.8 – Hydrophobic surface mapping of A) Recombinant Type I Sculpin AFP; B) $PPro_{10}$; C) $PGlu_{10}$ showing charged hydrophilic surface. Protein models generated by J. R. J. Healey (mapped by B. Graham)

In addition to IRI activity, AF(G)Ps display unwanted ice shaping which promotes the formation of needle-like ice crystals which damage cell membranes.[38] This is one of the overriding factors preventing their application to cell cryopreservation, and the source of their cytotoxicity. Cryo-confocal microcapillary microscopy has emerged as a tool for monitoring ice crystal shaping,[39] and was employed here (experimental performed by M. Marcellini and S. Deville), Figure 2.9. A non-IRI active dye, sulforhodamine B, provided contrast against the ice (which appears dark). A control using pure PBS showed no shaping whilst zirconium acetate (ZrAc), which is a strong ice shaping, produced hexagonal crystals.[39] $PPro_{19}$ did not induce shaping supporting the concept that polyproline inhibits ice crystal growth without inhibiting or binding to a specific plane of ice. Specifically, unlike PVA which is thought to bind ice, and AFGP which is known to, it is possible that this study provides a degree of substantiation for a specific mechanism of IR inhibition which – through the disordering of local waters – may inhibit ice crystal growth by preventing the energetic transfer of water across a disordered water-layer.

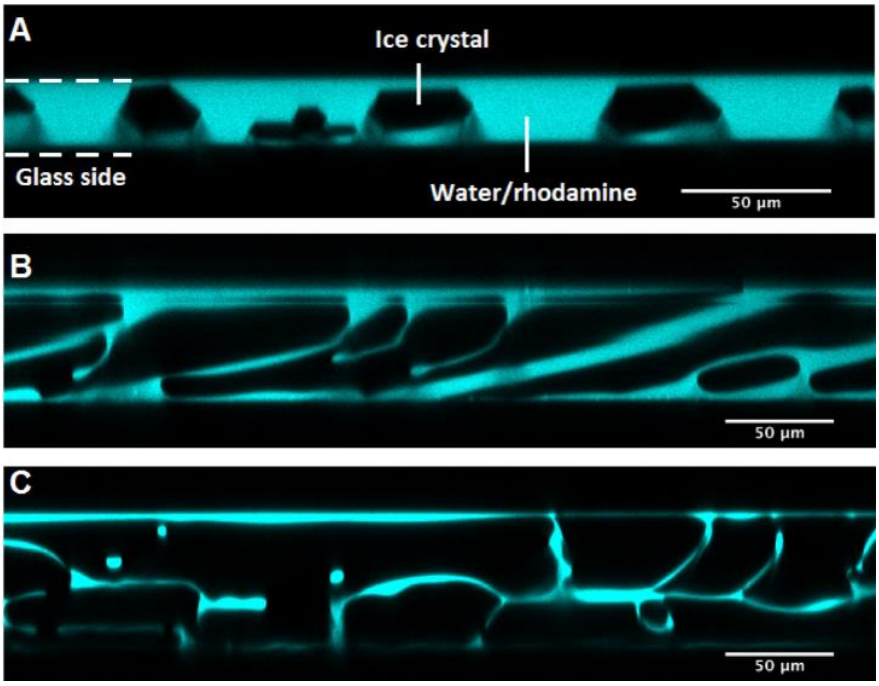

Figure 2.9 – Cross-section of ice crystals perpendicular to temperature gradient. A) ZrAc (positive control); B) $PPro_{19;}$ C) PBS (negative control). The ice crystals expel the dye while growing, appearing in black, while the remaining liquid fluoresces.

2.3iii – Cryopreservation with oligo- and poly- prolines

This apparent inability to dynamically shape ice and polyproline's intrinsic IRI activity suggested its wider application as a potential cellular cryoprotectant. Numerous biomedical procedures and practices (such as tissue engineering, gene therapy, and the manufacture of therapeutic proteins) depend upon the storage and transport of donor cells.[40] Principally, in order to access the full potential offered by stem cell therapy treatments, a ready, available, and on-demand supply of cellular material is essential. A reliable, replicable methodology for the cryopreservation of cell lines (preferably in the simpler monolayer format – providing phenotypically identical cells) is therefore highly desirable. In comparison, *in vitro* cell cultures are less favourable, as they undergo phenotypic and genetotypic changes when propagated over long periods of time[41,42] It is therefore necessary to freeze these cell lines in the presence of large volumes (of typically cytotoxic) cryoprotective organic solvents such as DMSO, which acts to limit the effective rise in extracellular solute concentration during freezing, lowering cryo-induced cellular damage. Repeated DMSO exposure, however, can result in the mutation of DNA methylation profiles and induces phenotypic drift.[43,44,45] Low cellular recoveries are also a factor, with embryonic stem cells generally giving only 5% cellular recovery when exposed to commercial formulations containing between just 5 – 10% DMSO. [46–48,49,50]

Of the IRI species developed to date, several have been subject to cell freezing studies. Matsumura *et al*. have developed polyampholytes[51] which are cryoprotective in spite of their moderate IRI activity.[33,34] Wang *et al.* have demonstrated the significant IRI activity of graphene oxide.[52] Ben *et al.* have developed low molecular weight surfactants which also inhibit ice growth.[36] A major setback is that the above synthetic IRIs are not biodegradable nor bioresorbable and have not been applied to significant challenge of cell monolayer storage.

To explore polyproline as a biocompatible, biodegradable and bioresorbable macromolecular cryopreservative A549 cells were employed as prototypical adherent cell line.[53]

Performed by Trisha L. Bailey, the protective osmolyte proline (which has no intrinsic IRI activity, see Appendix) was used as a secondary cryoprotectant to protect against osmotic stress. A549 cells were incubated with 200 mM proline or media alone for 24 hours. The solution was then removed and replaced with 10% DMSO with $PPro_{11}$, and after 10 minutes exposure, all excess solvent was removed followed by controlled freezing to –80°C and storage. Cells were subsequently thawed and the total number of viable cells assessed by trypan blue staining.

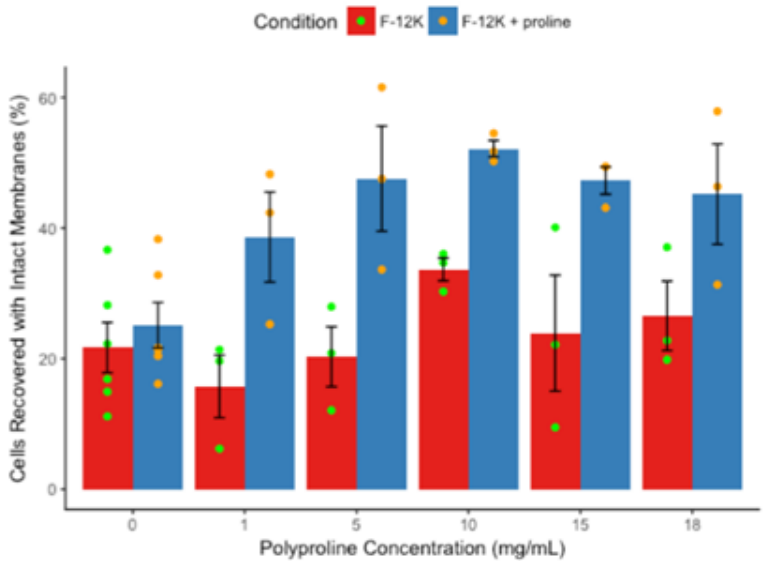

Figure 2.10 – A549 Cryopreservation. Error bars ± S.E.M from n= 3 with two nested replicates. # $P < 0.05$ compared to 10% DMSO treatment; * $P < 0.05$ compared to 200 mM proline exposure with 10% DMSO treatment. Performed and Graphed by T. L. Bailey.

Figure 2.10 shows that the industrial 'gold standard' (DMSO) which gives just 27% cellular recovery under the employed conditions. Addition of polyproline to 10% DMSO failed to give any additional protection. However, cells which had been pre-conditioned with 200 mM proline for 24 hrs before exposure to 5 $mg.mL^{-1}$ $PPro_{11}$/10% DMSO dramatically increased

recovery of viable cells to 53%. Increasing the concentration of polyproline beyond 10 mg.mL^{-1} did not increase recovery further.[54] This is a significant improvement in cell recovery and demonstrates the successful application of a simplistic, yet potent, antifreeze protein mimic.

Red blood cells haemolysis assays were also carried out, which indicated that polyproline was effectively non-haemolytic and biocompatible across the concentration range, Figure 2.11, with ~ 96% of red blood cells intact after exposure (10 mg.mL^{-1}).

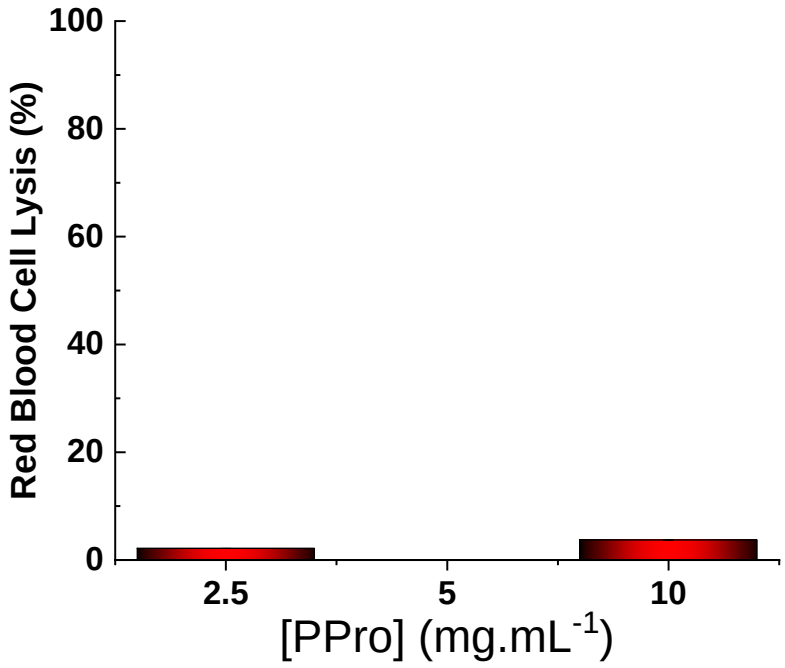

Figure 2.11 – Red blood cell hemolysis assay for poly(proline) ($PPro_{15}$) at 37 ºC.

Over a 24 hour period, significant cytotoxicity (signified by reduced cellular viability) with respect to poly(proline) is observed at concentrations in excess of 5 mg.mL^{-1}. Figure 2.12. However, these results are substantially better than what is observed for DMSO alone. Additionally, toxicity is only observed over extended periods, and given that the cryopreservation strategy employed requires only fleeting exposure to poly(proline) – no greater than 10 minutes – before removal of both DMSO/poly(proline) and subsequent freezing

as a monolayer, this is of little concern. Furthermore, the thawing of cells by addition of warm media will further dilute any residual poly(proline), minimising any long term cytotoxic effect.

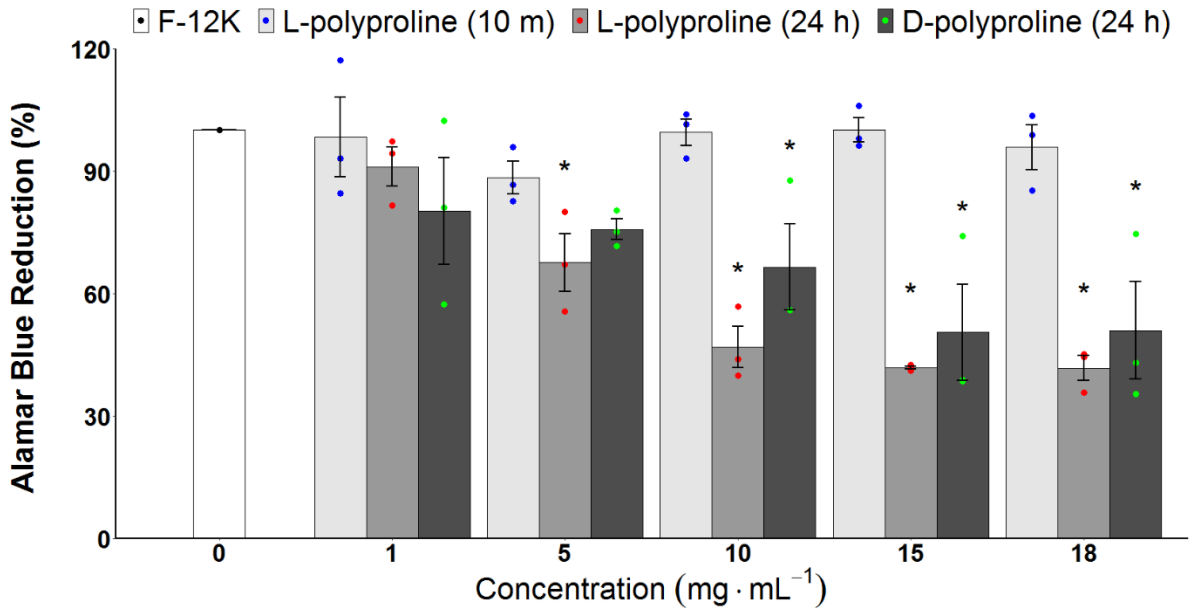

Figure 2.12 – Long Exposure (24 hrs) of A549 Cells to PPro. % Cell Recovery determined by alamar blue (resazurin) reduction. Error bars ± S.E.M from n= 3; * $P < 0.05$ compared to PPro-free control. Performed and Graphed by T. L. Bailey.

2.3iv – Preparation of poly(L-proline) *via in-situ N*-Carboxyanhydrides and ROP

The ability to produce poly(proline) on a large scale maybe an attractive proposition, given that we have demonstrated that it is a potent additive for cell-monolayer cryopreservation. However, production through Steglich coupling is not a practical method for anything other than small quantities, particularly due to its low efficiency and invariably low yield (1-10%). It is therefore not economically scaleable, requiring unrealistically large quantities of reagent to give very little product. The effective step-growth process is also self-limiting, with steric hindrance of the proline ring preventing chain growth. As already discussed, preparation of poly(proline) through *N*-carboxyanhydride synthesis and subsequent polymerisation has proved challenging, due to the instability of the NCA. Recent literature work by Schlaad *et al.*[55] and Endo and co-workers[56–62,63] has shown the ability to prepare *N*-carboxyanhydrides *in-situ*, subsequently generating the polypeptide of interest in high yield, through an effective transition state. Furthermore, Endo and co-workers has shown – to a very limited extent – the ability to prepare poly(proline) through this method,[64] and is the only example of its kind to date. However, this preparation was sparse in detail, low yielding, and gave no molecular weight or dispersity characterisation. Additionally, the poly(proline) prepared was insoluble in water and numerous organic solvents (including DMF and DMSO) – implying poly(proline) had only been produced in very high molecular weights by this method. In spite of this, as this approach does not require NCA isolation, it may have adapted application here for the mass, economical, production of poly(proline), Figure 2.13.

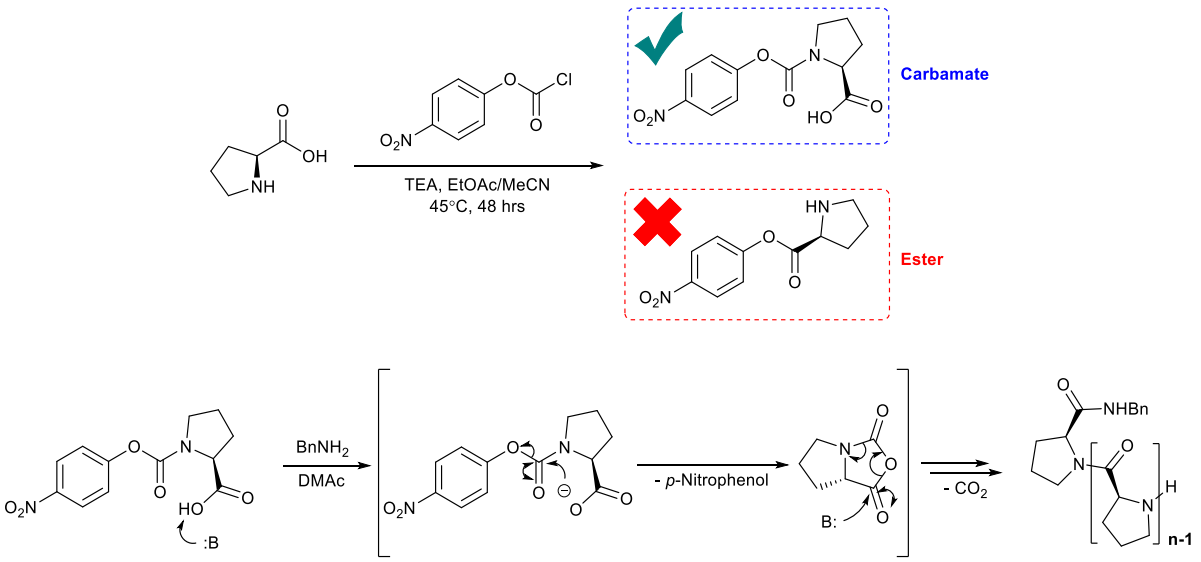

Figure 2.13 – Generation of Carbamate Precursor and *in-situ* NCA Generation/ROP

Attempts to prepare the carbamate as per the literature precedent were inconsistent, however. Use of a non-nucleophilic base (TEA) to scavenge HCl and improve yield relative to the literature (33%), resulted in the generation of 4-nitrophenoxide. Able to attack an otherwise transient intermediate (**1**, Figure 2.14), this competitive side reaction led to the production of the inactive ester product (Crude LCMS Fragment at 277 m/z = Ester + ACN), Figure 2.14. Column chromatography (9:1 chloroform:acetone) allowed isolation of the carbamate, but in less than expected yield (20%). As the ester is unable to undergo the cyclisation process to the NCA, it is a dead-end product, with any nucleophilic step growth to the polypeptide by intramolecular nucleophilic attack of the amine ultimately restricted by its own steric bulk.

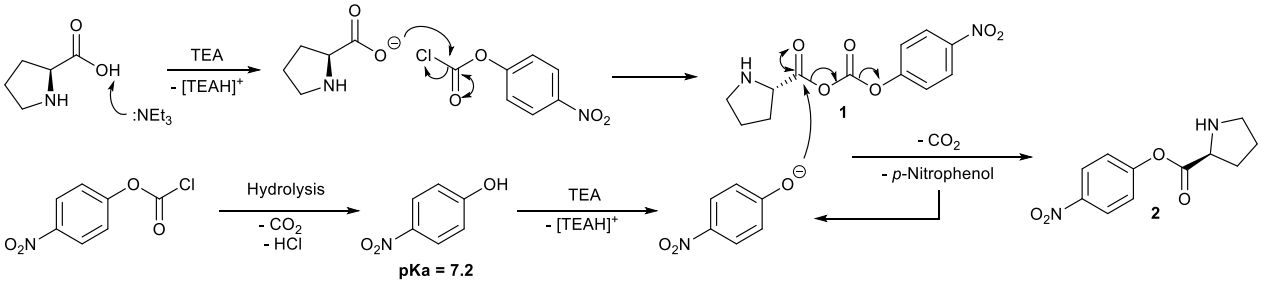

Figure 2.14 – Likely mechanism of ester formation during proline-4-nitrophenoxy carbonyl synthesis

However, once isolated, *in-situ* cyclisation of the carbamate to the NCA and subsequent ROP was found to be effective Table 2.3 – Entry 1, giving well defined oligo(proline) in substantially improved yield (relative to Steglich coupling).

	[M]:[$BnNH_2$]	$M_{n,}$ [a] ($g.mol^{-1}$)	$Đ_{,}$ SEC [a] (-)	DP [a] (-)	Yield
1	28.8 : 1	720	1.08	6	27.1% (Crude)
2	11.8 : 1	18,900	1.42	164	Negligible (Purified)
		1700	1.18	15	

Table 2.3 – Characterisation of polyprolines prepared through in-situ NCA/ROP protocol. [a] Determined by SEC (DMF)

Unlike Endo's previous work, poly(proline) was obtained in low molecular weight and low dispersity. Importantly, the Mw's of the poly(proline) acquired was similar to the oligomers previously prepared by Steglich coupling, suggesting that this method is applicable for scaleable production of poly(proline) as a macromolecular cellular cryoprotectant.

In the interests of improving yield further, attempts were made to prevent ester formation outright during carbamate preparation. Taking inspiration from Endo's later work on sarcosine,[62] we later substituted the use of free proline for the *tert*-butoxy protected equivalent, deactivating the α-carboxylic acid. When reacted with the 4-nitrophenol chloroformate, this selectively led to the ^{t}Bu-carbamate product in 84% yield before brief exposure to 50% TFA in DCM, cleaving the protecting group to reveal the free acid/carbamate derivative. *In-situ* polymerisation followed – Table 2.3, Entry 2 – with a lower excess (12 : 1 *vs* 29 : 1) of benzylamine used in order to produce longer poly(proline) chains, of the same order as those produced in the Steglich coupling (DP ~ 15). Despite the significantly reduced mass loss in the new procedure, the *in-situ* NCA/ROP protocol led to the formation of trace quantities of very long poly(proline) chains, of approximately 18 kDa molecular weight. The desired shorter

chains of approximately 1.7 kDa were also produced (and were significantly more pronounced by GPC), however, the mass of all fractions recovered was negligible (< 0.1 mg). This indicates that a large proportion of the proline carbamate was converted to very short oligomers (below the molecular weight cut-off of the dialysis tubing) or failed to polymerise at all. Given the steric hindrance of poly(proline), it is probable that the prolines have a propensity to form short stretches, with longer sequences disfavoured, rendering the synthesis of defined lengths problematic to achieve in practice. Further work is required in order to optimise this method and realise its potential to provide large quantities of poly(proline), economically.

2.4 – Conclusions

In summary, here we have introduced poly(proline) as a minimum (bio)synthetic antifreeze protein mimic. We have demonstrated polyproline has ice recrystallization inhibition activity, hypothesised to be due to its 'patchy' amphipathic PPII helical structure. This assertion has an important impact upon the understanding of IRI mechanistic action, disproving the necessity for hydroxyl groups and potentially supporting a theory of activity dependent upon the disruption of local water ordering in the absence of ice binding. Crucially, having elucidated some key structural motifs and asserted the supremacy of amphipathy, the observations made here may now allow for the enhanced rational design of potent AF(G)P mimetics, expanding the synthetic space which may be explored.

Poly(proline) was further found to significantly improve the cryopreservation of cell monolayers/adherent cell culture, with a remarkable increase from 20% (DMSO alone) to > 50% in total cell recovery post cryopreservation, thought to be a result of ice recrystallisation inhibition. This ultimately demonstrates a new macromolecular approach for the storage of complex cells to enable next generation therapies.

Transient exposure of poly(proline)/DMSO, followed by the removal of the excess solvent, limits the cytotoxicity associated with long-term exposure to poly(proline). As such, this may impart biomedical benefits in comparison to existing high-solvent-concentration vitrification techniques, making poly(proline) an appealing candidate to other cryoprotective species. Furthermore, being comprised only of native amino acids, poly(proline) is an ideal motif in the emerging field of macromolecular cryoprotectants. Unlike some synthetic polymers, poly(proline) may be accessed by both chemical and biochemical methods, making it a versatile new tool in cell biology and biomedicine.

2.5 – Experimental

Materials

L and D-proline, poly-L-proline mol wt 1,000-10,000 ($PPro_{10\text{-}100}$), ethyl (hydroxyimino) cyanoacetate (OxymaPure^{TM}), *N*-(3-dimethylaminopropyl)-*N′*-ethylcarbodiimide hydrochloride (EDCI), dichloromethane (DCM), phosphate-buffered saline preformulated tablets, and hydrochloric acid (37%) were purchased from Sigma Aldrich Co Ltd (Gillingham, UK) and used without further purification. Dialysis Membrane Spectra/Por 7 Flexible 38mm FWT 1000 MWCO 4.6 mL/cm was purchased from Fischer Scientific (Loughborough, UK) and used directly. Phosphate-buffered saline (PBS) solution was prepared using preformulated tablets in 200 mL of Milli-Q water (>18.2 Ω mean resistivity) to give [NaCl] = 0.138 M, [KCl] = 0.0027 M, and pH 7.4. $PPro_{10}$ and $PPro_{20}$ (>90%) were purchased bespoke from Peptide Protein Research Ltd (Fareham, UK) and were used without further purification. $PPro_{10}$: m/z (ESI, -ve) 988.0 (100%, -1); $PPro_{20}$: m/z (ESI, +ve) 491.0 (20%, +4), 654.3 (100%, +3), 981.0 (30%, +2).

Physical and analytical methods

^{1}H and ^{13}C NMR Spectra (300 – 400 MHz and 75 – 100 MHz, respectively) were recorded using one of a Bruker DPX-300/400 Spectrometer under standard NMR conditions. Chemical shifts were recorded in ppm and referenced to solvent residual peaks, using ACD Labs NMR Spectroscopy software.

ESI MS experiments were performed on an Agilent 6130B Single QUAD ESI-LC MS spectrometer in either positive or negative mode with an H_2O/MeOH (80:20) eluent feed, with samples dissolved in water, methanol or ethanol, unless otherwise stated.

IR experiments were carried out on a Bruker Vector 22 (ATR) FTIR Spectrometer in either the solid or thin film (volatile organic solvent) phase, with background subtraction.

SEC (size exclusion chromatography) was acquired a DMF Agilent 390-LC MDS instrument equipped with differential refractive index (DRI), viscometry (VS), dual angle light scatter (LS) and dual wavelength UV detectors. The system was equipped with 2 x PLgel Mixed D columns (300 x 7.5 mm) and a PLgel 5 µm guard column. The eluent is DMF with 5 mmol NH_4BF_4 additive. Samples were run at 1 mL/min at 50'C. Poly(methyl methacrylate) standards (Agilent EasyVials) were used for calibration. Analyte samples were filtered through a nylon membrane with 0.22 µm pore size before injection. Respectively, experimental molar mass ($M_{n,SEC}$) and dispersity (Đ) values of synthesized polymers were determined by conventional calibration (relative to poly(methyl methacrylate) standards) using Agilent GPC/SEC software. Refractive index recorded.

Experimental Methods

Ice recrystallization inhibition (splat) assay

Ice recrystallisation inhibition was measured using a modified splat assay. [1] A 10 µL sample of polymer dissolved in PBS buffer (pH 7.4) was dropped 1.40 m onto a chilled glass coverslip, resting on a thin aluminium block placed on dry ice. Upon hitting the coverslip, a wafer with diameter of approximately 10 mm and thickness 10 µm was formed instantaneously. The glass coverslip was transferred onto the Linkam cryostage and held at -8^{o}C under N_2 for 30 minutes. Photographs were obtained using an Olympus CX 41 microscope with a UIS-2 20x/0.45/∞/0-2/FN22 lens and crossed polarizers (Olympus Ltd, Southend-on-Sea, UK), equipped with a Canon DSLR 500D digital camera. Images were taken of the initial wafer (to ensure that a polycrystalline sample had been obtained) and again after 30 minutes. Image processing was conducting using Image J, which is freely available. In brief, five of the largest ice crystals in the field of view were measured and the single largest length in any axis recorded. The average (mean) of these five measurements was then calculated to find the largest grain dimension along any axis. This was repeated for three individual wafers, and the average (mean) of these three values was calculated to give the mean largest grain size (MLGS). The average value was compared to that of a PBS buffer negative control.

Surface hydrophobicity mapping of proteins

NMR solution phase (AFP Sculpin) and X-Ray crystal structures of proteins and peptides of interest were acquired from the Protein Data Bank and other publicly accessible sources, or computationally modelled in-house ($PPro_{10}$ and $PGlu_{10}$) by Dr. Joseph J. R. Healey. Structures were rendered in PyMOL (Schrödinger LLC, Cambridge, MA), which is freely available for educational use, and surfaces on the structures were displayed. An open source script “color_h” was used to colour the protein surface according to the Eisenberg hydrophobicity scale of its

constituent amino acids, from red (hydrophobic) to white (hydrophilic). For the homo-polypeptides where scaling is not possible, aliphatic hydrogen and carbon were defined as hydrophobic whilst oxygen, hydrogen and nitrogen as hydrophilic, utilising the same colour scheme. Due to the lack of hydrogen bond donors in a $PPro_{10}$ PPII helix, this was considered representative.

Cell culture

Performed by Trisha L. Bailey. Human Caucasian lung carcinoma cells (A549) were obtained from the European Collection of Authenticated Cell Cultures (Salisbury, UK) and grown in 175 cm^2 cell culture Nunc flasks (Corning Incorporated, Corning, NY). Standard cell culture medium was composed of Ham's F-12K (Kaighn's) Medium (F-12K) (Gibco, Paisley, UK) supplemented with 10 % USA-origin foetal bovine serum (FBS) purchased from Sigma Aldrich Co Ltd (Gillingham, UK), 100 units/mL penicillin, 100 µg/mL streptomycin, and 250 ng/mL amphotericin B (PSA) (HyClone, Cramlington, UK). A549 cells were maintained in a humidified atmosphere of 5 % CO_2 and 95% air at 37 °C and the culture medium was renewed every 3–4 days. The cells were S4 subcultured every 7 days or before reaching 90 % confluency. To subculture, cells were dissociated using 0.25 % trypsin plus 1 mM EDTA in balanced salt solution (Gibco) and reseeded at $1.87x10^5$ cells per 175 cm^2 cell culture flasks.

Cell solution preparation

Performed by Trisha L. Bailey. Solutions for cell incubation experiments were prepared by dissolving the individual compounds in F-12K supplemented with 10 % FBS and 1X PSA (solutions used as freezing buffers did not contain PSA) and sterile filtered prior to use.

Cytotoxicity Measurements

Performed by Trisha L. Bailey. Cells were seeded at 6·104 cells per well in 200 µL of cell culture medium with indicated concentrations of polyproline in 96-well plates (ThermoFisher).

Cells were incubated for 24 h in a humidified atmosphere of 5% CO_2 and 95% air at 37 °C. Following the incubation period, resazurin sodium salt (Sigma Aldrich) was dissolved in phosphate buffered saline (Sigma Aldrich) and added to wells in an amount of 1/10th initial well volume. Absorbance was measured at 570/600 nm every 60 minutes until control cells reached ~ 70 % reduction, and the viability reported relative to the control cells.

Haemolysis assay

Samples containing 250 µL ovine red blood cells (RBCs) and 250 µL of PPro solution (at twice the indicated concentration) were incubated at 37 °C for 1 hour. After centrifugation, 10 µL of the supernatant was added to 90 µL of PBS buffer in a 96 well plate. The absorbance was measured at 450 nm and compared against a PBS buffer and deionised water (to lyse cells) controls to determine the % haemolysis relative to the controls.

Statistical analyses

Performed by Trisha L. Bailey. Data were analysed with a one-way analysis of variance (ANOVA) on ranks followed by comparison of experimental groups with the appropriate control group (Holm–Sidak method) followed by Tukey's post hoc test. Excel 2013 (Microsoft, Redmond, WA) and R (R Foundation for Statistical Computing, Vienna, Austria) were used for the analyses. Data sets are presented as mean ± (SEM).

Cryopreservation of A549 cell monolayers

Performed by Trisha L. Bailey. Cells to be frozen in the monolayer format were seeded at $0.4X10^6$ cells per well in 500 µL of cell culture medium in 24-well plates (Corning Incorporated, Corning, NY). Plates had a total available volume of 3.4 mL with an approximate growth area of 1.9 cm^2, no coverslips were used and plates were used with the accompanying lid. Cells were allowed to attach to the entire free surface of the bottom of the well and formed a confluent layer not greater in height than one cell. Before experimental treatments, cells were

allowed to attach for 2 h to the plates in a humidified atmosphere of 5% CO_2 and 95% air at 37°C. The medium was exchanged against medium that was or was not supplemented with solutes as indicated in the figure. Control cells received no additional solutes and experimental cells were incubated with 23.1 mg/mL L-proline for 24 h in a humidified atmosphere of 5% CO_2 and 95% air at 37 °C. Following the incubation period, the culture medium was removed and cells were exposed for 10 min at room temperature to different concentrations of solutes dissolved in F-12K supplemented with 10% FBS and 10% DMSO. After 10 min, the freezing solutions were removed and the plates placed inside a CoolCell® MP plate (BioCision, LLC, Larkspur, CA), transferred to a -80 °C freezer and frozen at a rate of 1 °C/min. After 24 h at -80 °C, cells were rapidly thawed by addition of 500 µL cell culture medium warmed to 37 °C. Cells were placed in a humidified atmosphere for 24 h and then dissociated using 0.25% trypsin plus 1 mM EDTA in balanced salt solution. The number of viable cells was then determined by counting with a haemocytometer (Sigma Aldrich Co Ltd) at room temperature after 1:1 dilution of the sample with 0.4% trypan blue solution (Sigma Aldrich Co Ltd). The initial cell medium was discarded such that any non-attached cells were not included in the assessment. The percentage of recovered cells was calculated by dividing the number of cells with intact membranes after freezing and thawing by the number of cells present prior to freezing (i.e. after application of pre-treatments), multiplied by 100.

Confocal Microscopy sample preparation and measurements

Performed by Moreno Marcellini/Sylvian Deville. The solution of 20 mg/mL of poly(proline) in PBS was prepared as previously reported. This solution was stained with 60 µL/mL of 1 mM solution of Sulphorhodamine B in deionized water. The fluorophore absorbs the 552 nm wavelength laser light and emits in a wide band: The fluorescent light was integrated in the 575-625 nm range. Water at the liquid/solid phase transition expels all ions, such that the ice crystals will be constituted by pure water. In this way, we can highlight the ice crystals that

upon freezing will grow in the solution as black bodies in the fluorescent liquid. The experimental setup for a similar experiment has been described elsewhere.[3] A thin Hale-Shaw cell was built as follows: on a squared thin glass slide (20 x 20 mm^2, thickness $\lambda \approx 170$ μm, VWR) a 10 μl drop was deposited by using a pre-calibrated pipette. The sessile drop was carefully covered with a circular thin glass slide (Ø=15 mm, $\lambda \approx 170$ μm, VWR). The circular contour of such Hale-Shaw cell was sealed with nail polish (L'Oreal). With time, the solvent of the seal eventually evaporates, making the seal porous. The sample was therefore rapidly mounted on the cryostage and frozen only once, while the seal was still effective. The sample was discarded after the experiment.

Confocal Microscopy Measurement: To simulate – to a first approximation – the protocol of splat experiments reported elsewhere, [4] the sample was brought as quickly as possible (a few minutes) at the minimum temperature $T_{min} \approx -22°C$ that the cryostage can sustain. Nevertheless, this protocol is largely unable to provide the same crystallization feature of the splat experiments owing to the ice crystallization in a fraction of a second being more feasible with the latter. At a temperature below –15°C ice crystals burst from the cold side towards the hot side. The rapid imaging rate of the microscope is able to capture the growing ice crystal and the flow of fluorescent liquid.

Synthetic Procedures

General procedure for the synthesis of polyproline peptides $PPro_n$

EDCI (0.50 g, 2.60 mmol) was dissolved in dry DCM (20 mL) and stirred at room temperature under a flow of dry nitrogen for 20 minutes, followed by cooling to 0 ºC. Within 5 minutes of cooling, L- or D-proline (0.30 g, 2.60 mmol, 1 eqv) and OxymaPure™ (0.37 g, 2.60 mmol, 1 eqv) were added together to the reaction mixture, resulting in an instantaneous colour change to yellow. The mixture was stirred on ice under nitrogen for 1 further hour, and then warmed to RT with stirring overnight. The dark yellow solution was condensed *in vacuo*, dissolved in Milli-Q water (10 mL) acidified to pH 3-4 with 3M HCl, and a minimum volume of methanol added until residual solids dissolved. Dialysis (> 1 kDa) for 48 hours was subsequently performed with regular water changes. The resulting solution was freeze dried, yielding an off-white solid. 31.4 mg (10.4%). The DL racemate, $P(DL)Pro_n$, utilised a 1:1 ratio of L- and D-proline (2.60 mmol prolines).

Attempted synthesis of poly-L-proline from *in-situ* *N*-carboxyanhydride (NCA) generation and ring-opening polymerisation (*via* Free α-amine)

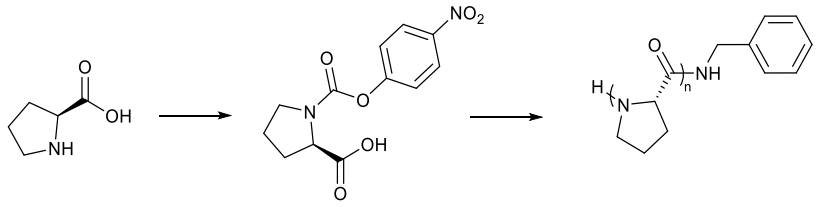

L-Proline (7.6 g, 66.0 mmol) was dissolved in ethyl acetate (50 mL) containing acetonitrile (20 mL) and 4-nitrophenylchloroformate (15.83 g, 78.55 mmol, 1.2 eqv) added. Triethylamine (12 mL, 86.10 mmol, 1.3 eqv) was then introduced dropwise, and the mixture stirred overnight at room temperature. The solution was then reduced *in vacuo* to a thick oil and loaded onto silica gel for purification by column chromatography (9:1 chloroform/acetone), R_f = 0.73, Fractions

6 – 10, yielding an off-white solid. 3.69 g (20.0 %). m/z (ESI, -ve) Expected 376.1, Observed 376.1 [100%, M + Proline – H_2O – H^+].

This solid was subsequently dissolved into dry DMAc, under N_2, and then sparged with nitrogen for 20 minutes. Benzylamine was then added (50 µL) and the mix was heated at 60ºC for 3 days with stirring. The mixture was then exposed to air, condensed to a thick oil *in vacuo* and subjected to SEC analysis. 1 g (27.1%).

Attempted synthesis of poly-L-proline from *in-situ* *N*-carboxyanhydride (NCA) generation and ring-opening polymerisation (*via* Protected α-amine)

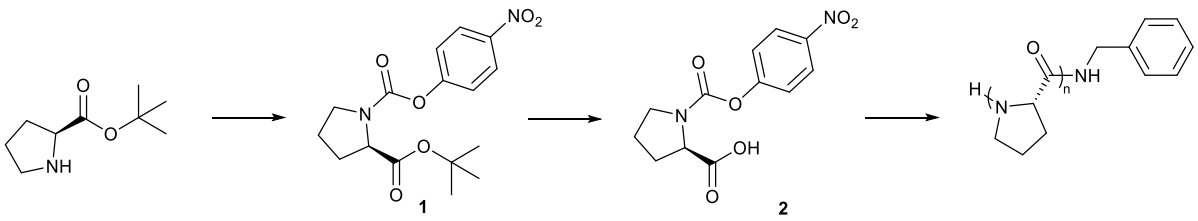

Preparation of 1: L-Proline *tert*-butyl ester (600 mg, 3.50 mmol) was dissolved in THF (30 mL) and 4-nitrophenylchloroformate (1.06 g, 5.26 mmol, 1.5 eqv) added, in conjunction with triethylamine (0.75 mL, 5.38 mmol, 1.53 eqv), and the mixture stirred overnight at room temperature. After 18 hours the solution was reduced *in vacuo* to a thick oil and then precipitated from ice cold water (~ 45 mL), to give a white solid which was filtered, rinsed with acetone, and then condensed *in vacuo*. The solid residue was then desiccated overnight, to give the arylated product. 1.03 g (87.4 %). m/z (ESI, +ve) Expected 359.3, Observed 359.2 [100%, M+Na^+].

Preparation of 2 and *in-situ* Polymerisation: **1** (910 mg, 2.71 mmol) was exposed to 50% trifluoroacetic acid in DCM for 1 hour on ice, and condensed *in vacuo*, yielding a brown oil. m/z (ESI, –ve) Expected 393.3, Observed 393.1 [100%, M+TFA^-].

The oil was rapidly dissolved into dry DMAc, under N_2, and sparged with nitrogen for 20 minutes. Excess acidity was removed with triethyl amine (13 µL) – until pH 7 – and then benzylamine added (25 µL). The mix was heated at 60ºC for 4 days with stirring. The mixture was then exposed to air, condensed to a thick oil *in vacuo*, and dissolved up into water (~ 40 mL) and dialysed (MWCO 1 kDa), with regular water changes until the loss of the yellow *p*-nitrophenol by-product. The contents of the dialysis bag were then freeze dried to give a very thin translucent film of negligible mass.

Failed and redundant syntheses of (*S*)-tetrahydro-1*H*,3*H*-pyrrolo[1,2-c]oxazole-1,3-dione (L-Proline NCA)

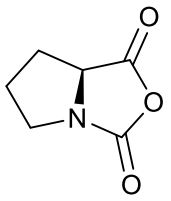

Free Amino Acid Method: L-proline (0.1 g, 100 mg, 0.87 mmol) was suspended in dry EtOAc (50 mL) with stirring, and heated to 50°C. Triphosgene (0.5 eqv, 0.13 g, 0.43 mmol) was added in whole, and the reaction mixture stirred for one hour (until dissolved). The intermediate was subsequently condensed *in vacuo* and the yellow oily residue redissolved in dry EtOAc (60 mL), added to pre-swollen DEAM-PS (3 eqv, 0.82g, 2.61 mmol) in dry EtOAc (20 mL), and stirred at RT for 2 hours. The filtrate was recovered and condensed *in vacuo*, the solid having been washed with further dry EtOAc (20 mL) at the pump. The off-white crude residue obtained was redissolved in dry EtOAc (5 mL) and crystallised from pentane (20 mL), with cooling to –20°C overnight, yielding yellow crystals. Recrystallisation from EtOAc (5 mL) and cold pentane (30 mL) at –20°C yielded an off-white solid. 25 mg. (Product Absent by ^{1}H and ^{13}C NMR – 0%). Compound previously reported.[25]

***N*-Boc Protected Method:** *N*-Boc-L-Pro-OH (0.1 g, 100 mg, 0.46 mmol) was suspended in dry THF (15 mL) with stirring under nitrogen**.** DEAM-PS (3 eqv, 0.44 g, 1.39 mmol) was added and allowed to equilibrate for 1hr 30 minutes, followed by the slow addition of Triphosgene (0.37 eqv, 51.00 mg, 0.17 mmol) in THF (5 mL), drop wise, at –7°C. The reaction mixture was stirred for a further 30 minutes on ice, and then quickly warmed to 40°C for 5 minutes, with stirring at RT overnight. The mixture was then filtered, washed with dry THF (100 mL), and condensed *in vacuo*, yielding the crude mixture which was subsequently dried under reduced pressure (4 hrs). The crude was then dissolved in EtOAc/Pentane (15 mL, 1:2), chilled at –5°C and then extracted once with ice cold water (50 mL). The organic phase was subsequently dried over $MgSO_4$, filtered and condensed *in vacuo*, yielding a clear oil featuring an off-white solid. 32 mg (53 %). IR (ATR): 2961 cm^{-1} (-OH); 1744, 1720, 1700, 1650 cm^{-1} (C=O). GC-MS (360°C): 12.67 min, m/z = 57.1 (309924, Unknown) 70.1 (1551485,-H^+N=$CHCH_2CH_2CH_2$-), 114.0 (1188295, -HN-$CH(CO_2^+)$-$CH_2CH_2CH_2$-). Compound previously reported.[24]

Modified *N*-Boc Protected Method: *N*-Boc-L-Pro-OH (0.5 g, 2.32 mmol) was dissolved in dry THF (20 mL) under nitrogen. Triphosgene (0.37 equiv, 0.25 g, 0.65 mmol) was added under vigorous stirring and after 10 minutes, triethylamine (1.1 equiv, 0.35 mL, 2.55 mmol) added dropwise over 15 minutes at –15°C, and the reaction mixture stirred for 1.5 hrs at RT under nitrogen. The reaction mixture was then cooled to 0°C to allow for complete precipitation of the triethylammonium salt and was removed by filtration. The filtrate was subsequently condensed *in vacuo* and dried under reduced pressure. The crude was dissolved in dry ethyl acetate (10 mL), chilled, and then extracted once with ice-cold water (30 mL). The organic phase was died over $MgSO_4$, filtered, and condensed *in vacuo*. The oily residue was subsequently chilled to – 20°C overnight under nitrogen, yielding white crystals. 0.301 g. (Product Absent – 0%). IR (ATR): 2967, 2985, 2716 (CH), 1828, 1779, 1736, 1701, 1632

(C=O), 1478, 1423 (CH), 1257, 1211 cm^{-1} (CO). GC-MS (360°C): Uninformative. Compound previously reported.[25]

Attempted Syntheses of Poly-L-Proline

The crude material from the *N*-Boc Protected Method (0.301 g) was dissolved in dry THF (5 mL), under nitrogen with benzylamine (0.1 mL), and stirred vigorously for 24 hours. A large excess of diethyl ether (50 mL) was added and the mixture centrifuged (10k RPM 10 minutes). No polymeric material precipitated.

2.6 – References

1 C. Budke and T. Koop, *ChemPhysChem*, 2006, **7**, 2601–2606.

2 P. M. Naullage, L. Lupi and V. Molinero, *J. Phys. Chem. C*, 2017, **121**, 26949–26957.

3 T. Inada and S. S. Lu, *Cryst. Growth Des.*, 2003, **3**, 747–752.

4 M. I. Gibson, *Polym. Chem.*, 2010, 1, 1141–1152.

5 M. I. Gibson, C. A. Barker, S. G. Spain, L. Albertin and N. R. Cameron, *Biomacromolecules*, 2009, **10**, 328–333.

6 C. A. Knight, C. C. Cheng and A. L. DeVries, *Biophys. J.*, 1991, **59**, 409–18.

7 D. E. Mitchell, G. Clarkson, D. J. Fox, R. A. Vipond, P. Scott and M. I. Gibson, *J. Am. Chem. Soc.*, 2017, **139**, 9835–9838.

8 D. E. Mitchell and M. I. Gibson, *Biomacromolecules*, 2015, **16**, 3411–3416.

9 K. L. Gorres and R. T. Raines, *Crit. Rev. Biochem. Mol. Biol.*, 2010, **45**, 106–124.

10 C. I. Biggs, T. L. Bailey, Ben Graham, C. Stubbs, A. Fayter and M. I. Gibson, *Nat. Commun.*, 2017, **8**, 1546.

11 C. A. Knight, D. Wen and R. A. Laursen, *Cryobiology*, 1995, 32, 23–34.

12 T. Congdon, R. Notman and M. I. Gibson, *Biomacromolecules*, 2013, **14**, 1578–1586.

13 C. P. Garnham, R. L. Campbell and P. L. Davies, *Proc. Natl. Acad. Sci.*, 2011, **108**, 7363–7367.

14 C. S. Strom, X. Y. Liu and Z. Jia, *J. Biol. Chem.*, 2004, **279**, 32407–17.

15 G. Yoshimatsu, N. Sakata, H. Tsuchiya, M. Ishida, F. Motoi, S. Egawa, S. Sumi, M.

Goto and M. Unno, *Transplant. Proc.*, 2013, **45**, 1875–1880.

16 R. Sabins, *Handbook of Biological Statistics*, John Wiley & Sons Inc., Hoboken, New Jersey, 2010.

17 T. R. Congdon, R. Notman and M. I. Gibson, *Biomacromolecules*, 2016, **17**, 3033–3039.

18 V. R. Bouvet, G. R. Lorello and R. N. Ben, *Biomacromolecules*, 2006, **7**, 565–571.

19 Y. Tachibana, G. L. Fletcher, N. Fujitani, S. Tsuda, K. Monde and S. I. Nishimura, *Angew. Chemie - Int. Ed.*, 2004, **43**, 856–862.

20 R. B. Merrifield, *J. Am. Chem. Soc.*, 1963, **85**, 2149.

21 M. I. Gibson and N. R. Cameron, *J. Polym. Sci. Part A Polym. Chem.*, 2009, **47**, 2882–2891.

22 E. Gutierrez, B. S. Shin, C. J. Woolstenhulme, J. R. Kim, P. Saini, A. R. Buskirk and T. E. Dever, *Mol. Cell*, 2013, **51**, 35–45.

23 C. Deng, J. Wu, R. Cheng, F. Meng, H. A. Klok and Z. Zhong, *Prog. Polym. Sci.*, 2014, 39, 330–364.

24 O. P. Gulín, F. Rabanal and E. Giralt, *Org. Lett.*, 2006, **8**, 5385–5388.

25 M. Gkikas, H. Iatrou, N. S. Thomaidis, P. Alexandridis and N. Hadjichristidis, *Biomacromolecules*, 2011, **12**, 2396–2406.

26 T. J. Deming, *Nature*, 1997, **390**, 386–389.

27 A. A. Adzhubei, M. J. E. Sternberg and A. A. Makarov, *J. Mol. Biol.*, 2013, **425**, 2100–2132.

28 P. Wilhelm, B. Lewandowski, N. Trapp and H. Wennemers, *J. Am. Chem. Soc.*, 2014,

136, 15829–15832.

29 A. V Mikhonin, N. S. Myshakina, S. V Bykov, S. A. Asher and V. Pennsyl, *J. Am. Chem. Soc.*, 2005, **127**, 7712–7720.

30 Protein Circular Dichroism Data Bank, 2016, CD0004553000.

31 J. L. S. Lopes, A. J. Miles, L. Whitmore and B. A. Wallace, *Protein Sci.*, 2014, **23**, 1765–1772.

32 S. Lui, W. Wang, E. von Moos, J. Jackman, G. Mealing, R. Monette and R. N. Ben, *Biomacromolecules*, 2007, **8**, 1456–1462.

33 D. E. Mitchell, M. Lilliman, S. G. Spain and M. I. Gibson, *Biomater. Sci.*, 2014, **2**, 1787–1795.

34 D. E. Mitchell, N. R. Cameron and M. I. Gibson, *Chem. Commun.*, 2015, **51**, 12977–80.

35 M. I. Gibson, C. A. Barker, S. G. Spain, L. Albertin and N. R. Cameron, *Biomacromolecules*, 2009, **10**, 328–333.

36 C. J. Capicciotti, M. Leclere, F. A. Perras, D. L. Bryce, H. Paulin, J. Harden, Y. Liu and R. N. Ben, *Chem. Sci.*, 2012, **3**, 1408–1416.

37 A. Kwan, K. Fairley, P. I. Anderberg, C. W. Liew, M. M. Harding and J. P. Mackay, *Biochemistry*, 2005, **44**, 1980–1988.

38 H. Chao, P. L. Davies and J. F. Carpenter, *J. Exp. Biol.*, 1996, **199**, 2071–2076.

39 M. Marcellini, C. Noirjean, D. Dedovets, J. Maria and S. Deville, *ACS Omega*, 2016, **1**, 1019–1026.

40 A. Fowler and M. Toner, *Ann. N. Y. Acad. Sci.*, 2005, **1066**, 119–135.

41 G. Walsh, *Nat. Biotechnol.*, 2006, **24**, 769–76.

42 G. Seth, *Methods*, 2012, **56**, 424–31.

43 K. Brockbank and M. Taylor, *Adv. biopreservation*, 2007, **5**, 157–196.

44 M. Iwatani, K. Ikegami, Y. Kremenska, N. Hattori, S. Tanaka, S. Yagi and K. Shiota, *Stem Cells*, 2006, **24**, 2549–2556.

45 K. Kawai, Y.-S. Li, M.-F. Song and H. Kasai, *Bioorg. Med. Chem. Lett.*, 2010, **20**, 260–5.

46 P. Mazur, *Science*, 1970, **168**, 939–49.

47 P. Mazur, J. Farrant, S. P. Leibo and E. H. Chu, *Cryobiology*, 1969, **6**, 1–9.

48 X. Stéphenne, M. Najimi and E. M. Sokal, *World J. Gastroenterol.*, 2010, **16**, 1–14.

49 B. C. Heng, C. P. Ye, H. Liu, W. S. Toh, A. J. Rufaihah, Z. Yang, B. H. Bay, Z. Ge, H. W. Ouyang, E. H. Lee and T. Cao, *J. Biomed. Sci.*, 2006, **13**, 433–445.

50 Q. Xu, W. J. Brecht, K. H. Weisgraber, R. W. Mahley and Y. Huang, *J. Biol. Chem.*, 2004, **279**, 25511–6.

51 K. Matsumura and S. H. Hyon, *Biomaterials*, 2009, **30**, 4842–4849.

52 H. Geng, X. Liu, G. Shi, G. Bai, J. Ma, J. Chen, Z. Wu, Y. Song, H. Fang and J. Wang, *Angew. Chem. Int. Ed.*, 2017, **56**, 997–1001.

53 B. Stokich, Q. Osgood, D. Grimm, S. Moorthy, N. Chakraborty and M. A. Menze, *Cryobiology*, 2014, **69**, 281–290.

54 R. C. Deller, M. Vatish, D. A. Mitchell and M. I. Gibson, *Nat. Commun.*, 2014, **5**, 3244.

55 A. Doriti, S. M. Brosnan, S. M. Weidner and H. Schlaad, *Polym. Chem.*, 2016, **7**, 3067–3070.

56 S. Yamada, M. Goto and T. Endo, *Macromol. Chem. Phys.*, 2015, **216**, 1348–1354.

57 S. Yamada, A. Sudo, M. Goto and T. Endo, *RSC Adv.*, 2014, **4**, 29890–29896.

58 S. Yamada, S. Atsushi, M. Goto and T. Endo, *J. Polym. Sci. Part A Polym. Chem.*, 2013, **51**, 4565–4571.

59 S. Yamada, K. Ikkyu, K. Iso, M. Goto and T. Endo, *Polym. Chem.*, 2015, **6**, 1838–1845.

60 S. Yamada, K. Koga and T. Endo, *J. Polym. Sci. Part A Polym. Chem.*, 2012, **50**, 2527–2532.

61 S. Yamada, K. Koga, A. Sudo, M. Goto and T. Endo, *J. Polym. Sci. Part A Polym. Chem.*, 2013, **51**, 3726–3731.

62 Y. Shiraki, S. Yamada and T. Endo, *J. Polym. Sci. Part A Polym. Chem.*, 2017, **55**, 1674–1679.

63 Y. Kamei, A. Nagai, A. Sudo, H. Nishida, K. Kikukawa and T. Endo, *J. Polym. Sci. Part A Polym. Chem.*, 2008, **46**, 2649–2657.

64 Y. Kamei, A. Sudo, H. Nishida, K. Kikukawa and T. Endo, *J. Polym. Sci. Part A Polym. Chem.*, 2008, **46**, 2525–2535.

CHAPTER 3

Photo-activatable ice recrystallisation inhibitors

3.1 – Chapter Abstract

Antifreeze proteins (AFP) are capable of binding to specific planes of ice and are potent ice recrystallisation inhibitors (IRIs). Their activity is controlled though modulation of protein expression *via* light regulated expression systems, whereas when used in application areas the activity is 'always on'. This chapter outlines the development of a series of photo-activatable IRI inhibitors, and is the first reported method for such external control over AFP activity using a photo switch based on the photo-reversible dimerization of anthracene. Truncated peptide sequences based on the consensus repeat sequence from Type I AFPs (TAANAAAAAAA) were conjugated to an anthracene unit featuring a dilysine solubilising linker, and the conjugates dimerised with exposure to UV-light. Dimerization (causing a head to head coupling and hence breaking the peptide sequence, giving a mirrored stretch) reduced activity compared to the non-dimerized derivative. This proof of concept study shows a new route towards providing spatio-temporal control over antifreeze protein function, potentially providing a blueprint for the design of advanced materials with applications in cryosurgery and biomedicine.

3.2 – Chapter Introduction

Antifreeze proteins (AFPs) exist in the blood serum of a number of marine and insectoid species, in addition to plants, which inhabit extremely cold climates. Their presence has the remarkable effect of restricting ice crystal growth,[1] allowing species like the right-eyed flounder to survive without freezing solid in icy waters.

During the summer months (when the oceans are warmer), a gene circuit inhibits the synthesis of AFPs by the liver. As temperatures begin to fall in the autumn (and the ocean grows colder), the fish begin to require protection, and a drop in available sunlight results in the pituitary gland inhibiting the production of the growth hormone which prevents AFP gene transcription, facilitating AFP biosynthesis.[2] There is no simple way to gain localised, spatiotemporal control over AFP function in therapeutic applications, and providing 'on-demand' protection against ice crystal growth is inherently complex, but would be particularly desirable in numerous fields, such as cryosurgery.

The use of cryogens – such as liquid nitrogen and carbon dioxide – in biomedical procedures has long been established as a viable method for the localised destruction of diseased tissue, and 'Cryosurgery' is often used for the removal of unwanted growths; particularly moles, warts, and benign/malignant melanomas.[3] Cryotherapy also finds use in invasive medical procedures, specifically in the treatment of tumours and cancerous growths on organs such as the lungs, kidneys, and liver. In this context 'Cryoablation' destroys the malignant tissue through the induction of cell apoptosis, ice crystal growth (causing catastrophic cell damage), and the effects of freezing ultimately cutting shutting off the tissues blood supply resulting in tissue ischemia.[4,5] However, extensive damage to surrounding healthy tissues in both Cryosurgery and Cryoablation is a fundamental problem with the cryogenic approach. Many patients suffer varying levels of pain post-surgery and are prone to the formation of blisters and

scarring.[6] The ability to restrict or inhibit this surrounding tissue damage, however, would ultimately alleviate pain, limit the formation of unsightly scarring or skin defects, improve recovery time, and enhance patient compliance. Therefore, there is clear potential to develop an ice recrystallisation inhibitor which is capable of being selectively activated by an external, non-invasive, photo-stimulus to ensure that the surrounding tissues are protected from cold damage, restricting cryodamage to the diseased region, Figure 3.1. Light is a desirable trigger, as it has high spatial resolution and is easy to apply, and the wavelengths can be tuned as required. Such photo triggers have found wide application in areas such as hydrogels,[7,8] light triggered polymerizatinon[9–11] and even to gain control over gene level expression.[12,13]

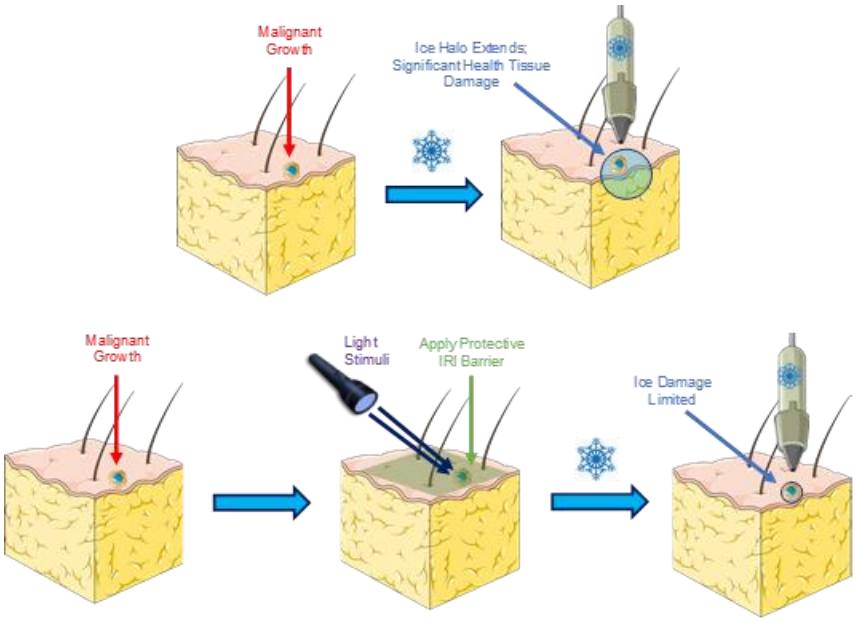

Figure 3.1 – Hypothesised protection of tissue through photo-controlled IRI.

There are very few examples of photo (or any stimulus) control of IRI activity, with Ben and co-workers reporting on the development of azobenzene derived carbohydrate (fluoro)surfactants which showed moderate, but significantly different, IRI activities between the isomerized derivatives.[14,15] Sonnischen and co-workers have demonstrated the use of azobenzene linkages to deform antifreeze proteins upon exposure to light, modulating their IRI activity.[16] Gibson and co-workers have used catechols to reversibly assemble polymeric IRIs

through co-ordination of Fe^{3+} ions, leading to pseudo-star polymers with increased activity.[17] However, this method does not enable remote control. Other than these isolated examples, there are no reports, to the best of our knowledge, of dynamically controllable IRIs. In contrast, there is vast literate on the use of photo-reactive units to control materials properties. Azobenzene has featured heavily in the literature as a biological photoswitch, Woolley and co-workers have comprehensively reviewed its deployment in this context.[18] Importantly, the ability to 'red-' or 'blue-shift' the photodimerization wavelengths of azobenzene's through aromatic functional group substitution is particularly important, allowing for application in sensitive biological systems where UV exposure would otherwise cause harm.

Most notably, azobenzene has found use in the photocontrol of the helical conformations and solution structures of several proteins and DNA, and has been applied to controlling protein cross-linking, DNA transcription, and protein activity.[16,19,20] Azobenzene incorporation into peptides has also provided for the artificial introduction of a β-like turn in normally a-helical structures through the application of a light stimulus.[18] This ability to order, and disorder, a protein was exploited by Aemissegger and co-workers, who demonstrated that the incorporation of an azobenzene motif could solicit the formation of a well defined β-hairpin solution structure of a peptide when in the *trans* conformation, whilst the protein-photoswitch conjugate promoted peptide oligomerization when *cis*.[21] Furthermore, azobenzene derived tethered ligands have also been applied to the selective activation and deactivation of biological receptors and ion channels, such as nicotinic acetylcholine,[22] potentially providing a therapeutic effect.

Similarly, anthracene derived species represent a second class of photo-triggers in biological molecules, as individual Anthracene units are capable of 'dimerizing' into a cycloaddition product upon exposure to UV light. Some previous applications have included the incorporation of anthracene into DNA binding proteins,[23] increasing protein binding affinity

when dimerized, whilst glycosylated anthracene derivatives have also shown promise as protein cleaving agents when irradiated.[24] More recently, anthracene modified DNA has demonstrated dissimilar binding towards complementary DNA strands when dimerized, illustrating the potential role of DNA duplex formation in the control of a photochromic system.[25] Intriguingly, despite anthracene chemistry being well established, the conjugation of anthracene to biological molecules is however heavily underexplored. To effect a similar molecular weight increase, anthracene's ability to undergo an on-water Diels-Alder [4+4] cycloaddition under UV irradiation represents an attractive mechanism,[26–28] resulting in a doubling of molecular weight for the AFP-conjugate species by the amalgamation of two distinct chains in solution. Similarly, the ability of some Safranine dyes to demonstrate IRI activity[29] – presumably through pi-pi stacking interactions – suggests that a small molecule with a conjugated aromatic system would likewise allow for supramolecular assembly in solution, and the induction of IRI activity. In addition, the 'on-water' effect – whereby certain reactions proceed at an accelerated rate in water – which is observed for Diels-Alder cycloadditions, would potentially allow for a reversible transformation in aqueous solution. This would provide for a tuneable, activatable/deactivatable photoswitch, allowing us to control *in-situ* IRI activity with exposure to UV light. Figure 3.2 As such, this chapter outlines the development of photo-switchable IRI inhibitors derived from truncated type I AFP peptides based on the consensus repeat sequence, which undergo photo-reversible dimerization by virtue of anthracene end groups, in order to modulate activity.

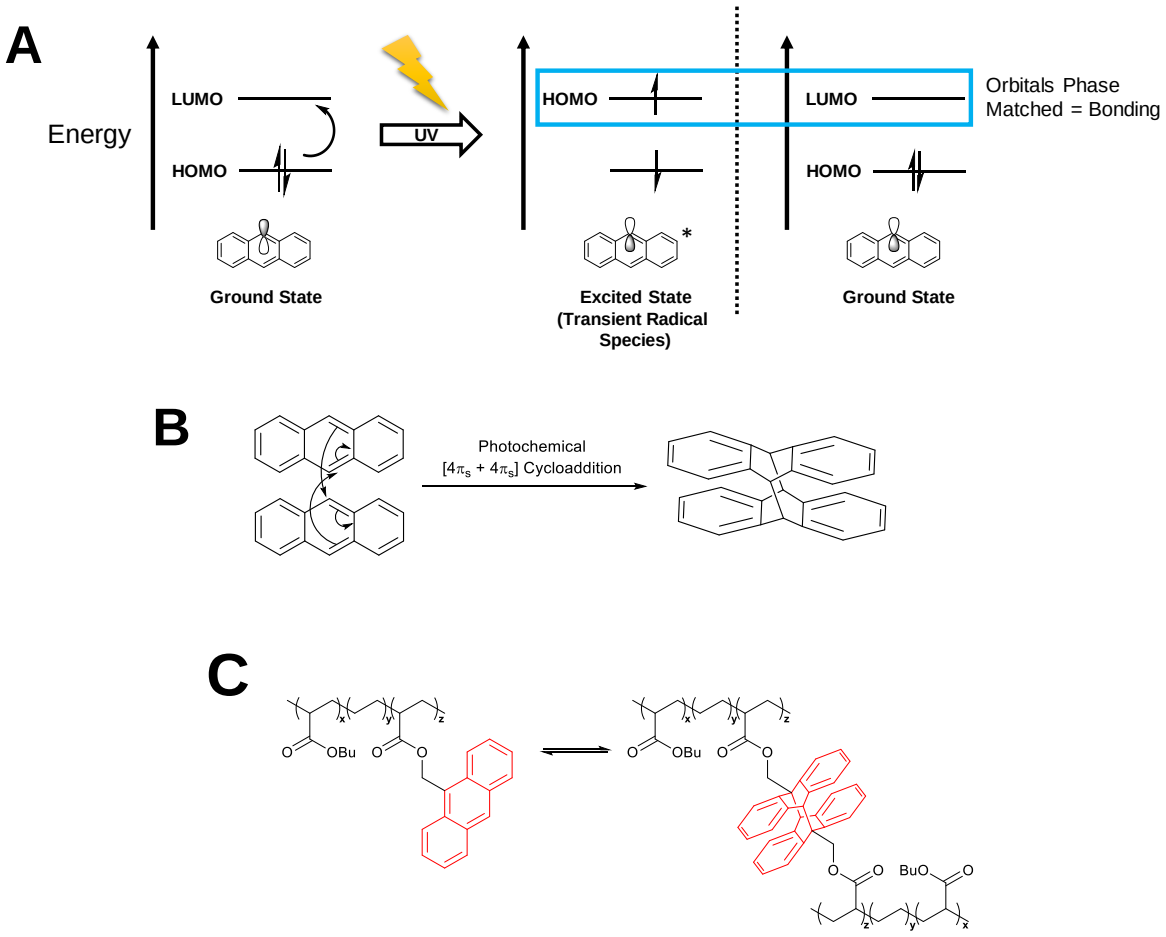

Figure 3.2 – A) Molecular orbital diagram showing the photolysis induced excitation of anthracene, resulting in; B) a concerted [$4\pi_s + 4\pi_s$] Diels-Alder cycloaddition of two anthracene units, forming a photodimer. C) Literature example of polymer cross-linking utilizing the anthracene/photodimer motif.[30]

3.3 – Results and Discussion

3.3i – Rational design and synthesis of the photoconjugates

A symmetrically functionalized anthracene derivative with peptide conjugation in the 9-position was devised (Figure 3.3), restricting the total number of possible photodimers to 2 and favouring the *ht* isomer, due to the steric hindrance of the protein chains disfavouring *hh*. Figure 3.3. In addition, this would allow for a 'linear' peptide sequence, running from end-to-end. Truncated 11 or 22-residue peptides based on the consensus 11-mer repeat sequence of a Type I AFP were obtained from solid phase peptide synthesis; TAANAAAAAAA.[31]

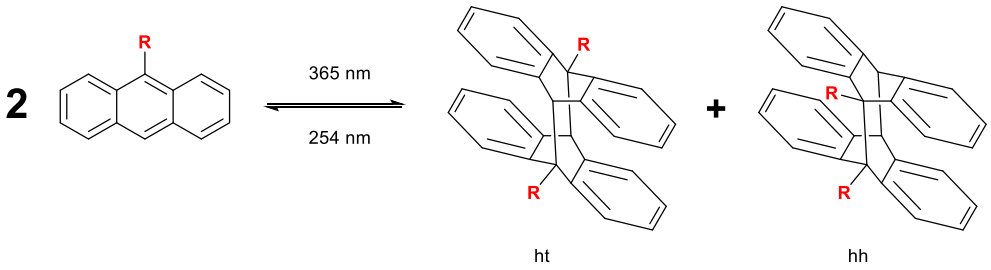

Figure 3.3 – Photodimerisation of anthracene rings under UV (365 nm) light, giving 2 photoproducts, where R is the peptide stretch (*N*-termini conjugated).

However, the high proportion of alanine in the Type I antifreeze protein (> 81 %) would, when conjugated to the hydrophobic anthracene framework, give poor aqueous solubility. Aggregation/micellization of the AFP would likely result in polar solvents, and could be expected to precipitate when dimerized in aqueous solution.

In order to avoid neutralization of activity and hydrophilic/phobic domain obfuscation, a polar di-amino acid spacing linker was introduced, to aid solubilisation. Figure 3.4. This would also act to prevent the steric bulk of the anthracene rings hindering the proximal threonine hydroxyl group of the bioconjugated protein – which has been hypothesised as necessary for AFP activity.

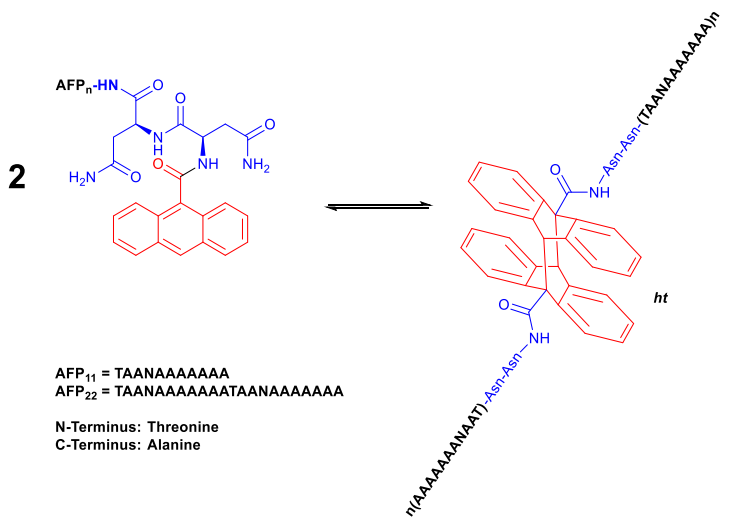

Figure 3.4 – Proposed monomeric and photo-dimeric products with asparagine (Asn) linkers.

Asparagine – as one of the most polar amino acids – was initially selected for its enhanced solubility, and a synthetic route to the monomeric photoresponsive unit designed, Scheme 3.1. Due to the presence of arginine in the 'variable' positions of some AFP Type I strains (*TAA*AAAAAAA),[31] including the species employed here, it was assumed that the introduction of this di-amino acid arginine linker directly before the protein would have no effect on AFP activity, and would be well tolerated.

However, as per Scheme 3.1, attempts to prepare the initial arginine-arginine dipeptide (Product **A**) failed. Mass spectrometry of the coupling product indicated a mass fragment of 466.7 m/z (Product **B** + H_3O^+ + 2 x Acetonitrile), with no observable fragments associated with the anticipated product and its mass of 402.21 g/mol^{-1}. Whilst the primary amide side chain of arginine is generally stable (including those internalised arginines present within the AFP chain), terminal arginines are however capable of undergoing dehydration under carbodiimide coupling conditions.

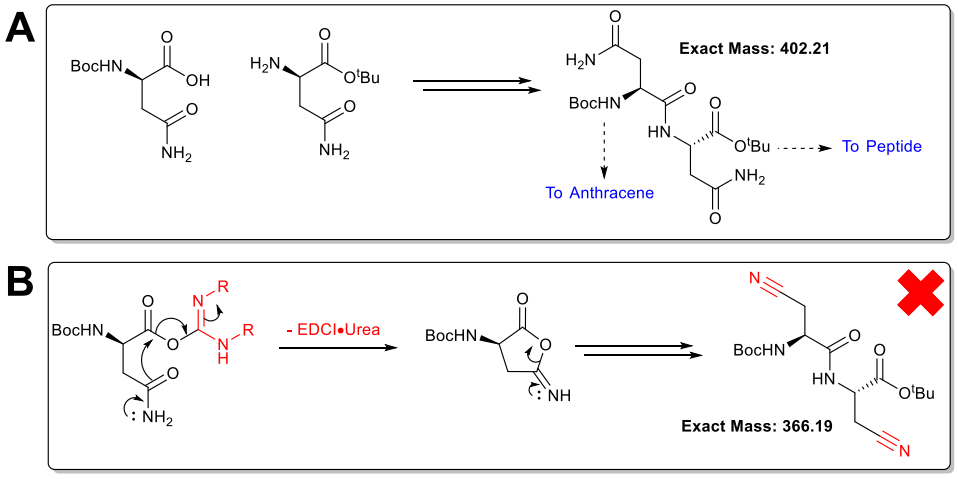

Scheme 3.1 – A) Attempted coupling of arginine derivatives. B) Intramolecular dehydration.

As such, the absence of the product by mass spectrometry made clear that unforeseen dehydration of the amide groups to nitriles had occurred, which upon acid exposure may have further oxidised to carboxylic acids and thereby complicated protein coupling. This warranted the substitution of arginine for a similarly polar amino acid, lysine, Scheme 3.2.

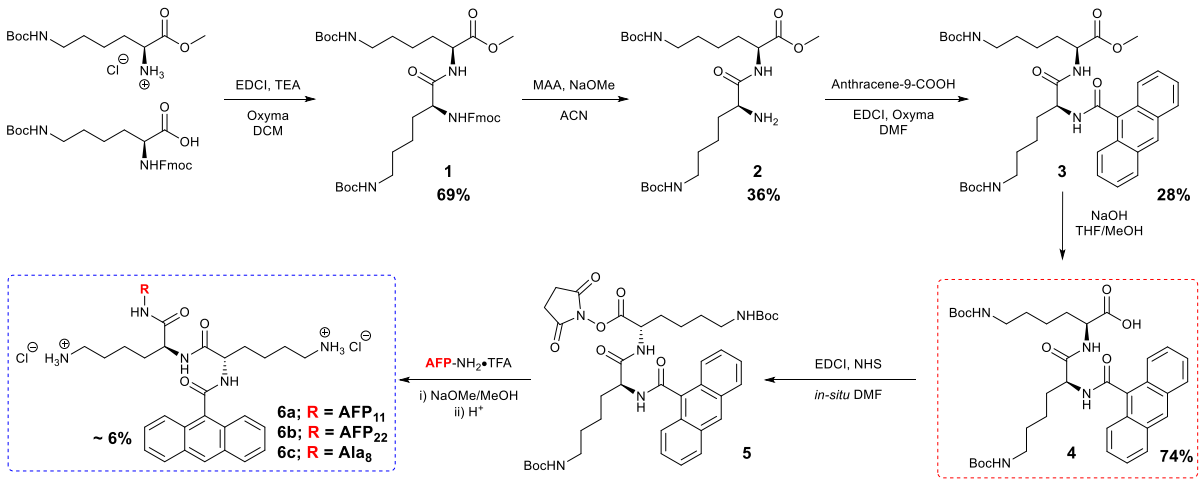

Scheme 3.2 – Optimised synthetic route for the synthesis of the anthracene-AFP conjugates, and prepared candidates (blue box). EDCI - 1-Ethyl-3-(3-dimethylaminopropyl)carbodiimide. TEA – Triethylamine. MAA – Mercaptoacetic acid. ACN – Acetonitrile. DMF – Dimethyl formamide. THF – Tetrahydrofuran. NHS – *N*-Hydroxysuccinimide. AFP-Antifreeze peptide. TFA – Trifluoroacetic acid.

Preparation of product **4** was expedient and simple. Removal of the Fmoc protecting group in the presence of a methyl ester to give intermediate **2** was achieved through the combinative use

of mercaptoacetic acid (MAA) and sodium methoxide (DBU is a viable non-nucleophilic alternative). The avoidance of secondary amines (usually used for Fmoc deprotection) prevented the inadvertent cleavage or amidation of the methyl ester, with the mercaptoacetic acid effectively scavenging the dibenzofulvene (DBF) by-product produced. The use of heat (50 ºC) is however essential, as this step will fail to proceed at room temperature (as observed by LCMS). Similarly, the conjugation of anthracene and lysine to give **3** fails to proceed in dichloromethane at both room temperature and at 60 ºC; and so DMF is required.

Prior to conjugating the antifreeze peptide to the photoresponsive unit, it was necessary to first estimate the overall solubility of the final AFP-photoconjugate. An alanine probe was therefore prepared. Although AFP Type I is water soluble, it has a defined secondary structure and is α-helical, despite being comprised of >70% alanine. Poly(alanine), however, is notoriously water insoluble, and has the propensity to form β-sheets. As such, it was necessary to ensure that the AFP-$(Lysine)_2$-Anthracene species would remain soluble when conjugated, despite the high proportion of alanine in the 11 and 22 residue stretches of AFP (>81%). By synthesising and conjugating poly(alanine), it would be possible to determine to model the solubility of the final conjugates. Scheme 3.3.

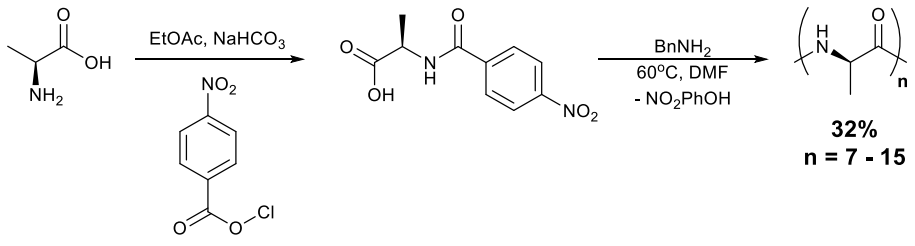

Scheme 3.3 – *In-situ* synthesis of poly(alanine) *via N*-Carboxyanhydride ROP.

Oligo alanine was obtained by the *in situ* ring opening polymerization of L-alanine *N*-carboxy anhydride (NCA). To enable NCA formation, the method of Endo *et al.*[32] was used whereby the carboxylic acid was activated by functionalisation with *para*-nitrophenyl chloroformate.

Subsequent addition of benzyl amine (as the initiator) in a [M]:[I] ratio of 0.4:1 led to the formation of the NCA, inducing ring opening polymerization. Poly(alanine) was isolated with a DP of 8, Mn of 790 $g.mol^{-1}$ and a low dispersity of 1.1 (likely resulting from fractionation during dialysis). This molecular weight was close to that of AFP_{11} and hence was suitable for initial studies.

Attachment of the poly(alanine) stretch to **4** was achieved by condensation coupling and the conjugate was observed by mass spectrometry at 1613.8 m/z (Experimental), and when deprotected, was soluble in aqueous solution at a concentration of 3.5 $mg.mL^{-1}$. This indicated that the similarly hydrophobic and alanine rich antifreeze peptides would likely have good solubility when conjugated. However, the conjugate was visibly aggregative in phosphate buffered saline, seemingly demonstrating better solubility when in saline alone (0.137 M NaCl), and hence saline was used for all subsequent IRI activity studies.

Attachment of the truncated antifreeze protein (e.g. AFP_{22}) to **4** was then performed, typically by the preparation of the *N*-hydroxysuccinimide ester, followed by NHS displacement by the *N*-terminus of the peptides. Due to the presence of threonine in the AFP peptide stretch, subsequent hydrolysis by sodium methoxide followed, as despite the unreactivity of threonine's α-alcohol group, it was necessary to ensure that it had not formed any unwanted ester linkages. The Boc groups were subsequently removed with hydrochloric acid to give the final products (**6a; AFP_{11} / 6b; AFP_{22}**) as the dihydrochloride salt, which were dialysed to remove low molecular weight contaminants, reacidified, and isolated as a solid salt. Mass spectrometry of the final AFP-22 conjugate indicated an absence of unconjugated protein (which possesses a high molecular weight, above the MWCO of the dialysis tubing), therefore indicating complete conversion.

Importantly, it was found that the dialysis bags continued to fluoresce under UV light (265 nm) after 72 hours, indicating retention of a high-molecular weight anthracene motif and thus indicative of successful conjugation. High resolution mass spectrometry of **6b** indicated the successful attachment of the peptide stretch, exhibiting several indicative fragments (Table 3.1), notably at 556.3 m/z (Mass + $4H^+$ + $2H_2O$). Furthermore, the free AFP_{22} peptide starting material (Appendix, 864.74 m/z) was no longer visible, Figure 3.5. High degrees of fragmentation were observed, given the many possible ions produced during the mass spectrometry of a protein.

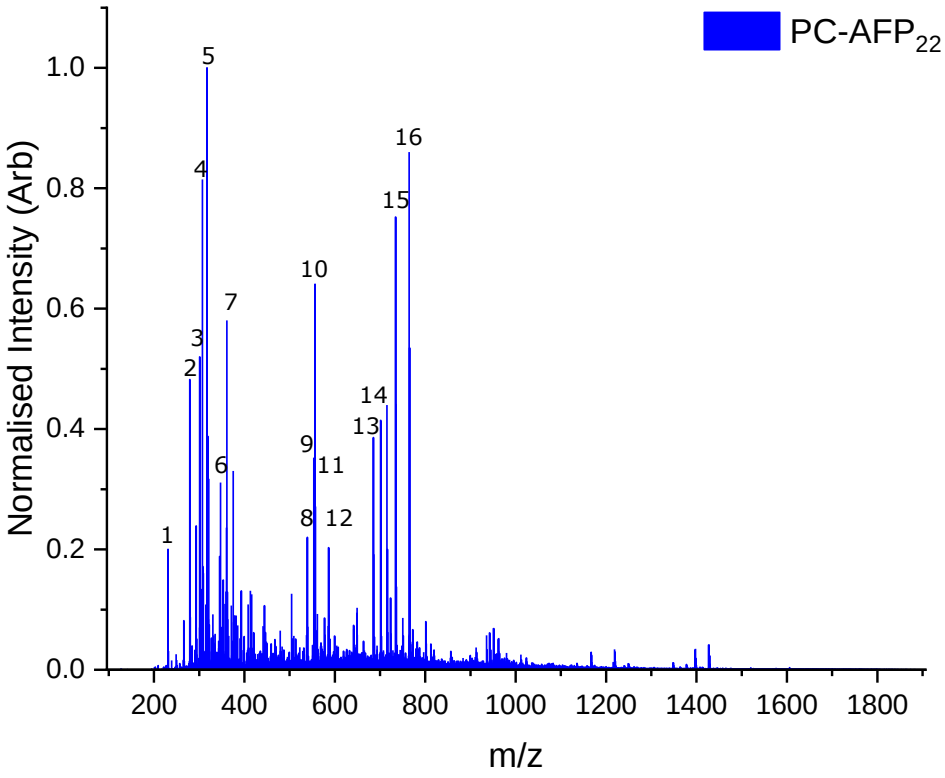

Figure 3.5 – Anthracene-AFP_{22} HR/LCMS spectra. Annotated signals in Table 3.1.

The low intensity / minor signals (< 0.2 Normalised Arb) in the 300 – 1100 m/z range are attributable to numerous γ and b fragments in numerous charge states, and are typical of a charged protein sample.

#	Proposed ion fragment/charge	$m/z_{(OBS)}$	$m/z_{(EXPECTED)}$	% Intensity
1	XKK^{2+}	231.0	231.2	20
2	$XKKT^{2+}$ (K Sidechains: $=NH2^{+}$)	279.2	280.1	48
3	$a_5^{+2} - H$	301.1	302.7	52
4	$b_5\text{-}H_2O^{+2}$	307.3	307.7	81
5	$XKKTA^{+2}$	317.3	317.3	100
6	b_9^{+3}	321.3	320.5	32
7	$b_{11}\text{-}H_2O^{+3}$	361.2	361.9	58
8	$a_{11}^{+2} - H_2$	539.3	537.3	22
9	$TAANAAA\text{-}H_2O$	553.5	553.3	35
10	$Anthracene\text{-}AFP_{22} + 4H^{+} + 2H_2O$	556.3	556.8	64
11	b_{18}^{+3}	557.3	558.0	27
12	b_{12}^{+2}	586.3	586.8	20
13	$b_6\text{-}H_2O$	685.4	685.4	39
14	$AAAAAAANA^{+}$	701.4	701.4	41
15	$b_{16}\text{-}H_2O^{+2}$	734.4 735.4	734.9	75 44
16	a_{17}^{+2}	764.4 765.4	765.4	86 53

Table 3.1 – $Anthracene\text{-}AFP_{22}$ HR/LCMS major fragments. X = Anthracene unit.

3.3ii – Characterisation and IRI activity of the photoconjugates

With the anthracene conjugates to hand, their photo-responsive behaviour could be explored. Figure 3.6 shows the UV-Vis absorption spectra of the unconjugated anthracene-dilysine dihydrochloride salt in both water and methanol. As per literature precedent, the classical anthracene multiplet in the UV-Visible 340 – 390 nm region, with $\lambda_{max} \approx 365$ nm, in both H_2O and MeOH.

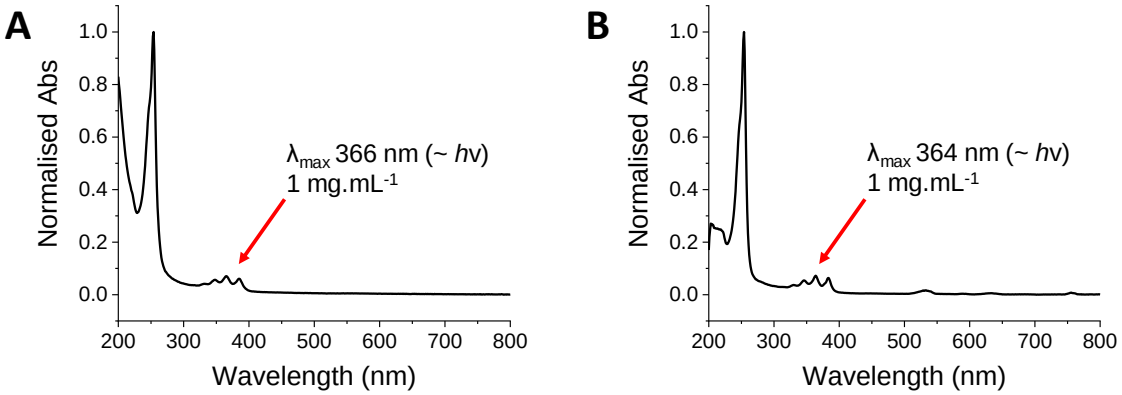

Figure 3.6 – UV-Vis Spectra of unconjugated anthracene-dilysine dihydrochloride in A) H_2O and B) MeOH.

In order to establish the extent of dimerisation upon irradiation and ensure complete formation of the photoproduct, UV exposure trials were then conducted, Figure 3.7. The anthracene-dilysine-poly(alanine) photoconjugate, **6c**, hereafter referred to as PC-Ala, was initially used to trial the photo dimerization processes. After 24 hour exposure of the PC-Ala in aqueous solution, to both a High Powered UV-CrossLinker and a Fibre Optic UV lamp (both at 365 nm), a complete loss of the multiplet in addition to the loss of the satellite peak at 255 nm was observed. This is consistent with cycloaddition induced dimerization of the anthracene motifs and provided proof of principle that the peptide conjugation does not inhibit this process due

to steric hindrance. This ultimately corroborates the concept and viability of the on-water photoswitch for IRI.

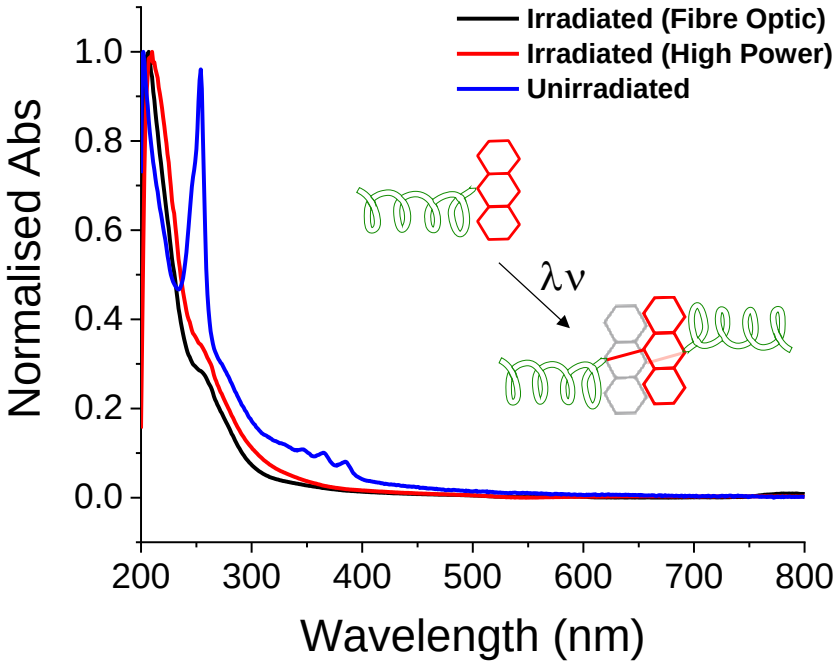

Figure 3.7 – Irradiation trials of the PC-Ala photoconjugate.

The two peptide candidates; **6a** (PC-AFP$_{11}$) and **6b** (PC-AFP$_{22}$) were subsequently irradiated in pure water under UV 365 nm light, and after 1 hour, complete conversion to the dimerised product was observed by UV-Vis spectroscopy, Figure 3.8. Complete loss of the triplet was again observed, in conjunction with a shift in the satellite peak. Importantly, when irradiated, no visible solution change occurred – ruling out inadvertent precipitation of the photo product dimer, which would otherwise impact upon concentration.

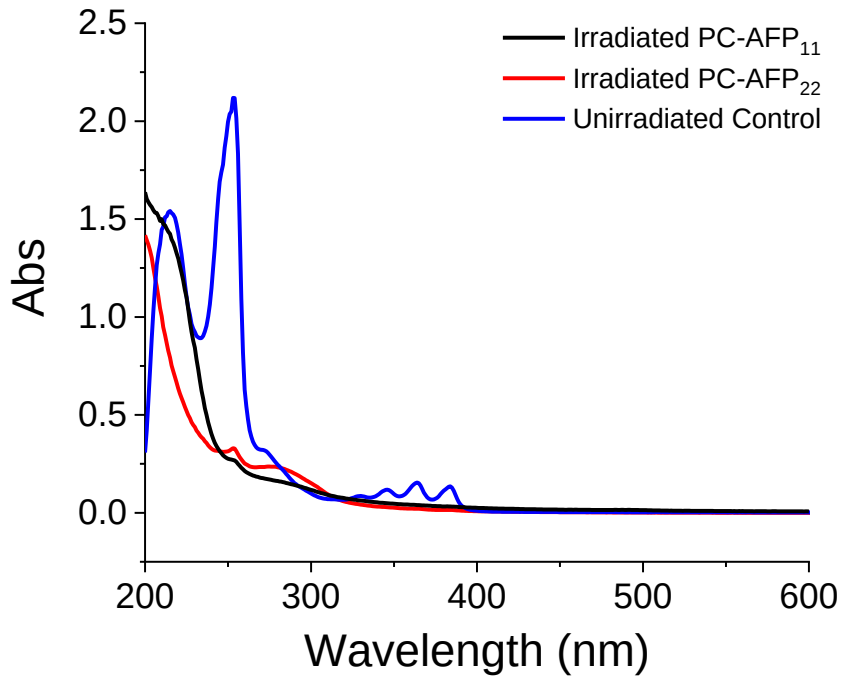

Figure 3.8 – Irradiation effect upon the UV-Vis spectra of the Anthracene-AFP photoconjugates.

Fluorescence analysis of the PC-AFP_{22} species further exhibited a 72% decrease in 360/40 nm emission post irradiation, further indicating successful dimerisation. Mass spectrometry monitoring of the photo-dimerization process showed complete removal of the undimerised monomers, but no peaks associated with the dimer products were observed. Therefore, HPLC was used. HPLC analysis of the PC-AFP_{22} in its dimerised state relative to an undimerised 9-ACA control, Figure 3.9, indicated the presence of the dimeric form only (without prominent secondary signals), as corroborated by literature confirming that a photo-driven process can be used to control the size of the AFP conjugates.[33,34]

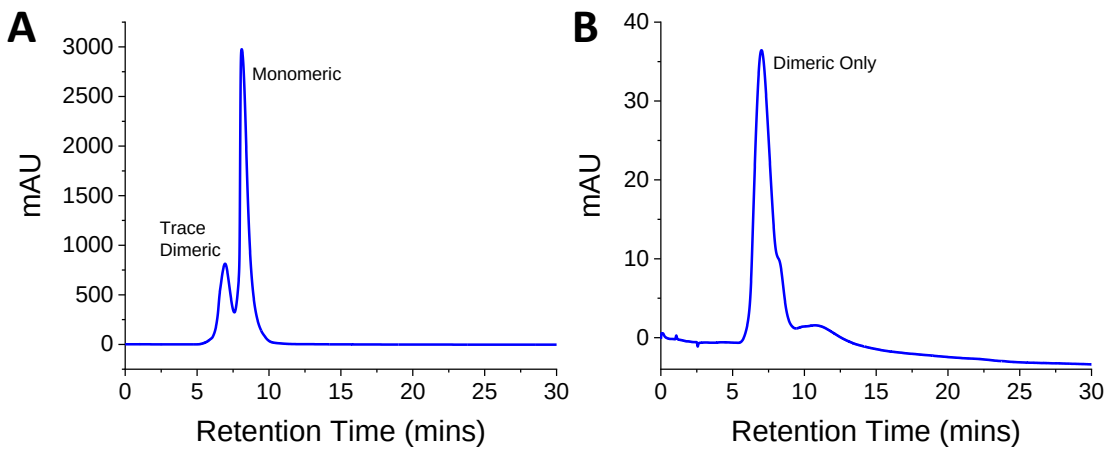

Figure 3.9 – HPLC Spectra of A) 9-ACA Control; and B) PC-AFP$_{22}$ (6b) Dimer at 213 nm.

Circular dichroism (CD) spectroscopy was employed to further investigate the dimerization process. Figure 3.10. Free AFP$_{11}$ showed a small degree of β-sheet character, as suggested by fitting analysis (ESI) and corroborated by literature,[35] as would be expected for a short alanine-rich stretch. Free AFP$_{22}$ was closer in nature to an α-helix (peak at 222 nm) which is seen for full length Type I AFP. These differences in secondary structure are crucial to understanding the observed IRI activity (discussed below). When conjugated to the anthracene-dilysine, the PC-AFP$_{22}$ monomer had similar features to the free peptide but showed slight shifting and a stronger inclination in the second band at ~ 235 nm, implying some deviation in the secondary structure as a result of the attachment of the anthracene unit. This is possibly a result of helical seeding by the lysine residues and/or contributions from the aromatics in the 190 – 200 nm region. When irradiated with UV light (to induce dimerization), the same PC-AFP$_{22}$ species lost its CD signature but retained a slight inclination of its former (unirradiated) signal morphology. Given the system possesses a central chromophore which is geometrically achiral, it is possible that it only has a small electronic chirality arising from coupling with the peptide chromophores, as a result, the induced CD could be expected to be comparatively small – further corroborating dimerisation.[36]

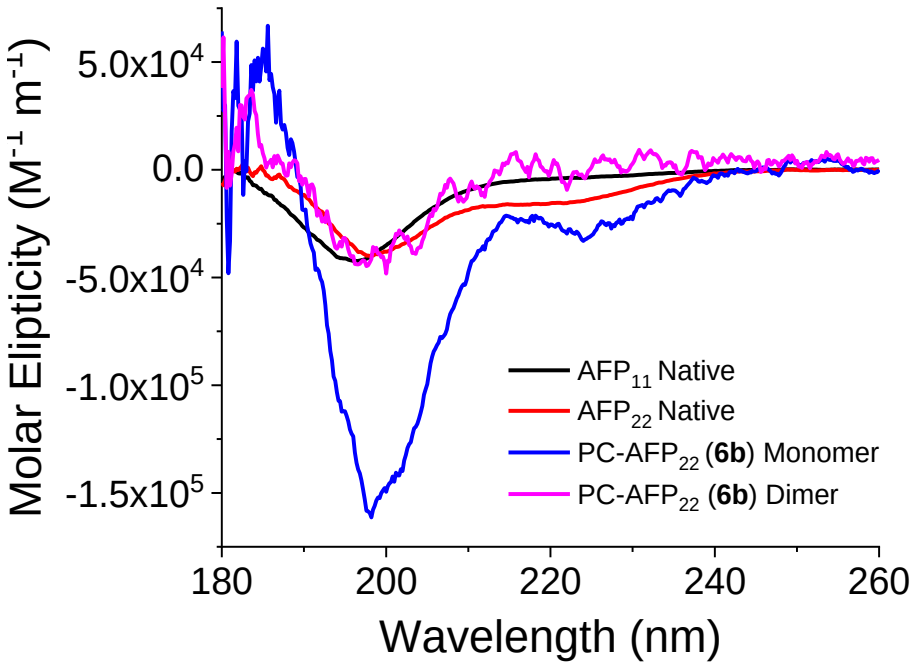

Figure 3.10 – CD Spectra of Anthracene-AFP Conjugates in H_2O.

With the photo-controlled dimerization process confirmed, the peptides were then evaluated for IRI activity. IRI activity was determined by the 'splat' assay, whereby a polynucleated ice wafer is annealed at – 8 °C, and the average crystal size determined after 30 minutes. Smaller crystal sizes indicate greater activity.

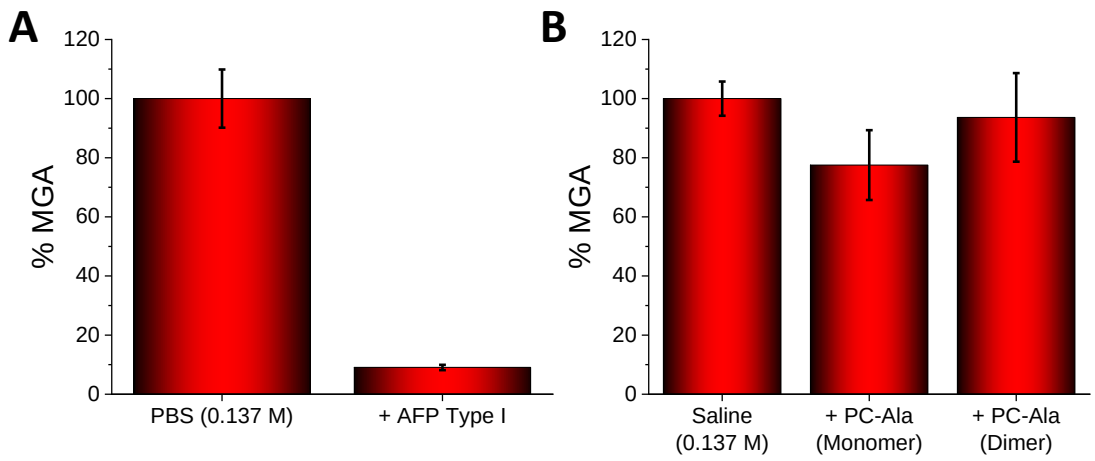

Figure 3.11 – A) Effect upon PBS ice crystal size of AFP Type I (2 µg.mL^{-1}). B) Effect upon saline ice crystal size by the PC-Ala photoconjugates (both at 3.5 mg.mL^{-1}). IRI activity measured as a function of solute concentration. MGA = Mean grain area relative to a PBS or saline control, expressed as %. Error bars represent the ± standard deviation from three independent measurements.

In comparison to type I antifreeze protein (Figure 3.11A) – a naturally occurring AFP with significant potency at very low concentration (9% MGA at 2 µg.mL^{-1}) – it was found that the negative control – PC-Ala – had essentially no activity (and was statistically similar) in both the monomeric and dimerised states at 3.5 mg.mL^{-1}, exhibiting > 80 % MGA at its upper limit (Figure 3.11B). This confirmed that the anthracene-dilysine motif conjugated to a homopeptide had no intrinsic IRI activity (in spite of its amphipathy)[37,38,39], and this alanine conjugate was therefore employed as a negative control. In contrast to AFP type I, which is comprised of 40 residues (sequence; DTASD(A)$_7$T(A)$_{10}$TAKAAAEAAAATAAAAR), the simplified free antifreeze peptides of 22 and 11 residues (repeat sequence; TAANAAAAAAA) were both found to have no activity in solution at their solubility limits of 0.9 and 1 mg.mL^{-1}, respectively. Figure 3.12.

Similarly, when conjugated to the anthracene-dilysine photounit, the PC-AFP$_{11}$ species showed no activity in either the monomeric or dimeric state (solubility limit 1 mg.mL^{-1}), and was statistically worse than PC-Ala control. This is ultimately unsurprising, given that it has been

previously reported that simply attaching (supposedly IRI active) proteins to nanoparticles or other central cores does not increase IRI activity.[40,41–43]

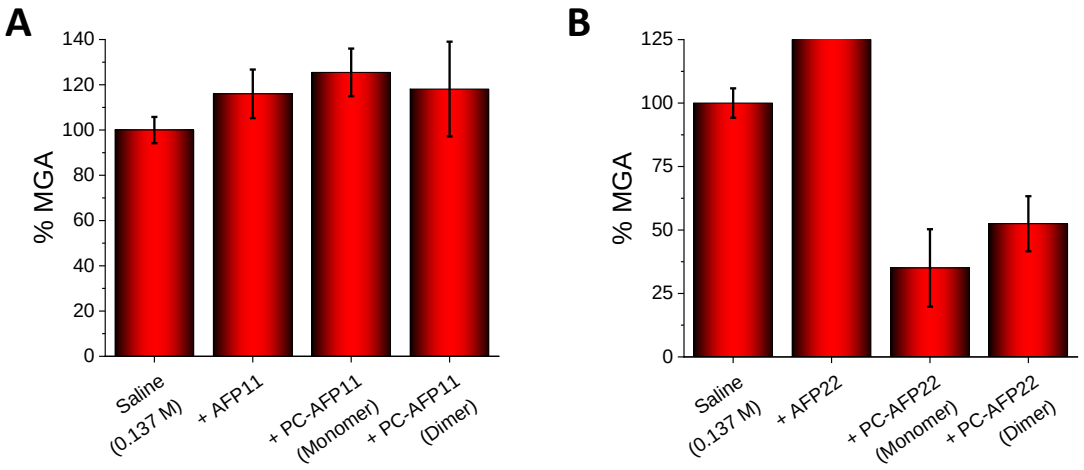

Figure 3.12 – A) Effect upon saline ice crystal size of the native AFP_{11} and $PC\text{-}AFP_{11}$ derivatives (both at 1 $mg.mL^{-1}$). B) Effect upon saline ice crystal size of the native AFP_{22} (0.9 $mg.mL^{-1}$ – giving very large crystals) and $PC\text{-}AFP_{22}$ derivatives (at 0.6 $mg.mL^{-1}$). IRI activity measured as a function of solute concentration. MGA = Mean grain area relative to a PBS or saline control, expressed as %. Error bars represent the ± standard deviation from three independent measurements.

Intriguingly, despite the clear lack of IRI activity for $PC\text{-}AFP_{11}$ and PC-Ala – and free AFP_{22} in and of its self – conjugation to give $PC\text{-}AFP_{22}$ resulted in appreciable IRI activity being observed. At its solubility maximum of 0.6 $mg.mL^{-1}$ the monomeric candidate exhibited 35% MGA, this potentially represents the first example of an AFP having its activity regulated by the addition of an end group. As for full length AFPs, addition of fusion proteins (e.g. as a large end-group) results in no change in activity,[44] and the same is observed for double hydrophilic blocks of poly(vinyl alcohol).[45] This potency eclipses the observed activity reported for the optimised poly(Fulvo-*co*-Diol) 17 kDa species previously reported by us,[46] representing a highly potent IRI inhibitor at sub-milligram concentrations, and is comparable with the activity of shorter chains of PVA (n=56) – Figures 3.13 and 3.14 (Data set provided by Congdon and co-workers).[47] This onset of IRI activity maybe associated with the secondary structure of the

free AFP_{22} in-particular, which when coupled with the large bulky anthracene hydrophobic domain – and the associated lysine units – has seeded a particularly amphipathic conformation and a stabilised secondary structure (optimised for ice face interaction).

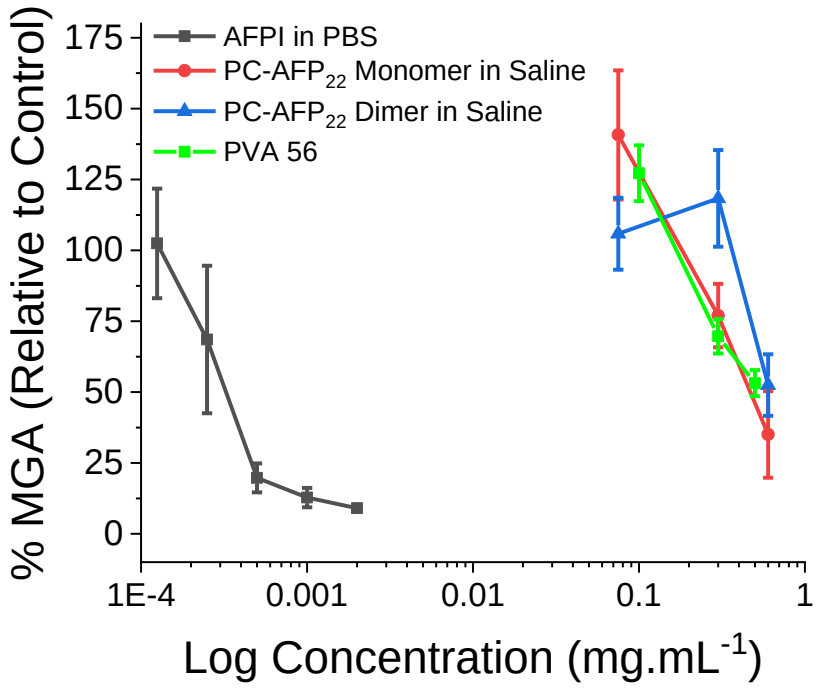

Figure 3.13 – Comparative % MGA of AFP Type I and the anthracene-AFP_{22} derivatives, relative to PVA 56. IRI activity measured as a function of Log solute concentration. MGA = Mean grain area relative to a PBS control, expressed as %. Error bars represent the ± standard deviation from three independent measurements.

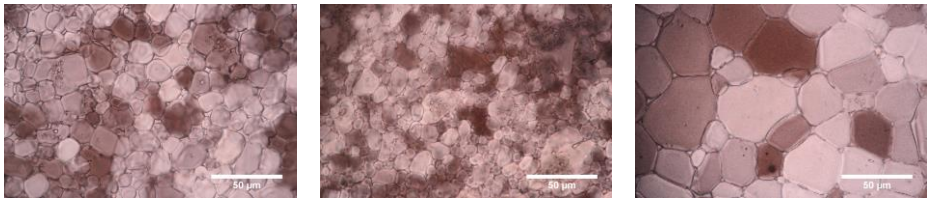

(TAANAAAAAAA)$_2$(22)
0.6 mg.mL^{-1}
Dimerised

(TAANAAAAAAA)$_2$(22)
0.6 mg.mL^{-1}
Unimerised

(TAANAAAAAAA)$_2$(22)
0.9 mg.mL^{-1}
Free Peptide

Figure 3.14 – Comparison between the undimerised and dimerized anthracene-AFP$_{22}$ conjugates and free AFP$_{22}$.

Photodimerisation however, leading to a head-to-head peptide orientation, had a very weak effect on the IRI activity of the PC-AFP$_{22}$ candidate. Despite dropping to 52 % MGA post-irradiation, the data was statistically identical to the monomer, with both candidates losing their effect completely below 0.3 mg.mL^{-1} – indicating a very narrow activity window.

In order to determine the structural phenomenon responsible for inferring IRI activity upon the PC-AFP$_{22}$ series, attempts were made to elucidate solution structures of the candidates.

Due to the perceived ability of the monomeric candidates to undergo pi-pi stacking interactions, potentially forming a supramolecular architecture in solution, dynamic light scattering (DLS) experiments were employed. Table 3.2.

Sample (Saturated in H_2O)	Averaged Z-Avg (d.nm)	Averaged Counts
PC-AFP$_{22}$ Undimerised (0.6 mg.mL^{-1})	1352.0	8454.2
PC-AFP$_{22}$ Dimerised (0.6 mg.mL^{-1})	1680.7	267.6
Native AFP$_{22}$ (0.9 mg.mL^{-1})	1259.0	132.4
Native AFP$_{11}$ (1.0 mg.mL^{-1})	392.6	229.2

Table 3.2 – DLS Data for the PC-AFP$_{22}$ photoconjugates.

The free AFP$_{22}$ peptide was found to have a larger diameter in comparison to the free AFP$_{11}$, which may be consistent with a helical (and therefore more spherical) species versus a planar

β-sheet. Both PC-AFP$_{22}$ species had proximal Z-averages, with the dimerised derivative showing a slight increase which would be expected of the larger unit. However, interestingly, the undimerised equivalent shows a very large counts recording of around 8500 versus 270 for the dimer. As a fit of the number of objects 'hit' by the laser, this may indicate that there are a very large number of monomer units in close proximity in solution. This may indicate the formation of fibres in solution as a result of pi-pi stacking interactions, which would be impacted in the photodimer. In order to further investigate the possibility of fibre formation in solution, attempts to analyse the solution structure of the PC-AFP$_{22}$ species by Small-angle X-Ray Scattering (SAXS) were ultimately unsuccessful. The low saturated solution concentration of the photoconjugate fell below the detection limit of the instrument (Figure 3.15).

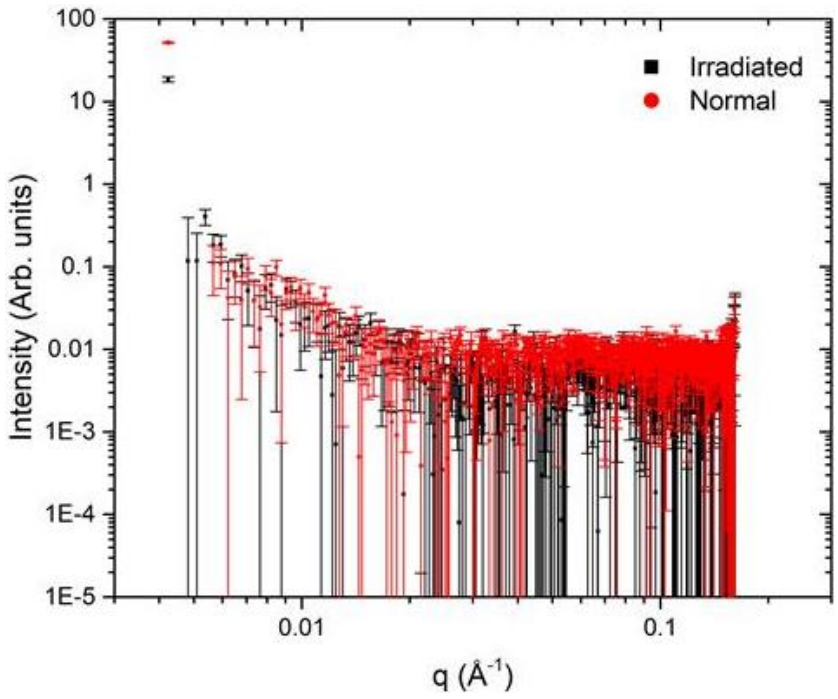

Figure 3.15 – SAXS Data of the AFP$_{22}$-PC irradiated and unirradiated samples, after background buffer subtraction. Performed and Graphed by Dr. Steven Huband.

Similarly, low temperature wide-angle x-ray scattering (WAXS) studies further failed to signify any difference between the two samples (Figure 3.16). Hexagonal ice was formed during the freezing of our control sample (saline) and this was compared to the ice formed

when the irradiated and non-irradiated samples were frozen, potentially indicating differences in the structures of the ice produced. This would have allowed us to infer information on potential supramolecular ordering of the photoconjugates.

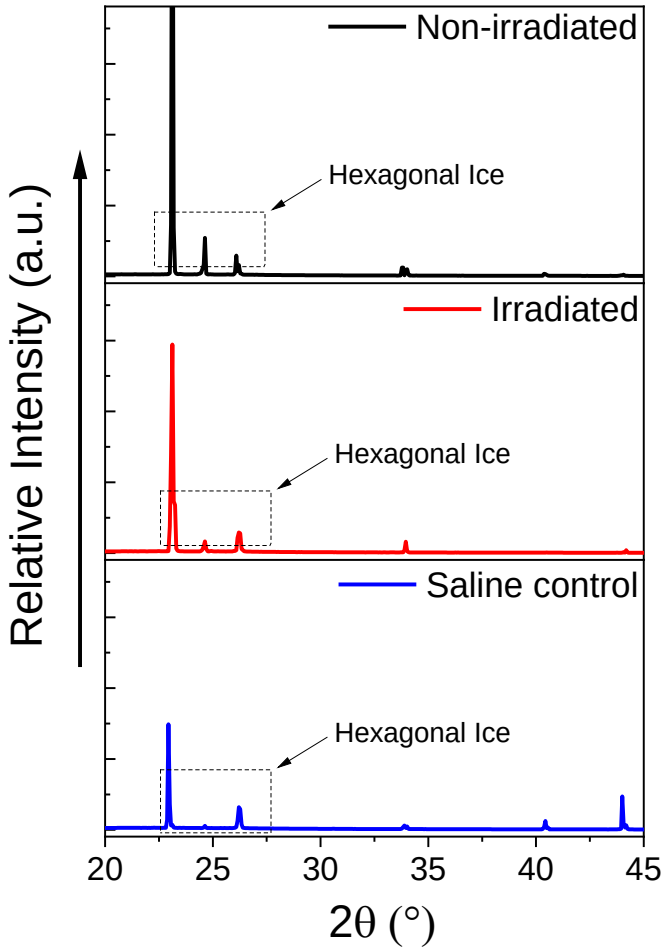

Figure 3.16 – Low temperature WAXS X-Ray diffraction patterns between the frozen irradiated and unirradiated PC-AFP$_{22}$ species at the saturated concentration versus a saline control. Performed and Graphed by Alice E. R. Fayter.

However, the diffraction patterns of the two samples are effectively identical, and both resemble hexagonal ice, similar to the control. Peaks are present at the same (characteristic) angles for each sample (22.75 °, 24.6 °, and 26 °, corresponding to ice faces 100, 002, 101, respectively). As such, differences between the samples could not be determined by X-ray

scattering. The differences in intensity between the samples can be attributed to a percentage of the crystallites orienting to diffract the X-ray beam.

3.3iii – Synthesis, characterisation, and IRI analysis of poly(vinyl alcohol) photoconjugates

Preparation of poly(vinyl)alcohol derived candidates was also pursued. It was hypothesised that, as the most potent synthetic IRI species discovered to date, incorporating PVA into the photoconjugate architecture may provide another exploitable avenue for activatable IRI activity, and may permit tuning of PVAs potency.

Due to the similarity in IRI activity with PVA_{56}, and in order to compare the activity of these protein-conjugates with a polymer-conjugate, a ~ DP11 stretch of poly(vinyl)alcohol was to be conjugated to the photoconjugate motif in the same manner. It is well established that a DP20 stretch of PVA is IRI active, with activity 'off' below DP14.[48] As such, we hypothesised that the formation of a dimer through photoirradiation would result in the formation of a contiguous DP22-stretch of PVA from 2 x (inactive) DP11 units, and would potentially result in activatable, potent, IRI activity with a greater on/off activity gap.

Initially, $PVAc_{11}$-NHS was acquired and the NHS group displaced by 1-amino-3-azido-propane, to give a reactive azide tether. **4** was functionalised with a complementary alkyne unit. Despite literature precedent, attempts to prepare candidate **8** were however hindered by the failure of the alkyne-azide click reaction between $PVAc_{11}$-$NH_2(CH_2)_3N_3$ and **7** to proceed, Scheme 3.4, and no product was observed, with **7** remaining visible by LCMS.

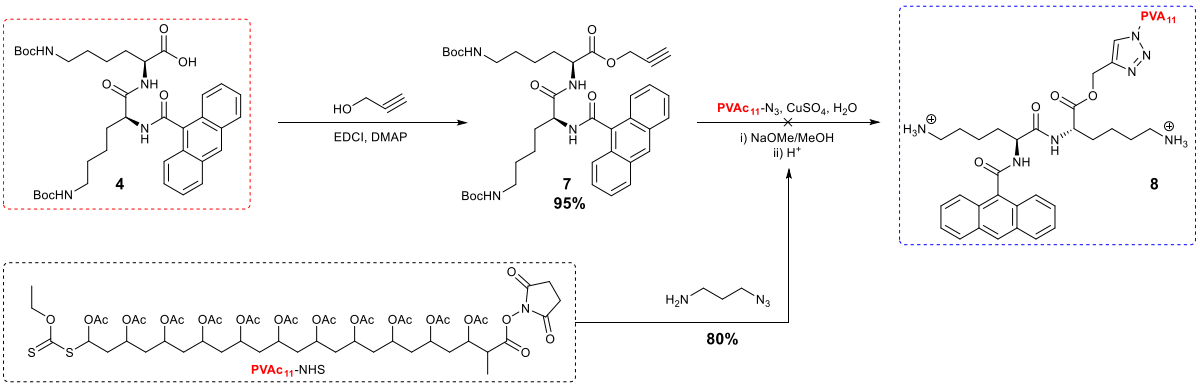

Scheme 3.4 – Attempted azide-alkyne 'click' to prepare the Anthracene-PVA Derivative.

A revised synthetic route was subsequently devised, Scheme 3.5. $PVAc_{11}$-NHS was instead functionalised with *tert*-butyl (2-aminoethyl)carbamate, and the Boc group subsequently removed, yielding a free primary amine. This allowed for direct conjugation to the photoconjugate motif in the same manner as the AFP candidates.

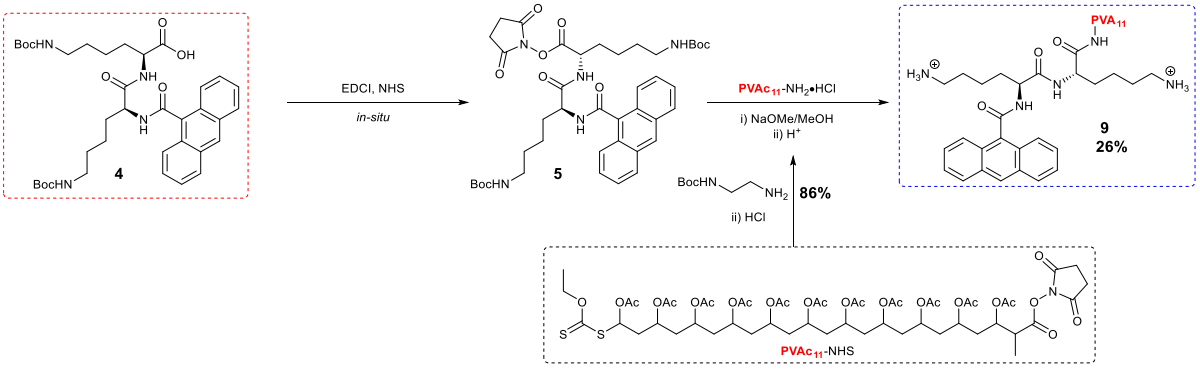

Scheme 3.5 – Revised synthetic route to the Anthracene-PVA Derivative.

As previous, **9** (PC-PVA) was subsequently dialysed, reacidified, and reduced to a solid salt, in 25% yield. It was again found that the dialysis bags continued to fluoresce under UV light (265 nm) after 72 hours, indicating retention of a high-molecular weight anthracene motif and thus indicative of successful conjugation. High resolution mass spectrometry of PC-PVA again indicated the successful attachment of the PVA stretch, exhibiting numerous fragment ions (Figure 3.17 and Table 3.3). Furthermore, the free $PVAc_{11}$-NH_2 starting material was no longer visible, with loss of the characteristic Gaussian Distribution of PVAc fragments.

The mass of broad, low intensity / minor signals (< 0.2 Normalised Arb) in the 200 – 2000 m/z range are attributable to the unprotected PVA fragments which fly poorly.

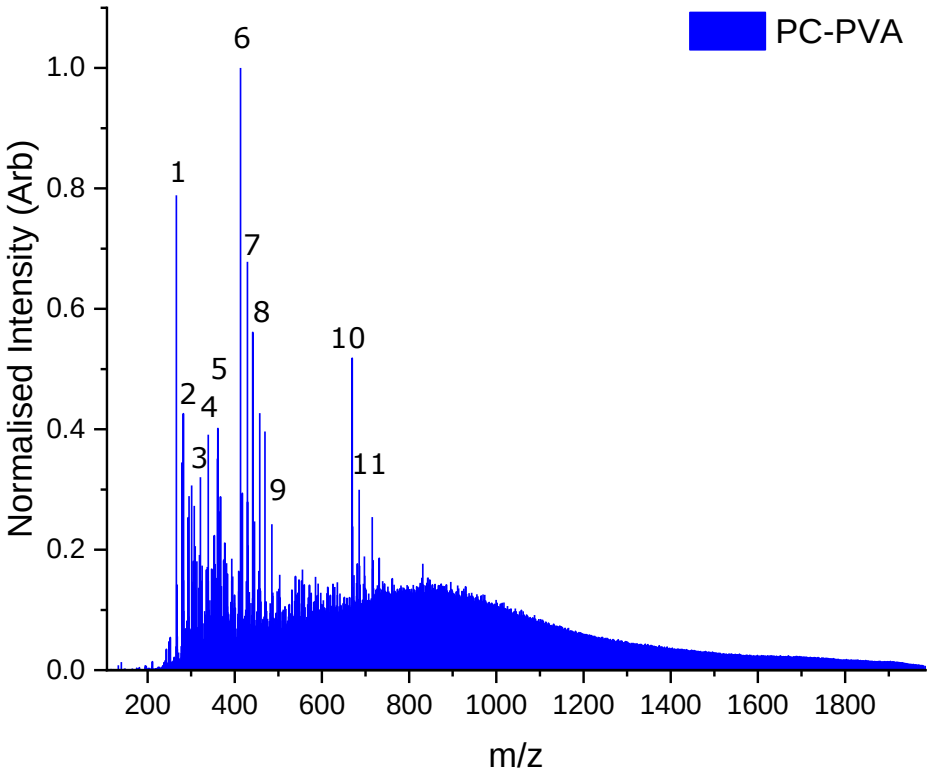

Figure 3.17 – Anthracene-PVA HR/LCMS spectra. Annotated signals in Table 3.3.

#	Proposed ion fragment/charge	m/z(OBS)	m/z(EXPECTED)	% Intensity
1	$HSHCOH(PVA)_5^+ - H_2O$	266.2	266.1	79
2	$XKK(Z)^{+2}$ (Na)	282.2	282.6	43
3	$HSHCOH(PVA)_5^+$ (K)	321.2	322.1	32
4	$XKK(Z)(PVA)_1^{+2} – H_2O$ (K)	339.2	339.6	39
5	$XKK(Z)(PVA)_2^{+2} – H_2O$ (K)	361.2	361.6	40
6	$XKK(Z)(PVA)_4^{+2}$ (K)	413.3	414.7	100
7	$XKK(Z)(PVA)_6^{+2}$ (H_3O^+)	429.2	429.8	68
8	$HSHCOH(PVA)_7^+$ (H^+) – H_2O	441.3	442.2	56
9	$HSHCOH(PVA)_{10}^+$ (H^+) – H_2O	485.3	486.2	24
10	$XKK(Z)(PVA)_3^+$ (Na) – H_2O	669.4	668.4	52
11	$XKK(Z)(PVA)_2^+$ (Na)	685.3	686.4	30

Table 3.3 – Anthracene-PVA HR/LCMS major fragments. X = Anthracene unit, Z = Linker.

As per previous, PC-PVA was irradiated in pure water under UV 365 nm light, and after 1 hour, complete conversion to the dimerised product was observed by UV-Vis Spectroscopy, Figure 3.18. Again, no visible solution change occurred.

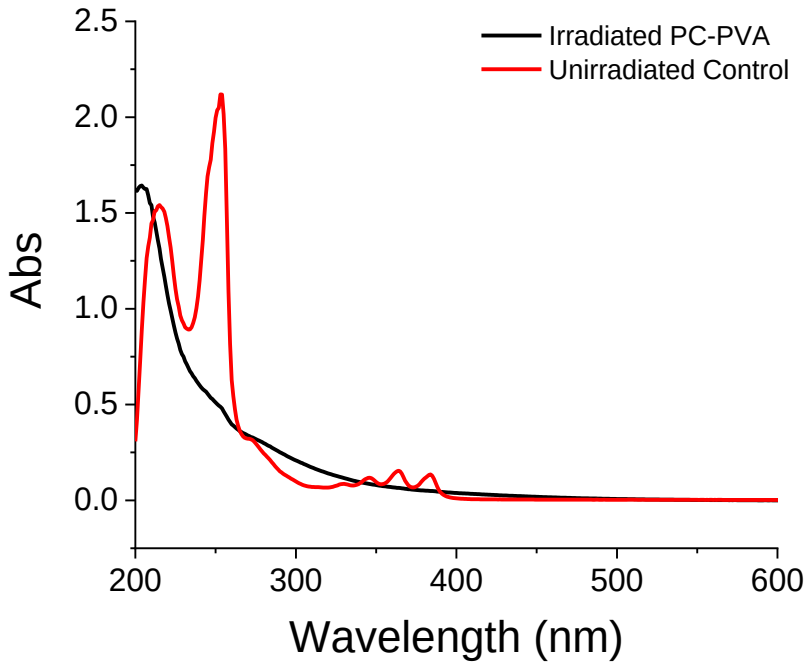

Figure 3.18 – Irradiated PC-PVA Photoconjugate.

Dimerisation was further confirmed by HPLC (Figure 3.19), as above, with only the dimeric species observed.

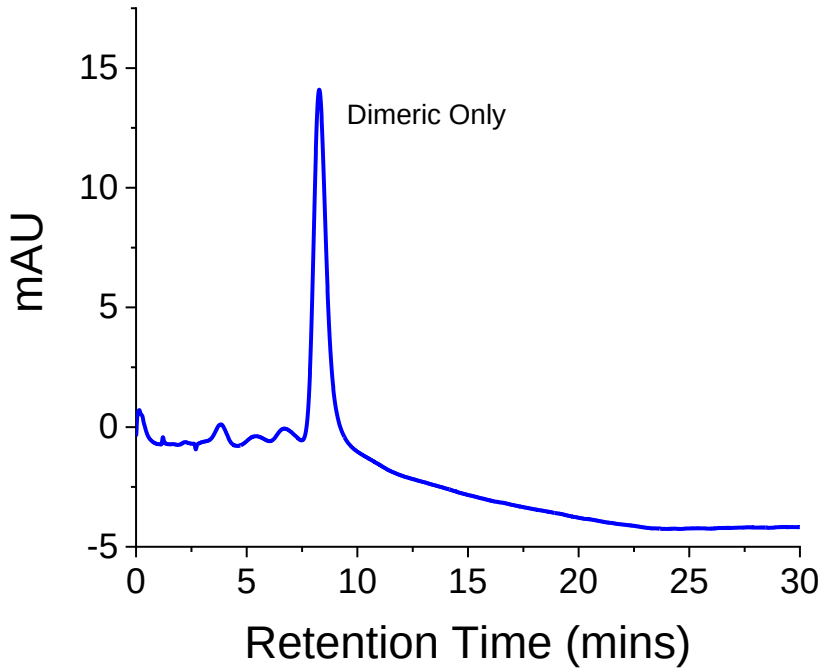

Figure 3.19 – HPLC Trace of Dimerised PC-PVA Photoconjugate at 213 nm. Control in Figure 3.9A.

The dimerised PC-PVA demonstrated a less significant 36% decrease in 360/40 fluorescence after irradiation, but had markedly lower initial fluorescence intensity as the monomer. When also coupled with the weaker intensity of the anthracene 'triplet' banding of the PC-PVA candidate (compared to the PC-AFP_{22}) by UV spectroscopy, Figure 3.20, this points towards the well-established phenomenon of fluorescence quenching, which is associated with PVA.

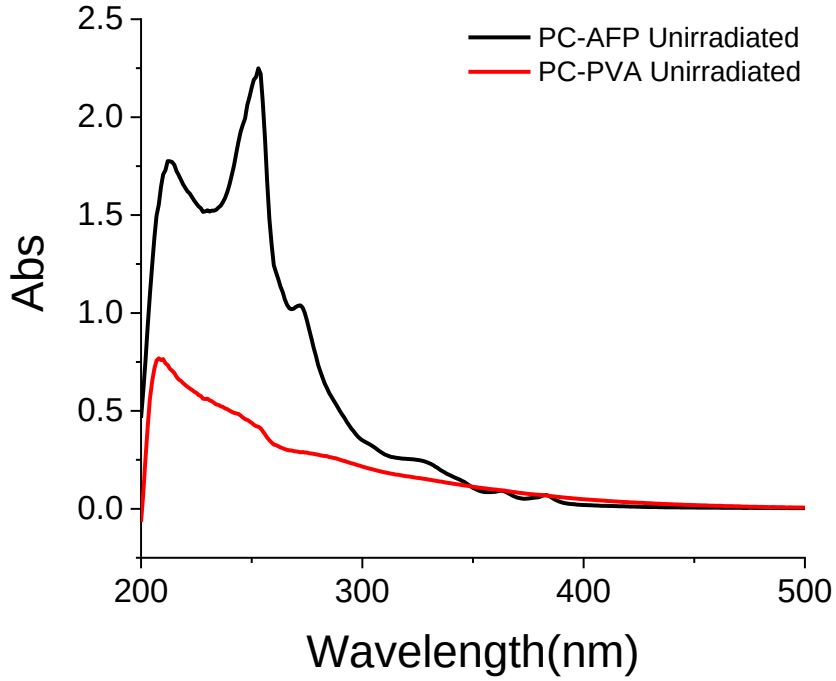

Figure 3.20 – Comparison of Unirradiated PC-AFP$_{22}$ and PC-PVA Photoconjugates.

However, activity was ultimately disappointing. It was clear that whilst possessing greater solubility (of the order of 5.7 mg.mL^{-1}), these species did not hold any meaningful IRI activity, with crystals in the presence of the undimerised candidate consistently ~ 70 – 80% of their original size across the concentration range. Dimerisation resulted in generally weaker activity, and at lower concentration, seemingly resulted in the growth of ice crystals above and beyond PBS alone. Figure 3.21.

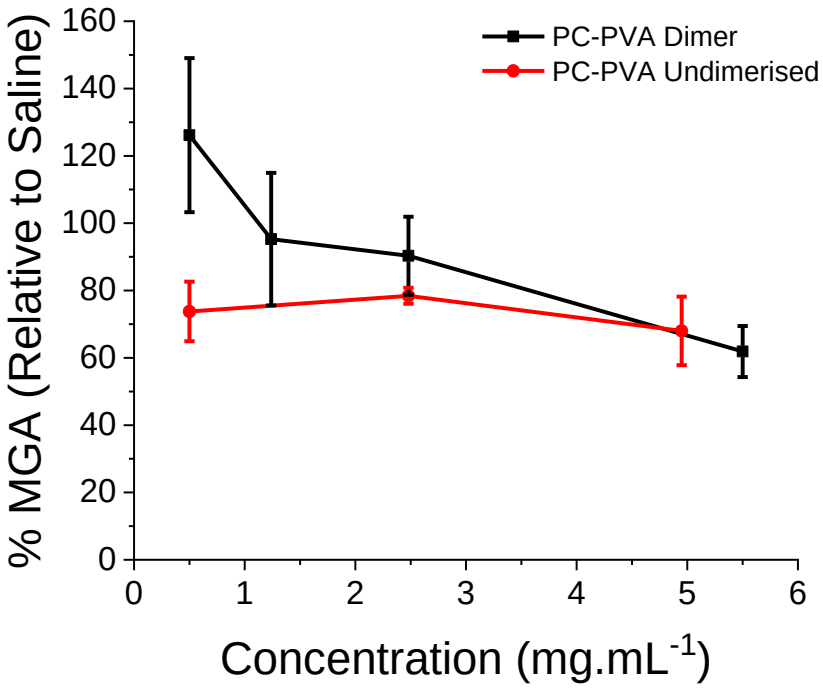

Figure 3.21 – 'Splat' Assay of the dimerised and undimerised PC-PVA photoconjugate. IRI activity measured as a function of solute concentration. MGA = Mean grain area relative to a saline control, expressed as %. Error bars represent the ± standard deviation from three independent measurements.

PVA is however well recognised as being intolerant to functionalisation, with often minor structural modifications resulting in the sudden loss of IRI activity.[47] The incorporation of a large hydrophobic central 'core' – the anthracene unit – restricting the rotational freedom of the PVA to explore the ice crystal face, and thereby also acting as modification preventing the formation of a truly contiguous PVA stretch, is likely a key problem.

Circular dichroism analysis of both the dimerised and undimerised poly(vinyl)alcohol derivatives failed to demonstrate any appreciable CD Spectra (Appendix A), whilst DLS analysis indicated no significant observable difference between the two photo-isoforms. Table 3.4.

Sample (~ 1 mg.mL^{-1} in H_2O)	Averaged Z-Avg (d.nm)	Averaged Counts
PC-PVA Undimerised	638.2	148.2
PC-PVA Dimerised	565.2	292.6

Table 3.4 – DLS Data for PC-PVA photoconjugates.

3.4 – Conclusions

Four IRI inactive species; poly(alanine)$_8$, poly(vinyl alcohol)$_{11}$, and two truncated antifreeze peptides of 11 and 22 residues – and comprised of the same repeat sequence as observed in the native AFP type I protein – were each conjugated to a rationally designed anthracene photoresponsive unit featuring a solubilising di-lysine linker.

Conjugation of these species did not introduce any IRI activity upon the poly(alanine), PVA, or AFP_{11} candidates, and irradiation of the conjugates with 365 nm light leading to the formation of photodimers also failed to induce IRI. The free poly(alanine), AFP_{11} and AFP_{22} peptides were also found to be IRI inactive. PVA being intolerant to functionalisation and AFP-11 being β-sheet like would account for this. However, functionalisation of the AFP_{22} stretch with the anthracene-di-lysine unit successfully introduced IRI activity to the conjugate, of similar order and potency to short PVA chains (n=56) at low concentration (35% MGA at 0.6 $mg.mL^{-1}$). Activity of this order is previously unreported for synthetic candidates and may represent an exploitable avenue of synthetic space in the preparation of future, hyper-potent AF(G)P mimetics. This result further shows that it may be possible to reduce antifreeze proteins to their basic repeat unit, so that they are accessible by solid phase peptide synthesis rather than recombinant expression, with modulable activity by the addition of end-group units. We hypothesise that this enhancement was due to the anthracene stabilising the secondary structure in the short peptide, supported by circular dichroism measurements.

However, irradiation of the conjugate led to an 18% drop in IRI activity upon photodimer formation, which was confirmed by UV-Vis and HPLC. As suggested by dynamic light scattering experiments, this activity drop may be attributed to the impaired ability to form a supramolecular solution structure (as observed in Safranine O), due to less efficient pi-pi stacking as a result of disrupted aromaticity in the photodimer product, resulting in a weaker

ice face interaction. However, whilst the ‘activity gap’ between the photodimer and monomer candidates were statistically within error, the clear difference in ice crystal size suggests that this candidate ultimately represents the first species devised to date with an appreciable IRI disparity when irradiated, relative to the nearest literature precedent. This species may serve as the future basis for a highly potent switchable inhibitor with an enhanced activity gap, with applications in cryosurgery.

3.5 – Experimental

Materials

NHFmoc-Lys-ε-(NHBoc)-OH, *N*-α-Boc-L-asparagine, L-asparagine *tert*-butyl ester hydrochloride were purchased from Fisher Scientific UK Limited (Loughborough, UK) and NH_3Cl-Lys-ε-(NHBoc)-OMe was purchased from Fluorochem Limited (Glossop, UK). Dichloromethane, EDCI, OxymaPure™, triethylamine, hydrochloric acid solution (12M), sodium chloride, sodium hydroxide, sodium hydrogen carbonate, sodium carbonate, magnesium sulphate, sodium sulphate, acetonitrile, mercaptoacetic acid, 25% sodium methoxide in methanol, methanol, acetone, hexane, 9-anthracene carboxylic acid, dimethyl formamide, dimethyl acetamide, diethyl ether, alanine, ethyl acetate, 4-nitrophenyl chloroformate, benzylamine, *N*-Boc-ethylenediamine, 1,4-dioxane, *N*-hydroxysuccinimide, Amberlyst IR120 resin (hydrogen form), DMAP, propargyl alcohol, sodium ascorbate, $CuSO_4$, *tert*-butanol, Amberlyst(R) A26 hydroxide form were purchased from Sigma Aldrich Co Ltd (Gillingham, UK). AFP_{11} and AFP_{22} were purchased from Peptide Protein Research Limited (Bishops Waltham, UK). Celite 545 was purchased from VWR Limited (Lutterworth, UK). PVAc was provided by Christopher Stubbs in the Gibson Group (University of Warwick, UK). All were used without further purification. Phosphate-buffered saline (PBS) solution was prepared using preformulated tablets in 200 mL of Milli-Q water (>18.2 Ω mean resistivity) to give [NaCl] = 0.138 M, [KCl] = 0.0027 M, and pH 7.4.

Antifreeze protein type I was provided by Dr. Muhammad Hasan,
Sequence: DTASDAAAAAAATAAAAAAAAATAKAAAEAAAATAAAAR;
Mw: 3285.53 g/mol^{-1}.

Physical and analytical methods

^{1}H and ^{13}C NMR Spectra (300 – 400 MHz and 75 MHz, respectively) were recorded using a Bruker DPX-300/400 Spectrometer under standard NMR conditions. Chemical shifts were recorded in ppm and referenced to solvent residual peaks, using MestReNova NMR Spectroscopy software.

ESI MS experiments were performed on an Agilent 6130B Single QUAD ESI-LC MS spectrometer in either positive or negative mode with an H_2O/MeOH (80:20) eluent feed, with samples dissolved in water, methanol or acetonitrile, unless otherwise stated.

Absorption UV/Vis (Ultra-violet/visible spectroscopy) spectra were acquired on an Agilent Technologies Cary 60 Variable Temperature UV-Vis spectrophotometer at room temperature fitted with Holographic Grating (27.5 × 35 mm, 1200 lines/mm, blaze angle 8.6° at 240 nm), a double beam, Czerny-Turner monochromator, 1.5 nm fixed spectral bandwidth, full spectrum Xenon pulse lamp single source, dual silicon diode detectors, quartz overcoated optics, non-measurement phase stepping wavelength drive, room light immunity. Analysis undertaken using Agilent CaryWin UV Scan software. All sample spectra were acquired in Hellma Analytics High Precision Quartz UV Cuvettes. Machine was zeroed and solvent background subtracted.

Irradiation experiments were carried out in a Vilber Lourmat™ Biolink™ BLX UV Crosslinker (Vilber, Germany) containing 5 x 8 W tubes (365 nm).

HPLC experiments were conducted on an Agilent 1260 Infinity II LC System (Bioinert) fitted with a quaternary pump and C18 reverse phase column. Detection was carried out with the UV module, and the UV lamp set at 213 nm. All samples were dissolved in methanol with an injection volume of 100 µL, flow rate of 1 ml/min, and gradient solvent system (Initial: 100% MeOH to 50:50% MeOH/H_2O), at room temperature, over a 30-minute run time.

Circular Dichroism experiments were conducted on a standard Jasco J-1500 CD Spectrometer utilising 1 mm quartz cuvettes containing 200 µL of appropriately diluted aqueous sample, with measurements taken in the 260 – 180 nm range at a voltage not exceeding 600. Solvent (water) backgrounds were subtracted.

Fluorescence measurements were made using a BioTek Synergy HT multi-detection microplate reader and Gen5 software (*BioTek* Instruments, Winooski, VT).

Dynamic light scattering was conducted using a NanoZs (Malvern Instruments, UK). Scattered light was detected at 173º and the observed count rates recorded. Hydrodynamic radii (where appropriate) were determined using the manufacturer's software. Diameters are an average of 3 measurements using at least 10 scans.

SAXS and WAXS experiments (performed by Dr. Steven Huband and Alice E. R. Fayter, respectively) were carried out on a 5m Xenocs Xeuss 2.0 SAXS instrument equipped with dual microfocus (Cu/Mo) sources and a Pilatus 300K hybrid photon counting detector. A CryoStage sample mount was used in conjunction with the low temperature WAXS experiments.

Solubilization of insoluble samples for analysis

Insoluble samples for splat and instrument analyses were made up in a pure water solution (1 mL) and centrifuged (10K RPM, 10 minutes). The supernatant was then wholly removed and reduced to dryness in a glass phial. The net weight difference of the phial was then calculated – giving the mass of material soluble in pure water (1 mL) at a saturated concentration. Either saline or PBS (as applicable, 1 mL) was then added, vortexed (and complete re-suspension confirmed), to give a wholly soluble solution of known concentration in saline/PBS.

Ice recrystallization inhibition (splat) assay

Ice recrystallization inhibition was measured using a modified splat assay.[1] A 10 µL sample of the species of interest, dissolved in PBS or saline buffer (pH 7.4 or 7, respectively), was dropped 1.40 m onto a chilled glass coverslip, resting on a thin aluminium block placed on dry ice. Upon hitting the coverslip, a wafer with diameter of approximately 10 mm and thickness 10 µm was formed instantaneously. The glass coverslip was transferred onto the Linkam cryostage and held at -8^{o}C under N_2 for 30 minutes. Photographs were obtained using an Olympus CX 41 microscope with a UIS-2 20x/0.45/∞/0-2/FN22 lens and crossed polarizers (Olympus Ltd, Southend-on-Sea, UK), equipped with a Canon DSLR 500D digital camera. Images were taken of the initial wafer (to ensure that a polycrystalline sample had been obtained) and again after 30 minutes. Image processing was conducted using Image J, which is freely available (National Institutes of Health, Bethesda, MD). In brief, the number of ice crystals in the field of view was measured, and the measurement repeated for three independent wafers. The average (mean) of these three measurements was then calculated to find the mean grain area (MGA). The average value and error was compared to that of a PBS or saline buffer, as appropriate, as a negative control.

Synthetic Procedures

Synthesis of methyl N^2-(N^2-(((9*H*-fluoren-9-yl)methoxy)carbonyl)-N^6-(*tert*-butoxycarbonyl)-L-lysyl)-N^6-(*tert*-butoxycarbonyl)-L-lysinate (1)

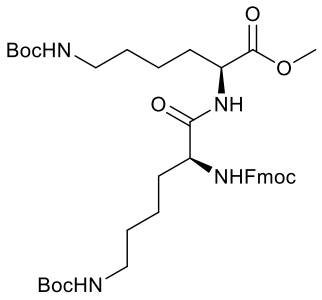

NHFmoc-Lys-ε-(NHBoc)-OH (0.5 g, 1.07 mmol) was dissolved in DCM (20 mL) with stirring, to which EDCI (0.246 g, 1.2 eqv, 1.28 mmol), OxymaPure™ (0.182 mg, 1.2 eqv, 1.28 mmol), and TEA (0.18 mL, 1.2 eqv, 1.28 mmol) were added. NH_3Cl-Lys-ε-(NHBoc)-OMe (0.348 g, 1.1 eqv, 1.17 mmol) was subsequently added, and the reaction mixture stirred at RT for 18 hours. The crude mix was subsequently extracted with dilute hydrochloric acid solution (x2 , 25 mL, pH 5 – 6), then saturated sodium hydrogen carbonate solution (x2, 30 mL), and finally brine (x1, 30 mL). The organic phase was dried over $MgSO_4$, filtered, and condensed *in vacuo*. The white solid was then crystallised from diethyl ether (30 mL), washed, filtered, and condensed *in vacuo*, yielding a colourless solid. 520 mg (68.6%). ^{1}H NMR (400 MHz, $CDCl_3$) δ = 7.82 – 7.21 (m, 8H), 6.82 (s, 1H), 5.71 (s, 1H), 4.75 (s, 2H), 4.56 (s, 1H), 4.38 (d, *J* = 5.7 Hz, 2H), 4.21 (t, *J* = 6.7 Hz, 2H), 3.73 (s, 3H), 3.22 – 2.98 (m, 4H), 1.86 (s, 2H), 1.71 (s, 2H), 1.58 – 1.24 (m, 26H). ^{13}C NMR (100 MHz, $CDCl_3$) δ = 172.71 (MeO**C**=O), 171.89 (NH**C**=O), 156.32 (2 x Boc **C**=O + Fmoc NH**C**=O), 143.95 (Fmoc), 141.37 (Fmoc), 127.83 (Fmoc), 127.21 (Fmoc), 125.22 (Fmoc), 120.08 (Fmoc), 79.27 (**C-*tert***) 67.27 (**C**OC=ONH), 54.73 (alpha-**C**), 52.53 (O**Me**), 52.21 (alpha-**C**), 47.21 (**C**H-Pent-Fmoc), 40.05, 32.23, 31.59, 29.56, 29.51, 28.54 (6 x **C**H_3), 22.52, 22.37. m/z (ESI, +ve) Observed 733.5 [100%, Na^+].

Synthesis of methyl N^6-(*tert*-butoxycarbonyl)-N^2-(N^6-(*tert*-butoxycarbonyl)-L-lysyl)-L-lysinate (2)

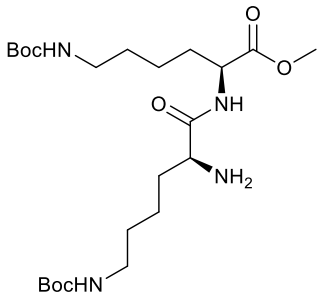

1 (1.4 g, 1.97 mmol) was dissolved in acetonitrile (10 mL), whilst mercaptoacetic acid (700 µL, 0.928 g, 10.07 mmol, 5.1 eqv) was added dropwise to a 25% solution of sodium methoxide in methanol (900 µL, 0.852 g, 15.76 mmol, 8 eqv) at 0ºC. To this pre-stirred solution, the solution of **1** in acetonitrile was added, and the combined mixture stirred for 12 hours, with heating at 50ºC. The mixture was then acidified to pH 5 – 6 with hydrochloric acid solution (1M) added dropwise, and the precipitated salts were filtered. The filtrate was subsequently condensed *in vacuo*, redissolved in methanol (5 mL), and the mercaptoacetic acid-dibenzofulvene by-product precipitated from water (20 mL). The milky-mixture was then filtered through a pad of Celite with water eluent, and the filtrate condensed *in vacuo*. Isolation of **2** followed through dissolution of the dry filtrate in acetone (10 mL) and then precipitation from hexane (30 mL), giving an off-white solid. 350 mg (36.4%). m/z (ESI, +ve) Observed 511.4 [100%, Na^+]. ^{1}H NMR (300 MHz, CH_3OH+D_2O) δ = 4.18 (t, *J* = 6.7 Hz, 1H), 3.82 (s, 1H), 3.55 (s, 3H), 2.90 – 2.77 (m, 4H), 2.02 (d, J = 2.4 Hz, 1H), 1.77 – 1.52 (m, 4H), 1.35 – 1.09 (m, 26H). ^{13}C NMR (101 MHz, MeOD) δ = 173.76 (MeO**C**=O), 173.16 (NH**C**=O), 158.51 (2 x Boc **C**=O), 128.50, 127.96, 126.12, 120.72, 79.82 (**C-*tert***), 58.29, 55.94, 54.68, 53.28, 52.79 (O**Me**), 41.01, 34.91, 33.63, 31.97, 30.60, 30.44, 28.79 (6 x **C**H_3), 24.12, 23.12, 18.38.

Synthesis of methyl N^2-(N^2-(anthracene-9-carbonyl)-N^6-(*tert*-butoxycarbonyl)-L-lysyl)-N^6-(*tert*-butoxycarbonyl)-L-lysinate (3)

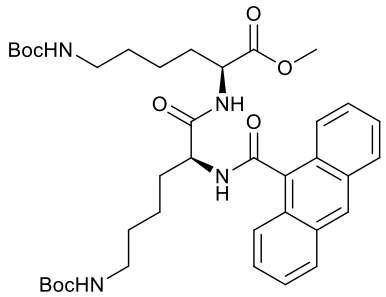

Anthracene-9-carboxylic acid (356 mg, 1.60 mmol, 2.2 eqv) was dissolved in DMF (30 mL) with stirring, and EDCI (154 mg, 0.86 mmol, 1.2 eqv), OxymaPure™ (114 mg, 0.86 mmol, 1.2 eqv), and TEA (112 µL, 0.86 mmol, 1.2 eqv) were added. **2** (350 mg, 0.72 mmol) was subsequently added, and the reaction mixture stirred at RT for 18 hours. The crude mix was then condensed to low volume *in vacuo* (~ 5 mL) and diluted with chloroform (30 mL), before being extracted with dilute hydrochloric acid solution (x2 , 25 mL, pH 5 – 6), then saturated sodium hydrogen carbonate solution (x2, 30 mL), and finally brine (x1, 30 mL). The organic phase was then re-acidified to pH 5 – 6 with hydrochloric acid solution (1M) and a column was packed with pre-rinsed Amberlyst beads (A26 hydroxide form). The acidified mix was then poured through the column, eluting and washing with THF (3 x 10 mL). The collected eluent was then dried over $MgSO_4$, filtered, and condensed *in vacuo*, yielding an orange oil. 140 mg (28.2%). m/z (ESI, –ve) Observed 691.4 [100%, M-H^+]. ^{1}H NMR (400 MHz, $CDCl_3$) δ = 8.52 (s, 1H), 8.09 – 7.11 (m, 9H), 5.09 – 4.74 (m, 1H), 4.43 (m, 1H), 4.23 – 3.88 (m, 1H), 3.40 (s, 3H), 3.23 – 2.97 (m, 5H), 2.11 – 1.58 (m, 9H), 1.55 – 0.76 (m, 26H). ^{13}C NMR (101 MHz, $CDCl_3$) δ = 174.54 (MeO**C**=O), 168.62 (NH**C**=O), 156.25 (2 x Boc **C**=O), 154.32 (Anthracene NH**C**=O), 135.56 – 119.72 (Anthracene), 79.07 (**C-*tert***), 57.43, 56.87, 56.49 – 55.84, 54.79, 52.35 (O**Me**), 50.32, 46.71, 45.63 – 45.14, 42.30, 41.17, 40.60, 40.02, 39.11, 37.34, 35.60,

35.25, 34.06, 33.82, 33.62, 33.47, 32.46, 29.80, 28.45 (6 x **C**H_3), 27.61, 27.42, 26.64, 26.26, 25.16, 22.60, 22.00, 15.66, 15.43, 15.21, 14.89, 14.23, 13.43.

Synthesis of methyl *N*^{2}-(*N*^{2}-(anthracene-9-carbonyl)-*N*^{6}-(*tert*-butoxycarbonyl)-L-lysyl)-*N*^{6}-(*tert*-butoxycarbonyl)-L-lysine (4)

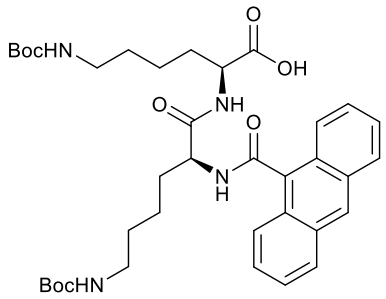

3 (140 mg, 0.20 mmol) was dissolved in methanol/water (1:1, 20 mL) and a large excess of sodium hydroxide added (500 mg, 62.5 eqv), and the mixture stirred at RT for 18 hours. The mixture was then acidified with hydrochloric acid solution (1M), dropwise, until pH 5 – 6. The mixture was then condensed *in vacuo*, and the product precipitated and isolated from acetone, giving a pale yellow solid. 100 mg (73.7%). m/z (ESI, -ve) Observed 677.3 [100%, M-H$^+$]. ^{1}H NMR (300 MHz, $CDCl_3$) δ = 8.42 – 7.00 (m, 9H), 5.22 (s, 1H), 4.84 (s, 2H), 4.59 – 3.92 (m, 4H), 3.83 (s, 1H), 3.68 – 3.51 (m, 1H), 3.12 – 2.81 (m, 5H), 2.65 (d, J = 5.5 Hz, 1H), 1.97 – 1.52 (m, 4H), 1.52 – 1.11 (m, 29H). ^{13}C NMR (75 MHz, $CDCl_3$) δ = 173.95 (NH**C**=O), 157.74 (2 x Boc **C**=O), 156.89 (Anthracene NH**C**=O), 135.71 – 125.24 (Anthracene), 79.16 (**C-*tert***), 69.76, 69.12, 55.38, 42.92, 39.07, 37.59, 36.06, 34.41, 33.85, 29.73, 28.54 (6 x **C**H_3), 23.82, 14.28, 13.52.

Synthesis of poly(alanine)

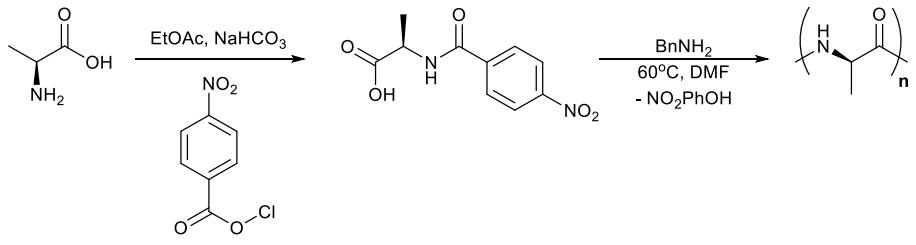

Alanine (0.25 g, 2.81 mmol) was dissolved in ethyl acetate (40 mL) with sodium hydrogen carbonate (0.286 g, 5.62 mmol, 2 eqv). 4-Nitrophenylchloroformate (0.689 g, 3.37 mmol 1.2 eqv) was subsequently added with stirring, and the mixture heated at 45ºC overnight. The solids were filtered and the filtrate washed with saturated sodium hydrogen carbonate solution (20 mL), and then with water (5 x 40 mL). The organic phase was then condensed *in vacuo*. Acetone (30 mL) was then added to the solid residue, and the acetone soluble portion removed in solution and condensed once more, to give a white solid (100 mg) which was then dissolved in dry DMAc (15 mL). The solution was subsequently sparged under a flow of dry nitrogen and heated at 60ºC for 18 hours, in the presence of benzylamine (0.1 mL) under N_2. After which, the solution was precipitated from water (35 mL) and centrifuged (10k RPM, 10 minutes), the solution decanted, and the precipitate re-dissolved in acetone (5 mL) and re-precipitated from water (45 mL) x 5. The precipitate was isolated as an oily brown solid, which was dissolved in methanol and negatively dialysed (1 kDa MWCO) to yield 80 mgs of poly(alanine). (32%). Mn_{SEC} 790 g.mol^{-1}, 1.1 Đ.

Synthesis of 2,2,10-trimethyl-4,9-dioxo-33-thioxo-3,34-dioxa-32-thia-5,8-diazahexatriacontan-11,13,15,17,19,21,23,25,27,29,31-undecayl undecaacetate ($PVAc_{11}$-NHBoc)

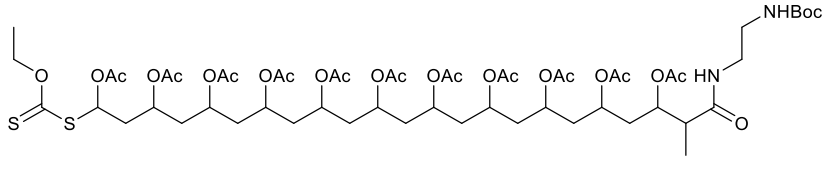

$PVAc_{11}$-NHS (0.85g, 0.66 mmol, Mn 1294 g/mol^{-1}, 1.2 Đ) was dissolved in DMF (5 mL) and *N*-Boc-ethylenediamine (210 mg, 210 µL, 2 eqv, 1.31 mmol) added, and the mixture stirred overnight. The solution was then condensed *in vacuo*, redissolved in acetone (5 mL) and precipitated from water (45 mL) five times, and then centrifuged (11k RPM, 20 minutes). The residual mass was taken up into acetone (5 mL) and condensed again, to give an orange/brown solid. 470 mg (56.1%). m/z (ESI, +ve) Observed 1320.6 [20%, DP_{11} + $2H_2O$ + H^+].

Synthesis of 23-((2-aminoethyl)amino)-1-((ethoxycarbonothioyl)thio)-22-methyl-23-oxotricosan-1,3,5,7,9,11,13,15,17,19,21-undecayl undecaacetate ($PVAc_{11}$-NH_2)

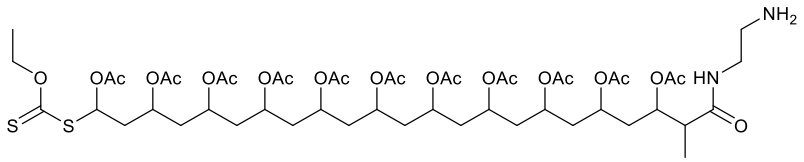

$PVAc_{11}$-NHBoc (0.47g, 0.37 mmol) was dissolved in 1,4-dioxane (20 mL) and 6M HCl added (1 mL), and the reaction mixture stirred overnight. The mixture was subsequently condensed *in vacuo* to give a brown solid. 370 mg (85.5%). m/z (ESI, -ve) Observed 1277.4 [20%, DP_{11} + Acetonitrile + H_2O + Cl^-].

Representative / Optimised Procedure for Conjugative Coupling

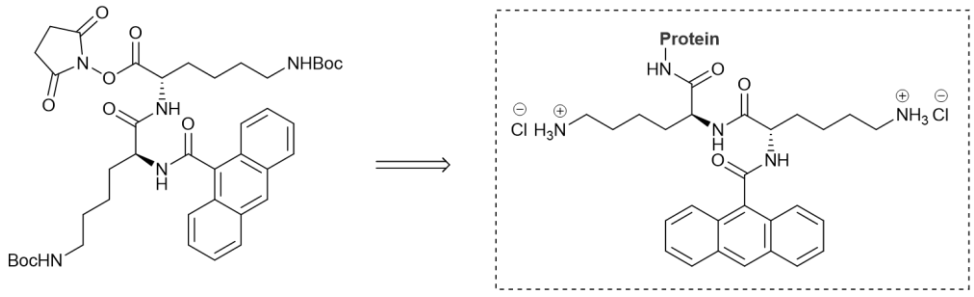

4 (30 mg, 0.044 mmol) was dissolved in dry DMF or DMAc and DCM (1:1, 5 mL) under a flow of dry nitrogen, and EDCI (17 mg, 2 eqv, 0.088 mmol) added, followed by *N*-hydroxysuccinimide (10 mg, 2 eqv, 0.088 mmol). The mixture was allowed to stir for 30

minutes to allow for the formation of **5** *in-situ*. Then, either the antifreeze protein (AFP-22•TFA, 5 mg) or the poly(vinyl)acetate (111 mg) species for conjugation was dissolved up in dry DMF or DMAc (2.5 mL) under a flow of dry nitrogen, and injected into the main flask, followed by a large excess of TEA (100 µL). The flask was then stirred for 4 days under dry nitrogen, with heating at 50ºC. The flask was subsequently cooled, exposed to air, and a large excess of sodium methoxide/methanol solution added (2 mL) – giving pH 12 and a fluorescent pink colour change, and then stirred for 1 hour. After which, the flask was acidified to pH 1 with HCl (6M), resulting in decolourisation, and stirred for 1 further hour. After the removal of the protecting/end groups, the mixtures were then diluted with methanol (3 mL) and water (50 mL) and dialysed against water for 3 days (1 kDa dialysis tubing), with regular water changes. Upon completion, sedimentation was apparent, and the dialysis bags continued to fluoresce under long wave ultraviolet light, indicating the presence of a conjugated/large molecular weight anthracene unit within the bag. Both species were then reacidified to pH 2 with HCl (6M), and condensed *in vacuo* to give the final photoconjugate products, **6b** (AFP-22, 5.7 mg, 5.7%) and **9** (PVA, 12.5 mg, 25.7%). The initial candidates **6a** (AFP-11, 1 mg) and **6c** (Ala_8, 3.5 mg) were similarly prepared, but through a modified procedure and were low yielding. Mass Spectrometry of **6c** (as the Di-ε-Lys-Fmoc protected derivative) indicated a single peak present at 1613.8 m/z (100%), corresponding to the [Conjugate Mass + $Cl^{\bullet} - H^{+}$].

Redundant Procedure for the Synthesis of 23-((3-azidopropyl)amino)-1-((ethoxycarbonothioyl)thio)-22-methyl-23-oxotricosan-1,3,5,7,9,11,13,15,17,19,21-undecayl undecaacetate ($PVAc_{11}$-N_3)

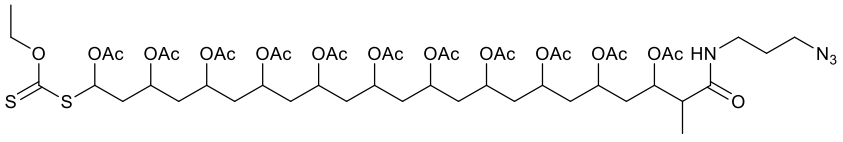

$PVAc_{11}$-NHS (0.85g, 0.66 mmol, Mn 1294 g/mol^{-1}, 1.2 Đ) was dissolved in DMF (5 mL) and 3-azido-1-propanamine added (1.2 eqv, 0.792 mmol 77 µL) with stirring. After 16 hours, the reaction mixture was condensed *in vacuo*, dissolved in acetone (5 mL) and precipitated from water (45 mL), three times, giving a brown solid. 640 mg (80.1%). m/z (ESI, +ve) Observed 1259.5 [45%, DP_{11} + MeOH + H_3O^+].

Redundant Procedure for the Synthesis of *N*-(3-azidopropyl)-3,5,7,9,11,13,15,17,19,21,23-undecahydroxy-23-mercapto-2-methyltricosanamide (PVA_{11}-N_3)

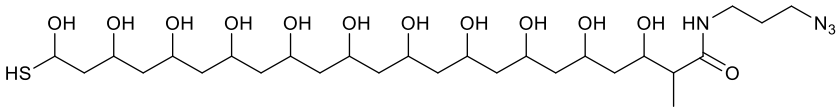

$PVAc_{11}$-N_3 (0.64 g, 0.571 mmol) was dissolved in methanol (20 mL) and a large excess of sodium methoxide in methanol (10 mL, 25%) added, and the mixture stirred overnight at RT. After which, the solution was passed through a column packed with acidic Amberlyst IR120 resin (hydrogen form) for neutralisation, and the eluent (pH 7) condensed *in vacuo* yielding a brown solid. 220 mg (58.5%). m/z (ESI, +ve) Observed 673.4 [75%, DP_{10} + $2H_2O$ + Na^+].

Redundant Procedure for the Synthesis of prop-2-yn-1-yl N^2-(N^2-(anthracene-9-carbonyl)-N^6-(*tert*-butoxycarbonyl)-L-lysyl)-N^6-(*tert*-butoxycarbonyl)-L-lysinate (7)

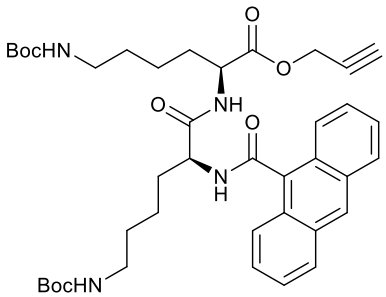

4 (50 mg, 0.0737 mmol) was dissolved in DMF (10 mL) and EDCI (1.2 eqv, 0.0884 mmol, 17 mg) added, followed by DMAP (0.1 eqv, 0.00737 mmol, 1 mg) with stirring. Propargyl alcohol

(1.2 eqv, 0.0884 mmol, 5 µL) was then added dropwise, and the reaction mixture stirred for 12 hours at RT. The crude mix was subsequently extracted with dilute hydrochloric acid solution (x 2, 25 mL, pH 5 – 6), then saturated sodium hydrogen carbonate solution (x2, 30 mL), and finally brine (x1, 30 mL). The organic phase was dried over $MgSO_4$, filtered, and condensed *in vacuo*, yielding a yellow solid. 50 mg (94.6%). ^{1}H NMR (300 MHz, $CDCl_3$) δ 8.45 – 6.83 (m, 9H), 4.99 – 4.65 (m, 2H), 3.94 – 3.14 (m, 3H), 3.11 – 2.77 (m, 6H), 2.34 (s, 1H), 1.98 – 1.29 (m, 28H). ^{13}C NMR (101 MHz, $CDCl_3$) δ 183.28 (Ester), 171.58 (NH**C**=O), 168.69 (NH**C**=O), 156.30 (2 x Boc **C**=O), 134.24 - 125.63 (Anthracene), 79.24 (**C-*tert***), 54.77, 40.08, 35.48, 33.31, 32.73, 29.80, 29.80, 28.56, 28.47, 28.43 (6 x **C**H_3), 22.92, 22.03, 21.56, 14.76, 1.12. m/z (ESI, +ve) Observed 834.6 [100%, Mass + Acetone + Acetonitrile + H_3O^+].

Failed Procedure for the Synthesis of Anthracene-Dilysine•HCl-PVA Conjugate by Alkyne-Azide Click Chemistry (8)

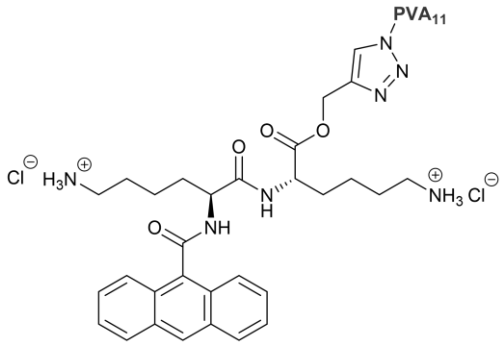

Attempt 1: 7 (50 mg, 0.0698 mmol) was dissolved in a 1:1 solution of water/*tert*-butanol (20 mL) and the PVA_{11}-N_3 (220 mg) was added with stirring. Sodium ascorbate (0.00698 mmol, 0.1 eqv, 1.4 mg) in water (100 µL) was added, followed by $CuSO_4$•$5H_2O$ (0.00698 mmol, 0.1 eqv, 1.4 mg) in water (100 µL). The reaction mixture was stirred for 36 hours at RT, and then condensed *in vacuo*.

Attempt 2: The dry residue was re-dissolved in a 2:1 solution of DMF/water (15 mL) and further sodium ascorbate (0.1396 mmol, 2 eqv, 28 mg) and $CuSO_4$•$5H_2O$ (0.1396 mmol, 2 eqv,

28 mg) were added. The reaction mixture was stirred for a further 24 hours at 60ºC, and then condensed *in vacuo*.

Failed Synthesis of *tert*-butyl (*tert*-butoxycarbonyl)-L-asparaginyl-L-asparaginate (11)

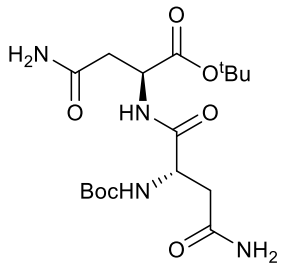

EDCI (0.083 g, 0.431 mmol, 1 eqv) was dissolved in DCM (50 mL) with stirring under a flow of dry nitrogen. *N*-α-Boc-L-asparagine (0.1 g, 0.431 mmol, 1 eqv) and OxymaPure™ (0.0612 mg, 1 eqv, 0.431 mmol) were then added, followed by L-asparagine *tert*-butyl ester hydrochloride (0.0968 g, 0.431 mmol, 1 eqv). TEA was then added (0.1 mL, 1.66 eqv, 0.712 mmol), and the reaction mixture stirred at RT for 18 hours. The crude reaction mix was then condensed *in vacuo*, re-dissolved in ethyl acetate (50 mL), and washed with 0.1M HCl (3 x 30 mL), followed by 1M Na_2CO_3 (3 x 30 mL), and saturated brine (30 mL). The organic phase was then dried over $MgSO_4$, filtered, and condensed *in vacuo*. m/z (ESI, +ve) Observed 466.7 [100%, Dehydrated Product + H_3O^+ + 2 x Acetonitrile].

3.6 – References

1 P. L. Davies, *Trends Biochem. Sci.*, 2014, 39, 548–555.

2 G. L. Fletcher, D. R. Idler, A. Vaisius and C. L. Hew, *Fish Physiol. Biochem.*, 1989, **7**, 387–393.

3 W. K. Yiu, M. T. Basco, J. E. Aruny, S. W. K. Cheng and B. E. Sumpio, *Int. J. Angiol.*, 2007, 16, 1–6.

4 A. Fowler and M. Toner, *Ann. N. Y. Acad. Sci.*, 2005, 1066, 119–135.

5 D. K. Whittaker, *Ann. R. Coll. Surg. Engl.*, 1984, **66**, 313–318.

6 J. Prohaska and T. Badri, *Cryotherapy*, StatPearls Publishing, 2018, vol. 37.

7 A. M. Kloxin, M. W. Tibbitt, A. M. Kasko, J. A. Fairbairn and K. S. Anseth, *Adv. Mater.*, 2010, **22**, 61–66.

8 T. E. Brown and K. S. Anseth, *Chem. Soc. Rev.*, 2017, 46, 6532–6552.

9 B. P. Fors and C. J. Hawker, *Angew. Chemie - Int. Ed.*, 2012, **51**, 8850–8853.

10 C. Fu, Z. Huang, C. J. Hawker, G. Moad, J. Xu and C. Boyer, *Polym. Chem.*, 2017, **8**, 4637–4643.

11 B. Wenn, M. Conradi, A. D. Carreiras, D. M. Haddleton and T. Junkers, *Polym. Chem.*, 2014, **5**, 3053–3060.

12 M. Yamada, Y. Suzuki, S. C. Nagasaki, H. Okuno and I. Imayoshi, *Cell Rep.*, 2018, **25**, 487–500.

13 S. A. Reis, B. Ghosh, J. A. Hendricks, D. M. Szantai-Kis, L. Törk, K. N. Ross, J. Lamb, W. Read-Button, B. Zheng, H. Wang, C. Salthouse, S. J. Haggarty and R.

Mazitschek, *Nat. Chem. Biol.*, 2016, **12**, 317–323.

14 M. K. Adam, Y. Hu, J. S. Poisson, M. J. Pottage, R. N. Ben and B. L. Wilkinson, *Carbohydr. Res.*, 2017, **439**, 1–8.

15 M. K. Adam, J. S. Poisson, Y. Hu, G. Prasannakumar, M. J. Pottage, R. N. Ben and B. L. Wilkinson, *RSC Adv.*, 2016, **6**, 39240–39244.

16 A. Müller, H. Kobarg, V. Chandrasekaran, J. Gronow, F. D. Sönnichsen and T. K. Lindhorst, *Chem. - A Eur. J.*, 2015, **21**, 13723–13731.

17 D. J. Phillips, T. R. Congdon and M. I. Gibson, *Polym. Chem.*, 2016, **7**, 1701–1704.

18 A. A. Beharry and G. A. Woolley, *Chem. Soc. Rev.*, 2011, 40, 4422–4437.

19 J. Garner and M. M. Harding, *Org. Biomol. Chem.*, 2007, **5**, 3577–3585.

20 I. Filpponen, H. Sadeghifar and D. S. Argyropoulos, *Nanomater. Nanotechnol.*, 2011, **1**, 7.

21 A. Aemissegger, V. Kräutler, W. F. Van Gunsteren and D. Hilvert, *J. Am. Chem. Soc.*, 2005, **127**, 2929–2936.

22 E. Bartels, N. H. Wassermann and B. F. Erlanger, *Proc. Natl. Acad. Sci.*, 2006, **68**, 1820–1823.

23 G. A. Bullen, J. H. R. Tucker and A. F. A. Peacock, *Chem. Commun.*, 2015, **51**, 8130–8133.

24 M. Hasegawa, A. Suzuki, S. Matsumura and K. Toshima, *Sci. Technol. Adv. Mater.*, 2006, **7**, 169–174.

25 J. H. R. Tucker, L. Giordano, Z. Zhao, J. Manchester, D. M. Bassani, J. S. Vyle and J.-L. H. A. Duprey, *J. Am. Chem. Soc.*, 2012, **134**, 10791–10794.

26 H. Bouas-Laurent, A. Castellan, J. P. Desvergne and R. Lapouyade, *Chem. Soc. Rev.*, 2000, **29**, 43–55.

27 M. M. Maturi, G. Fukuhara, K. Tanaka, Y. Kawanami, T. Mori, Y. Inoue and T. Bach, *Chem. Commun.*, 2016, **52**, 1032–1035.

28 A. Dawn, N. Fujita, S. Haraguchi, K. Sada and S. Shinkai, *Chem. Commun.*, 2009, **0**, 2100–2102.

29 R. Drori, C. Li, C. Hu, P. Raiteri, A. L. Rohl, M. D. Ward and B. Kahr, *J. Am. Chem. Soc.*, 2016, **138**, 13396–13401.

30 L. López-Vilanova, I. Martínez, T. Corrales and F. Catalina, *Eur. Polym. J.*, 2014, **56**, 69–76.

31 M. E. Houston, H. Chao, R. S. Hodges, B. D. Sykes, C. M. Kay, F. D. Sönnichsen, M. C. Loewen and P. L. DAvies, *J. Biol. Chem.*, 1998, **273**, 11714–11718.

32 Y. Kamei, A. Sudo, H. Nishida, K. Kikukawa and T. Endo, *J. Polym. Sci. Part A Polym. Chem.*, 2008, **46**, 2525–2535.

33 H. Wei, Q. Wang, H. Cheng, X. Zhang, L. Kan, B. Li and N. Ma, *New J. Chem.*, 2019, **43**, 2658–2664.

34 H. Kihara and M. Yoshida, in *IOP Conference Series: Materials Science and Engineering*, IOP Publishing, 2014, vol. 54, p. 012020.

35 Y. Mu, B. Tang and M. Yu, *Phys. Rev. E - Stat. Nonlinear, Soft Matter Phys.*, 2014, **89**, 032711.

36 A. Wakai, H. Fukasawa, C. Yang, T. Mori and Y. Inoue, *J. Am. Chem. Soc.*, 2012, **134**, 4990–4997.

37 M. K. Adam, C. Jarrett-Wilkins, M. Beards, E. Staykov, L. R. MacFarlane, T. D. M. Bell, J. M. Matthews, I. Manners, C. F. J. Faul, P. D. J. Moens, R. N. Ben and B. L. Wilkinson, *Chem. - A Eur. J.*, 2018, **24**, 7834–7839.

38 D. E. Mitchell, G. Clarkson, D. J. Fox, R. A. Vipond, P. Scott and M. I. Gibson, *J. Am. Chem. Soc.*, 2017, **139**, 9835–9838.

39 C. I. Biggs, C. Stubbs, B. Graham, A. E. R. Fayter, M. Hasan and M. I. Gibson, *Macromol. Biosci.*, 2019, 1900082.

40 M. I. Gibson, C. Biggs, L. E. Wilkins, A. E. R. Fayter, M. Walker and M. Hasan, *Polym. Chem.*, 2019, **10**, 2986–2990.

41 L. L. C. Olijve, M. M. R. M. Hendrix and I. K. Voets, *Macromol. Chem. Phys.*, 2016, **217**, 951–958.

42 C. Stubbs, L. E. Wilkins, A. E. R. Fayter, M. Walker and M. I. Gibson, *Langmuir*, 2018, **35**, 7347–7353.

43 C. A. Stevens, R. Drori, S. Zalis, I. Braslavsky and P. L. Davies, *Bioconjug. Chem.*, 2015, **26**, 1908–1915.

44 C. I. DeLuca, R. Comley and P. L. Davies, *Biophys. J.*, 1998, **74**, 1502–1508.

45 T. R. Congdon, R. Notman and M. I. Gibson, *Biomacromolecules*, 2016, **17**, 3033–3039.

46 B. Graham, A. E. R. Fayter, J. E. Houston, R. C. Evans and M. I. Gibson, *J. Am. Chem. Soc.*, 2018, **140**, 5682–5685.

47 T. Congdon, R. Notman and M. I. Gibson, *Biomacromolecules*, 2013, **14**, 1578–1586.

48 N. S. Vail, C. Stubbs, C. I. Biggs and M. I. Gibson, *ACS Macro Lett.*, 2017, **6**, 1001–4.

CHAPTER 4

Rationally designed amphipathic glycopolymers for ice growth inhibition

---

4.1 – Chapter Abstract

This chapter describes the synthesis of a series of facially amphipathic glycopolymers with IRI potency. Antimicrobial polymers are known to possess many of the desired structural characteristics we hypothesised as necessary for IRI potency – hydrophilicity, hydrophobicity, and rigidity.[1] Taking inspiration from previous work, four amphipathic monomers derived from norbornene and featuring different functionalities at the imide bridgehead were prepared. These monomers were (co)polymerized to a variety of molecular weights using Ring-opening Metathesis Polymerisation (ROMP) with Grubbs 3rd generation catalyst, and acetate protecting groups removed by treatment with methanolic sodium methoxide followed by ion exchange. The panel of amphipathic polymers were characterized by SEC, NMR and IR. 'Splat' analysis of the initial facially amphipathic derivative indicated significant IRI activity at low concentration (50 % MGA at 500 μg.mL^{-1}), levels of activity which have only been previously reported for PVA and naturally occurring AF(G)Ps. Of the sequentially modified architectures prepared, the significance of amphipathy is further asserted, with wholly hydrophilic derivatives displaying comparably weaker activity to facially amphipathic versions, which will be explored in greater detail. Copolymeric derivatives are also discussed, and were prepared in an effort to enhance both the solubility and activity profiles of the candidates, the optimised

derivative of which is capable of inhibiting ice growth to 40% MGA at 1.3 mg.mL^{-1}. This level of activity is remarkable, indicating that rational design of potent IRI species is possible, and that such activity can be feasibly incorporated into macromolecular architectures. Furthermore, the absence of dynamic ice shaping in the optimised candidate will be reported, in addition to SANS data, which suggests a similarity between the flat amphipathic ice binding surface of AFPs and the optimised copolymer – potentially suggesting a mechanistic mode of action.

4.2 – Chapter Introduction

Few IRIs are known, despite intense research in the field, due to a lack of understanding of the design principles. PVA,[2,3,4] metallohelices,[5] and some glycopeptides,[6] have shown the most promise as synthetic IR inhibitors to date. However, toxicity, relatively low potencies, and intolerance to (bio)chemical functionalisation thereby leading to loss of activity, have hindered the development and exploitation of the next generation of AF(G)P mimetics. It is clear, that to access the next class of highly potent IR inhibitors, a rational design blue-print for activity must be devised. However, this task is not trivial. Whilst AFPs have been better characterised leading to the identification of defined ice-binding faces *via* structural biology methods[7], there are no crystal structures available of AFGPs – which are believed to possess substantially different architectures.[8,9] As such, the exact structural motifs required for IRI are unknown. Solution NMR and circular dichroism studies do however suggest that AFGPs form a polyproline II type helix, with the glycans (deemed essential for ice shaping)[10] on one face, and peptides on the opposite, forming a facially amphipathic structure (Figure 4.1).[8] It has emerged however in recent literature that this segregated display of hydrophobic/hydrophilic groups, rather than the presentation of a distinct 'ice binding site' may be the essential feature for IRI activity.[11–13]

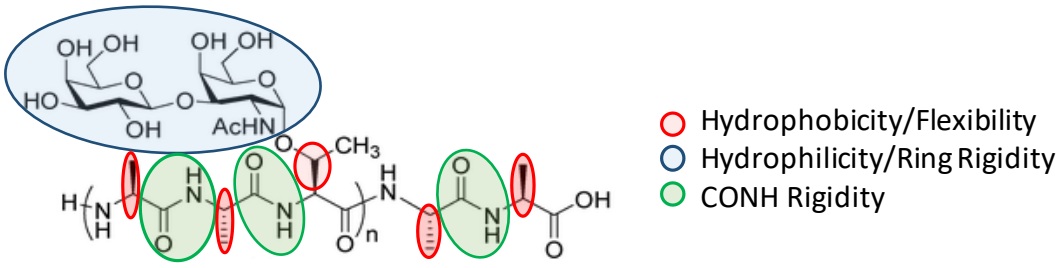

Figure 4.1 – $(AFGP)_n$ Repeat architecture, showing structural features along a PPII helix.

In particular, our recent work on polyproline serves as a representative example of a very small class of viable cryoprotective additives. Through the adoption of an polyproline type-II helix,

and the presentation of an amphipathic surface structure, polyproline exhibited moderate IRI activity and had markedly improved performance versus poly(hydroxy)proline – asserting the need for amphipathy over hydroxyl group presentation alone.[14] In addition, molecular modelling recently revealed that the hydrophobic face, not the glycans, of AFGP interact with the ice, and that the spatial segregation along the polyproline II helix is essential.[15] In conjunction with polyproline, Gibson and co-workers have further shown that self-assembled metallohelicies with 'patchy' amphipathy are potent IRIs,[5] which supports a hypothesis that well defined ice binding domains and hydrogen bonding centres are not essential for IRI.[16] Amphipathy has also been seen to be important in ice nucleation.[17] This evidence suggests that IRI, but not detrimental dynamic ice shaping,[18] could be selectively introduced into new and emerging (bio)materials, if precise control over hydrophilic/phobic domains is possible. The design of macromolecules with solvent-exposed hydrophobic domains is, however, non-trivial. Block copolymeric amphiphiles spontaneously self-assemble into micelles/vesicles to reduce hydrophobic domain contact with water, and hence only 'water loving' surfaces are exposed.[19]

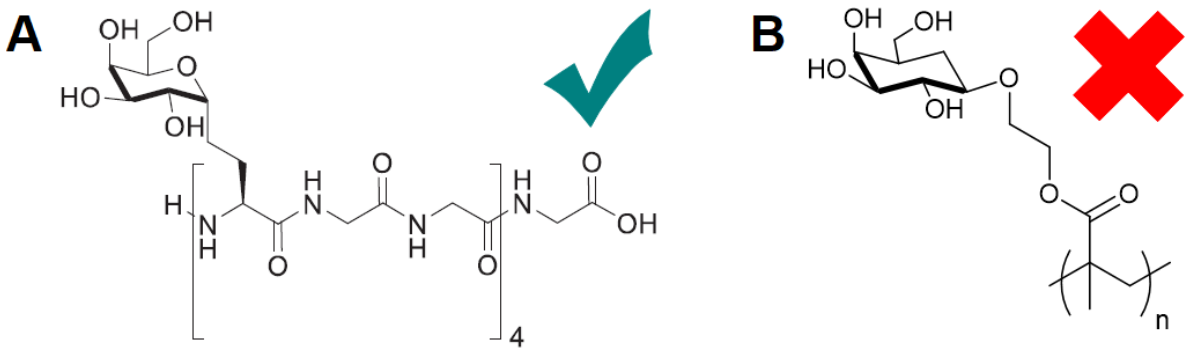

Figure 4.2 – Structural flexibility compared between active and inactive glycopeptides.

In the pursuit of structural mimickery of AFGP, a large number of carbohydrate derived species have been developed. Ben and co-workers have demonstrated the potential and IRI potency of synthetic glycopeptide mimetics of AFGP [6,20,21,22,23,24] and their application to cell

cryopreservation (Figure 4.2A).[25,26,13,27] Similarly, Cameron and co-workers have previously reported on a series of glycopolymers, which had very weak IRI activity (Figure 4.2B).[28]

These species were (unlike AFGP and Ben's amide rich peptides) highly flexible, with little spatial segregation of the hydrophobic backbone and hydrophilic glycosyl units. From this, it is clear that in order to mirror the complex architecture of AFGP, featuring both rigidity to allow for a spatially segregated hydrophilic and hydrophobic domain, but sufficient flexibility so as to not be wholly insoluble, traditional radical polymerisation techniques such as RAFT (leading to sp3 hybridised centres) are not apposite. Backbone rigidity is therefore advantageous, and so an unsaturated polymer chain, featuring sp^2 hybridised centres, would be desirable.

Tew and co-workers have explored the use of structural rigidity in the development of a series of facially amphipathic cationic polymers, with opposing positive charges and lipophilic domains to mimic the function of antimicrobial peptides.[1,29,30] These synthetic mimics of antimicrobial peptides (SMAMPs) are thought to cause disruption of the bacterial cell membrane by charge permeation, with amphipathy as the prerequisite for potency. Specifically, the key design step was the use of ROMP to introduce rigid alkene backbones, balancing the polymers hydrophobicity/philicity and thereby maintaining both the overall solubility of the material and ensuring the presentation of the hydrophobic faces. These candidates have ultimately shown particular potency as potential antimicrobials.[1,31] Considering the above rationale, we aimed to design and synthesise a locally-rigid, facially amphipathic glycopolymer series, utilising ROMP to introduce local rigidity. The anticipated potency would represent a blue-print in rational IRI design, demonstrating the ability to incorporate high levels of activity into simple macromolecular architectures through the optimisation of defined architectural motifs.

4.3 – Results and Discussion

4.3i – Synthesis of amphipathic homopolymers

In order to probe and validate the structural features necessary to incorporate potent ice recrystallisation activity into synthetic polymers, sequentially modified polymers were to be prepared. In the first instance, it was desirable to synthesise both a wholly hydrophilic derivative and an amphipathic derivative, based on the Tew architecture. It was hypothesised that a hydrophilic derivative – lacking a significant hydrophobic domain – would produce little to no IRI effect, whilst an amphipathic structure would display greater potency, as has been previously asserted in the literature. A wholly hydrophobic derivative on the other hand, was neither designed or assessed, as it would have likely demonstrated so little solubility as to make analysis impossible.

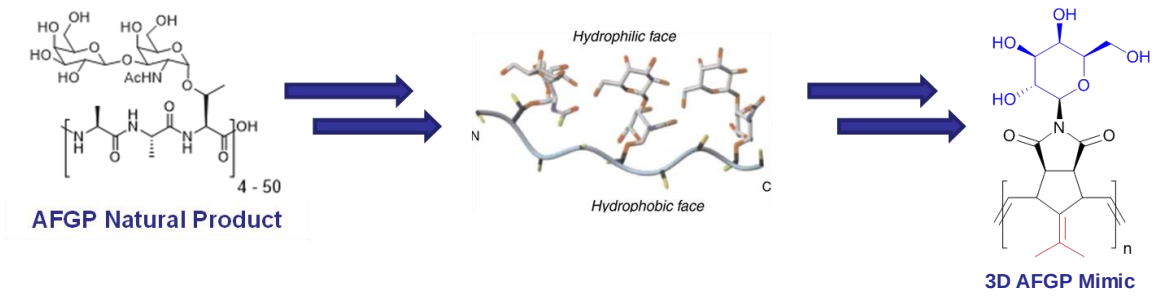

Figure 4.3 – Proposed structural framework. The solution state structure of AFGP,[7] with the disaccharide units spatially segregated from the hydrophobic peptide backbone.

Two monomeric candidates were designed, both containing a hydrophilic carbohydrate domain, and with one (the intrinsically amphipathic derivative) containing a hydrophobic fulvene 'fulvo' motif at the ring bridge head (**M1**). The other more hydrophilic species, containing an 'oxo'-ether in the same position (**M2**), Figure 4.4.

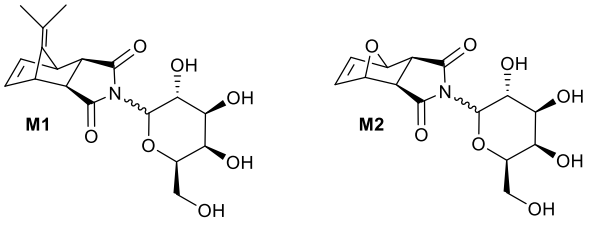

Figure 4.4 – Rationally designed monomeric architectures.

The norbornene-imide was selected due to its versatility and regular exploitation as a ROMP monomer, with a high propensity to undergo polymerisation. As such, its preparation by Diels-Alder cycloaddition and subsequent decoration is well understood and readily achieved.

Initially, a six-step synthetic route was identified based on the retrosynthetic analysis of the desired candidates, Figure 4.5 and Scheme 4.1. The 'fulvo' and 'oxo' bridge heads represented simple, large hydrophobic and hydrophilic units respectively, and the Diels-Alder precursors were inexpensive and commercially available. Galactose in particular was selected as the carbohydrate motif owing to its presence in AFGP,[6,10] with activity believed to stem from its hydration profile.[32] This would further allow for the subsequent analysis and comparison of hydrophilic group substitution and tolerance, enabling a conclusion to be drawn on the essentiality and role of the galactose motif in particular.

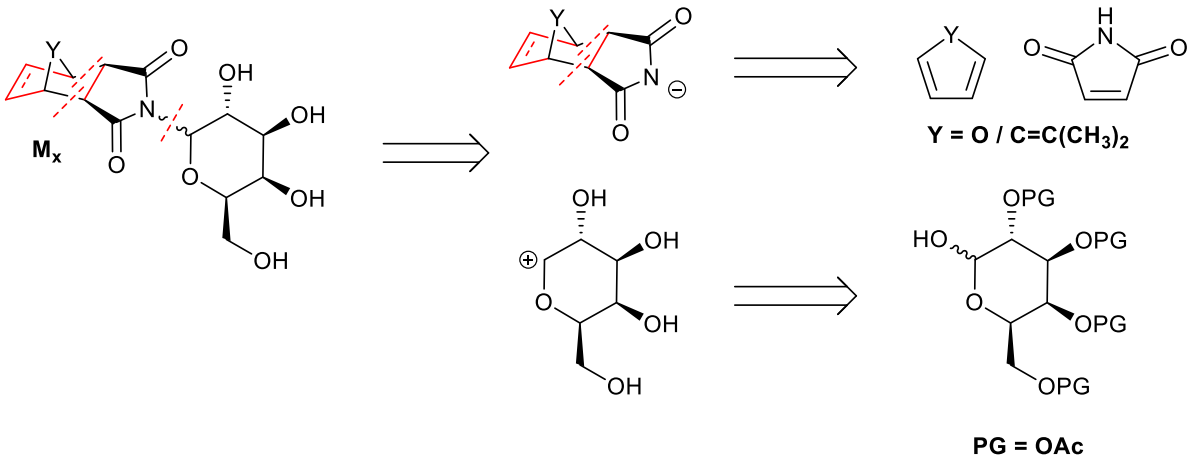

Figure 4.5 – Retrosynthesis of proposed candidates.

As per Scheme 4.1, galactose was to be acetylated under standard conditions with pyridine (**1**), and then regioselectively deprotected at the anomeric position to yield the free hydroxyl group (**2**) for amidation. Initial attempts to perform the acetylation step with $ZnCl_2$ were impractical as a result of the harsh conditions (heat and Lewis acidic) yielding a difficult to isolate tar which failed to crystallise as expected. Additionally, it was not necessary to set the stereochemistry at the anomeric centre during acetylation (with $ZnCl_2$ giving the alpha product), as the subsequent steps will render this superfluous. Pyridine was therefore opted for preferentially. It was however preferable that the final sugar-conjugate (**M1**) be stereopure at the anomeric centre, therefore avoiding obtaining a random and irregular polymer with potentially distorted IRI activity. Importantly, earlier work by Ben and co-workers noted that inactivity was induced in *C*-linked AFGP mimetics by substituting the galactose moiety for glucose, implying a potential intolerance to epimerisation in some AFGP mimetics.[20,32] Ammonium carbonate was selected due to its reported selectivity during deacetylation of the anomeric centre, giving predominately α-stereochemistry.[33,34] The acidic norbornene imide (**3a/b**) would be simultaneously prepared *via* Diels-Alder [4+2] cycloaddition, and the two fragments coupled at the imide nitrogen *via* the Mitsunobu protocol – giving the protected monomer products (**M1**/**M2**). Polymerisation was to follow, before acetate deprotection with sodium methoxide in methanol, to give the final candidates (**6a/b**). Grubbs' third generation catalyst was selected to perform the olefin metathesis, due to its superior control over molecular weight, polymer dispersity, its improved stability profile with respect to air and moisture, and its ability to initiate the polymerisation step up to x1,000,000 faster than the second generation equivalent. [35–37,38]

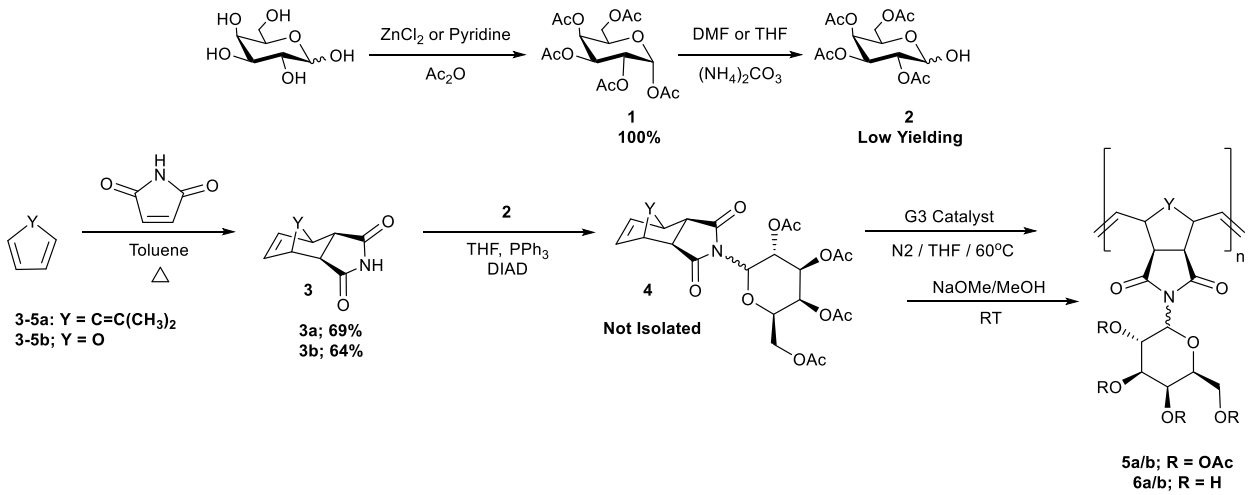

Scheme 4.1 – Initial Synthetic Route.

It was necessary under the above scheme and conditions to specifically deprotect the sugar acetates with NaOMe/MeOH instead of hydrazine, owing to the propensity of the imide ring system to otherwise undergo Wolff-Kishner reduction or the latter stage of a Gabriel synthesis. Furthermore, it was essential to not deprotect prior to polymerisation, due to both cross-linking effects and the risk of premature precipitation often encountered during ROMP with exposed hydroxyl groups and increasing molecular weight.[39]

The Diels-Alder cycloaddition products, **3a/b**, were successfully obtained in diastereoisomerically pure yields of 69 % and 64 %, respectively, exclusively giving the desired (and superiorly stable) *exo,exo* isomer owing to thermodynamic control (> 81 ºC).[40] Figure 4.6. Isomeric purity is necessary, due to the weaker ability of the *endo,endo* equivalent to effectively undergo ring-opening metathesis due to poorer sterics, impacting upon polymerisation kinetics.[41]

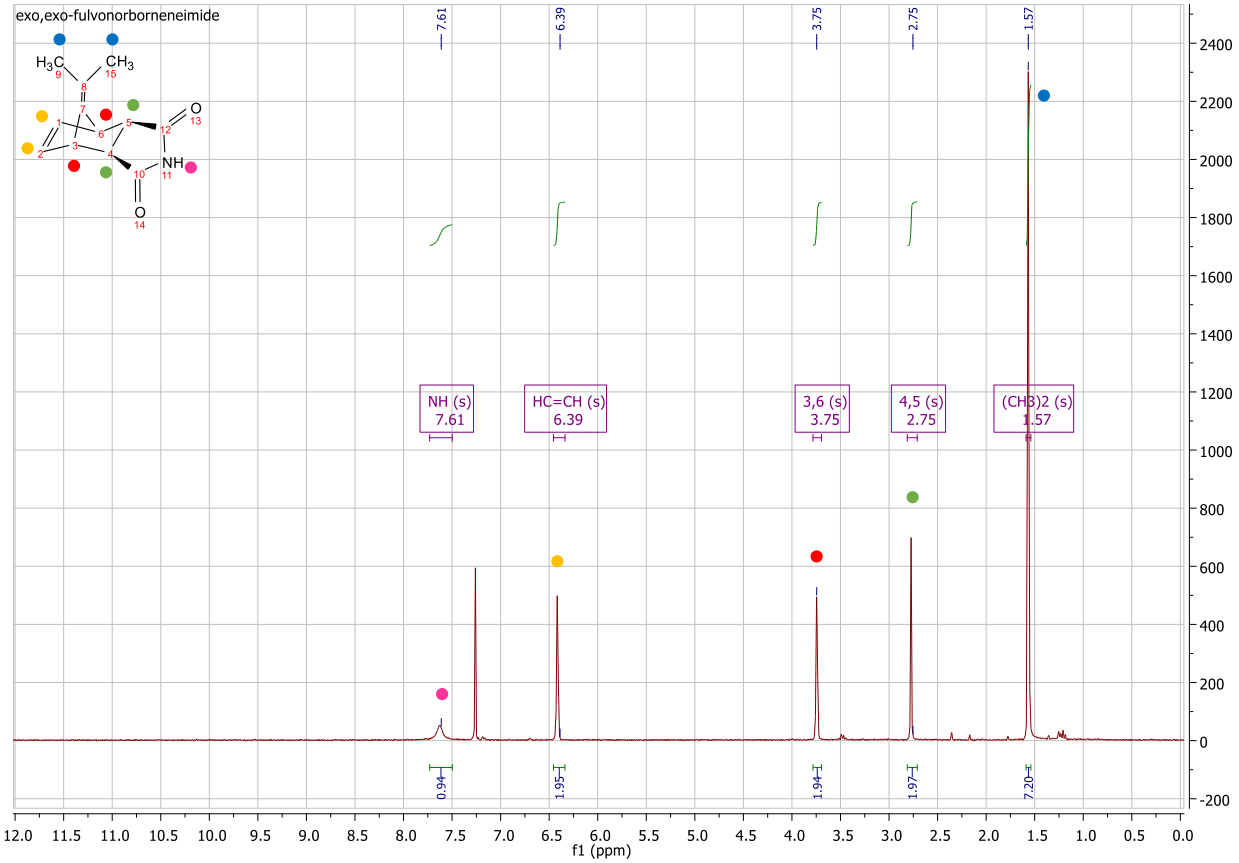

Figure 4.6 – ^{1}H NMR ($CDCl_3$) of diastereoisomerically pure *exo,exo*-fulvonorborneneimide.

Selective deprotection of the anomeric hydroxyl to give species **2**, was however problematic in practice. The rate of deacetylation with ammonium carbonate was often slow and incomplete, the extent of which was inconsistent and irreproducible, and appeared to give a substantial mixture of anomers – contrary to literature precedent (Appendix A). Substitution for benzylamine [42] furnished a smoother and complete deprotection, but again provided a mixture of the α/β diastereoisomers (Appendix A) which are not readily separable due to their similarity. The mixture of isomers were however used 'as is' and carried forward to the next stage (Mitsunobu coupling), where solely β-stereochemistry was obtained, due to the supremacy of neighbouring group participation over backside attack (Scheme 4.2).

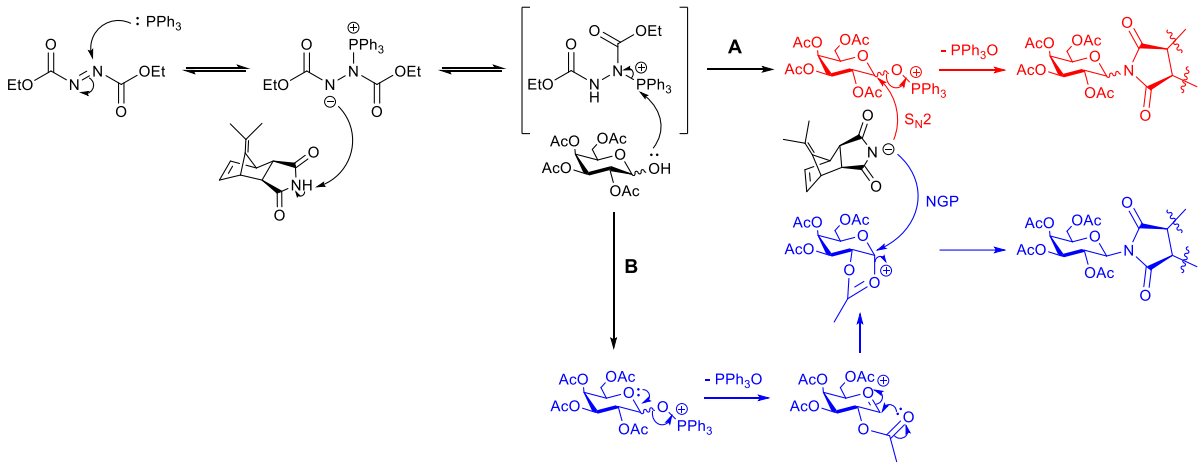

Scheme 4.2 – Attempted Mitsunobu Synthesis of **M1**.

Repeated recrystallisation, as recommended by the literature precedent,[1] failed however to adequately remove the large quantities of the triphenyl phosphine oxide (TPPO) by-product present in the reaction mixture, produced 1:1 with the product (Appendix A). Thin layer chromatography (TLC) of the crude mixture indicated a significant abundance of additional (unknown) components (Appendix A) complicating separation by column chromatography. The crude mixture had broad-spectrum solubility in organic solvents, and proximal R_f values were observed between the two main spots, suggesting similar polarity between TPPO and **M1**. Complexation with hot, ethanolic-$ZnCl_2$,[43] had little-to-no effect on removing the contaminant, with no crystallisation observed. This suggested the reaction was inefficient, incomplete, and would prove difficult to purify. Revision of the synthetic route was therefore necessary to provide the monomer in isolatable quantities, Scheme 4.3.

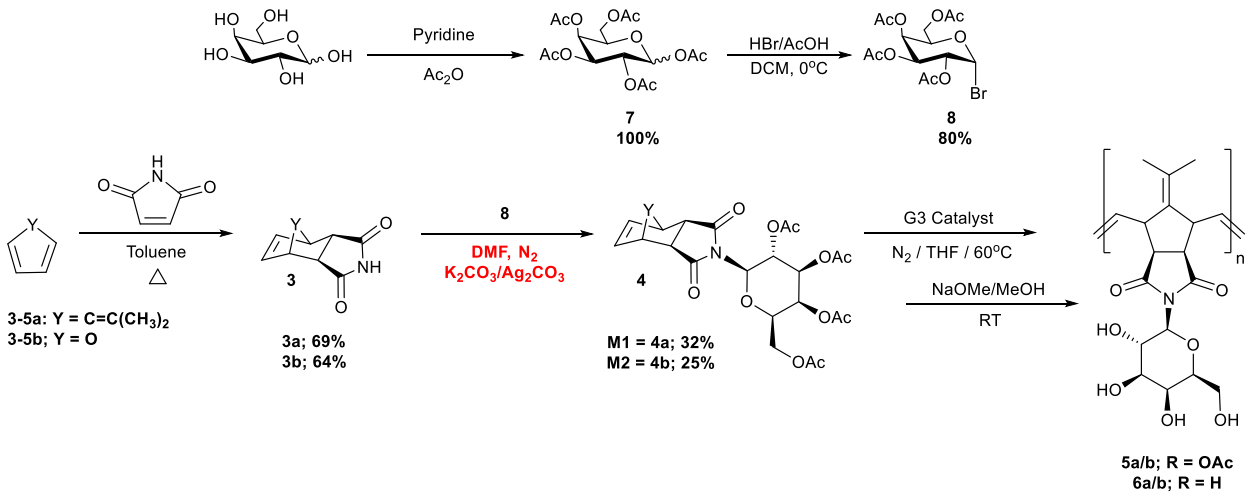

Scheme 4.3 – Revised Scheme for the synthesis of **M1/2**.

M1/2 were to be instead synthesized by Koenigs–Knorr coupling of acetobromo-α-D-galactose (**6**) with *exo*,*exo*-[oxo/fulvene]norborneneimide. Bromination of the galactose pentaacetate was efficient, providing a reactive tether of defined stereochemistry, α (100 %), in good yield (80 %).

Initial trials to optimise the coupling process of **3** and **8** were carried out. Attempts to generate the phthalate salt of the acidic **3a** with potassium hydroxide, followed by a simple displacement reaction were not fruitful. In the absence of a carbohydrate activator, the salt was ineffective at instigating a simple S_N2 displacement of the R-Br bond. Additional attempts with potassium carbonate in DMF at both 50 and at 90 ºC also produced no observable product by ^{1}H NMR or LCMS. This indicated that the reaction would only proceed through an intermediary oxonium ion assisted by a carbohydrate promoter.

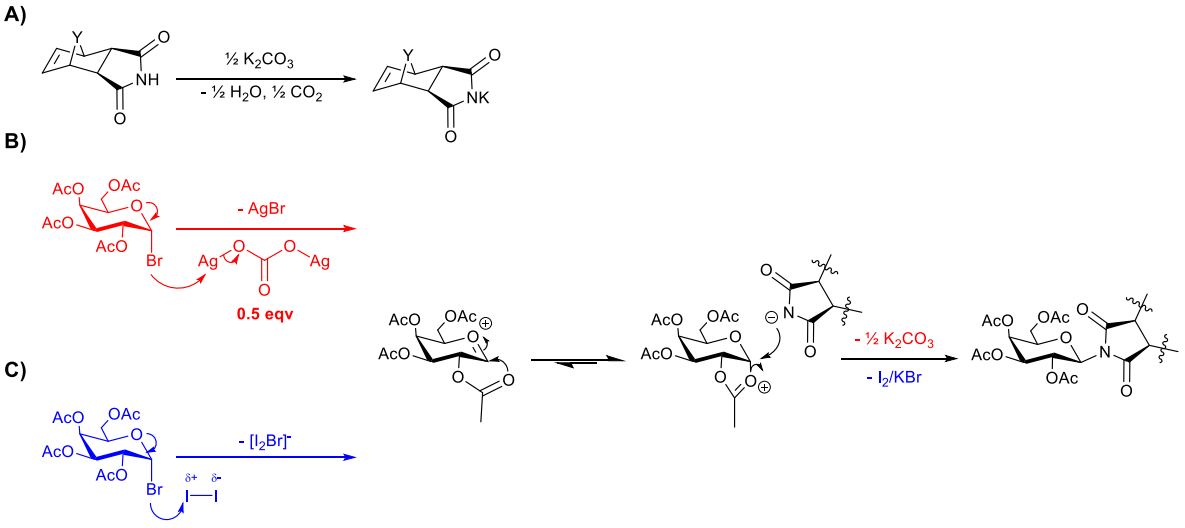

Scheme 4.4 – Trialed carbohydrate conjugation strategies A) Preparation of the norborneneimide salt *in-situ.* B) Silver carbonate promotion. C) Iodine (Lewis-acid) promotion.[44]

As such, *in-situ* couplings were attempted. The first, using iodine as a Lewis acid catalytic promoter [45,46] in conjunction with potassium carbonate (for imide activation), led to the formation of the new monomer product **M1**. However, this procedure was impractical, requiring intricate manipulations and separate preparatory techniques for the imide and carbohydrate to avoid neutralisation.

The second was simpler and efficient. Silver carbonate was identified [47] and in a preliminary run, was found to be the most suitable catalyst, capable of activating the imide at ½ an equivalent without any sign of orthoester formation by ^{1}H NMR.[48,49] The β-stereochemistry of the product was ensured by the presence of neighbouring group participation at C2, preventing the formation of an α-linkage. This led to the clean generation of **M1**, under mild, basic (K_2CO_3) conditions. As with the prior method of preparation, the stereochemical outcome is preferable, as lacking the increased steric hinderance associated with the alpha-form, **M1** was expected to be more solvent accessible when polymerised.

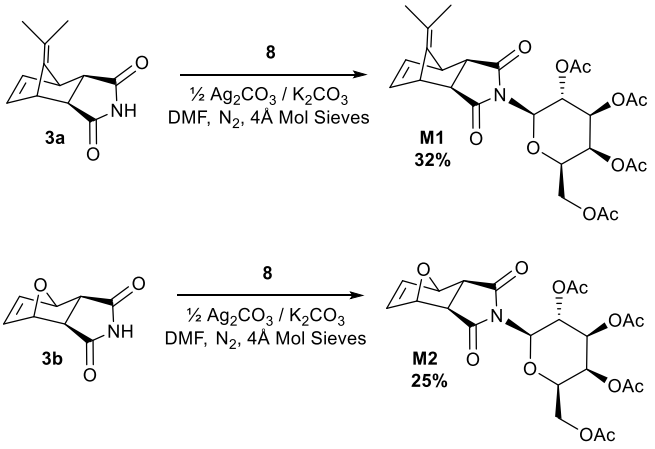

Scheme 4.5 – Optimised coupling route.

Now optimised as per Scheme 4.5, **M1** was obtained in a yield of 32 % (Figure 4.7), whilst the oxo-ether derivative, **M2** was obtained through the same procedure at 25 % yield.

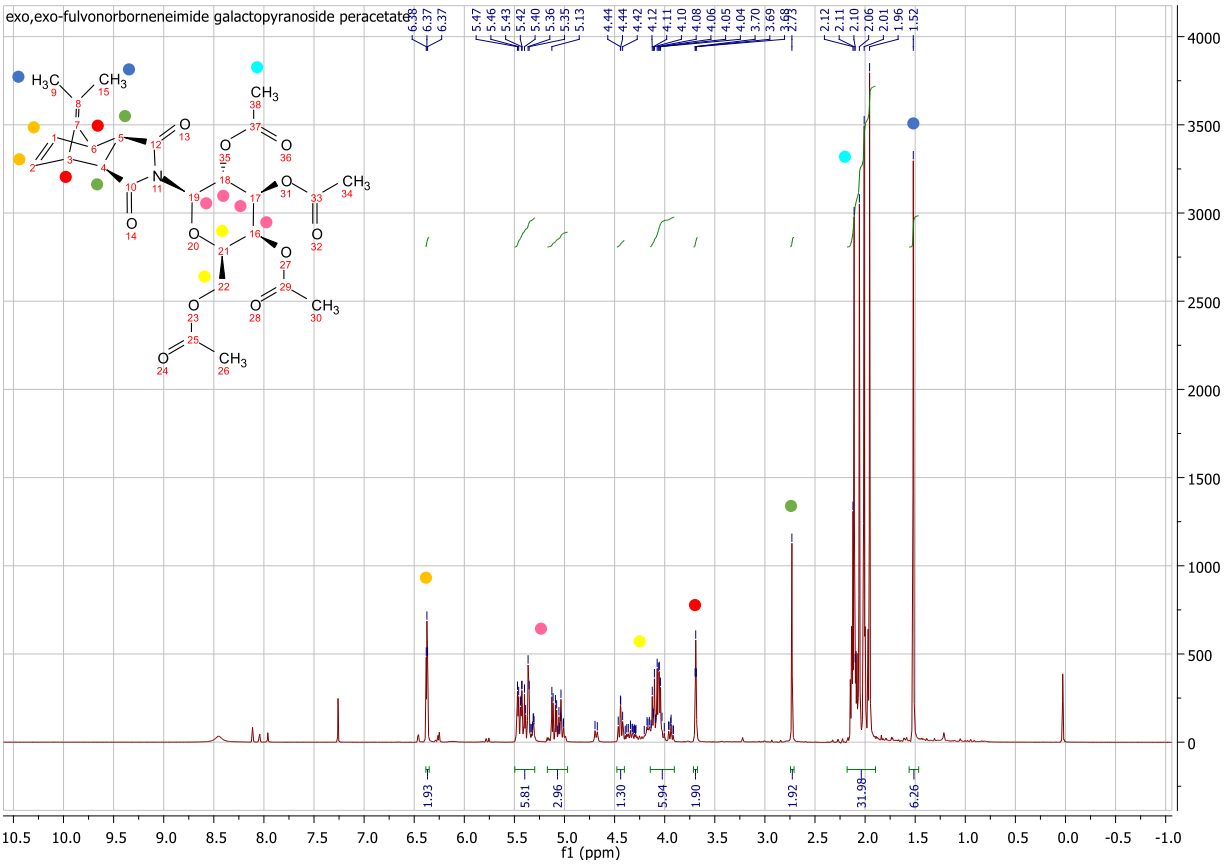

Figure 4.7 – ^{1}H NMR ($CDCl_3$) of **M1**.

Polymerisation was subsequently attempted, as per the ring opening metathesis polymerisation protocol, Scheme 4.6.

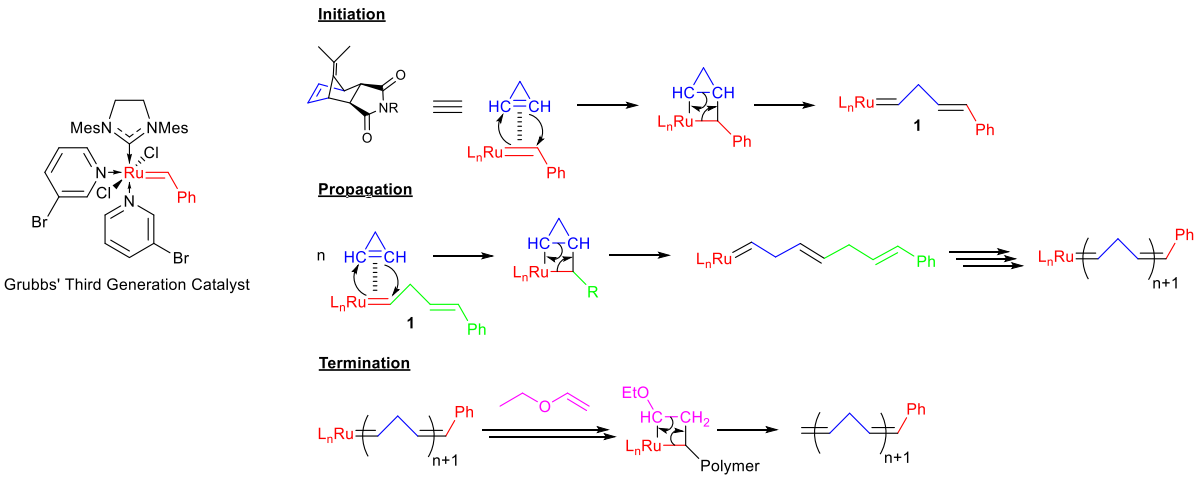

Scheme 4.6 – Mechanism of ring-opening metathesis polymerisation.

The rate of this homopolymerisation with Grubbs' third generation catalyst was judged to be rapid and non-reversible, with a ^{1}H NMR kinetics study of the unconjugated norborneneimide starting material (**3**) showing an absence of the 6.37 ppm monomeric triplet at time zero, indicating instantaneous polymerisation (Appendix A). The alkene proton signals stemming from the polymeric backbone in the 6.54 ppm region were consistent and unchanged over this interval, further suggesting that no ring closing metatheses occurred.

In order to prepare the macromolecular architectures of interest, polymerisation of the candidates **M1** and **M2**, with Grubbs' 3rd Generation Catalyst in THF under inert atmosphere then followed. Table 4.1. Molecular weight targeting yielded two polymeric candidates at approximately 10 kDa Mw and of narrow dispersity (≈ 1.2 Đ). (See Materials & Methods).

	$M_{n(THEO)}$ ($g.mol^{-1}$) [a]	$M_{n\ (SEC)}$ ($g.mol^{-1}$) [a]	Đ (-) [a]	DP (-) [a]	Conv % [b]
poly(Fulvo)	25,000	10,300	1.21	28	100
poly(Oxo)	10,000	7,300	1.18	22	100

Table 4.1 – Homopolymer characterisation [a] Determined by SEC. [b] Determined by ^{1}H NMR. [c] Single species.

4.3ii – The IRI activity of the amphipathic homopolymers

Utilising the 'splat' cooling assay, as first pioneered by Knight and co-workers,[3] the homopolymeric candidates could be assessed for IRI activity. In short, a 10 µL sample of the species of interest, dissolved in PBS buffer (pH 7.4), was dropped 1.40 m onto a chilled glass coverslip, resting on a thin aluminium block placed on dry ice. Upon hitting the coverslip, a frozen wafer with diameter of approximately 10 mm and thickness 10 µm forms instantaneously. The glass coverslip is transferred onto the Linkam cryostage and held at -8°C under N_2 for 30 minutes. Photographs are obtained of the initial wafer (to ensure that a polycrystalline sample had been obtained) and again after 30 minutes. In brief, the number of ice crystals in the field of view are measured, and the measurement repeated for three independent wafers. The average (mean) of these three measurements was then calculated to find the mean grain area (MGA). The average value and error was compared to that of a PBS buffer negative control.

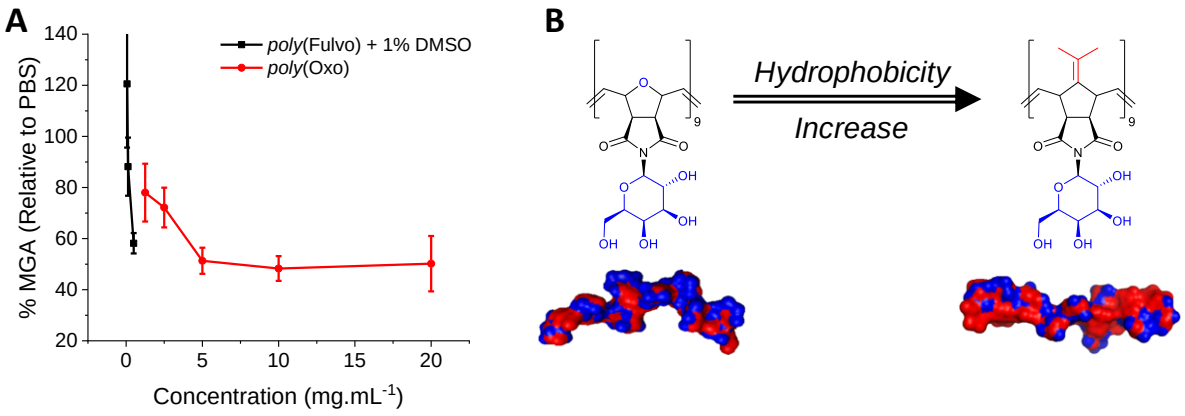

Figure 4.8 – A) IRI activity of the initial homopolymeric candidates. B) Difference in surface amphipathy of poly(Oxo) and poly(Fulvo), respectively. IRI activity measured as a function of solute concentration. MGA = Mean grain area relative to a PBS control, expressed as %. Error bars represent the ± standard deviation from three independent measurements.

The poly(Fulvo) derivative was found to be highly insoluble in water, and indeed polymers derived from it (the **M1** monomer) containing the 'fulvo' motif were significantly less soluble on the whole, than those derived from **M2** (containing the 'oxo'-ether units). Solubility limits of the derived candidates were therefore established through UV-Vis spectroscopy and Beer-Lambert Plots (Materials & Methods). The hydrophobic nature of the 6,6-dimethylfulvene bridge head coupled with the aggregatory effect of sugar hydroxyls likely led to solution phase aggregation of the poly(Fulvo) species. This necessitated the addition of 1% DMSO to aid with dissolution for IRI assay (with a 1% DMSO/PBS control used accordingly). The poly(Oxo) on the other hand lacked a prominent hydrophobic domain, and possessed high water solubility. Poly(Oxo) was found to inhibit ice crystal growth by approximately 50% MGA at concentrations above 5 $mg.mL^{-1}$, Figure 4.8A, demonstrating greater activity than many previously reported IRI active polymers.[50,51] The activity plateau between 5 and 20 $mg.mL^{-1}$ is likely due to aggregation. The poly(Fulvo) derivative featuring the hydrophobic face was however, considerably more active, inhibiting ice crystal growth by ~ 50% MGA at just 0.5 $mg.mL^{-1}$ (solubility limit), supporting the facially amphipathic hypothesis for IRI. This makes clear the core importance of hydrophobic domain inclusion for IRI potency. Molecular models corroborate this (Figure 4.8B), and illustrate the relative increase in hydrophobicity across the poly(Oxo) and poly(Fulvo) homopolymers. Crucially, this validated our hypothesis that rational design of IRI active species was in principle possible, and that hydrophobicity as a core design motif may allow us to access highly potent architectures.

However, the overall low polymer solubility of poly(Fulvo) is self-limiting, ultimately preventing sufficient solubilisation of additional fulvo units necessary for accessing greater levels of activity.

4.3iii – Synthesis and IRI activity of amphipathic copolymers

In an effort to access greater IRI activity whilst benefiting from improved solubility, a series of (co)polymers were synthesised, Table 4.2 and Figure 4.9.

	$M_{n(THEO)}$ (g.mol^{-1}) *[a]*	$M_{n\ (SEC)}$ (g.mol^{-1}) *[a]*	Đ (-) *[a]*	DP (-) *[a]*	Conv % *[b]*
poly(**Diol**) *[c]*	10,000	2200	1.01	14	100
		5300	1.01	34	
		8,400	1.02	54	
poly(**FPEG**)	10,000	35,900	1.38	133	100
poly(**Fulvo-*co*-Diol)-11**	5,000	10,700	1.12	14,35	94/97
poly(**Fulvo-*co*-Diol)-17**	10,000	16,800	1.10	22,54	100
poly(**Fulvo-*co*-Diol)-35**	25,000	34,600	1.26	47,112	100
poly(**Fulvo-*co*-Oxo**)	10,000	7,700	1.35	11,11	100/96
poly(**Fulvo-*co*-FPEG**)	10,000	55,600	1.47	76,58	71

Table 4.2 – (Co)polymer characterisation [a] Determined by SEC. [b] Determined by ^{1}H NMR. [c] Single species.

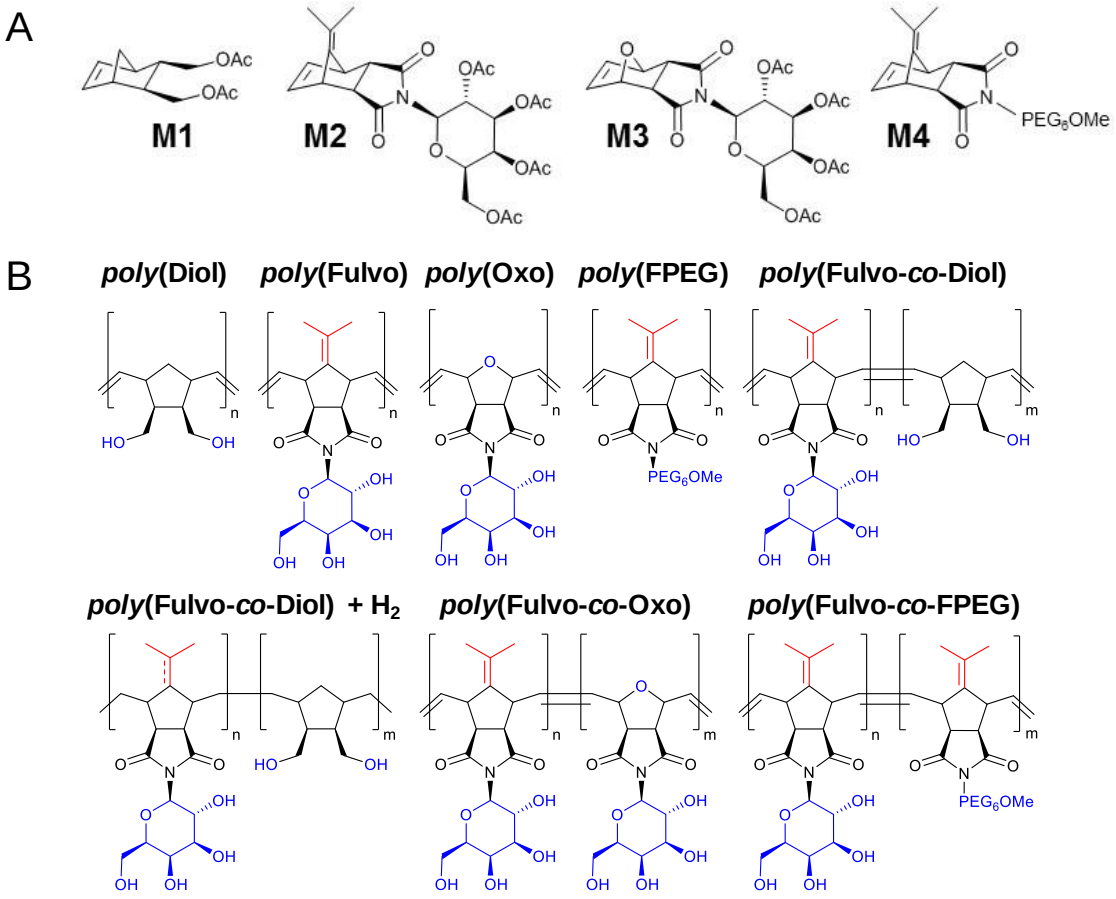

Figure 4.9 – A) Monomers prepared herein and; B) (Co)polymeric library prepared from the monomers.

In the first instance, a 1:1 statistical copolymer was prepared from the **M1** and **M2** monomeric candidates, to give poly(Fulvo-*co*-Oxo). We hypothesised that the incorporation of randomly interspersed Oxo units (**M2**), breaking up intramolecular aggregation, would improve solubility and consequently enhance activity (stemming from the greater solvated fulvo motifs).

In practice, the poly(Fulvo-*co*-Oxo) co-polymer had significantly improved solubility as anticipated from the introduction of the oxygen bridgehead motif, and slightly improved overall IRI activity relative to poly(Fulvo) – 39 % MGA at 20 $mg.mL^{-1}$. Figure 4.10A. This demonstrates that some co-monomer incorporation is tolerated, unlike PVA,[2] with example ice wafers are shown in Figure 4.10B/C.

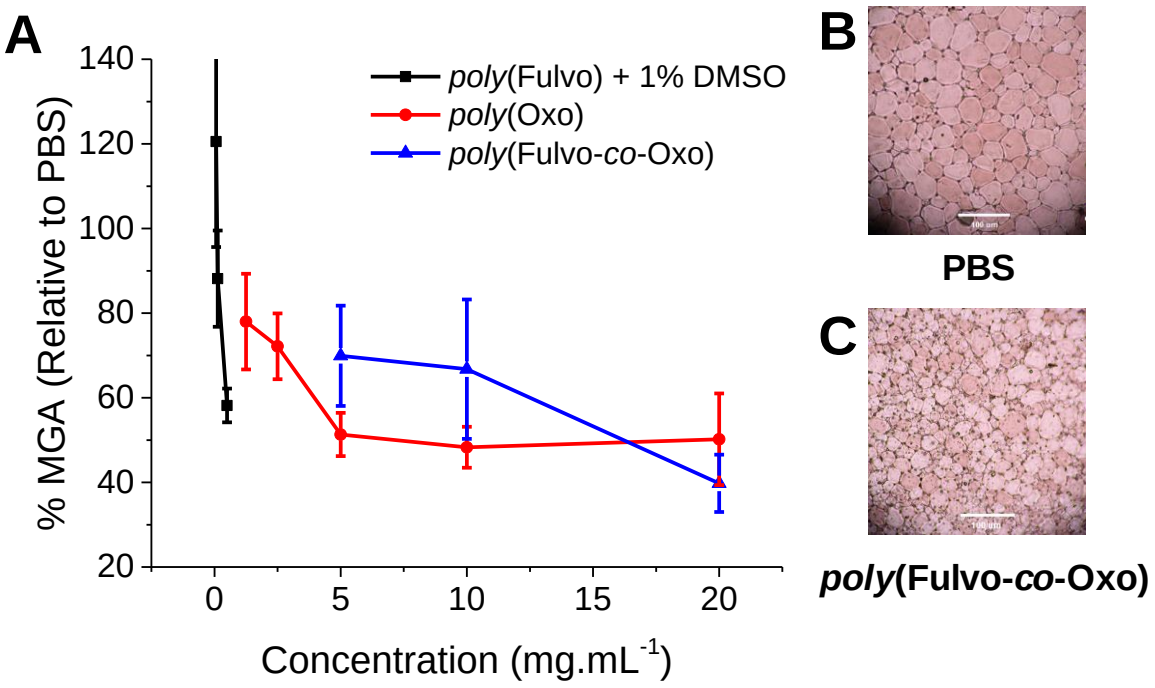

Figure 4.10 – A) IRI activity of statistical copolymer versus homopolymers. B) Splat wafer of PBS and C) poly(Fulvo-*co*-Oxo) at 20 mg.mL^{-1}. Cryomicrographs taken after 30 mins at –8 °C. Scale bars 50 µM across. IRI activity measured as a function of solute concentration. MGA = Mean grain area relative to a PBS control, expressed as %. Error bars represent the ± standard deviation from three independent measurements.

However poly(Fulvo-*co*-Oxo) had a relative lack of potency compared to poly(Fulvo) at low concentrations, and it is likely that the non-ideal copolymerization kinetics of the oxo (**M2**) and fulvo (**M1**) co-monomers will have led to a blocky, rather than statistical copolymerization, ultimately leading to aggregation.[39,52] Previously, Musa and co-workers has highlighted the propensity of monomers with diverse bridgeheads to possess vastly different kinetics with respect to the oxidative addition step on the adjacent ring alkene.[38] SEC analysis – Figure 4.11 – confirms aggregation, likely as a result of micellization/internalization of hydrophobic domains, with a bimodal trace observed depending on eluent.

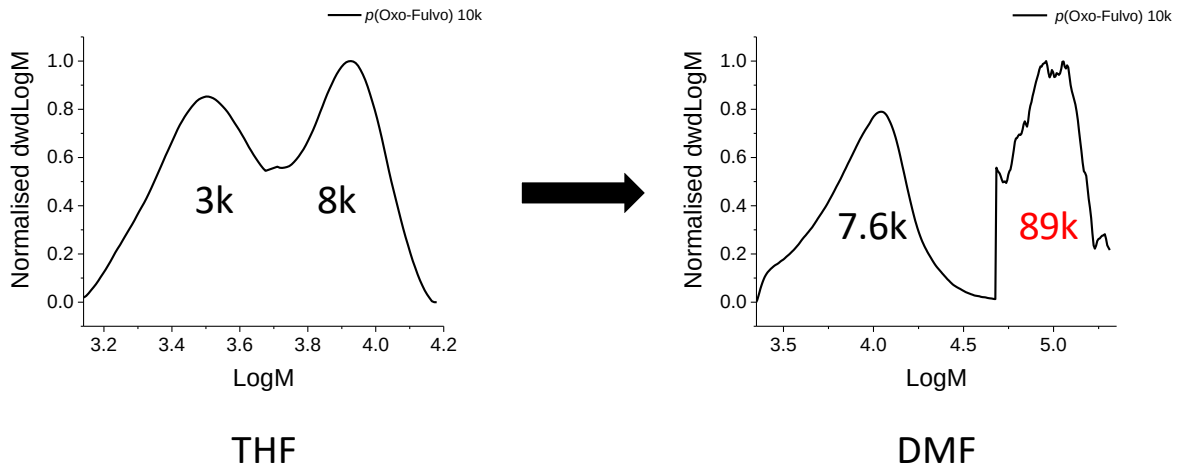

Figure 4.11 – SEC/GPC Trace of poly(Fulvo-*co*-Oxo) in THF and DMF.

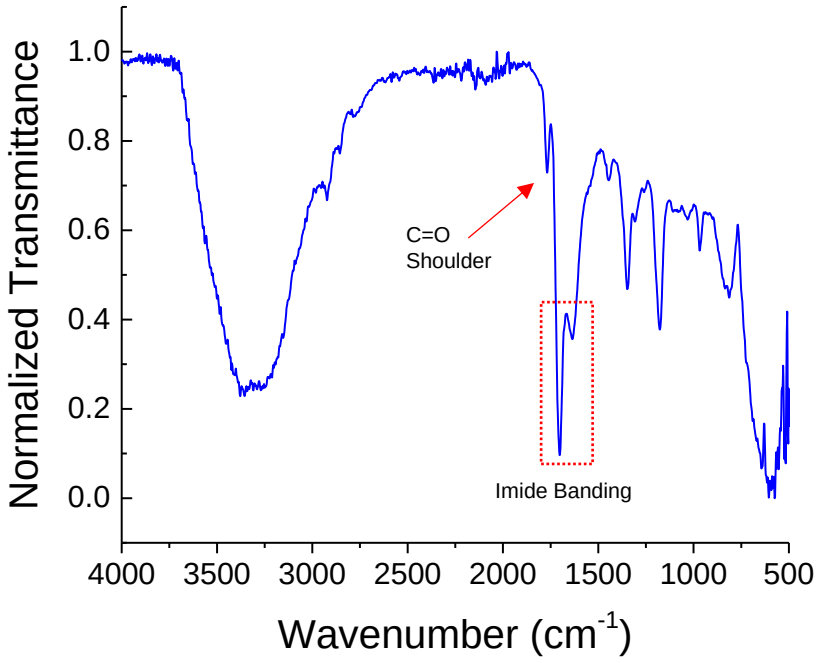

Figure 4.12 – IR Spectra of poly(Fulvo-*co*-Oxo) indicating incomplete deacetylation.

In addition, Infrared analysis (Figure 4.12) indicated the incomplete removal of the acetate protecting groups (in contrast to the homo polymers) – with a second carbonyl environment observed at ~ 1750 cm^{-1}. This would tend to confirm the block like character of the copolymer,

suggesting an internalized domain structure and/or aggregation, with some hydrophobic surfaces being solvent inaccessible and hence limiting the total activity poly(Fulvo-*co*-Oxo).

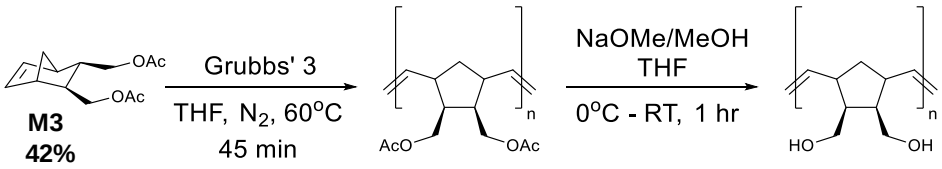

Scheme 4.7 – Polymerisation of a norbornenediol.

In order to improve solubility and retain activity, a norbornene diol monomer (**M3**) with a non-hydrophilic bridgehead was investigated, Scheme 4.7. De-acetylated homopolymers of **M3**, poly(Diol), were found to have surprisingly low solubility and no activity at their solubility limit of 0.59 mg.mL^{-1} (2-8 kDa). A higher molecular weight species (30 kDa) also displayed no activity at 52 µg.mL^{-1}. This is presumably due to strong, intramolecular hydrogen bonding.

However, when **M3** was incorporated as a co-monomer with the (IRI active) 'fulvo' monomer **M1** to give poly(Fulvo-*co*-Diol), an overall increase in solubility was achieved. Poly(Fulvo-*co*-Diol)-17 had remarkable IRI activity; 40 % MGA at just 1.3 mg.mL^{-1}, Figure 4.13. This is likely due to the diol-units breaking up intramolecular hydrogen bonding as a result of being randomly interspersed in the copolymer in a more statistical manner than **M2**. As such, the kinetically proximal, non-electron withdrawing hydrophobic bridgehead of **M3**, as opposed to the polar and highly disruptive nature of the oxygen bridge head present in poly(Fulvo-*co*-Diol), has led to greater solvation of the potent fulvo stretches without aggregation/encapsulation. This polymer also showed strong molecular weight dependence on activity, and a distinct solubility trend. 17 kDa (1.3 mg.mL^{-1}) had significantly more activity than 11 kDa (3.4 mg.mL^{-1}). This is in agreement with the effects observed for many AFGPs, PVA,[53] and IRI active proteins (such as those extracted from the freeze-tolerant plant Seabuckthorn)[54], where a strong molecular weight dependence has been demonstrated – with

increasing activity observed at higher molecular weights. Increasing the molecular weight to 35 kDa lowered the solubility of the copolymer (0.39 mg.mL^{-1}, due to aggregation), and hence activity fell, indicating a 'goldilocks zone'.

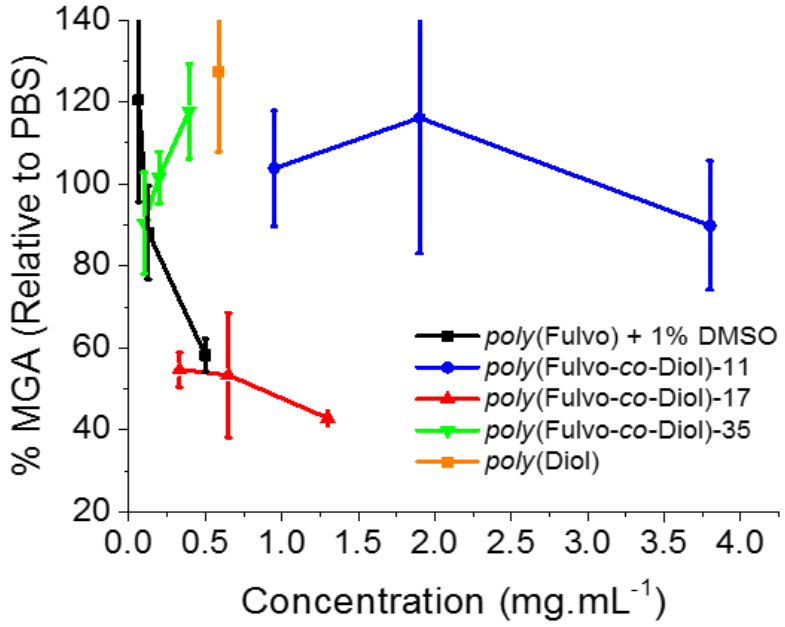

Figure 4.13 – IRI activities of the poly(Fulvo-*co*-Diol) molecular weight series. IRI activity measured as a function of solute concentration. MGA = Mean grain area relative to a PBS control, expressed as %. Error bars represent the ± standard deviation from three independent measurements.

In order to probe the tolerance to functionalisation, and the importance of the carbohydrate motif as the hydrophilic domain in particular, the glycan unit was replaced with a short oligo(ethylene glycol), PEG, chain. Two candidates, poly(Fulvo-*co*-FPEG) and poly(FPEG), were obtained – Scheme 4.8 and Figures 4.14 and 4.15. Monomethylation of the PEG chain was surprisingly simple to achieve, similar to literature precedent,[55–57] with a yield of 90%.

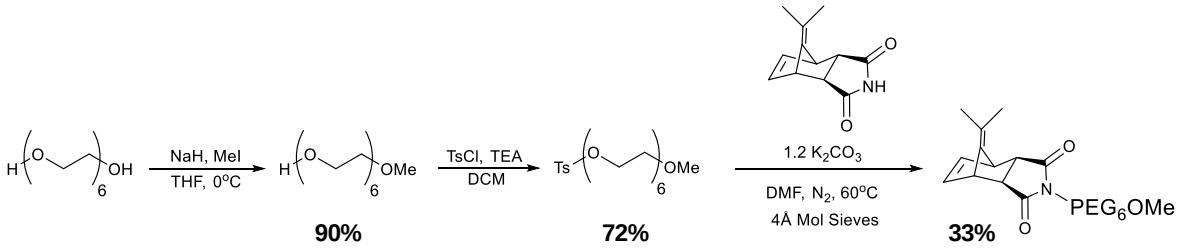

Scheme 4.8 – Monomethylation and tosylation of PEG and conjugation to the monomer unit.

At 55 kDa Mw, poly(Fulvo-*co*-Diol) had comparable solubility (~ 0.43 mg.mL^{-1}) to the poly(Fulvo-*co*-Diol) 35 kDa derivative. However, only very slight activity was observed (~ 80 % MGA), much weaker than poly(Fulvo-*co*-Diol) 17k at similar concentration. Likewise, poly(FPEG) was inactive at 36 kDa Mw despite having an improved maximum solubility of 0.65 mg.mL^{-1}. The decreased activity observed in both cases may therefore stem from the large and flexible PEG pedant being able to adopt numerous confirmations, thereby reducing overall amphipathy.

Crucially, the small molecule monomers of poly(Fulvo), poly(Diol), and poly(FPEG) were all very weakly active, with **M1** inhibiting at just 83 % MGA (280 µg.mL^{-1}) – implying the supremacy of long range order and the need for a macromolecular system in IRI.

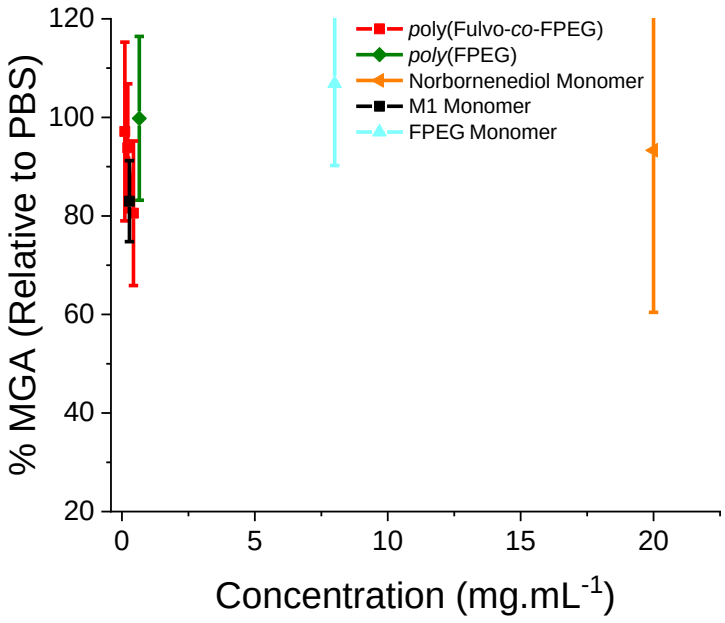

Figure 4.14 – IRI activities of weak to inactive candidates. IRI activity measured as a function of solute concentration. MGA = Mean grain area relative to a PBS control, expressed as %. Error bars represent the ± standard deviation from three independent measurements.

Similarly, hydrogenation attempts upon the alkene backbone of poly(Fulvo-*co*-Diol)-17 (Scheme 4.9) in order to increase flexibility and observe the effect of decreased rigidity on our structures, resulted in a wholly insoluble (and un-assayable) polymer.

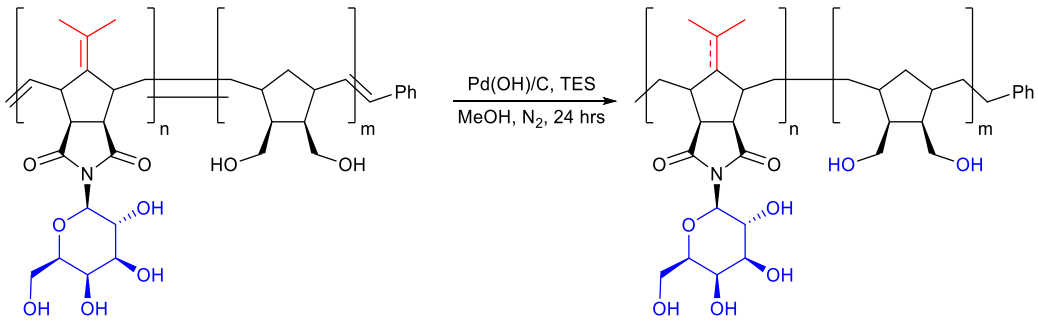

Scheme 4.9 – Hydrogenation of the poly(Fulvo-*co*-Diol)-17 species with palladium (II) hydroxide over carbon and triethyl silane.

These observations demonstrate that precise macromolecular engineering is essential to achieve a potent IRI mimetic.

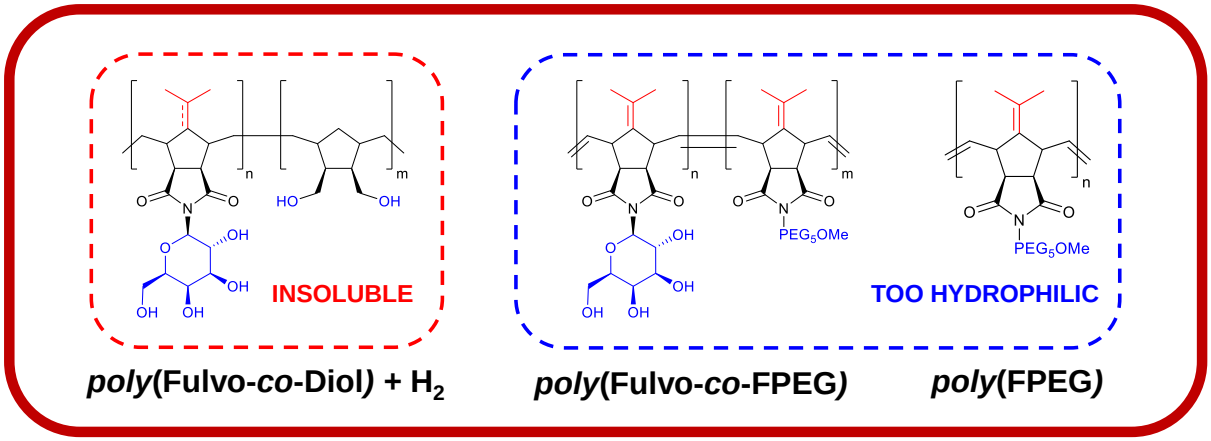

Figure 4.15 – Inactive modified species.

AF(G)Ps bind to specific ice crystal faces,[58,59] leading to dynamic ice shaping (unwanted in cryopreservation[60]). In order to elucidate the mode of mechanistic action in inhibiting ice crystal growth, and to determine applicability for biomedical translation, DIS assays were performed. Performed by Alice E. R. Fayter, Control ice crystals (Figure 4.16A) showed no dynamic ice shaping, but addition of AFGPs (Figure 4.16B) produced distinctive spicular (needle-like) crystals. Poly(Fulvo-*co*-Diol)-17 (Figure 4.16C) did not lead to ice shaping, ruling out strong / specific ice face recognition and showing that these effects can be separated by macromolecular design. Moreover, as no membrane-puncturing spicular needles are formed, this study indicates that these species do not possess the same cytotoxic profile as AFGPs and may have application in biomedicine.

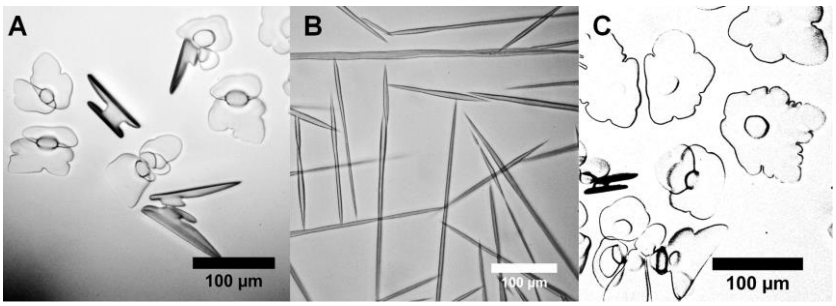

Figure 4.16 – Ice morphology analysis. A) Water. B) AFGP-8. C) poly(Fulvo-*co*-Diol)-17 at 0.72 mg.mL^{-1}.

In order to determine the morphology and evaluate the solution conformation and rigidity of the lead poly(Fulvo-*co*-Diol) candidate, small angle neutron scattering (SANS) was employed. Figure 4.17 (and Appendix). Performed by Judith E. Houston and Rachel C. Evans, two molecular weight derivatives of the poly(Fulvo-*co*-Diol) series, 11 kDa and 17 kDa were used. The estimated persistence lengths (b_t) for poly(Fulvo-*co*-Diol)-11 and poly(Fulvo-*co*-Diol)-17 were found to be 38.9 and 44.4 Å, respectively. Whilst the overlap may actually occur at a lower q region, and is masked by aggregate scattering, these values should be taken as the minimum persistence lengths for each polymer. Each b_t is much larger than the monomer length (~10 Å) which suggests that the chain backbones are locally stiff.[61] Furthermore, given the approximate contour length, L, of both polymer chains (490 Å and 760 Å for poly(Fulvo-*co*-Diol)-11 and poly(Fulvo-*co*-Diol)-17, respectively), the large b_t suggests rigid rather than highly flexible aggregates, of potentially rod-like structures. This rigidity coupled with the intrinsic amphipathy of the polymers is aligned with the hypothesized semi-rigid (and generally amphipathic) ice binding faces of AFP's,[7,62] and the flexible hydrophilic 'glycan face' of AFGPs, providing evidence that facial amphipathy is a key motif for introducing IRI activity into a diverse range of polymers.

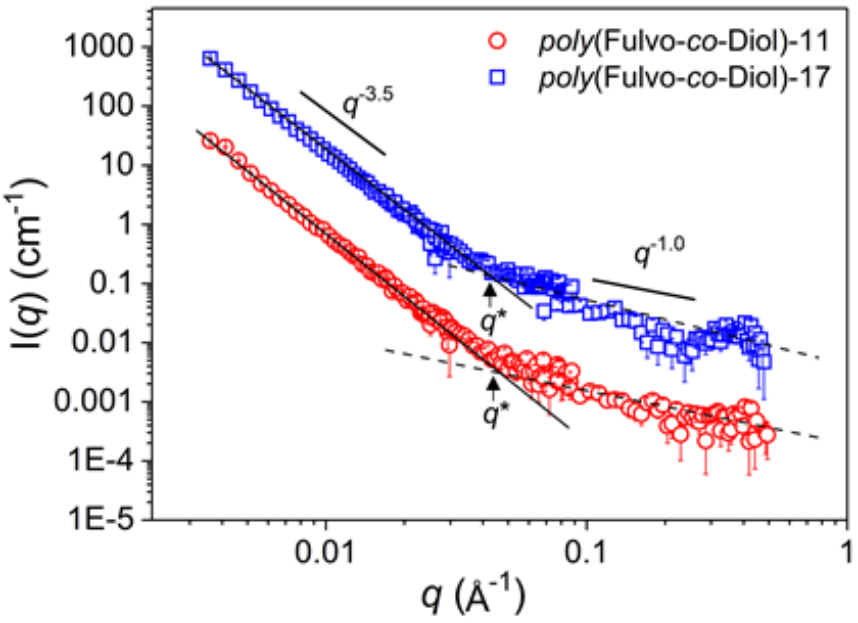

Figure 4.17 – SANS data for poly(Fulvo-*co*-Diol)-11 (100%, red) and poly(Fulvo-*co*-Diol)-17 (100%, blue) in D_2O at 25 °C. Straight lines show -3.5 and -1 decays for comparison.

4.4 – Conclusions

We have designed and synthesized facially amphipathic glycopolymers to mimic the solution confirmation and function of antifreeze glycoproteins. It was found that the addition of hydrophobic faces, opposing the glycan units, introduced potent IRI activity, but that substitution with a more hydrophilic ether unit removed activity. These results support a mechanism for IRI activity which is dependent upon local water ordering rather than an essential ice binding unit, and there was no evidence of dynamic ice shaping; with small angle neutron scattering supporting a locally rigid confirmation, as seen for AF(G)Ps, supporting the hypothesis of amphipathy as the driver for activity.

These results further suggest that the presence of hydroxyls alone are not essential for IRI, and that amphipathic domain structure is key. It is notable that none of poly(Diol), poly(Fulvo-*co*-Diol) or poly(Oxo) were capable of introducing potent IRI activity except poly(Fulvo-*co*-Diol) at very high concentration, implying that hydroxyl units themselves may not infer IRI activity.

A combination of ice binding assays, modelling and small-angle neutron scattering (SANS) ultimately provides compelling evidence that local amphipathy is an essential motif for introducing IRI activity, providing design rules for new materials to mimic AFGP function.

4.5 – Experimental

Materials

6,6-dimethylfulvene, furan, 5-norbornene-2-exo,3-exo-dimethanol, hexaethylene glycol, tosyl chloride, maleimide, toluene, diethyl ether, galactose, acetic anhydride, pyridine, *p*-toluene sulfonyl chloride, hexaethylene glycol, methyl iodide, sodium hydride (as a 60% dispersion in mineral oil), dichloromethane (DCM), hydrobromic acid in acetic acid (33%), triethylsilane, palladium hydroxide/carbon, methanol, ethanol, tetrahydrofuran (THF), triethylamine, potassium carbonate, silver carbonate, dimethylformamide (DMF), 4 Angstrom molecular sieves, ethanol, ethyl vinyl ether, Grubbs' 3rd generation metathesis catalyst, sucrose, sodium sulphate and deuterium oxide (D_2O) were purchased from Sigma Aldrich Co Ltd (Gillingham, UK) and used without further purification. Phosphate-buffered saline (PBS) solution was prepared using preformulated Figure 4.ts (Sigma Aldrich Co Ltd, Gillingham, UK) in 200 mL of Milli-Q water (>18.2 Ω mean resistivity) to give [NaCl] = 0.138 M, [KCl] = 0.0027 M, and pH 7.4.

Physical and analytical methods

^{1}H and ^{13}C NMR Spectra (300 – 400 MHz and 75 – 100 MHz, respectively) were recorded using one of a Bruker DPX-300/400 Spectrometer under standard NMR conditions. Chemical shifts were recorded in ppm and referenced to solvent residual peaks, using MestReNova NMR Spectroscopy software.

ESI MS experiments were performed on an Agilent 6130B Single QUAD ESI-LC MS spectrometer in either positive or negative mode with an H_2O/MeOH (80:20) eluent feed, with samples dissolved in water, methanol or ethanol, unless otherwise stated.

IR experiments were carried out on a Bruker Vector 22 (ATR) FTIR Spectrometer in either the solid or thin film (volatile organic solvent) phase, with background subtraction.

SEC/GPC data was acquired on either a THF or DMF (as applicable) Agilent 390-LC MDS instrument equipped with differential refractive index (DRI), viscometry (VS), dual angle light scatter (LS) and dual wavelength UV detectors. System equipped with a PL-AS RT/MT2 autosampler, Shimadzu SPD-M20A microarray detector, a PL-gel 3 μm (50 × 7.5 mm) guard column and 2 × PL-gel 5 μm mixed-D columns (300 x 7.5 mm). Samples were filtered and suspended in the relevant HPLC grade solvent (THF containing 2% TEA; DMF with 5 mmol NH_4BF_4 additive), with a flow rate of 1 mL/min^{-1} at 50ºC. Refractive index recorded. Analyte samples were filtered through a nylon membrane with 0.22 μm pore size before injection. Respectively, experimental molar mass (Mn,SEC) and dispersity (Đ) values of synthesized polymers were determined by conventional calibration (relative to poly(methyl methacrylate) standards – Agilent EasyVials, 690 – 271400 Da) using Agilent GPC/SEC software. Refractive index recorded.

Absorption UV/Vis (Ultra-violet/visible spectroscopy) spectra were acquired on an Agilent Technologies Cary 60 Variable Temperature UV-Vis spectrophotometer at room temperature

fitted with Holographic Grating (27.5 × 35 mm, 1200 lines/mm, blaze angle 8.6° at 240 nm), a double beam, Czerny-Turner monochromator, 1.5 nm fixed spectral bandwidth, full spectrum Xenon pulse lamp single source, dual silicon diode detectors, quartz overcoated optics, non-measurement phase stepping wavelength drive, room light immunity. Analysis undertaken using Agilent CaryWin UV Scan software. All sample spectra were acquired in Hellma Analytics High Precision Quartz UV Cuvettes.

Small-angle neutron scattering (SANS) experiments were performed by Judith E. Houston/Rachel C. Evans on the KWS-2 instrument at FRM-2 research reactor in Garching (Germany).[63] A q-range of 3.6×10^{-3} to 0.48 $Å^{-1}$ was achieved utilizing an incident neutron wavelength of 5 Å with a spread of $\Delta\lambda/\lambda = 20\%$ and sample-to-detector distances of 1.5, 8 and 20 m, as $q = (4\pi/\lambda)\sin(\theta/2)$, where λ is the wavelength and θ is the scattering angle. The samples were prepared in D_2O to provide good scattering contrast and placed in rectangular quartz cuvettes (Hellma, pathlength = 1 mm) and maintained at 25.0 ± 0.5 °C. The two-dimensional raw scattering data were corrected for detector sensitivity, electronic and background noise, empty cuvette contribution, and then azimuthally integrated to give the one-dimensional intensity $I(q)$ using the instrument software QtiKWS. The data was converted to the absolute scale (cm^{-1}) through reference to the scattering from a secondary standard sample (Plexiglas). Finally, the data was corrected for the solvent contribution, which was measured separately.

Experimental Methods

Solubilization of insoluble samples for analysis

Insoluble samples for splat and UV-Vis analyses (see below) were added to a PBS solution and centrifuged (10K, 10 minutes) and the supernatant removed – to give a saturated solution of unknown concentration in PBS.

UV-Vis concentration determination of insoluble samples for analysis
Calibration: The spectrometer was calibrated with a DMSO 'blank' (machine zeroed and a background scan conducted). A stock solution of the species of interest was prepared (in DMSO) at a known concentration and serially diluted, and a spectrum acquired for each concentration in the 200 – 800 nm range (600 nm/min scan rate, 1.00 nm data interval, 0.1 s average time), to give a Beer-Lambert calibration plot.
Sample Concentration Analysis: 200 – 400 µL (typically) of the sample of interest was taken as a saturated solution in PBS, and condensed *in vacuo*. The dry residue was subsequently re-dissolved in the same volume of DMSO, mixed, and drawn up to separate the liquor from the insoluble PBS salts. The UV-Vis spectrum was then acquired, as above, with dilution employed (and corrected for) where necessary. The λ_{max} of the primary peak was identified and the absorbance recorded and intersected against the line of best fit of the Beer-Lambert plot of the stock calibrants to give the saturated samples concentration in PBS solution.

Ice recrystallization inhibition (splat) assay

Ice recrystallization inhibition was measured using a modified splat assay.[1] A 10 µL sample of the species of interest, dissolved in PBS buffer (pH 7.4), was dropped 1.40 m onto a chilled glass coverslip, resting on a thin aluminium block placed on dry ice. Upon hitting the coverslip, a wafer with diameter of approximately 10 mm and thickness 10 µm was formed instantaneously. The glass coverslip was transferred onto the Linkam cryostage and held

at -8ºC under N_2 for 30 minutes. Photographs were obtained using an Olympus CX 41 microscope with a UIS-2 20x/0.45/∞/0-2/FN22 lens and crossed polarizers (Olympus Ltd, Southend-on-Sea, UK), equipped with a Canon DSLR 500D digital camera. Images were taken of the initial wafer (to ensure that a polycrystalline sample had been obtained) and again after 30 minutes. Image processing was conducted using Image J, which is freely available (National Institutes of Health, Bethesda, MD). In brief, the number of ice crystals in the field of view was measured, and the measurement repeated for three independent wafers. The average (mean) of these three measurements was then calculated to find the mean grain area (MGA). The average value and error was compared to that of a PBS buffer negative control.

Surface hydrophobicity mapping of polymers

Polymeric structures (containing 9 homo- or 9 regularly alternating hetero- ring opened monomer units) were assembled in ChemDraw Professional 16.0 (PerkinElmer Informatics Inc., Waltham, MA), assuming a 'classic' Grubbs' polymer architecture of 3:1 Trans/Cis along the unsaturated backbone. Chain end groups were not featured. The structures were then energy minimised in Chem3D and the resulting structures rendered in PyMOL (Schrödinger LLC, Cambridge, MA), which is freely available for educational use, and the surfaces on the structures were displayed. Hydrogens were then removed from the structure. The "color" command was then used to colour the polymer surface, with carbon (and so aliphatic hydrogen) defined as hydrophobic (red), whilst oxygen and nitrogen (and so imide/alcoholic hydrogens) were defined as hydrophilic (blue).

Sucrose Sandwich Ice Shaping Assay

Performed by Alice E. R. Fayter, samples dissolved in PBS buffer containing 45% sucrose were sandwiched between two glass coverslips and sealed with immersion oil. Samples were cooled to −50 °C on a Linkam Biological Cryostage BCS196 with T95-Linkpad system

controller equipped with a LNP95-Liquid nitrogen cooling pump, using liquid nitrogen as the coolant (Linkam Scientific Instruments UK, Surrey, U.K.). The temperature was then increased to −8 °C and held for 1 hour to anneal. The samples were then heated at 0.05 °C.min^{-1} until few ice crystals remained and then cooled at 0.05 °C.min^{-1} and the shape of ice crystals observed. Micrographs were obtained every 0.1 °C using an Olympus CX41 microscope equipped with a UIS-2 20x/0.45/∞/0−2/FN22 lens (Olympus Ltd., Southend on sea, U.K.) and a Canon EOS 500D SLR digital. Image processing was conducted using ImageJ.

Synthetic Procedures

General Procedure for the Synthesis of (3aR,4R,7R,7aS)-8-(propan-2-ylidene)-3a,4,7,7a-tetrahydro-1H-4,7-methanoisoindole-1,3(2H)-dione – (*exo,exo*-fulvonorborneneimide)

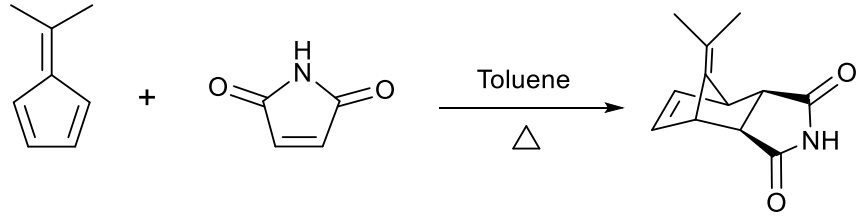

6,6-dimethylfulvene (2.4 mL, 2.12 g, 20 mmol) and maleimide (1.94 g, 20 mmol, 2 eqv) were dissolved in toluene (100 mL), and the reaction mixture stirred under reflux (135°C) for 24 hours, transitioning from a translucent orange solution to opaque after 60 minutes. The reaction mixture was then cooled to RT and condensed *in vacuo* to remove excess toluene and fulvene, and the solids washed with hot diethyl ether (3 x 20 mL) to yield the pure *exo,exo* product as a pale orange solid. 2.82 g (69%). ^{1}H NMR (300 MHz, $CDCl_3$) δ = 7.61 (1H, s, N**H**), 6.42 (2H, t, *J* = 1.96 Hz, **H**C=C**H**), 3.74 (2H, t, *J* = 1.88 Hz, Bridge Base 2 x C**H**), 2.78 (2H, s, Fused Ring 2 x C**H**), 1.57 (7H, s, 2 x **Me**). ^{13}C NMR (75 MHz, $CDCl_3$) δ = 206.96 (2 x HNR**C**=O), 137.67 (H**C**=**C**H / R_2-**C**=**C**-$(Me)_2$), 49.20 (**C**-C=O), 45.61 (**C**-HC=CH-**C**), 30.93 (2 x **Me**). IR (ATR): 3229 (NH), 3000 (C=C / C-H), 1759, 1705 (2 x C=O), 1369, 1345, 1182 (C-H), 689 cm^{-1} (C=C). m/z (ESI, -ve) Observed 202.1 [95%, $R2N^-$]. Compound previously reported.[64]

General Procedure for the Synthesis of (3aR,4R,7R,7aS)-3a,4,7,7a-tetrahydro-1H-4,7-epoxyisoindole-1,3(2H)-dione – (*exo,exo*-oxonorborneneimide)

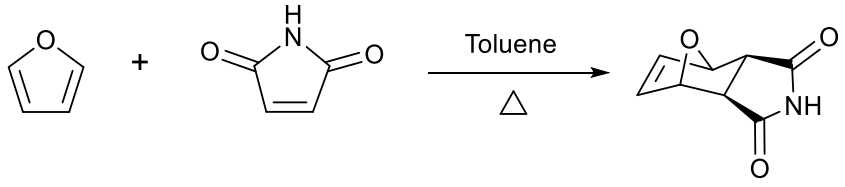

Furan (15 mL, 14.04 g, 206.26 mmol, 10 equiv) and maleimide (2.00 g, 20.60 mmol) were dissolved in toluene (20 mL), and refluxed at 95ºC for 48 hours, with the colourless mixture becoming white/opaque within 10 minutes. The reaction mixture was then cooled to RT, and then solids filtered and washed with cold toluene (100 mL) to give a white solid, and dried *in vacuo*. 2.19 g (64%). Characterization as previously reported. [65] ^{1}H NMR (300 MHz, $CDCl_3$) δ = 8.00 (1H, s, N**H**), 6.52 (2H, t, *J* = 0.91 Hz, **H**C=C**H**), 5.32 (2H, t, *J* = 0.92 Hz, Bridge Base 2 x C**H**), 2.89 (2H, s, Fused Ring 2 x C**H**). ^{13}C NMR (75 MHz, $CDCl_3$) δ = 162.34 (2 x **C**=O), 136.59 (H**C**=**C**H), 80.99 (**C**-O-**C**), 48.71 (2 x **C**-C=O). IR (ATR): 3194 (NH); 3101, 3065, 2866, 2724 (CH); 1834, 1801; 1773, 1702 (2 x C=O); 1626, 1579 (C=C); 1345, 1301 (CH); 1148; 1065, 938, 842 cm^{-1} (C=C). m/z (ESI, -ve) Observed 164.1 [100%, $M-H^+$].

General Procedure for the Synthesis of D-galactose pentaacetate

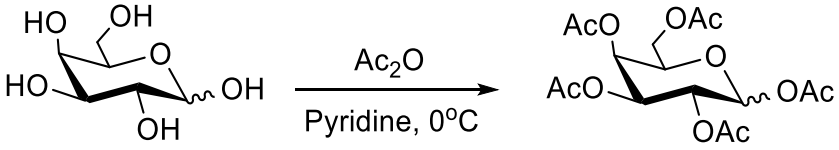

To a solution of D-galactose (1.00 g, 5.55 mmol) in pyridine (20 mL) on ice, acetic anhydride (20 mL) was added slowly with stirring, and allowed to warm to RT overnight. To the resulting reaction mix, $CHCl_3$ (30 mL) was added and the mixture extracted from a chilled solution of HCl (3 x 30 mL, 1M). The combined organic phases were then extracted with saturated $NaHCO_3$ solution (3 x 30 mL), washed with brine (30 mL), dried over Na_2SO_4, and condensed *in vacuo* to give a thick colourless oil. 2.26 g (Quant%). Characterization as previously reported. [66] ^{1}H NMR (300 MHz, $CDCl_3$) δ = 6.38 (1H, s, Anomeric **H-1**), 5.50 (1H, s, **H-4**), 5.34 (2H, s, **H-2,3**), 4.43 – 4.01 (3H, m, **H-5,6**',"), 2.27 – 1.92 (15H, m, 5 x **OAc**). 9:1 α:β. ^{13}C NMR (75 MHz, $CDCl_3$) δ = 170.14 – 168.92 (**C**=O-CH_3), 89.72 (**C-1**), 68.96 – 65.99 (**C-5,4,3,2**), 61.25 (**C-6**), 21.26 – 19.87 (5 x C-O**C**H_3). m/z (ESI, +ve) Observed 412.9 [100%, $M+Na^+$].

General Procedure for the Synthesis of Acetobromo-α-D-galactose

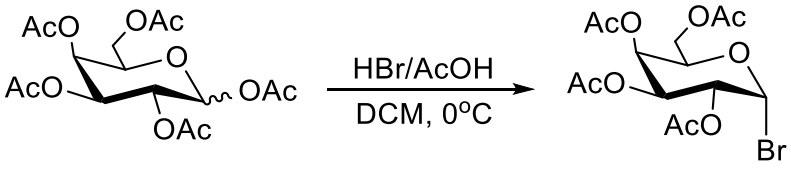

To a solution of D-galactose pentaacetate (1.62 g, 4.15 mmol) in anhydrous dichloromethane (20 mL) on ice, a large excess of hydrobromic acid in acetic acid (33% w/w, 5 mL, 27.81 mmol, 6.7 eqv) was added dropwise with stirring, and the reaction mix allowed to equilibrate for 1 hour with protection from ambient light. The resulting translucent orange solution was then extracted from a saturated solution of ice-cold $NaHCO_3$ (3 x 30 mL), leading to effervescence and a discolouration of the organic phase. The organic phase was then washed with ice-cold brine (30 mL), dried over Na_2SO_4, and condensed *in vacuo*, yielding a thick colourless oil, which slowly crystallised. 1.37 g (80%). Characterisation as previously reported. [67] ^{1}H NMR (300 MHz, $CDCl_3$) δ = 6.70 (1H, d, *J* = 3.20 Hz, Anomeric **H-1**), 5.52 (1H, d, *J* = 2.9 Hz, **H-3**), 5.40 (1H, dd, J_1 = 10.70 Hz, J_2 = 3.40 Hz, **H-4**), 5.10 – 4.99 (1H, m, **H-2**) 4.54 – 4.04 (3H, m, **H-5,6**',"), 2.19 – 1.96 (12H, m, 4 x **OAc**). 1:0 α:β. ^{13}C NMR (75 MHz, $CDCl_3$) δ = 163.12 (**C**=O-CH_3), 88.11 (**C-1**), 71.06 – 66.97 (**C-5,4,3,2**), 60.83 (**C-6**), 20.75 – 20.55 (C-O**C**H_3). m/z (ESI, -ve) Observed 427.1, 428.1 [100%, M+H_2O–H^+].

General Procedure for the Synthesis of ((1R,2S,3S,4R)-bicyclo[2.2.1]hept-5-ene-2,3-diyl)bis(methylene) diacetate – (5-Norbornene-2-*exo*,3-*exo*-dimethylacetate) – 'M1'

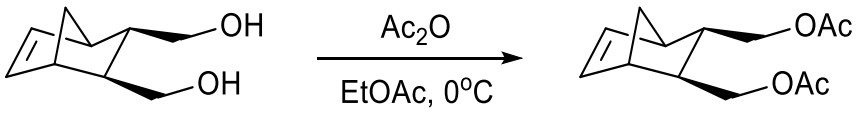

5-Norbornene-2-*exo*,3-*exo*-dimethanol (215.3 mg, 1.40 mmol) was dissolved in ethyl acetate (20 mL) on ice, and a large excess of acetic anhydride (10 mL) was added slowly with stirring, and allowed to equilibrate for one hour. The reaction mixture was subsequently condensed *in*

vacuo, re-dissolved in DCM (30 mL), and extracted from a saturated solution of $NaHCO_3$ (3 x 30 mL). The combined organic phases were then dried over Na_2SO_4, and condensed *in vacuo*¸ to give a thick colourless oil. Subsequent chilling at –20°C yielded a white crystalline solid. 140 mg (42%). ^{1}H NMR (300 MHz, $CDCl_3$) δ = 6.05 (2H, d, *J* = 2.3 Hz, **H-1**), 4.20 – 3.83 (4H, m, **H-4**), 2.61 (2H, s, **H-2**), 1.98 – 1.89 (6H, m, **H-6**), 1.73 (2H, d, J = 11.4 Hz, **H-3**), 1.44 – 1.17 (2H, m, **H-5**). ^{13}C NMR (75 MHz, $CDCl_3$) δ = 169.84 (2 x **C**=O), 136.27 (H**C**=**C**H), 64.39 (2 x **C**-OC=O), 43.79 (**C**-C=C), 41.55 (R_2**C**H2), 38.68 (**C**-C-OC=O), 29.83, 19.98 (O**Ac**). Compound previously reported.[68]

General Procedure for the Synthesis of (2R,3S,4S,5R,6R)-2-(acetoxymethyl)-6-((3aR,4R,7R,7aS)-1,3-dioxo-8-(propan-2-ylidene)-1,3,3a,4,7,7a-hexahydro-2H-4,7-methanoisoindol-2-yl)tetrahydro-2H-pyran-3,4,5-triyl triacetate – (*exo,exo-fulvonorborneneimide galactopyranoside peracetate)* – 'M2'

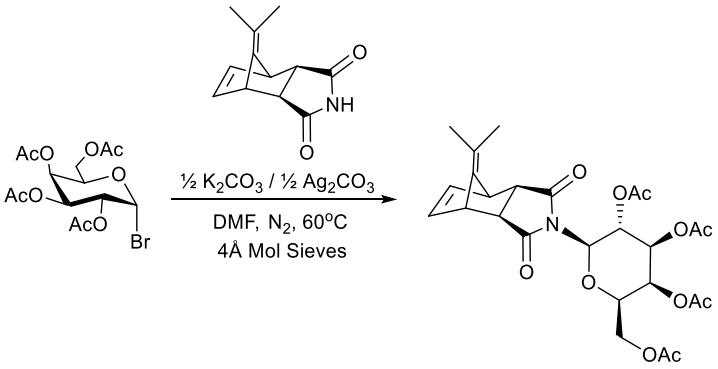

exo,exo-fulvonorborneneimide (326 mg, 1.61 mmol), K_2CO_3 (111 mg, 0.80 mmol, 0.5 eqv), and acetobromo-α-D-galactose (600 mg, 1.46 mmol, 0.91 eqv) were dissolved in dry, deoxygenated DMF (20 mL) with 4 Å molecular sieves. Ag_2CO_3 (201 mg, 0.73 mmol, 0.46 eqv) was subsequently added with stirring, the reaction protected from light, and allowed to equilibrate at 60°C overnight. The dark green/brown reaction crude was then filtered, and condensed *in vacuo* until a thick suspension remained, and re-dissolved in ethanol to precipitate the insoluble black solids of the silver oxide/bromide by-products, and again filtered. The

filtrate was dissolved in $CHCl_3$ (30 mL) and extracted with saturated $NaHCO_3$ solution (3 x 30 mL), and the organic phase washed again with saturated NaCl solution (30 mL), water (30 mL), dried over Na_2SO_4 and condensed *in vacuo.* Solids were then taken up into hot diethyl ether (30 mL), filtered, and the filtrate condensed again to give an off-white/beige solid. 250 mg (32%). ^{1}H NMR (300 MHz, $CDCl_3$) δ = 6.37 (2H, d, *J* = 10.5 Hz, **H**C=C**H**), 5.73 – 5.36 (2H, m, **H-1,4**), 5.36 – 4.97 (2H, m, **H-3,2**), 4.76 – 3.90 (4H, m, **H-5,6**',''), 3.71 (2H, s, Bridge Base 2 x C**H**), 2.74 (2H, s, Fused Ring 2 x C**H**), 2.09 – 1.94 (12H, m, 4 x **OAc**), 1.54 (4H, s, 2 x **Me**). ^{13}C NMR (75 MHz, $CDCl_3$) δ = 207.03 (2 x HNR**C**=O), 177.47 (R_2-**C**=C-$(Me)_2$), 170.36 – 168.92 (4 x **C**=OAc + R_2-C=**C**-$(Me)_2$), 89.69 (**C-1**), 70.87 (2 x **C**-OC=O), 68.74 – 66.43 (**C-2,3,4,5**; 4 x **C**-C=OAc), 61.24 (**C-6**), 49.21 (**C**-C=O), 45.58 (**C**-HC=CH-**C**), 30.90 (2 x **Me**), 20.87 – 19.61 (4 x O**Ac**).

General Procedure for the Synthesis of (2R,3S,4S,5R,6R)-2-(acetoxymethyl)-6-((3aR,4R,7R,7aS)-1,3-dioxo-1,3,3a,4,7,7a-hexahydro-2H-4,7-epoxyisoindol-2-yl)tetrahydro-2H-pyran-3,4,5-triyl triacetate – (*exo,exo-oxonorborneneimide galactopyranoside peracetate*) – 'M3'

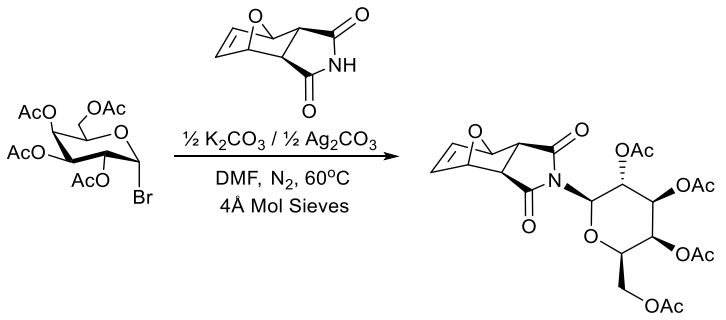

Synthetic procedure as described in the General Procedure for the Synthesis of exo,exo-fulvonorborneneimide galactopyranoside peracetate.

exo,exo-oxonorborneneimide (498 mg, 3.02 mmol), K_2CO_3 (210 mg, 1.51 mmol, 0.5 eqv), and acetobromo-α-D-galactose (1.13 g, 2.75 mmol, 0.91 eqv) were dissolved in dry, deoxygenated

DMF (20 mL) with 4Å molecular sieves. Ag_2CO_3 (380 mg, 0.73 mmol, 0.46 eqv) addition followed as previously prescribed. Workup as per previous, with the exception that toluene was used for the final wash in place of hot diethyl ether. Brown oil obtained, 340 mg (25%). ^{1}H NMR (300 MHz, $CDCl_3$) δ = 6.37 (1H, s, **H**C=C**H**), 5.73 – 4.99 (5H, m, **H-1,4,** 2 x **H**C-O), 4.53 – 3.90 (5H, m, **H-2,3,5,6**',''), 2.12 – 1.95 (14H, m, 4 x OAc). ^{13}C NMR (75 MHz, $CDCl_3$) δ = 174.57 – 167.20 (4 x **C**=OAc), 162.31 (2 x HNR**C**=O), 95.92 (H**C**=**C**H), 92.62 – 88.45 (**C**-O-**C**, **C-1**), 73.30 – 64.71 (**C-2,3,4,5**), 61.62 (**C-6**), 61.46 (2 x **C**-C=O), 24.59 – 18.45 (4 x O**Ac**).

General Procedure for the Synthesis of (3aR,4R,7R,7aS)-8-(propan-2-ylidene)-2-((2R,3R,4S,5R,6R)-3,4,5-trihydroxy-6-(hydroxymethyl)tetrahydro-2H-pyran-2-yl)-3a,4,7,7a-tetrahydro-1H-4,7-methanoisoindole-1,3(2H)-dione – (*exo,exo*-fulvonorborneneimide galactopyranoside)

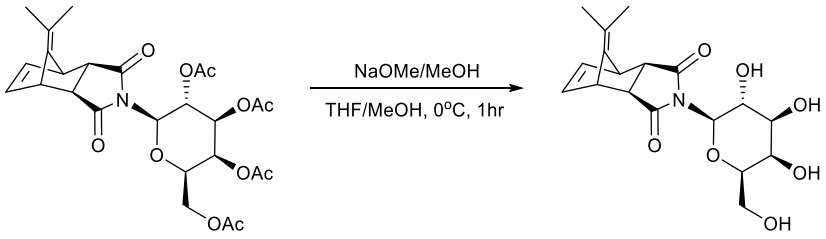

exo,exo-fulvonorborneneimide galactopyranoside peracetate (200 mg, 0.375 mmol) was dissolved in THF/Methanol (2:1, 15 mL) and a large excess of methanolic sodium methoxide (30%, 5 mL) added with stirring at 0°C. After 1 hour, the mixture (pH ~ 10) was neutralised on an Amberlite Ion Exchange column and flushed sequentially with THF (20 mL) and methanol (20 mL). The collected fraction (pH ~ 6–7) was subsequently condensed *in vacuo* to yield an off-white solid. 50 mg (36%). ^{1}H NMR (300 MHz, $CDCl_3$) δ = 6.17 (2H, s, **H**C=C**H**), 4.19 (4H, s, Carbohydrates), 3.45 (2H, s, Carbohydrates), 3.09 (2H, s, Bridge Base 2 x C**H**), 2.50 (2H, s, Fused Ring 2 x C**H**), 1.30 (3H, s, 2 x **Me**). ^{13}C NMR (75 MHz, $CDCl_3$) δ = 140.31 (2 x HNR**C**=O), 52.16 – 50.45 (**C-1,2,3,4,5,6**), 48.26 (**C**-C=O), 21.95(2 x **Me)**.

General Procedure for the Synthesis of 2,5,8,11,14,17-hexaoxanonadecan-19-ol – (*Monomethoxyhexaethylene glycol*)

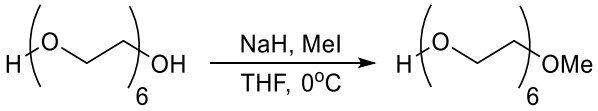

Hexaethylene glycol (1g, 0.89 mL, 3.54 mmol) was dissolved in THF (10 mL) and cooled on ice, and sodium hydride (60% dispersion in mineral oil, 142 mg, 1 eqv, 3.54 mmol) added. Methyl iodide (503 mg, 0.22 mL, 1 eqv, 3.54 mmol) was then added slowly, dropwise, and stirred for 1 hour. The reaction mixture was quenched with NH_4Cl, warmed to RT, and diethyl ether added (30 mL). The aqueous phase was separated and extracted with diethyl ether (3 x 30 mL), the organic phases combined, dried over Na_2SO_4, and condensed *in vacuo* to give a clear, off-yellow oil. 940 mg (89.5%). ^{1}H NMR (300 MHz, $CDCl_3$) δ = 3.75 – 3.46 (27H, m, ((C**H**$_2$C**H**$_2$O)$_5$(C**H**$_2$)$_2$O**H**), 3.32 (3H, s, O**Me**). ^{13}C NMR (75 MHz, $CDCl_3$) δ = 72.48 – 69.89 (**C**OR), 61.46 – 61.31 (**Me**), 58.64 – 31.38 (**C**H). m/z (ESI, -ve) Observed 313.9 [100%, M+H_2O–H^-]. Compound previously reported.[69]

General Procedure for the Synthesis of 2,5,8,11,14,17-hexaoxanonadecan-19-yl 4-methylbenzenesulfonate – (*Monomethoxyhexaethylene glycol monotosylate*)

Monomethoxyhexaethylene glycol (920 mg, 3.10 mmol), triethylamine (0.52 mL, 1.2 eqv, 3.73 mmol), and tosyl chloride (710 mg, 1.2 eqv, 3.73 mmol) were dissolved in DCM (30 mL) and stirred for 16 hours. Water (30 mL) was subsequently added, and the aqueous phase separated and extracted with DCM (3 x 30 mL). Organic phases were combined, condensed *in vacuo*, and solids precipitated from a minimal volume of cold THF (2 x 5 mL) and filtered. The organic liquor was then re-condensed, dissolved in DCM (30 mL), and washed with saturated $NaHCO_3$

solution (3 x 30 mL), dried over Na_2SO_4, and condensed again to yield a brown oil. 1 g (72%). ^{1}H NMR (400 MHz, $CDCl_3$) δ = 7.83 – 7.30 (4H, m, Aromatic), 4.16 (2H, td, J_1 = 4.9, J_2 = 1.7 Hz, PEG C**H**$_2$), 3.80 – 3.50 (26H, m, (C**H**$_2$C**H**$_2$O)$_5$), 3.37 (3H, t, J = 1.5 Hz, O**Me**), 2.72 (2H, s, Ar-**Me**). ^{13}C NMR (75 MHz, $CDCl_3$) δ = 144.80 (Aromatic), 132.96 – 126.32 (Aromatic), 72.38 – 68.64 (**C**OR), 61.64 (**Me**), 58.99 – 30.31 (**C**H), 21.63 (Ar-**Me**). m/z (ESI, +ve) Observed 473.1 [100%, M+Na$^+$]. Compound previously reported.[70]

General Procedure for the Synthesis of (3aR,4R,7R,7aS)-2-(2,5,8,11,14,17-hexaoxanonadecan-19-yl)-8-(propan-2-ylidene)-3a,4,7,7a-tetrahydro-1H-4,7-methanoisoindole-1,3(2H)-dione – (*exo,exo-fulvonorborneneimide-PEG$_6$)* – 'M4'

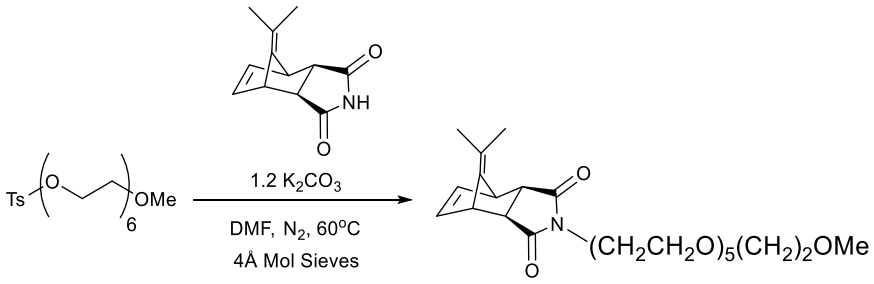

Monomethoxyhexaethylene glycol monotosylate (1 g, 3.33 mmol) was dissolved in DMF (50 mL) with 4Å molecular sieves, K_2CO_3 (470 mg, 1.5 eqv, 5.00 mmol), and *exo,exo*-fulvonorborneneimide (677 mg, 1.5 eqv, 5.00 mmol) at 60°C with stirring for 24 hours. The crude was filtered, condensed *in vacuo*, and re-dissolved in ethyl acetate (30 mL). Saturated $NaHCO_3$ solution (30 mL) was added, the organic phase separated, and washed a further three times (3 x 30 mL) with saturated $NaHCO_3$ solution, and brine (1 x 30 mL). The organic phase was then dried over Na_2SO_4 and reduced to a small volume (~ 5 mL), before being precipitated from diethyl ether to yield an off-white solid. 530 mg (33%). ^{1}H NMR (300 MHz, $CDCl_3$) δ = 6.34 (2H, q, J = 1.9 Hz, H**C=C**H), 3.74 – 3.36 (27H, m, (C**H**$_2$C**H**$_2$O)$_5$, Bridge Base 2 x C**H**), 3.30 (1H, 2, O**Me**), 2.68 (2H, d, J = 10.4 Hz, Fused Ring 2 x C**H**), 1.46 (7H, d, J = 16.0 Hz, C=C**(Me)**$_2$),. ^{13}C NMR (75 MHz, $CDCl_3$) δ = 177.88 – 177.39 (Imide 2 x R**C**=ON), 162.31

(Me_2-C=**C**), 140.9 (Me_2-**C**=C), 137.6 (H**C=C**H), 115.88, 71.87 – 67.09 (**C**OR), 61.57 (**Me**), 58.95 – 14.11 (**C**H, **C**NR). m/z (ESI, +ve) Observed 504.1 [100%, M+Na^+], 473.0 [75%, SM+Na^+].

General Procedure for the (co)polymerisation of the M1–M4 monomer libraries

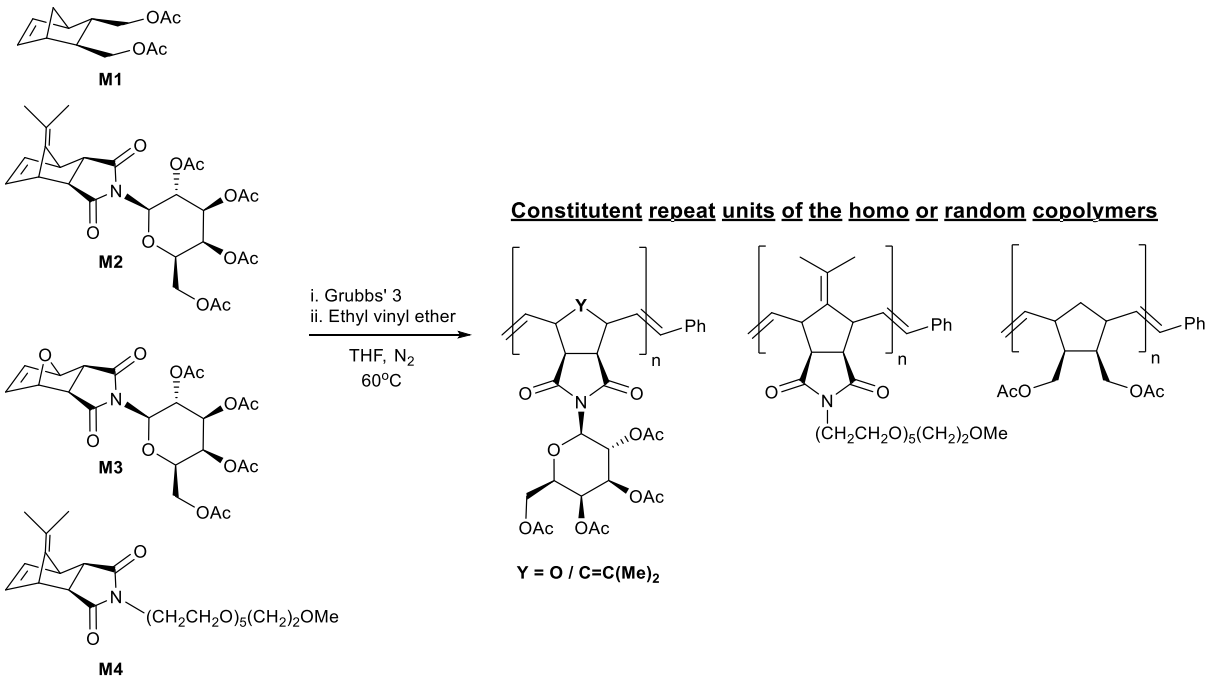

The monomer(s) and Grubbs' 3 metathesis catalyst (See Table 4.3, below) were weighed into separate Schlenk flasks (or for some monomers, as a solution of known concentration in dry THF) and each made up to 10 mL and 5 mL with anhydrous THF, respectively, and purged/degassed with N_2 for 20 minutes. Mesitylene (3 drops) was added to the monomer solution prior to degassing. The catalyst and monomer solutions were then combined and heated at 50°C for 1 hour under nitrogen, with stirring. The Schlenk flask was subsequently cooled under liquid nitrogen (–196°C), a drop removed (for ^{1}H NMR conversion), and a large excess of ethyl vinyl ether (5 mL) introduced, with stirring for a further 30 minutes. The polymer was then precipitated with a large excess (~ 45 mL) of an appropriate solvent (Table 4.3), and isolated by centrifugation (10K RPM, 10 minutes), to yield a solid mass (polymers generally brown through grey/beige). Polymers not containing acetate groups were then

reprecipitated under the same conditions at least twice, and finally dried under compressed air. (Table 4.3 and Figures 4.14 and 4.18 – 4.20, below, for further polymer characterisation data).

poly(Fulvo): ^{1}H NMR (300 MHz, $CDCl_3$) δ = 5.35 (s, Carbohydrates + Backbone), 4.34 (br s, Carbohydrates + Backbone), 3.65 (br s, Carbohydrates), 3.27 (br s, Carbohydrates), 2.92 – 2.22 (m, Carbohydrates + Norbornene Ring), 2.06 – 1.78 (m, Carbohydrates + Norbornene Ring), 1.75 – 1.53 (m, Norbornene Ring), 1.50 – 1.16 (m, Norbornene Ring + Methylene's), 1.07 – 0.75 (m, Norbornene Ring + Methylene's). Cis/Trans n/d.

poly(Oxo): ^{1}H NMR (300 MHz, $CDCl_3$) δ = 6.98 (m), 6.60 – 6.47 (m), 5.59 – 5.06 (m, Carbohydrates + Backbone), 4.77 – 4.31 (m, Carbohydrates), 4.26 – 3.90 (m, Carbohydrates + Norbornene Ring), 3.85 – 3.38 (m, Carbohydrates), 3.25 – 2.98 (m, Carbohydrates), 2.92 – 2.39 (m, Carbohydrates + Norbornene Ring), 2.24 – 1.94 (m, Ac), 1.01 – 0.77 (m, Norbornene Rings + Methylene's). Cis/Trans n/d.

poly(Fulvo-*co*-Oxo): ^{1}H NMR (400 MHz, *d*-DMSO) δ = 11.13 (s), 8.28 (s), 7.57 – 6.06 (m, Ph Chain End), 5.82 – 4.49 (m, Carbohydrates + Backbone), 4.26 – 3.86 (m, Carbohydrates + Norbornene Rings), 2.33 – 0.52 (m, Norbornene Rings + Methylene's). Cis/Trans n/d.

poly(Fulvo-*co*-Diol): ^{1}H NMR (400 MHz, *d*-DMSO) δ = 11.14 (br s), 7.36 (m, Ph Chain End), 5.54 – 4.62 (m, Carbohydrates + Backbone), 4.28 – 2.58 (m, Fulvo Norbornene Ring + Carbohydrates), 2.38 – 0.76 (m, Diol Norbornene Ring + Fulvo Methylene's). Cis/Trans n/d.

poly(Fulvo-*co*-FPEG): ^{1}H NMR (400 MHz, *d*-DMSO) δ = 11.13 (br s), 7.09 (s, Ph Chain End), 5.65 – 5.17 (m, Carbohydrates + Backbone), 4.43 (m), 4.20 – 3.95 (m, Carbohydrates + Norbornene Rings), 3.63 – 3.37 (m, PEG Pedant), 3.27 – 2.90 (m, PEG Pedant), 2.74 – 2.53 (m), 2.41 – 2.12 (m), 2.01 – 1.42 (m, Norbornene Ring + Methylene's), 1.34 – 0.82 (m). Cis/Trans n/d.

poly(Diol): ^{1}H NMR (400 MHz, *d*-DMSO) δ = 7.68 (s, Ph Chain End), 5.32 – 5.09 (m, Backbone), 4.98 – 4.86 (m, Backbone), 4.16 – 3.89 (m), 2.32 – 1.52 (m, Norbornene Ring), 1.39 – 0.76 (m, Methylene's). Cis/Trans 1:1.

poly(FPEG): ^{1}H NMR (400 MHz, *d*-DMSO) δ = 11.13 (br s), 7.09 (s, Ph Chain End), 5.60 – 5.20 (m, Backbone), 4.59 – 4.40 (m), 4.18 – 3.93 (m), 3.67 – 3.36 (m, PEG Pedant), 3.31 – 2.93 (m, PEG Pedant), 2.66 (s), 2.34 – 2.29 (m, Norbornene Ring) 1.83 – 1.41 (br s, Norbornene Ring + Methylene's). Cis/Trans 1:4.

poly(Fulvo-*co*-Diol) + H_2: ^{1}H NMR (400 MHz, *d*-DMSO) δ = 11.08 (s), 7.25 (br. s, Ph Chain End), 5.67 – 4.62 (m, Carbohydrates), 4.15 – 2.64 (m, Fulvo Norbornene Ring + Carbohydrates), 2.37 – 0.97 (m, Diol Norbornene Ring + Fulvo Methylene's), 0.96 – 0.76 (q, J = 7.7 Hz, Hydrogenated Fulvene), 0.66 – 0.32 (dq, J1 = 43.6, J1 = 7.9 Hz, Hydrogenated Fulvene). Cis/Trans n/d.

* n/d – Not possible to determine the cis/trans ratio in these instances due to unsaturated backbone signals overlapping with the carbohydrate signals.

Acetylated Polymer Species	Monomer (mg, mmol)		Grubbs' 3 mg, μmol	Mn_{THEO} ($g.mol^{-1}$) †	Ratio A:B:G3	Precipitation Solvent (from THF)	Yield (mg)
	Monomer A	Monomer B					
poly(Fulvo)	**M2** (191.1, 0.358)	-	7.1, 8.03	25,000	46.9:0:1	Diethyl ether	54.1
poly(Oxo)	**M3** (184.3, 0.372)	-	16.3, 18.43	10,000	20.2:0:1	Pentane	8.1
poly(Fulvo-*co*-Oxo)	**M2** (100, 0.187)	**M3** (97.1, 0.196)	17.7, 20.01	10,000	19.4:19.4:1	Hexane	39.3
poly(Fulvo-*co*-Diol)-17 *	**M2** (100, 0.187)	**M1** (45, 0.187)	16.6, 18.74	10,000	10:10:1	Diethyl ether	8.5
poly(Fulvo-*co*-FPEG)	**M2** (52.6, 0.0986)	**M4** (47.4, 0.0984)	8.9, 10.06	10,000	19.7:19.7:1	Diethyl ether	63.4
poly(Diol)	**M1** (50, 0.210)	-	9, 10.18	10,000	20.6:0:1	Ethanol	33.1
Non-Acetylated							
poly(FPEG)	**M4** (100, 0.208)	-	8.9, 10.06	10,000	20.7:0:1	Hexane	66.5

Table 4.3 – Polymer preparation summary † Derived from Mn_{THEO} = [M]/[C]•(Mw)•Y, where [M] is the initial monomer(s) concentration, [C] is initial catalyst concentration, Mw is the monomer molecular weight(s), and Y is = 1 (assuming 100% conversion). *Representative example.

Deacetylated Polymer Species	Deprotected Yield (mg)	Post-Deprotection Dissolution Solvent *	Post-Deprotection Precipitation Solvent
poly(Fulvo)	50.8	THF	Diethyl ether
poly(Oxo)	3.3	THF	Pentane
poly(Fulvo-*co*-Oxo)	9.1	THF	Diethyl ether
poly(Fulvo-*co*-Diol)-17	3.6	THF	Hexane
poly(Fulvo-*co*-FPEG)	12.8	THF	Hexane
poly(Diol)	8.2	MeOH/THF (1:1)	Diethyl ether

Table 4.4 – Deprotected polymer preparation summary * Addition of methanol maybe required (in addition to THF) to fully dissolve the deacetylated derivative.

General Procedure for the postpolymerisation modification (deacetylation) of acetylated polymer derivatives

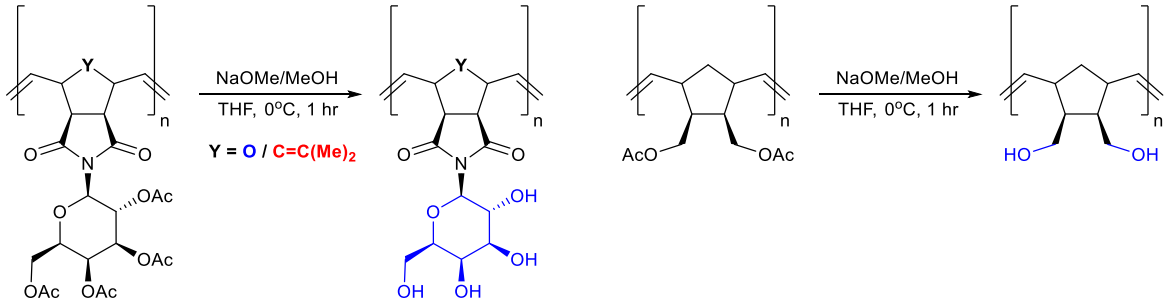

The acetylated polymeric materials (See Table 4.3, above) were dissolved in THF/Methanol (2:1, 15 mL) and a large excess of methanolic sodium methoxide (30%, 5 mL) added with stirring at 0°C. After 1 hour, the mixture (pH ~ 10) was neutralised on an Amberlite Ion Exchange column, and flushed sequentially with THF (20 mL) and methanol (20 mL). The collected fraction (pH ~ 6–7) was subsequently condensed *in vacuo*, and the deprotected polymer re-dissolved in an appropriate solvent (Table 4.4), and precipitated with a large excess (~ 45 mL) of an appropriate solvent (Table 4.4), and isolated by centrifugation (10K RPM, 10 minutes) to yield a solid mass (polymers generally brown through grey/beige). Polymers were then reprecipitated under the same conditions at least twice, and finally dried under compressed air. (Tables 4.3–4, above, and Figures 4.18 – 4.20, below, for polymer characterisation data).

General Procedure for the postpolymerisation modification (hydrogenation) of the polymer derivatives

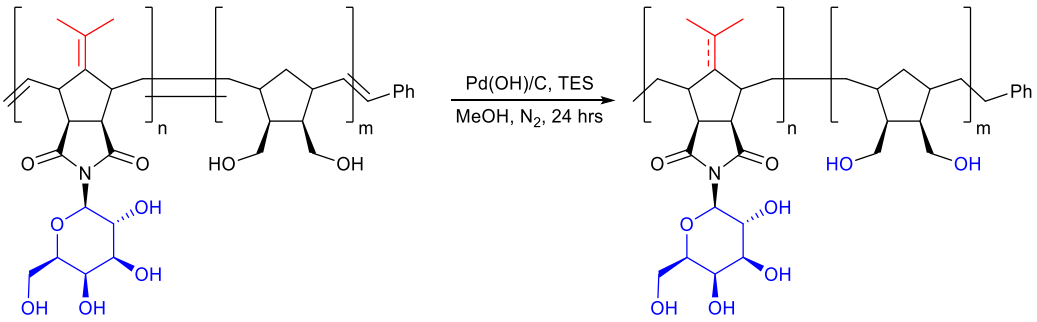

Deacetylated poly(Fulvo-*co*-Diol) 17k (13 mg) was dissolved in methanol (5 mL) in a sealed system, under a nitrogen atmosphere. A solution of $Pd(OH)_2/C$ (10 mg) in methanol (5 mL) was introduced with stirring, and nitrogen bubbled through the mix for 5 minutes. Triethylsilane (0.5 mL) was then added in whole, leading to instantaneous effervescence and the *in-situ* generation of molecular H_2. The reaction mix was allowed to stir for 16 hours, with balloons attached for back pressure. The reaction was then subsequently filtered through a Celite plug, flushed with methanol (20 mL) and THF (20 mL), and condensed *in vacuo* to give the hydrogenated copolymeric derivative as a red mass. 14.7 mg.

UV-VIS/Beer-Lambert plots of (insoluble) polymers and calibration curves

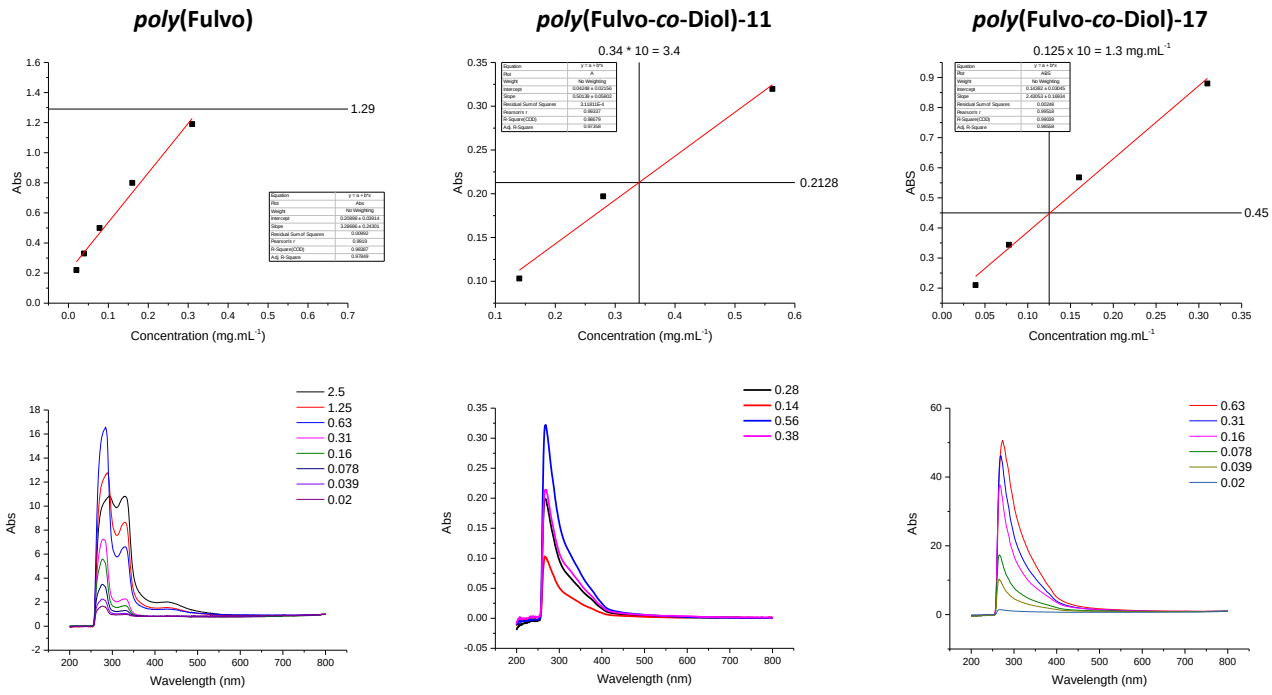

Figure 4.118 – Beer Lambert Plots (TOP) and UV-Vis spectra (BOTTOM) of the poly(Fulvo), poly(Fulvo-*co*-Diol)-11 and -17 polymer series, respectively

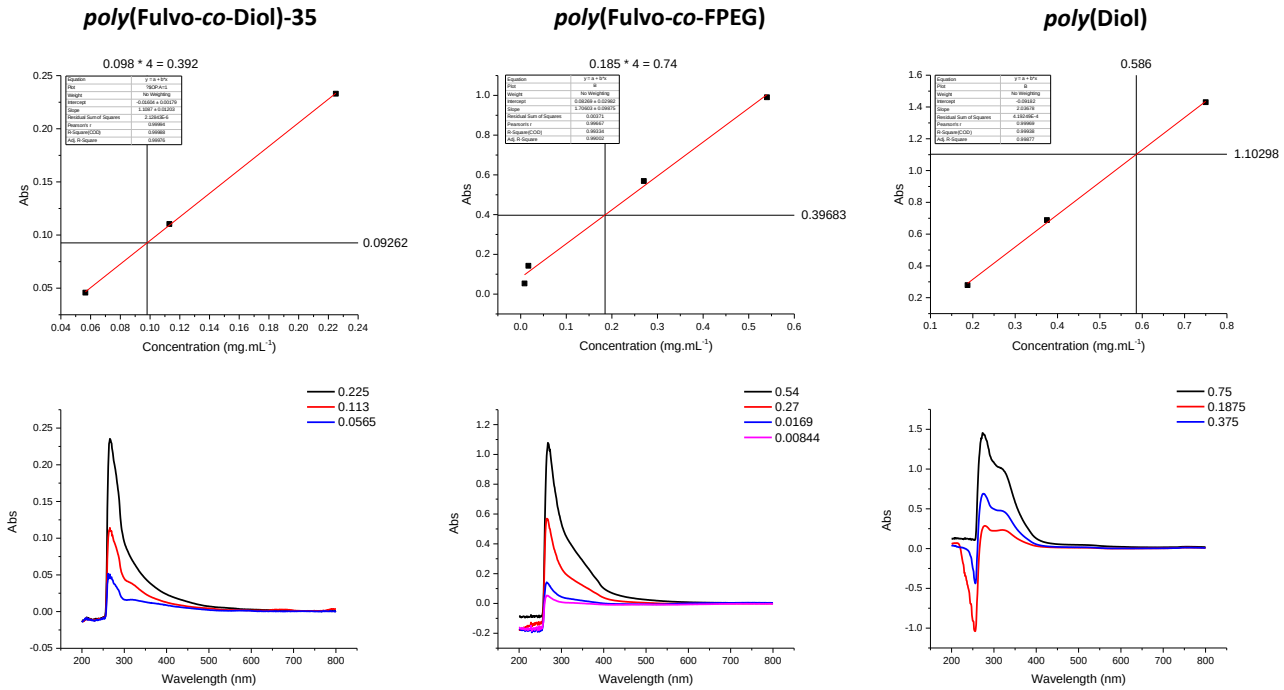

Figure 4.19 – Beer Lambert Plots (TOP) and UV-Vis spectra (BOTTOM) of poly(Fulvo-*co*-Diol)-35, poly(Fulvo-*co*-FPEG), and poly(Diol) polymer series, respectively.

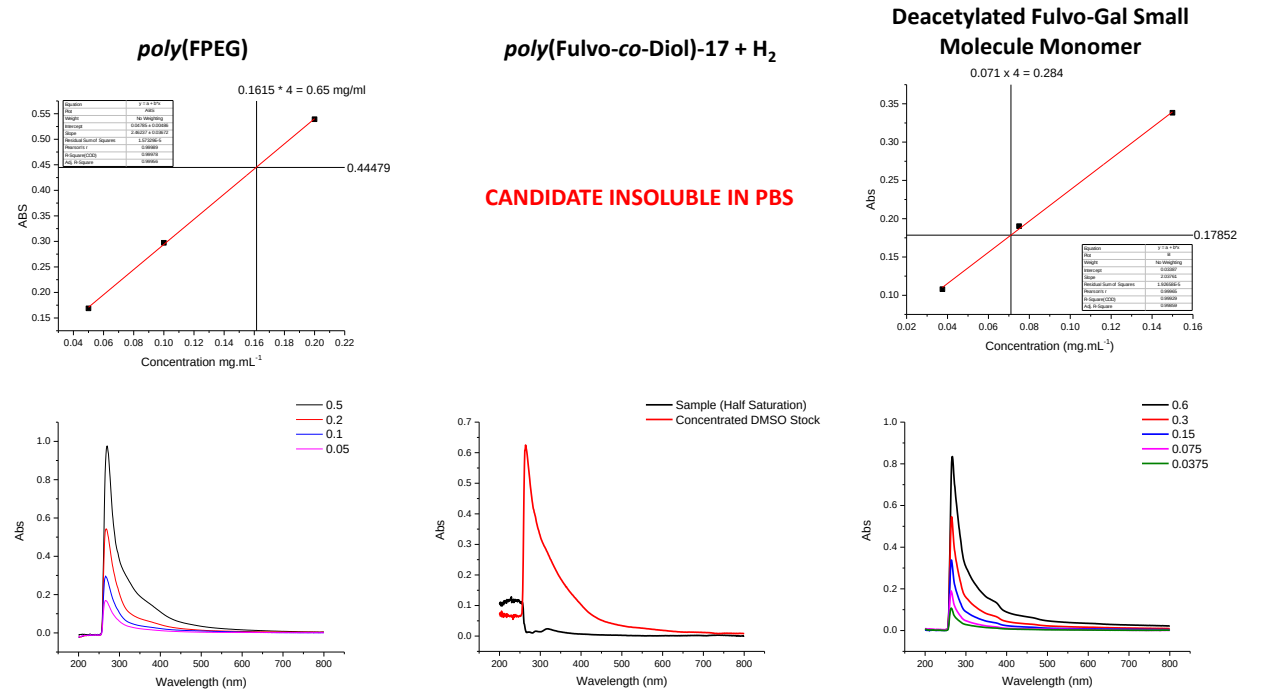

Figure 4.20 – Beer Lambert Plots (TOP) and UV-Vis spectra (BOTTOM) of the poly(FPEG) and poly(Fulvo-*co*-Diol)-17 + H_2 polymer series, and deacetylated Fulvo-Gal monomer series, respectively.

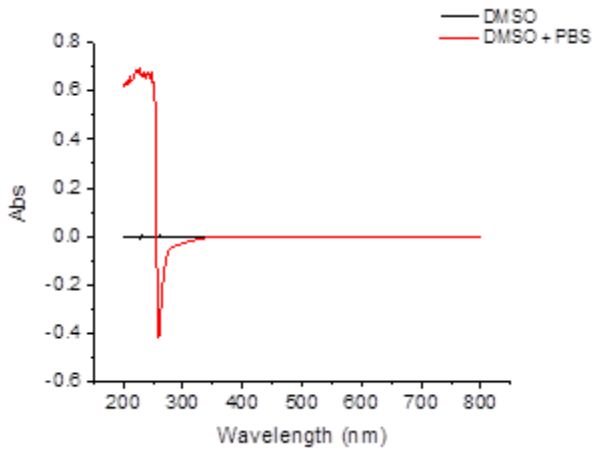

Figure 4.21 – UV/Vis spectrum of DMSO (background zeroed) and DMSO containing PBS salt

Unsuccessful and redundant general procedures

I. Example procedure for the syntheses of glycosyl (Glc/Gal/GalNAc) peraacetates

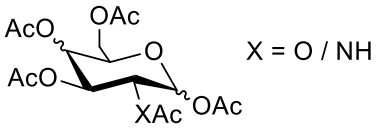

Zinc chloride (0.96 g, 7.04 mmol) was added quickly to acetic anhydride (20 mL) and the mixture heated to and stirred at 85ºC for five minutes, resulting in a dark brown solution. D-Glucose (4.00 g, 22.2 mmol) was added slowly with stirring and the mixture was heated for 1 further hour. The resulting thick black oil which was poured into chilled water (200 mL) and stirred vigorously to give a dark green solution and an off-white precipitate. The solid was recovered at the pump, washed with ice cold water (40 mL), and recrystallised from hot ethanol (20 mL). White crystals were isolated, washed with cold ethanol (10 mL) and dried *in vacuo*. 4.06 g (46.8 %). ^{1}H NMR (300 MHz, $CDCl_3$) δ = 6.32 (1H, d, $J_{1,2}$ = 3.7 Hz, Anomeric), 5.47 (1H, t, $J_{3,2}$ = $J_{3,4}$ = 9.9 Hz, H-3), 5.19 – 5.05 (2H, m, H-2,4), 4.26 (1H, dd, $J_{6,6'}$ = 12.5, $J_{6,5}$ = 4.1 Hz, H-6), 4.10 (2H, m, H-5,6'), 3.70 (q, EtOH), 3.48 (s, EtOH) 2.18 (3H, s, OAc), 2.09 (3H, s, OAc), 2.05 – 1.99 (9H, s, 3 x OAc), 1.24 (t, EtOH). m/z (ESI) 413.0 (95%, M+Na^+). Compound previously reported – as above.

II. Example procedure for the attempted syntheses of glycosyl (Glc/Gal/GalNAc) tetraacetates

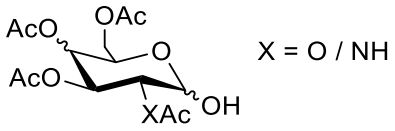

The glycosyl peracetate (1.00 g) was dissolved in DMF (20 mL) and ammonium carbonate (506 mg) or benzylamine (2 mL) added, and the mixture stirred at 30ºC for 48 hours. Chloroform (30 mL) was added and the mixture poured into ice cold HCl (1M, 20 mL). The

organic phase extracted and the aqueous washed with $CHCl_3$ (3 x 20 mL). The combined organic phases were washed with water (15 mL) and saturated $NaHCO_3$ solution (15 mL), dried over Na_2SO_4 and condensed *in vacuo* with an excess of *n*-Butanol, resulting in a yellow/brown gum. Glc $(NH_4)_2CO_3$: ^{1}H NMR (300 MHz, $CDCl_3$) δ = 5.51 (2H, dt, *J* = 7.2, 6.7 Hz), 5.26 (1H, t, *J* = 9.5 Hz), 5.00 – 4.65 (2H, m), 4.37 – 4.06 (3H, m, H-5,6$^{',''}$), 2.13 – 1.99 (12H, m, 4 x OAc). m/z (ESI) 371.0 (100%, M+Na^+). GalNAc ($BnNH_2$): ^{1}H NMR (300 MHz, $CDCl_3$) δ 5.71 (d, J = 9.5 Hz, 1H, Anomeric), 5.65 – 5.59 (m, 1H), 5.43 – 5.33 (m, 2H), 5.27 (dd, J = 11.2, 3.3 Hz, 1H), 4.60 (d, J = 9.6 Hz, 1H), 4.40 (dt, J = 14.1, 6.4 Hz, 3H), 4.19 – 3.93 (m, 4H), 3.76 (s, 2H), 2.16 – 1.95 (m, 13H, 1 x NHAc, 3 x Ac). Compounds previously reported.[71]

III. Example procedure for the attempted syntheses of glycosyl (Glc/Gal/GalNAc) *exo*-fulvonorborneneimide monomers (*via* mitsunobu coupling)

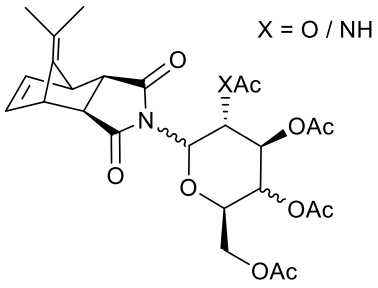

To the crude mono-deacetylated sugar (Galactose, 0.44 g) and *exo,exo*-fulvonorborneneimide (0.12g, 0.63 mmol, 0.5 eqv) were dissolved in dry THF (50 mL) under N_2 with triphenyl phosphine (0.17 g, 0.63 mmol, 0.5 eqv) and cooled to zero degrees. DIAD (0.13 mL, 0.13g, 0.63 mmol, 1 eqv) was added drop wise to the reaction mixture with stirring, and the reaction mixture kept at 0ºC for five minutes, before being warmed to RT and stirred for 48 hours. The crude orange solution obtained was condensed *in vacuo* to give a dark brown syrup, and was recrystallised from hot toluene to precipitate the excess TPPO, *exo,exo*-fulvonorborneneimide, and tetraacetate, and the filtrate again condensed. The residue was recrystallised from warm diethyl ether to afford an off-white crystalline product (20 mg), which was isolated and washed

with cold ether (100 mL), and the remaining solution condensed down to a yellow gum. Gum filtered through a plug of silica (Hexane/Ethyl acetate, 1:2), yielding a white crystalline solid (Trace %). ^{1}H NMR (300 MHz, $CDCl_3$) δ = 7.72 - 7.44 (m, TPPO), 6.41 (1H, t, *J* 1.9, HC=CH), 6.32 (s, Unknown), 5.59 – 4.83 (8H, m, Sugar), 4.47 (1H, t, *J* 6.6, Sugar), 4.27 – 3.89 (4H, m, Sugar), 3.74 (1H, t, *J* 1.9, Bridge 2 x CH), 3.48 (q, Diethyl ether), 2.77 (1H, s, Ring 2 x CH), 2.21 – 1.93 (17 H, m), 1.56 (s, H2O), 1.43 (t, Et2O), 1.29 - 1.20 (m, Unknown). ^{13}C NMR (100 MHz, $CDCl_3$) δ = 132.18, 128.60, 21.96. m/z (ESI): 227.1 (80%, $M+Na^+$), 279.1 (30%), 301.0 (100%, $TPPO+Na^+$), 371.0 (55%), 579.0 (95%, $M+2Na^+-H^+$), 857.1 (90%).

4.6 – References

1 S. Colak, C. F. Nelson, K. Nusslein and G. N. Tew, *Biomacromolecules*, 2009, **10**, 353–359.

2 T. Congdon, R. Notman and M. I. Gibson, *Biomacromolecules*, 2013, **14**, 1578–1586.

3 C. A. Knight, D. Wen and R. A. Laursen, *Cryobiology*, 1995, 32, 23–34.

4 T. Inada and S. S. Lu, *Cryst. Growth Des.*, 2003, **3**, 747–752.

5 D. E. Mitchell, G. Clarkson, D. J. Fox, R. A. Vipond, P. Scott and M. I. Gibson, *J. Am. Chem. Soc.*, 2017, **139**, 9835–9838.

6 S. Liu and R. N. Ben, *Org. Lett.*, 2005, **7**, 2385–2388.

7 C. S. Strom, X. Y. Liu and Z. Jia, *J. Biol. Chem.*, 2004, **279**, 32407–17.

8 D. H. Nguyen, M. E. Colvin, Y. Yeh, R. E. Feeney and W. H. Fink, *Biophys. J.*, 2002, **82**, 2892–2905.

9 N. M. Tsvetkova, B. L. Phillips, V. V. Krishnan, R. E. Feeney, W. H. Fink, J. H. Crowe, S. H. Risbud, F. Tablin and Y. Yeh, *Biophys. J.*, 2002, **82**, 464–473.

10 Y. Tachibana, G. L. Fletcher, N. Fujitani, S. Tsuda, K. Monde and S. I. Nishimura, *Angew. Chemie - Int. Ed.*, 2004, **43**, 856–862.

11 C. I. Biggs, T. L. Bailey, Ben Graham, C. Stubbs, A. Fayter and M. I. Gibson, *Nat. Commun.*, 2017, **8**, 1546.

12 C. J. Capicciotti, M. Leclere, F. A. Perras, D. L. Bryce, H. Paulin, J. Harden, Y. Liu and R. N. Ben, *Chem. Sci.*, 2012, **3**, 1408–1416.

13 C. J. Capicciotti, J. D. R. Kurach, T. R. Turner, R. S. Mancini, J. P. Acker and R. N.

Ben, *Sci. Rep.*, 2015, **5**, 9692.

14 B. Graham, T. L. Bailey, J. R. J. Healey, M. Marcellini, S. Deville and M. I. Gibson, *Angew. Chemie - Int. Ed.*, 2017, **56**, 15941–15944.

15 K. Mochizuki and V. Molinero, *J. Am. Chem. Soc.*, 2018, **140**, 4803–4811.

16 H. Geng, X. Liu, G. Shi, G. Bai, J. Ma, J. Chen, Z. Wu, Y. Song, H. Fang and J. Wang, *Angew. Chem. Int. Ed.*, 2017, **56**, 997–1001.

17 K. Liu, C. Wang, J. Ma, G. Shi, X. Yao, H. Fang, Y. Song and J. Wang, *Proc. Natl. Acad. Sci.*, 2016, **113**, 14739–14744.

18 M. Leclère, B. K. Kwok, L. K. Wu, D. S. Allan and R. N. Ben, *Bioconjug. Chem.*, 2011, **22**, 1804–1810.

19 Y. Mai and A. Eisenberg, *Chem. Soc. Rev.*, 2012, **41**, 5969–5985.

20 P. Czechura, R. Y. Tam, E. Dimitrijevic, A. V. Murphy and R. N. Ben, *J. Am. Chem. Soc.*, 2008, **130**, 2928–2929.

21 C. J. Capicciotti, R. S. Mancini, T. R. Turner, T. Koyama, M. G. Alteen, M. Doshi, T. Inada, J. P. Acker and R. N. Ben, *ACS Omega*, 2016, **1**, 656–662.

22 A. K. Balcerzak, S. S. Ferreira, J. F. Trant and R. N. Ben, *Bioorganic Med. Chem. Lett.*, 2012, **22**, 1719–1721.

23 J. F. Trant, R. A. Biggs, C. J. Capicciotti and R. N. Ben, *RSC Adv.*, 2013, **3**, 26005–26009.

24 A. K. Balcerzak, M. Febbraro and R. N. Ben, *RSC Adv.*, 2013, **3**, 3232–3236.

25 C. J. Capicciotti, J. S. Poisson, C. N. Boddy and R. N. Ben, *Cryobiology*, 2015, **70**, 79–89.

26 M. Leclère, B. K. Kwok, L. K. Wu, D. S. Allan and R. N. Ben, *Bioconjug. Chem.*, 2011, **22**, 1804–1810.

27 J. G. Briard, J. S. Poisson, T. R. Turner, C. J. Capicciotti, J. P. Acker and R. N. Ben, *Sci. Rep.*, 2016, **6**, 23619.

28 M. I. Gibson, C. A. Barker, S. G. Spain, L. Albertin and N. R. Cameron, *Biomacromolecules*, 2009, **10**, 328–333.

29 K. Lienkamp, A. E. Madkour, K.-N. Kumar, K. Nüsslein and G. N. Tew, *Chem. - A Eur. J.*, 2009, **15**, 11715–11722.

30 T. Eren and G. N. Tew, *J. Polym. Sci. Part A Polym. Chem.*, 2009, **47**, 3949–3956.

31 K. Lienkamp, A. E. Madkour, A. Musante, C. F. Nelson, K. Nüsslein and G. N. Tew, *J. Am. Chem. Soc.*, 2008, **130**, 9836–9843.

32 R. Y. Tam, S. S. Ferreira, P. Czechura, R. N. Ben and J. L. Chaytor, *J. Am. Chem. Soc.*, 2008, **130**, 17494–17501.

33 S. Chittaboina, B. Hodges and Q. Wang, *Lett. Org. Chem.* , 2006, **3**, 35–38.

34 Y. Yang, L. Yang, Y. Han, Z. Wu, P. Chen, H. Zhang and J. Zhou, *Bioorg. Chem.*, 2017, **72**, 42–50.

35 D. J. Walsh, S. H. Lau, M. G. Hyatt and D. Guironnet, *J. Am. Chem. Soc.*, 2017, **139**, 13644–13647.

36 A. R. Kudinov, D. S. Perekalin, S. S. Rynin, K. A. Lyssenko, G. V. Grintselev-Knyazev and P. V. Petrovskii, *Angew. Chemie - Int. Ed.*, 2002, **41**, 4112–4114.

37 T. L. Choi and R. H. Grubbs, *Angew. Chemie - Int. Ed.*, 2003, **42**, 1743–1746.

38 D. K. Hood and O. M. Musa, *Handbook of Maleic Anhydride Based Materials*, 2016.

39 M. A. Tallon, in *Handbook of Maleic Anhydride Based Materials*, ed. O. M. Musa, Springer International Publishing, Switzerland, 1st edn., 2016, pp. 387–388.

40 Carey and Sundberg, *Advanced organic chemistry 5th edition - Part A: Structure and Mechanisms*, 2007, vol. 65.

41 S. A. Kiselev, D. A. Lenev, A. A. Lyapkov, S. V. Semakin, G. Bozhenkova, F. Verpoort and R. V. Ashirov, *RSC Adv.*, 2016, **6**, 5177–5183.

42 D. A. Ryan, in *Doctoral Thesis*, p. 28.

43 D. C. Batesky, M. J. Goldfogel and D. J. Weix, *J. Org. Chem.*, 2017, **82**, 9931–9936.

44 R. M. Van Well, K. P. R. Kartha and R. A. Field, *J. Carbohydr. Chem.*, 2005, **24**, 463–474.

45 M. I. Gibson, G. J. Hunt and N. R. Cameron, *Org. Biomol. Chem.*, 2007, **5**, 2756–2757.

46 K. P. Ravindranathan Kartha, L. Ballell, J. Bilke, M. McNeil and R. A. Field, *J. Chem. Soc. Perkin Trans. 1*, 2001, 770–772.

47 K. Igarashi, *Adv. Carbohydr. Chem. Biochem.*, 1977, **34**, 243–283.

48 A. Wadouachi and J. Kovensky, *Molecules*, 2011, **16**, 3933–3968.

49 R. J. Williams, N. W. McGill, J. M. White and S. J. Williams, *J. Carbohydr. Chem.*, 2010, **29**, 236–263.

50 C. Stubbs, J. Lipecki and M. I. Gibson, *Biomacromolecules*, 2017, **18**, 295–302.

51 C. J. Capicciotti, J. F. Trant, M. Leclère and R. N. Ben, *Bioconjug. Chem.*, 2011, **22**, 605–616.

52 L. L. Kiessling and L. E. Strong, in *Alkene Metathesis in Organic Synthesis*, ed. A.

Fuerstner, Springer-Verlag, Berlin Heidelberg, 1st edn., 2013, pp. 219–220.

53 I. Takaaki and S. S. Lu, *Cryst. Growth Des.*, 2003, **3**, 747–752.

54 R. Deswal, R. Gupta and B. Sharma, *J. Proteins Proteomics*, 2016, **7**, 199–211.

55 C. Yu, B. Liu and L. Hu, *Tetrahedron Lett.*, 2000, **41**, 4281–4285.

56 P. G. McDougal, J. G. Rico, Y. I. Oh and B. D. Condon, *J. Org. Chem.*, 1986, **51**, 3388–3390.

57 W. R. Roush, H. R. Gillis and A. P. Essenfeld, *J. Org. Chem.*, 1984, **49**, 4674–4682.

58 J. A. Raymond, P. Wilson and A. L. DeVries, *Proc. Natl. Acad. Sci. U. S. A.*, 1989, **86**, 881–885.

59 C. A. Knight, E. Driggers and A. L. DeVries, *Biophys. J.*, 1993, **64**, 252–259.

60 H. Chao, P. L. Davies and J. F. Carpenter, *J. Exp. Biol.*, 1996, **199**, 2071–2076.

61 E. Buhler and F. Boué, *Macromolecules*, 2004, **37**, 1600–1610.

62 E. I. Howard, M. P. Blakeley, M. Haertlein, I. P. Haertlein, A. Mitschler, S. J. Fisher, A. C. Siah, A. G. Salvay, A. Popov, C. M. Dieckmann, T. Petrova and A. Podjarny, *J. Mol. Recognit.*, 2011, **24**, 724–732.

63 A. Radulescu, V. Pipich and A. Ioffe, *Nucl. Instruments Methods Phys. Res. Sect. A Accel. Spectrometers, Detect. Assoc. Equip.*, 2012, **689**, 1–6.

64 D. G. Lonergan and G. Deslongchamps, *Tetrahedron*, 1998, **54**, 14041–14052.

65 E. Villemin, M. F. Herent and J. Marchand-Brynaert, *European J. Org. Chem.*, 2012, **31**, 6165–6178.

66 L. Shi, G. Zhang and F. Pan, *Tetrahedron*, 2008, **64**, 2572–2575.

67 X. Yuan, S. Cheng, Y. Shi and W. Xue, *Synth.*, 2014, **46**, 331–335.

68 G. Asensio, C. Andreu and J. A. Marco, *Chem. Ber.*, 1992, **125**, 2233–2238.

69 T. Deng, X. Mao, Y. Li, S. Bo, Z. Yang and Z. X. Jiang, *Bioorganic Med. Chem. Lett.*, 2018, **28**, 3502–3505.

70 M. R. J. Vallée, L. M. Artner, J. Dernedde and C. P. R. Hackenberger, *Angew. Chemie - Int. Ed.*, 2013, **52**, 9504–9508.

71 V. Dimakos, J. J. W. Liu, Z. Ge and M. S. Taylor, *Org. Biomol. Chem.*, 2019, **17**, 5671–5674.

CHAPTER 5

Engineering ice inhibitory activity into new synthetic materials

---

5.1 – Chapter Abstract

Building upon the work of Chapter 4, this chapter outlines the development of a series of IRIs. Sequentially modified derivatives of simvastatin, and a chenodeoxycholic acid series, were synthesised. The bile acid series was rationally designed to feature the key properties and design motifs present in AFGP; helicity, amphipathy, and rigidity (with a defined domain structure). Likewise, intended as a mimic of the aromatically stacked Safranin O (a potent IRI), the statin series was used to probe the boundaries of IRI activity for hydrophobic small molecules, in order to determine whether activity can be modulated through minor structural modifications (as previously observed). Neither series demonstrated any meaningful IRI activity. However, this study has contributed to our understanding of the IRI structure-activity relationship, indicating that simple mimicry of core structural properties observed in AFGP and Safranine O is actually insufficient to incorporate IRI into a synthetic architecture.

5.2 – Chapter Introduction

The discovery of novel AF(G)P mimetics has, to date, almost exclusively focussed on the development of simplistic polymers and synthetic polypeptides, many of which have been identified through serendipity or trial-and-error screening.[1–3] Recently however, evidence of more rationally designed architectures have been presented in the literature and have been shown to possess significant IRI potency.

Ben and co-workers have worked extensively on the development of synthetic glycopeptides, with IRI activity similar to AFGP.[4] Recently they have shown small molecule inhibitors, with an optimised *O*-aryl-glycoside and *N*-aryl-D-aldonamide showing significant IRI activity (5 % MGA and 3 % MGA, respectively) at 22 mM (7.81 and 6.36 $mg.mL^{-1}$, respectively). Slow freezing (-40 ºC, with storage at -80 ºC) of red blood cells in the presence of the optimum brominated *O*-aryl-galactoside candidate + 15 % glycerol saw a 60 % recovery of red blood cells post-thaw, contrasted to 28 % without.[5,6] Similarly, a fluorinated *N*-aryl-D-aldonamide showed promise at enhancing the post-thaw colony forming ability of umbilical cord red blood cells (by ~ 15 % with 5 mM / 1.45 $mg.mL^{-1}$ doping).[7] These species clearly demonstrate potential application, but they are however not the most potent small molecule IRI candidates to have been prepared, and cryopreservative ability is ultimately limited with statistically identical post-thaw cellular recoveries to DMSO alone.

Most notably, is the work of Scott and Gibson and co-workers who have shown that enantiomerically pure amphipathic metal-organic frameworks – metallohelices – are capable of potently inhibiting ice crystal growth to 20 % MLGS at 20 µM.[8] These levels of activity are unprecedented amongst synthetic mimics, and comparable to hyper-potent AFGP-8 (~ 15 % MLGS at 5 µM). Likewise, Dori and co-workers recently reported on the activity of Safranine O, a small molecule IRI which is capable of supramolecular assembly in solution.[9] These

species are however inapplicable to biomedical translation, due to the potential cytotoxicity of transition metals and quaternised ammonium centres, respectively. However, in the absence of a definitive mechanism of action and given the common structural profile of these candidates (namely rigidity, amphipathy, and defined domain structure), a question is presented as to whether a more finite, considered approach to IRI design maybe employed in order to access clinically useful candidates with excellent IRI potency.

The potency of Safranine O is thought to stem from intramolecular pi-pi stacking, facilitating the formation of an extended – amphipathic – macromolecular architecture.[9] Contrarily, Ben and co-workers have successfully demonstrated the IRI activity of numerous (non-assembling) *O*-aryl-glycosides, indicating that potent IRI activity may not be the reserve of macromolecules alone.[6,10]

Without a universally established rational design blue print or mechanism of action, the potential synthetic space which may be explored in the process of discovering a, new, potent IRI inhibitor is prohibitively expansive. Recent work by Gibson and co-workers,[8] in addition to Chapters 2 and 4 herein, have however identified amphipathy (aided by structural rigidity) as potential design rationale in the preparation of IRI active species. As such, here we further explore these core structural motifs believed to be responsible for IRI activity, and investigate their incorporation into IRI inactive species by structural modification, with the aim of introducing IRI potency.

5.3 – Results and Discussion

5.3i – Synthesis and IRI analysis of Simvastatin derivatives

In order to explore the IRI activity field and further establish a range of small molecules which possess IRI potency (and which have been comparatively underexplored to date), attention was turned to the DrugBank archive. The repurposement of legacy pharmaceutical agents is of particular relevance, and the abundance of data present within the DrugBank provided a viable starting point for the initial assessment of potential chemical structures. A query was executed resulting in the display of a series of potential candidates of interest, matching the desired/prescribed criteria; Small molecule = true, LogP > 2 – and therefore possessing prominently hydrophobic character, regulatory approval = true – and therefore commercially sourceable. Results were then inspected and solubilities compared between the candidates. Of these results, Simvastatin represented the most intriguing candidate. Given its status as a small, rigid, hydrophobic small molecule – with some hydrophilic character – the IRI activity assessment of a small series of Simvastatin and its key metabolites was of specific interest, with the core structural motifs supposedly matching our hypothesised design rationale.

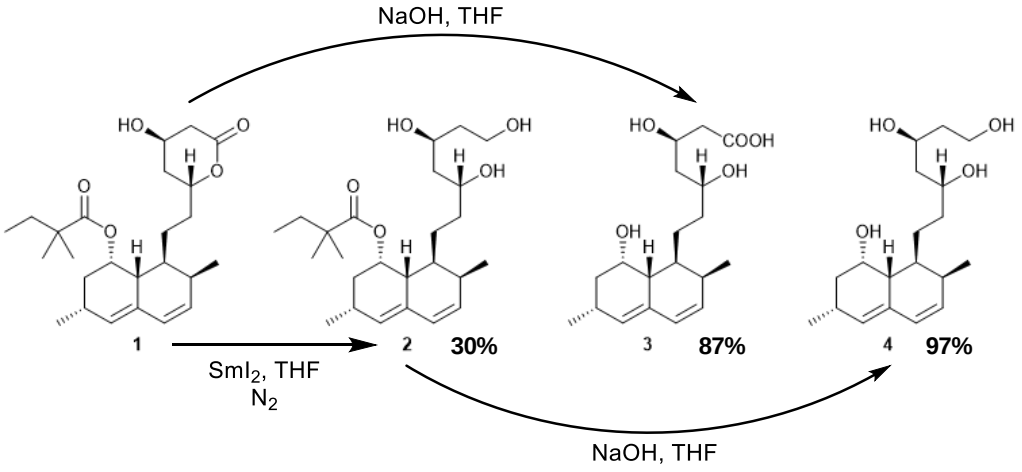

Figure 5.1 – Synthesis of the panel of simvastatin derivatives prepared for IRI activity assessment.

Due to Simvastatin's (**1**) low water solubility, three further synthetic derivatives were prepared, to i) enhance solubility (and potentially access greater magnitudes of activity) and ii) to explore the effect upon IRI activity by sequential modification and amplification of the hydrophilic domain (Figure 5.1).

In the first instance, a ring-opened candidate (**2**) was synthesised through the selective hydrolysis of the lactone ring by samarium iodide, in the presence of the butyric ester, cleanly affording the desired compound after chromatography in moderate yield (30%). **4** was subsequently accessed through saponification of **2** in 97% yield, whilst saponification of **1** yielded product **3** in equally excellent yield (87%). Importantly, these candidates have disparate hydrogen bonding capacities, potentially impacting upon IRI activity, and aqueous solubilities of **2**, **3**, and **4** were determined by UV-Visible spectroscopy. Subsequent IRI activity analysis indicated no activity across the series and comparable to a PBS control, Figure 5.2.

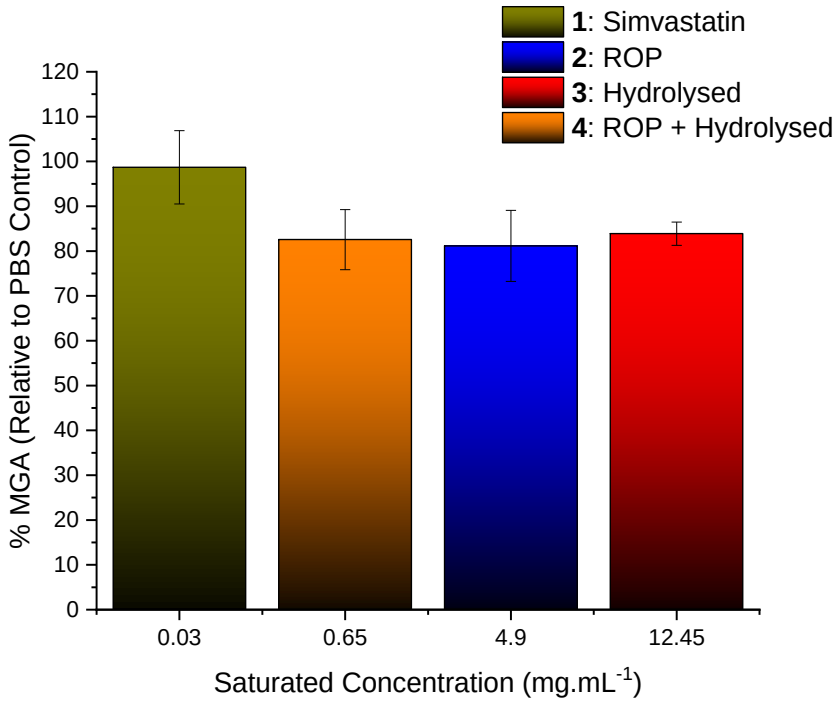

Figure 5.2 – IRI activities of the statin series at their saturated solution concentrations. IRI activity measured as a function of solute concentration. MGA = Mean grain area relative to a PBS control, expressed as %. Error bars represent the ± standard deviation from three independent measurements.

Simvastatin itself possessed no activity at a saturated solution concentration of 30 μg.mL^{-1},[11] and so enhancing solubility to access greater levels of potency was clearly vital. However, whilst the modified candidates demonstrated substantially increased solubility across the series, they too possessed weak activity. The ring opened and hydrolysed derivative (**4**) demonstrated enhanced solubility to Simvastatin itself (0.65 mg.mL^{-1}) but was comparatively less soluble than the other synthetic candidates – presumably due to aggregation facilitated by the free hydroxyl groups. The ring opened equivalent on the other hand (**2**) possessed substantially increased solubility, and further removal of the butyric acid ester and lactone hydrolysis (**3**) gave the highest solubility of the series at 12.45 mg.mL^{-1}, likely enhanced by salt formation in buffer. Whilst unable to form a supramolecular architecture, these candidates were unable to show potency in the same manner as non-assembling equivalents of proximal size and hydrophobicity. This indicates that designing a new IRI around simple design rules is astonishingly difficult, and a more elegant strategy is ultimately required.

5.3ii – Synthesis and IRI analysis of poly(bile acids)

Antifreeze glycoproteins are unique in their structural conformation, both intrinsically flexible and rigid, they are also amphipathic, featuring well defined regions of hydrophobicity and hydrophilicity. Mirroring these key structural properties on a simple framework may yield a viable candidate with enhanced IRI activity. However, rational design has thus far proven problematic. Amphipathic species have a tendency to aggregate and micellise, making exposure of both domains in solution – a crucial prerequisite for IRI function – challenging to achieve. As shown in Chapter 4, a rigid amphiphile has potential to infer enhanced IRI activity.

Naturally occurring bile acids, synthesised by the liver and found in the bile of mammals, have numerous biological functions, and are primarily involved in cholesterol metabolism. These species are unique, in that they are amphipathic and structurally rigid due to the presence of a conjugated hydrophobic ring system. Depending on the particular derivative, bile acids have a degree of flexibility due to the presence of alkyl chains, with hydrophilicity inferred from the presence of spatially segregated alcohol groups.

These properties make bile acids an interesting proposition for investigation herein, featuring highly analogous structural properties to AFGP, it is possible that certain bile acids may have IRI potency, particularly when polymerised. In addition, below the critical micelle concentration, bile acids are known for their ability to sit at the water/oil interface – due to the established importance of the hydrophobic domain in IRI activity – this property is of particular interest, potentially leading to a soluble IRI inhibitor with the necessary, substantive, hydrophobic character.

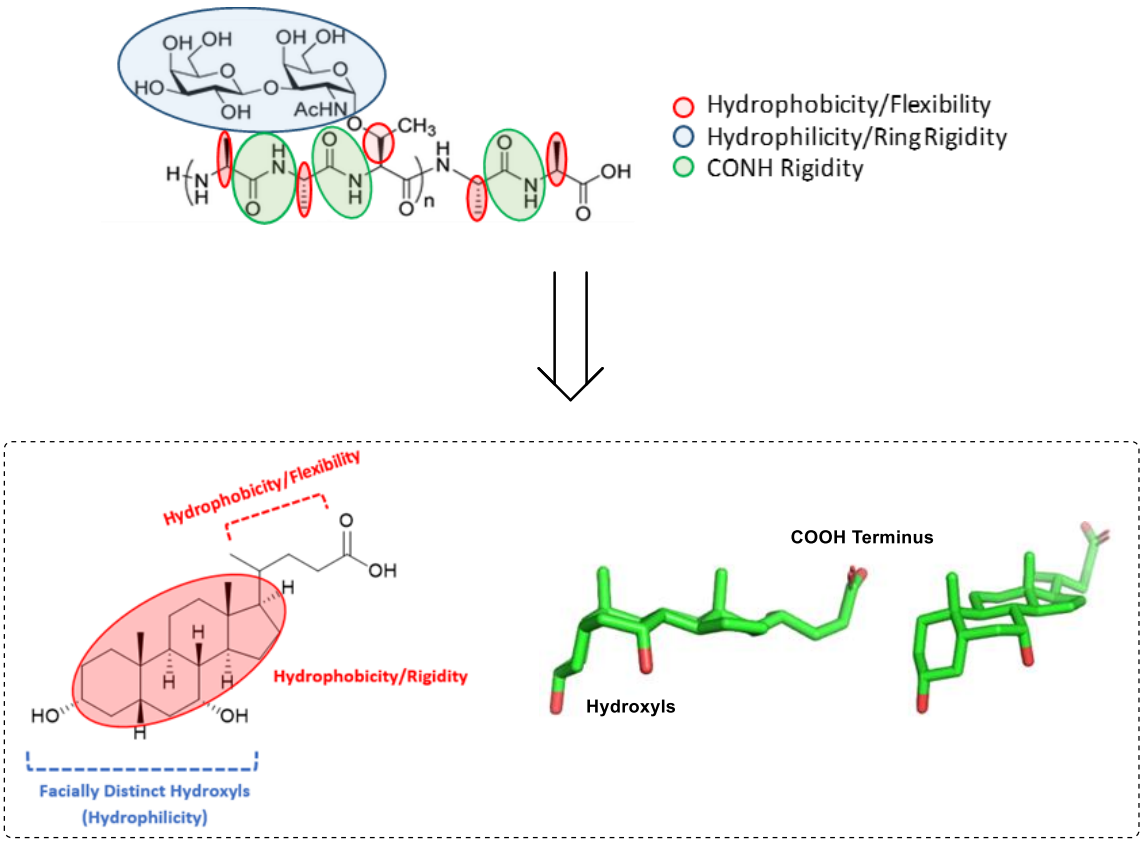

Figure 5.3 – Comparison of structural motifs of AFGP and chenodeoxycholic acid.

The preparation of macromolecular architectures of bile acids therefore warrants the use of a species with multiple sites of functionality. Chenodeoxycholic acid, Figure 5.3, represents an ideal bile acid candidate for investigation. It's spatially distinct hydroxyls, protruding from segregated positions on the rigid conjugated rings, and a flexible carboxylic acid tail, allow for polyesterification whilst retaining amphipathy and the core design criteria. Its synthetic versatility – and the recognised ability to easily and selectively functionalise at the C-3 hydroxyl group *via* ether formation, as shown by Chen and co-workers [12] – also lends itself to application herein.

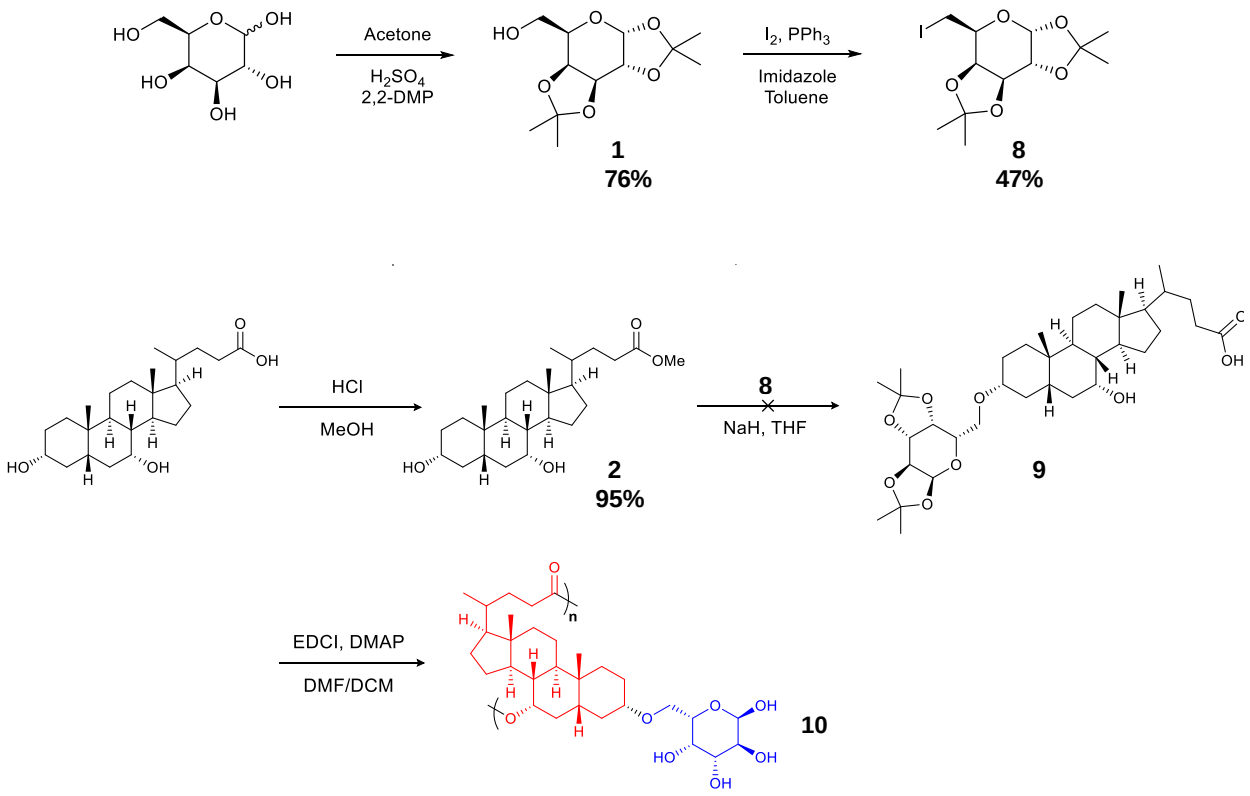

Scheme 5. 1 – Initial synthetic route for the generation of a poly bile acid-carbohydrate conjugate.

A strategy involving the selective mono-glycosylation of a chenodeoxycholic acid framework was devised, with the sugar acting as an 'enhanced' hydrophilic domain, larger and more pronounced than a lone free hydroxyl group. As per Chapter 4, galactose in particular was selected due to its natural occurrence as a constituent unit of the hydrophilic domain in AFGP. Scheme 5.1. It was hypothesised that, when polymerised as poly(chenodeoxycholic acid-3-galactopyranose), this system would be a predominantly hydrophobic rigid structure, with facially distinct 'patches' of hydrophilicity, and a degree of flex, representative of AFGP.

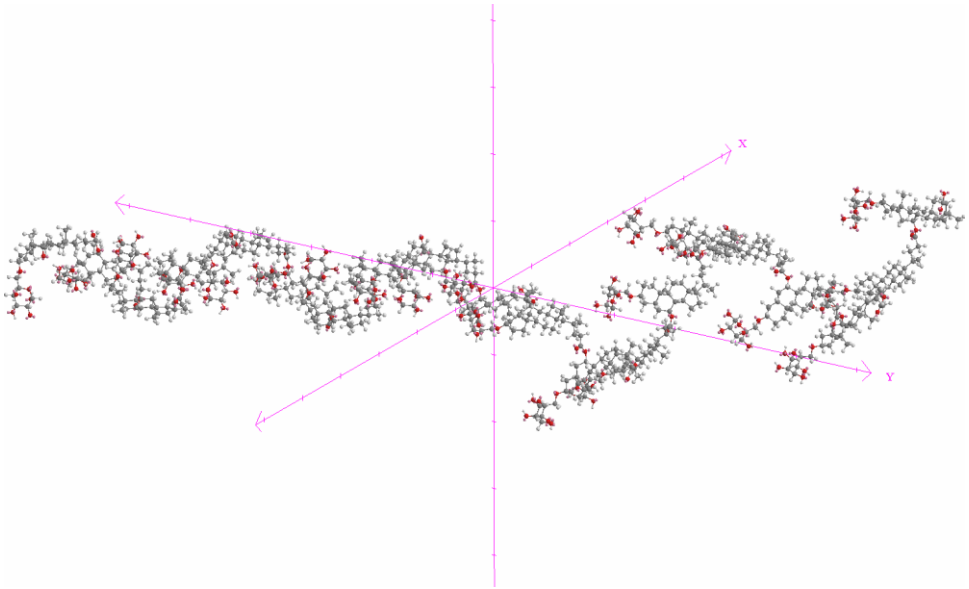

Figure 5.4 – Energy minimized model of the polymeric conjugate (featuring axes).

Furthermore, energy minimisation modelling (ChemDraw) of an N=20 stretch of the amphipathic poly(chenodeoxycholic acid-3-galactopyranose) indicated that the structure may have a propensity to adopt a helical structure (partly driven by the sugar unit), Figure 5.4. This is particularly interesting, given the PPII helix adopted by AFGP, the role which it plays in ensuring amphipathic domain presentation, and by extension, IRI activity.

In pursuit of the monomer **9**, stereopure 1,2:3,4-Di-O-isopropylidene-α-D-galactopyranose was first synthesised in good yield (76 %) with 2,2-dimethoxypropane in dry acetone, in the presence of a sulphuric acid catalyst. Iodination followed, giving the iodosugar for conjugation in reasonable yield (47 %). The chenodeoxycholic acid methyl ester was prepared in parallel (95 %), and in combination with the iodosugar, was subsequently subjected to Williamson conditions for ether synthesis, as per the literature precedent.

Despite the employ of dry solvents, air free-technique, and heating, mass spectrometry indicated the absence of the desired product, and instead showed a starting material dimer at 779.3 m/z [CDCA+Gal-6-OH+I^-]. Column chromatography of the crude mixture resulted in the isolation of the two distinct – unconjugated – reactants.

Although ether syntheses have the potential to be low yielding, and are heavily dependent upon the presence of moisture, solvent, kinetics, and the propensity of the reactants to undergo side reactions (such as E1cb of the alkylating agent), the outright failure of the step was surprising. The literature precedent has however only effectively demonstrated the use of methyl iodide as the alkylating agent – a comparatively smaller species to the iodosugar. Consequently, considering the steric bulk of the bile acid, it is possible that the formation of such an ether is highly unfavourable, given the resulting congestion around the C-3 position by the forcing together of the two ring systems. Furthermore, despite the inherent stability of ethers, given the close proximity of the sugar and bile acid when conjugated, it is possible that any ether formed would be so puckered and/or crowded as to render it particularly susceptible to hydrolysis. In addition, evidence of elimination by-products in the isolated carbohydrate were also observed, with characteristic alkene signals present in the 5.5 – 6.1 ppm range and complex epimer multiplets between 3 – 4 ppm, indicating that inactivation of the iodosugar may have also occurred *in situ*.

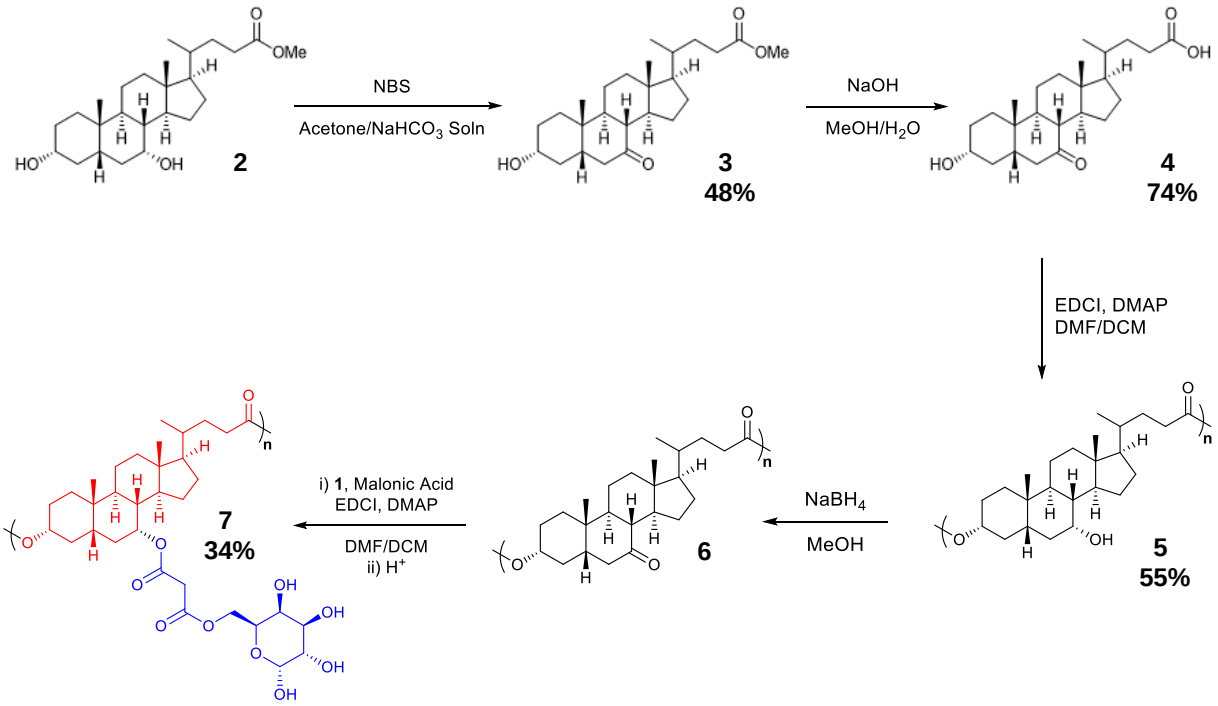

Scheme 5.2 – Revised synthetic scheme for the production of the poly bile acid-carbohydrate conjugate featuring a malonate spacing-linker, **7**. 6 was not isolated and was prepared *in-situ*.

Due to the failure of the selective coupling route, an alternative synthesis was therefore proposed, Scheme 5.2. As a result of the steric bulk hindering both hydroxyl positions, it was considered necessary to introduce a 'spacing' linker, which would give sufficient separation from the backbone ring system and the carbohydrate unit, so as to not slow or inhibit the conjugative glycosylation step. For conjugation, an ester at the more synthetically accessible ring-7 position was preferentially opted for, due to the failure to selectively install an ether at ring-3. Importantly, molecular modelling of this amended route suggested that the final product, **7**, would also possess the propensity to form a solvent accessible helical structure, Figure 5.5, at multiple molecular weights.

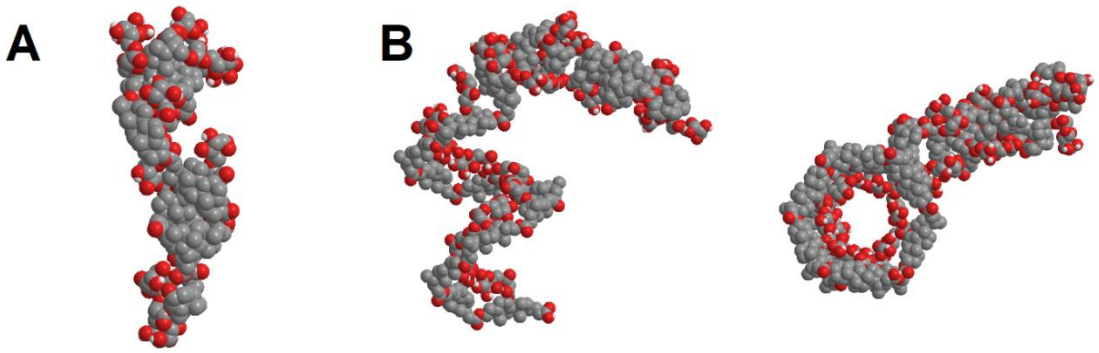

Figure 5.5 – Energy minimized model of 7 at varying molecular weights. A) DP10 Simulation, B) DP20 Simulations (Two angles).

As such, chenodeoxycholic acid methyl ester (**2**) was stereoselectively oxidised at the ring-7 position using *N*-bromosuccinimide to give 7-ketolithocholic acid methyl ester in 48% yield. The ring-7 position has fewer repulsive interactions and ease of accessibility towards bases across the unhindered equatorial face due to its axial conformation, this enhances its proclivity towards oxidation relative to the equatorial ring-3 position.[13] This temporary installation of a ketone, effectively acting as a protecting group, would allow for the stereoregular polymerisation of chenodeoxycholic acid through the ring-3 hydroxyl only. As per literature precedent, the ^{13}C NMR of the crude material, Figure 5.6, identified the 7-keto isomer as the major product of this step, and was easily isolated from the 3-ketolithocholic acid methyl ester by-product through column chromatography, Figure 5.7.

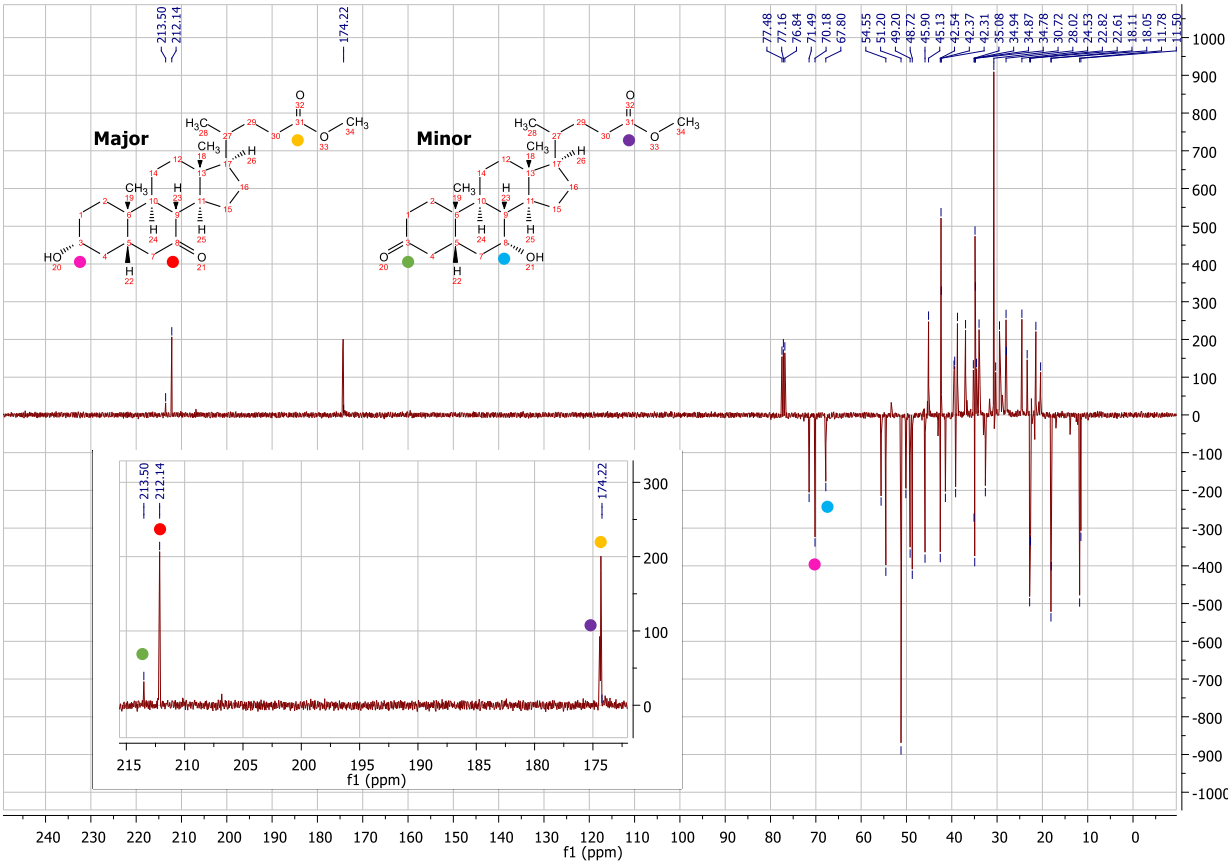

Figure 5.6 – ^{13}C NMR ($CDCl_3$) of (7/3)-ketolithocholic acid methyl ester (Crude).

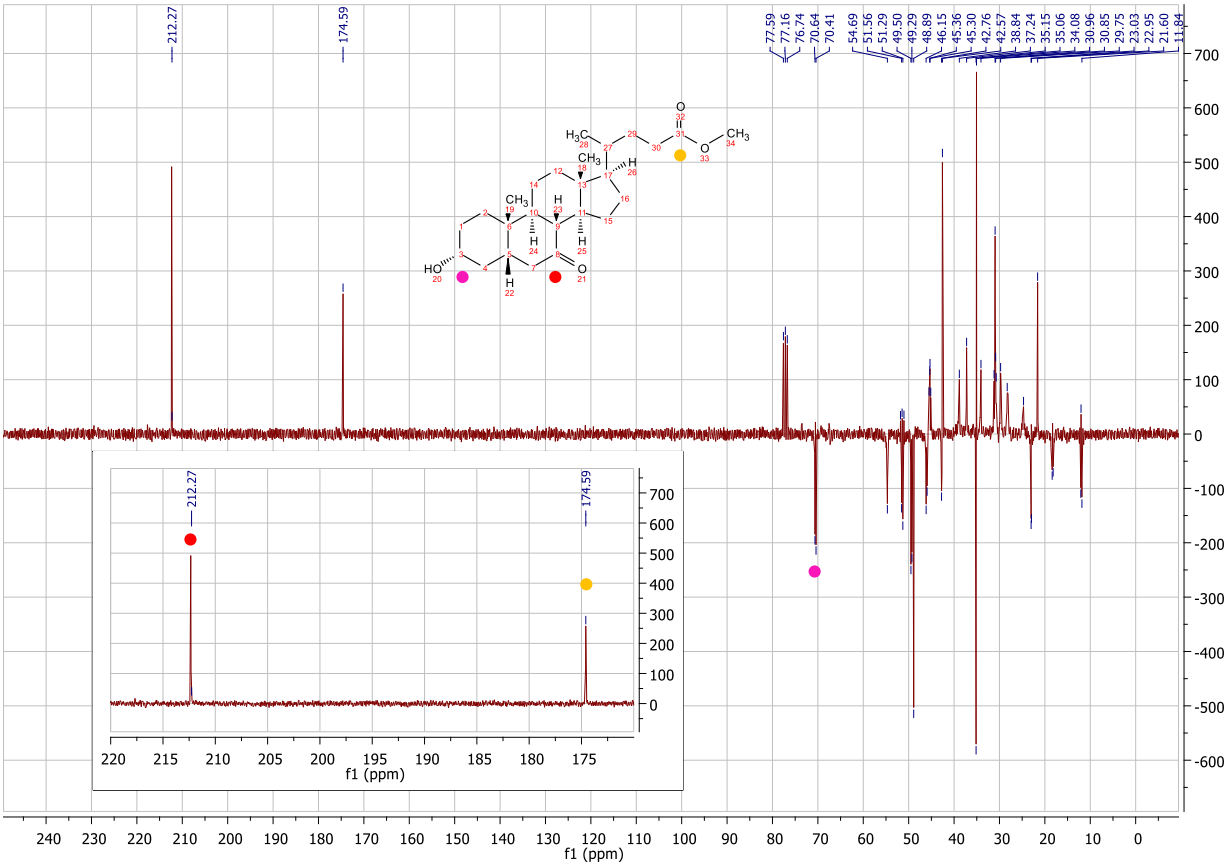

Figure 5.7 – ^{13}C NMR ($CDCl_3$) of 7-ketolithocholic acid methyl ester (Purified).

Subsequent ester hydrolysis and polycondensation *via* carbodiimide coupling yielded the 7-ketolithocholic acid derived polyester, **5**, Table 5.1.

Mass (mg)	Yield (%)	Mn_{THEO} (g.mol^{-1}) [a]	Mn_{OBS} (g.mol^{-1}) [a]	Đ [a]	DP [a]
130	31.0%	330,712	7353	1.02	20
			3446	1.03	9
			1575	1.01	4
			847	1.01	2

Table 5.1 – GPC/SEC and Yield data for poly(7-ketolithocholic acid). [a] Mn_{THEO} = molar mass assuming 100% condensation of starting material, Mn_{OBS} = molar masses as observed experimentally, Đ = dispersity, and DP = degree of polymerization, determined by SEC.

Due to the step-growth nature of polyesterification, a propagative series of molecular weights was obtained, giving a resolvable polydisperse mixture, Figure 5.8. This was of serendipitous importance in the rational design process, given that AFGP exists in nature as a polydisperse protein, as we believed that the production of a mixture of chain lengths may provide a more proximal mimic of AFGP.

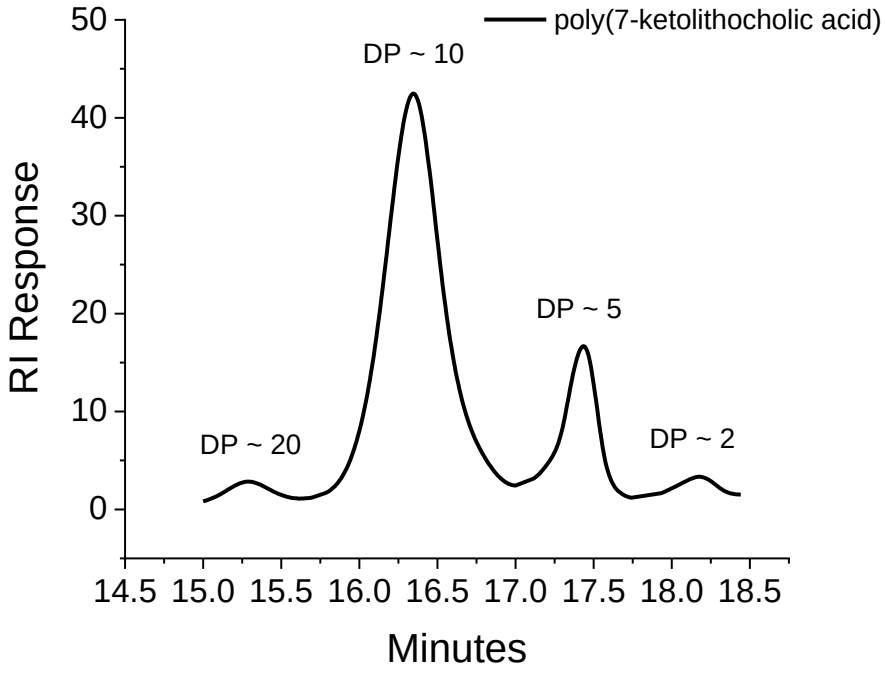

Figure 5.8 – SEC trace of poly(7-ketolithocholic acid).

Reduction of the 7-keto group was then necessary to restore the unmasked hydroxyl group, to which the glycosyl unit and linker were to be conjugated. In the pursuit of preparing a well-defined AFGP mimetic, stereoregularity was to be maintained. As such, it was necessary to determine an optimum method for effective reduction, and the return of uniform stereochemistry, to avoid scrambling of the ring-7 centre.

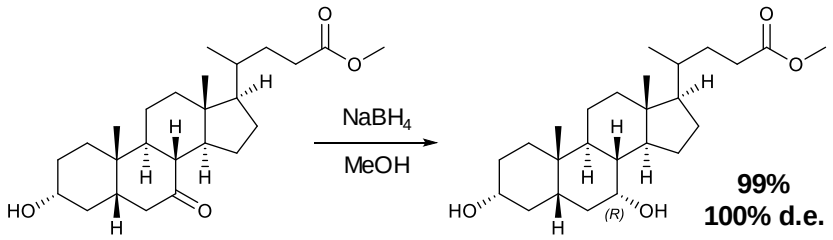

Figure 5.9 – Stereoselective reduction of 7-ketolithocholic acid methyl ester to CDCA methyl ester.

Utilising a sample of 7-ketolithocholic acid, it was found (as per literature precedent) that an excess of sodium borohydride in methanol was sufficient to return the original *R* stereochemistry of the ring-7 position, without any evidence of racemisation. Figure 5.10.

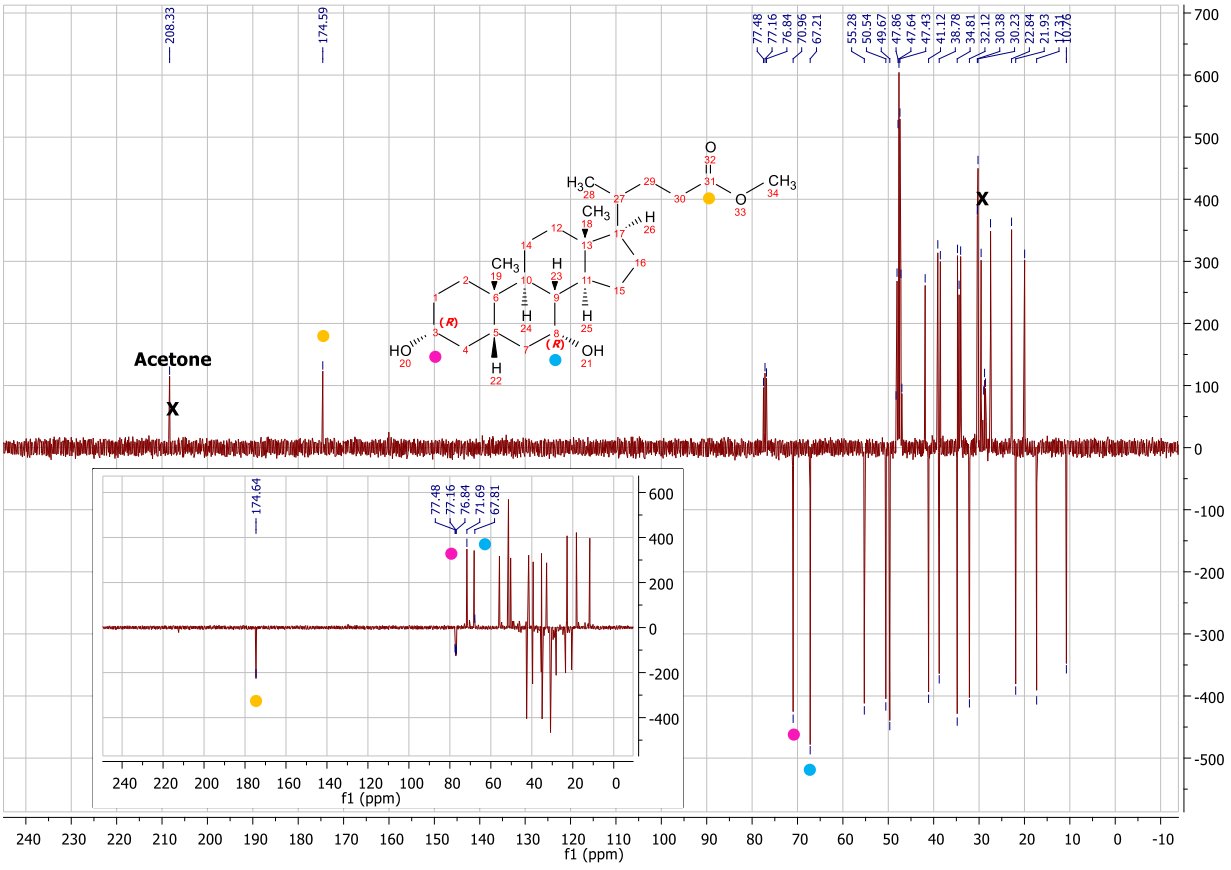

Figure 5.10 – ^{13}C NMR ($CDCl_3$) of chenodeoxycholic acid methyl ester (Post $NaBH_4$ Reduction).

Whilst the ability of sodium borohydride to reduce esters is limited in extent – often failing to do so entirely, except under harsh conditions or elevated temperature – the use of a 2-fold excess of $NaBH_4$ may nonetheless pose a risk to the integrity of the polymer chain, potentially

resulting in degradation. However, after four hours of exposure, the small molecule trial showed no evidence of hydrolysis of the terminal methyl ester, implying synthetic resilience. Nevertheless, in the interests of preventing polymer hydrolysis, exposure to sodium borohydride was limited to half the time employed for the small molecule.

Following the reduction of the ketone containing polymer, subsequent SEC analysis of the intermediate species indicated a shift in the molecular weight profile of the polymer mixture. The mixture contained DP10, DP5 and some smaller oligomeric fragments, as previous, whilst the DP20 derivative was seemingly absent. The strength of the DP10 signal was further intensified, implying that the DP20 stretch may have undergone significant hydrolysis. Figure 5.11A and B. This may suggest that, should it have formed an extended helical-like structure as hypothesised, that the strain of its coiling may have predisposed the DP20 stretch to ester reduction and degradation to a more stable chain length.

Now reduced, functionalisation of the disperse poly(chenodeoxycholic acid) mixture with the malonic acid linker and galactose unit by carbodiimide coupling was to follow. Conjugation of the previously prepared sugar, 1,2:3,4-Di-O-isopropylidene-α-D-galactopyranose, through the free 6-hydroxy position to the poly(chenodeoxycholic acid) mixture was achieved *in-situ* with 1 equivalence of malonic acid. In order to avoid any inadvertent backbone ester cleavage, the malonic acid was first incubated in the presence of a large excess of EDCI, in order to ensure no solution acidity remained. pH testing confirmed the neutrality of the coupling mixture, before introduction to the bile acid polymer. This further ensured the malonic acid carboxylic acids were activated, prior to attack by the bile acid alcohol groups. Delayed addition of a large excess of Gal-6-OH then ensured quantitative glycosylation to the activated, but uncoupled, malonic acid chain ends. Fleeting exposure to a dilute acidic solution in order to cleave the sugar acetal protecting groups followed, yielding the final “Deprotected” candidate. Subsequent SEC analysis, Figure 5.11B, showed little change in the molecular weight profile

of the polymer, indicating that the transient acid exposure did not result in significant ester backbone cleavage.

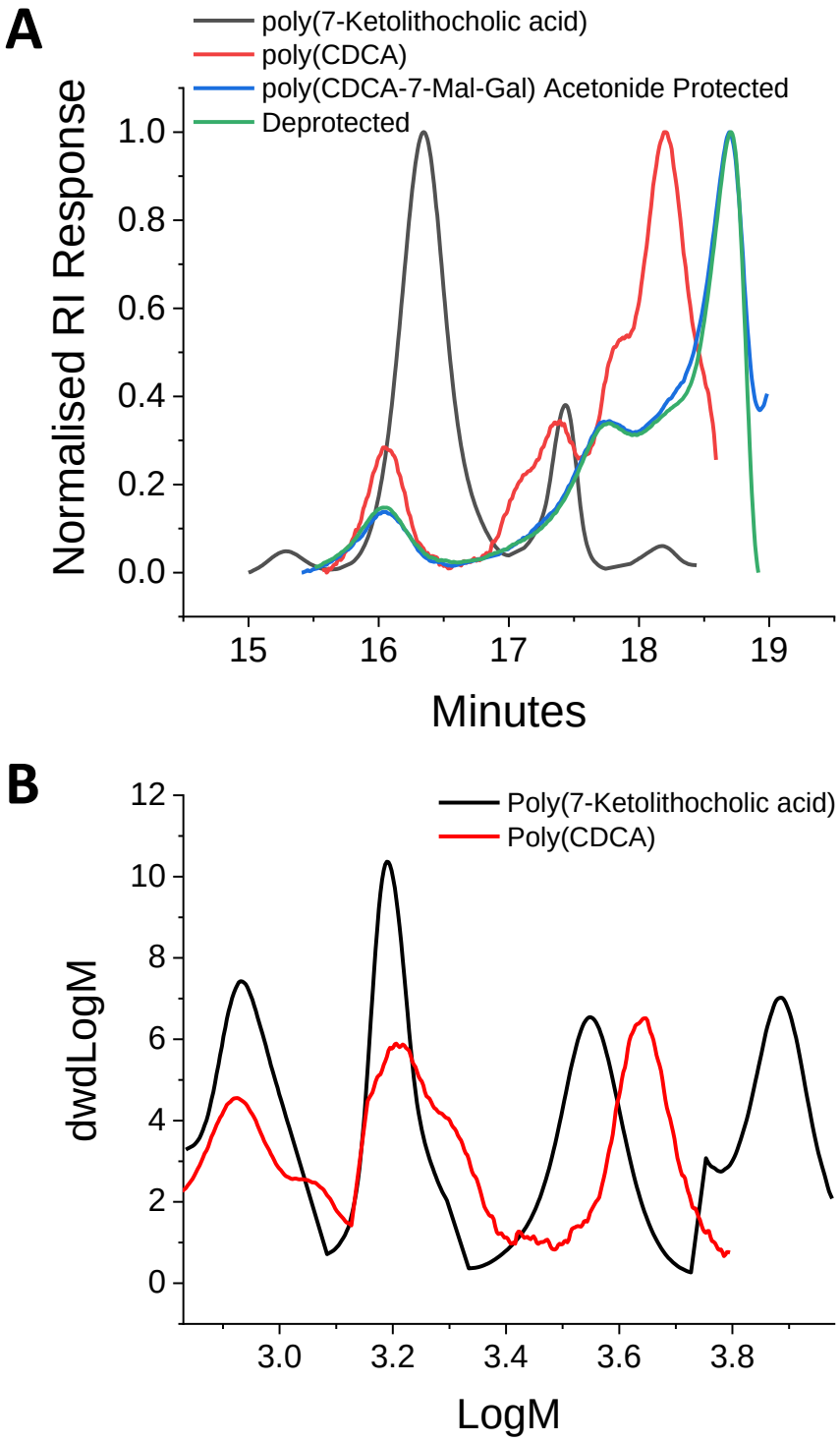

Figure 5.11 – A) Overlaid SEC RI traces of the polymeric bile acid series synthesised. B) Comparison between poly(7-ketolithocholic acid) and the reduced poly(CDCA).

Unusually, an expected shift in molecular weight associated with glycosylation was not observed, however, ^{1}H and ^{13}C NMR analysis indicated near quantitative glycosylation and successful installation of the malonic acid linker, Figure 5.12 and 5.13, respectively. Integration of the anomeric galactose C1 peak at 4.61 ppm relative to a bile acid C-3H signal at 2.29 ppm, indicated a ratio of ~ 1:3, respectively. Furthermore, the absence of the acetal signals in the ^{1}H NMR confirmed sugar deprotection. Importantly, repeated washing & precipitation from water – in which the final species had poor solubility – ensured the removal of any excess and unconjugated galactose and malonic acid.

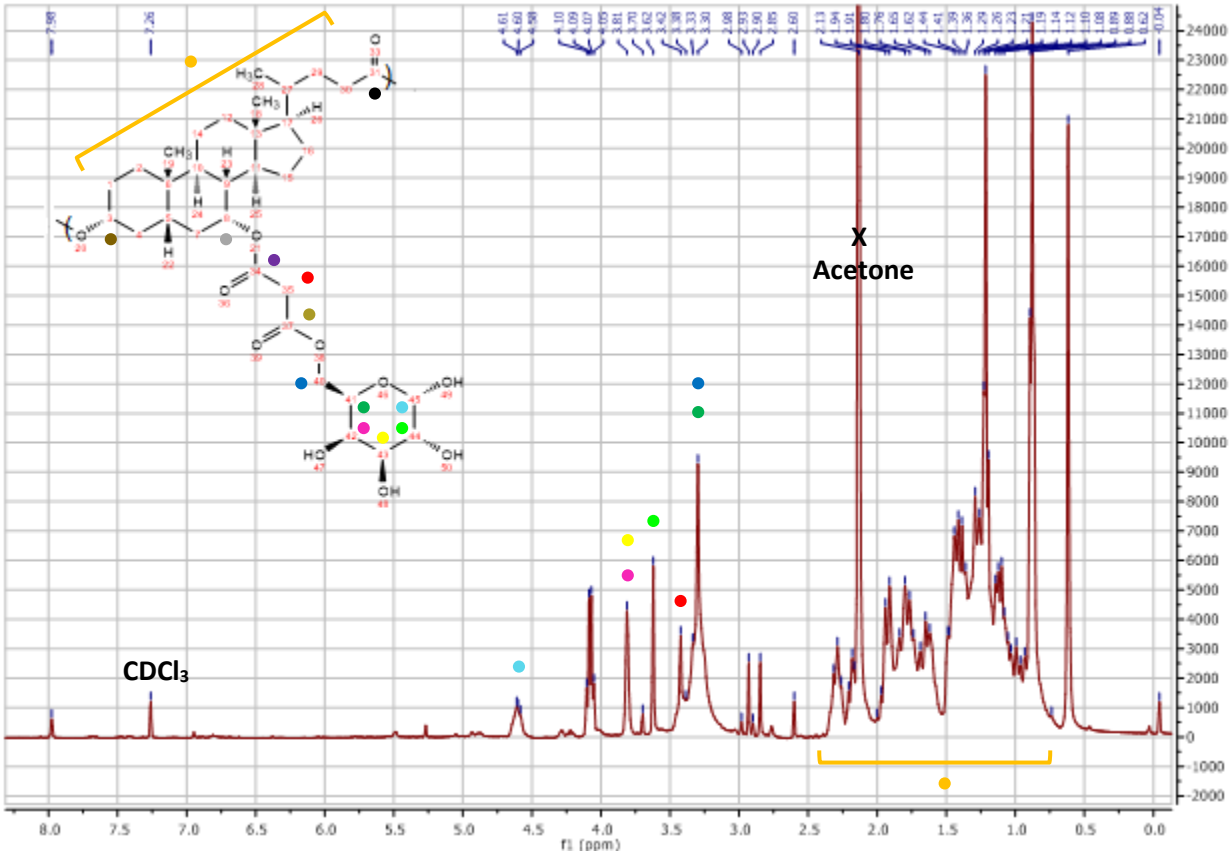

Figure 5.12 – ^{1}H NMR ($CDCl_3$) of the deprotected poly(chenodeoxycholic acid-7-malonate galactose).

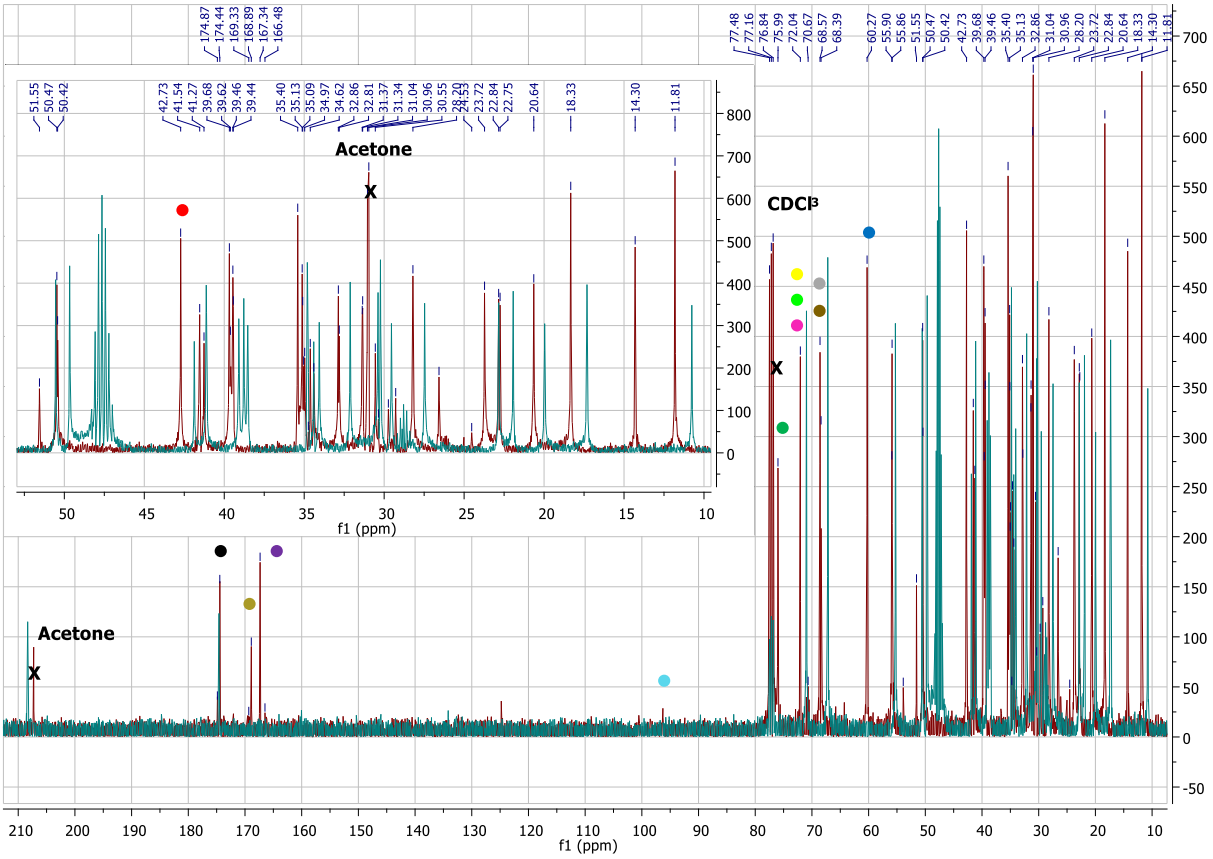

Figure 5.13 – Comparative ^{13}C NMR ($CDCl_3$) of the deprotected poly(chenodeoxycholic acid-7-malonate galactose) (Brown) and chenodeoxycholic acid methyl ester (Blue).

Once dried, the poly(chenodeoxycholic acid-7-malonic-6-galactopyranoside) candidate, **A**, along with the unconjugated poly(chenodeoxycholic acid) **B**, and poly(chenodeoxycholic acid-7-one) **C**, intermediates, and the chenodeoxycholic acid, **D**, starting material, were carried forward for splat testing and analysis, Figure 5.15. Due to low solubilities, the samples were tested at their saturated concentrations, which were determined by UV-Vis spectroscopy.

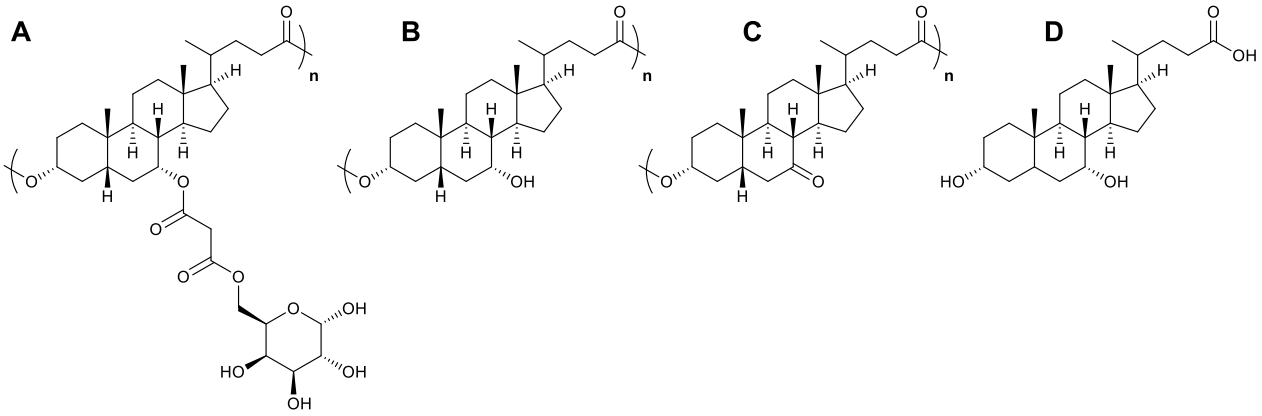

Figure 5.14 – Series of bile acid derivatives and polymers assayed for IRI activity.

Chenodeoxycholic acid (CDCA) was found to have very weak IRI activity, inhibiting the growth of ice crystals to ~ 80% of their original size at 90 μg.mL^{-1} (the CDCA solubility limit), Figure 5.15.

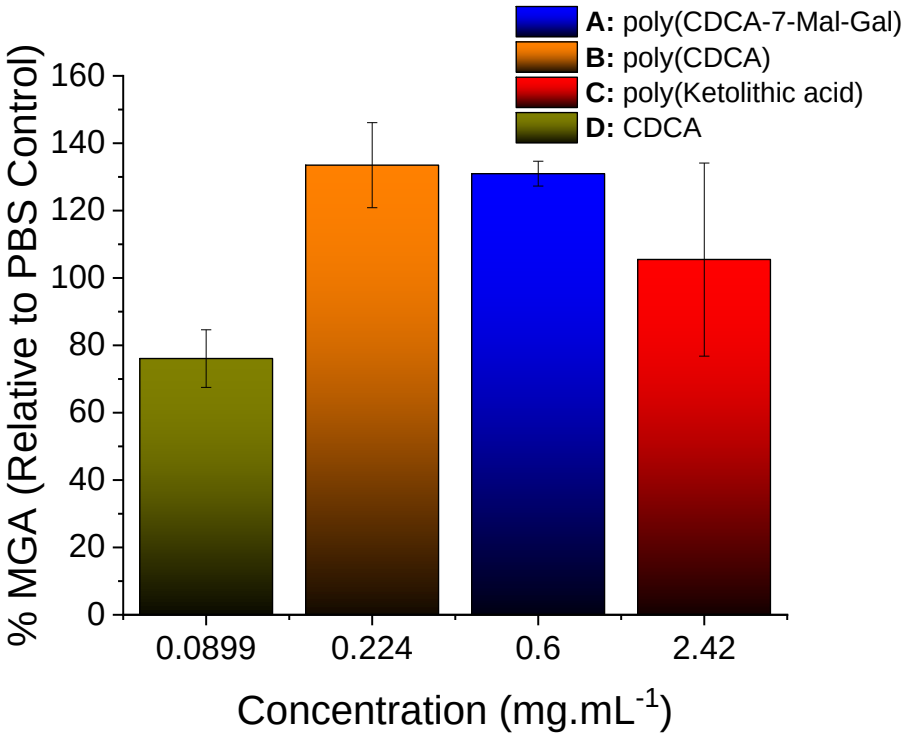

Figure 5.15 – IRI activities of the bile acid series. IRI activity measured as a function of solute concentration. MGA = Mean grain area relative to a PBS control, expressed as %. Error bars represent the standard deviation from three independent measurements.

In contrast, the synthetic candidates exhibited comparatively greater solubilities across the board, with polymeric CDCA (B) showing a near x2.5 increase in solubility in aqueous solution. This solubility jump would likely indicate that the formation of a rigid extended structure – potentially helical in nature – has resulted in a greater degree of solvent accessibility. Intriguingly, the poly(ketolithocholic acid) equivalent – differing only by the presence of a ketone group (in place of a hydroxyl) at the C-7 position – further demonstrates a near 10-fold increase in solubility. As a hydrogen bond acceptor only, **C** lacks the same H-bonding capacity as donor and acceptor **B**. This may infer that the poly(ketolithocholic acid) likely has a substantially different polarity profile and solution structure, aiding and abetting solubilisation. However, whilst neither candidate demonstrated any appreciable IRI activity, this may suggest it is possible to perform minor structural 'tweaks' to potent, but insoluble, IRI candidates in order to significantly enhance solubility (and potentially activity) without significant structural modification or amphipathic distortion (which has been shown to destroy potency – Chapter 4).

Conjugation of the malonic acid linker and galactose motif did little to rescue IRI activity. Whilst still possessing greater solubility than poly(CDCA), this bile acid-carbohydrate conjugate (**A**) was less soluble than poly(ketolithocholic acid) – suggesting that the free hydroxyl groups acted to both solubilise and aggregate, lowering overall solution concentration relative to **C**.

5.4 – Conclusions

A series of poly(bile acids) and corresponding small molecules were synthesised, as were a series of hydrophobic, small molecule, simvastatin derivatives. IRI activity was not induced in any of the prepared species, despite the inclusion of specific design motifs observed in other hyper-potent IRIs of both synthetic and natural origin.

The preparation of AFGP inspired poly(chenodeoxycholic acid) derivatives, which were designed to be; intrinsically amphipathic, polydisperse, highly rigid with some slight flexibility, and containing spatially segregated and defined hydrophobic / hydrophilic faces – mimicking AFGP – did not show the anticipated potency. These results indicate that simply replicating the baser structural properties of hyper-active species is not necessarily sufficient to effectively inhibit ice crystal growth. Furthermore, the observations reported herein may further suggest that a model of ice recrystallisation inhibition dependent upon ice-face binding is the primary mechanism by which crystal growth is actually impeded. AFGP and PVA have both been reported to bind to ice, whilst AFP is thought to order clathrate waters and therefore bind indirectly. In all cases, the three-dimensional spacing of both methyl and hydroxyl groups are thought to play a significant role – and despite the stereopurity of the prepared candidates – the lack of specific engineering of the geometric presentation of domains may be responsible for the observed failure of activity.

Similarly, sequentially modified Simvastatin derivatives – intended to mimic other small molecule species such as Safranine O – did not effectively inhibit ice crystal growth. Although unable to form a supramolecular architecture, the lack of potency when compared to other non-assembling small molecules would clearly indicate a fundamental presentative disparity – with functional groups potentially not optimised for specific ice facing binding.

Collectively, these results show that rational IRI design is unpredictable, and highly difficult.

5.5 – Experimental

Materials

Physical and analytical methods

^{1}H and ^{13}C NMR Spectra (300 – 400 MHz and 75 – 100 MHz, respectively) were recorded using one of a Bruker DPX-300/400 Spectrometer under standard NMR conditions. Chemical shifts were recorded in ppm and referenced to solvent residual peaks, using MestReNova NMR Spectroscopy software.

ESI MS experiments were performed on an Agilent 6130B Single QUAD ESI-LC MS spectrometer in either positive or negative mode with an H_2O/MeOH (80:20) eluent feed, with samples dissolved in water or methanol, unless otherwise stated.

SEC/GPC data was acquired on either a DMF Agilent 390-LC MDS instrument equipped with differential refractive index (DRI), viscometry (VS), dual angle light scatter (LS) and dual wavelength UV detectors. System equipped with a PL-AS RT/MT2 autosampler, Shimadzu SPD-M20A microarray detector, a PL-gel 3 μm (50 × 7.5 mm) guard column and 2 × PL-gel 5 μm mixed-D columns (300 x 7.5 mm). Samples were filtered and suspended in the relevant HPLC grade solvent (DMF with 5 mmol NH_4BF_4 additive), with a flow rate of 1 mL/min^{-1} at 50ºC. Refractive index recorded. Analyte samples were filtered through a nylon membrane with 0.22 μm pore size before injection. Respectively, experimental molar mass (Mn,SEC) and dispersity (Đ) values of synthesized polymers were determined by conventional calibration (relative to poly(methyl methacrylate) standards – Agilent EasyVials, 690 – 271400 Da) using Agilent GPC/SEC software. Refractive index recorded.

Absorption UV/Vis (Ultra-violet/visible spectroscopy) spectra were acquired on an Agilent Technologies Cary 60 Variable Temperature UV-Vis spectrophotometer at room temperature fitted with Holographic Grating (27.5 × 35 mm, 1200 lines/mm, blaze angle 8.6° at 240 nm), a double beam, Czerny-Turner monochromator, 1.5 nm fixed spectral bandwidth, full spectrum Xenon pulse lamp single source, dual silicon diode detectors, quartz overcoated optics, non-measurement phase stepping wavelength drive, room light immunity. Analysis undertaken using Agilent CaryWin UV Scan software. All sample spectra were acquired in Hellma Analytics High Precision Quartz UV Cuvettes.

Experimental Methods

Solubilization of insoluble samples for analysis

Insoluble samples for splat and UV-Vis analyses (see below) were added to a PBS solution and centrifuged (10K, 10 minutes) and the supernatant removed – to give a saturated solution of unknown concentration in PBS.

UV-Vis concentration determination of insoluble samples for analysis

Calibration: Depending on sample solubility, the spectrometer was calibrated with either a Acetone or Methanol 'blank' (machine zeroed and a background scan conducted). A stock solution of the species of interest was prepared (in Acetone or Methanol) at a known concentration and serially diluted, and a spectrum acquired for each concentration in the 200 – 800 nm range (600 nm/min scan rate, 1.00 nm data interval, 0.1 s average time), to give a Beer-Lambert calibration plot.

Sample Concentration Analysis: 200 – 400 µL (typically) of the sample of interest was taken as a saturated solution in PBS, and condensed *in vacuo*. The dry residue was subsequently re-dissolved in the same volume of Acetone or Methanol, mixed, and drawn up to separate the liquor from the insoluble PBS salts. The UV-Vis spectrum was then acquired, as above, with dilution employed (and corrected for) where necessary. The λ_{max} of the primary peak was identified and the absorbance recorded and intersected against the line of best fit of the Beer-Lambert plot of the stock calibrants to give the saturated samples concentration in PBS solution.

Ice recrystallization inhibition (splat) assay

Ice recrystallization inhibition was measured using a modified splat assay.[1] A 10 µL sample of the species of interest, dissolved in PBS buffer (pH 7.4), was dropped 1.40 m onto a chilled

glass coverslip, resting on a thin aluminium block placed on dry ice. Upon hitting the coverslip, a wafer with diameter of approximately 10 mm and thickness 10 μm was formed instantaneously. The glass coverslip was transferred onto the Linkam cryostage and held at -8ºC under N_2 for 30 minutes. Photographs were obtained using an Olympus CX 41 microscope with a UIS-2 20x/0.45/∞/0-2/FN22 lens and crossed polarizers (Olympus Ltd, Southend-on-Sea, UK), equipped with a Canon DSLR 500D digital camera. Images were taken of the initial wafer (to ensure that a polycrystalline sample had been obtained) and again after 30 minutes. Image processing was conducted using Image J, which is freely available (National Institutes of Health, Bethesda, MD). In brief, the number of ice crystals in the field of view was measured, and the measurement repeated for three independent wafers. The average (mean) of these three measurements was then calculated to find the mean grain area (MGA). The average value and error was compared to that of a PBS buffer negative control.

Surface hydrophobicity mapping of polymers

Structures of interest were assembled in ChemDraw Professional 16.0 (PerkinElmer Informatics Inc., Waltham, MA). The structures were then energy minimised in Chem3D and the resulting structures rendered with the surfaces displayed and hydrogens removed from the structure. Carbon (and so aliphatic hydrogen) defined as hydrophobic (grey), whilst oxygen (and so alcoholic hydrogens) were defined as hydrophilic (red).

Synthetic Procedures

Synthesis of (3*R*,5*R*)-3,5-dihydroxy-7-((1*S*,2*S*,6*R*,8*S*,8a*R*)-8-hydroxy-2,6-dimethyl-1,2,6,7,8,8a-hexahydronaphthalen-1-yl)heptanoic acid (Hydrolysed Simvastatin, 3)

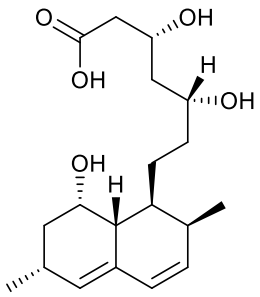

Simvastatin (100 mg) was dissolved in THF (10 mL) and a large excess of NaOH dissolved in H_2O was subsequently added (10 mL, 160 mg, 16.7 eqv). The reaction mixture stirred at RT for 36 hours, and then condensed *in vacuo*. The dry residue was dissolved in $CHCl_3$ (30 mL) and 1M HCl (30 mL), the organic phase separated, and extracted with water (3 x 30 mL). The organic phase was then dried over $MgSO_4$, filtered, and condensed *in vacuo*, to give a clear crystalline solid (70 mg, 86.6%). ^{1}H NMR (400 MHz, MeOD) δ = 6.00 (dd, *J* = 9.3, 5.8 Hz, 1H), 5.86 – 5.76 (m, 1H), 5.52 (s, 1H), 5.36 (s, 1H), 4.87 (s, 3H), 4.64 (d, *J* = 7.3 Hz, 1H), 4.27 (s, 1H), 4.23 – 4.11 (m, 1H), 3.70 (s, 1H), 3.62 (q, *J* = 7.1 Hz, 1H), 3.37 (s, 1H), 3.01 (s, 1H), 2.88 (s, 1H), 2.74 (dd, *J* = 17.7, 4.5 Hz, 1H), 2.60 – 2.27 (m, 5H), 2.08 – 1.91 (m, 3H), 1.89 – 1.69 (m, 2H), 1.65 – 1.49 (m, 4H), 1.41 (dd, *J* = 22.5, 10.5 Hz, 2H), 1.24 (ddd, *J* = 20.2, 14.3, 6.9 Hz, 3H), 1.15 – 1.03 (m, 8H), 0.96 – 0.80 (m, 7H). ^{13}C NMR (101 MHz, MeOD) δ 179.30, 175.35, 173.31, 134.16, 133.89, 133.15, 130.31, 129.52, 78.12, 71.76, 69.74, 68.29, 63.24, 44.7, 44.09, 43.03, 39.63 – 39.35, 39.63 – 38.56, 38.28, 38.04, 36.62, 35.96, 35.03 – 33.98, 33.76, 31.89, 30.69, 28.59, 25.80, 25.27, 23.67, 18.38, 14.14, 9.82. m/z (ESI,−ve) Observed 435.3 [100%, M-H$^+$]. Compound previously reported.[14]

Synthesis of (1*S*,3*R*,7*S*,8*S*,8a*R*)-3,7-dimethyl-8-((3*R*,5*S*)-3,5,7-trihydroxyheptyl)-1,2,3,7,8,8a-hexahydronaphthalen-1-yl 2,2-dimethylbutanoate (Ring Opened Simvastatin, 2)

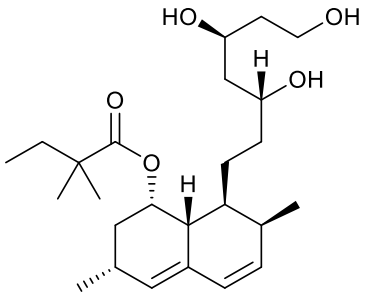

Simvastatin (100 mg) was dissolved in dry THF (5 mL) and samarium (II) iodide/THF solution (0.1M, 20 mL) was added under dry nitrogen, and the reaction mixture stirred at RT. After 36 hours, the reaction was exposed to air and saturated NH_4Cl solution was added slowly. The mixture was filtered, dissolved in ethyl acetate (50 mL) and extracted with saturated NH_4Cl solution (1 x 50 mL), followed by water (1 x 50 mL). The organic phase was subsequently condensed *in vacuo*, and the reduced syrup loaded onto silica gel and purified by column chromatography (EtOAc, 100%; R_f = 0.22, Fractions 17 – 23). The condensed fractions yielded a clear crystalline solid (30 mg, 29.7%). ^{1}H NMR (400 MHz, $CDCl_3$) δ 5.95 (d, *J* = 9.4 Hz, 1H), 5.76 (d, *J* = 5.8 Hz, 1H), 5.42 (d, *J* = 35.9 Hz, 2H), 4.08 (s, 1H), 3.96 – 3.61 (m, 4H), 2.47 – 2.18 (m, 4H), 2.04 – 1.84 (m, 2H), 1.75 – 1.45 (m, 10H), 1.42 – 1.30 (m, 1H), 1.21 (d, *J* = 12.9 Hz, 6H), 1.12 – 1.00 (m, 9H), 0.91 – 0.73 (m, 7H). ^{13}C NMR (101 MHz, $CDCl_3$) δ 178.49, 133.15, 131.65, 129.68, 128.39, 124.84, 72.79, 71.29, 68.29, 61.11, 43.06, 38.91, 37.86, 36.17, 35.15, 33.14, 31.00, 30.54, 30.07, 29.44, 27.36, 24.83, 24.23, 22.99, 22.71 – 22.32, 13.99, 9.39. m/z (ESI, +ve) Observed 445.4 [100%, $M+Na^+$].

Synthesis of (3*S*,5*R*)-7-((1*S*,2*S*,6*R*,8*S*,8a*R*)-8-hydroxy-2,6-dimethyl-1,2,6,7,8,8a-hexahydronaphthalen-1-yl)heptane-1,3,5-triol (Ring Opened and Hydrolysed Simvastatin, 4)

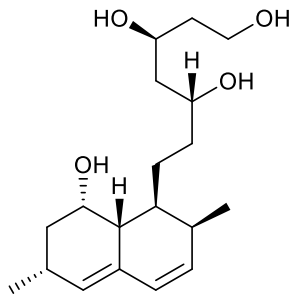

A sub-sample of **2** (20 mg) was dissolved in THF (10 mL) and a large excess of NaOH dissolved in H_2O was subsequently added (10 mL, 195 mg, 103 eqv). The reaction mixture stirred at RT for 36 hours, and then condensed *in vacuo*. The dry residue was dissolved in $CHCl_3$ (30 mL) and 1M HCl (30 mL), the organic phase separated, and extracted with water (3 x 30 mL). The organic phase was then dried over $MgSO_4$, filtered, and condensed *in vacuo*, to give a clear crystalline solid (15 mg, 96.8%).

Synthesis of ((3a*R*,5*R*,5a*S*,8a*S*,8b*R*)-2,2,7,7-tetramethyltetrahydro-5*H*-bis([1,3]dioxolo)[4,5-b:4',5'-d]pyran-5-yl)methanol (1,2:3,4-Di-O-isopropylidene-α-D-galactopyranose)

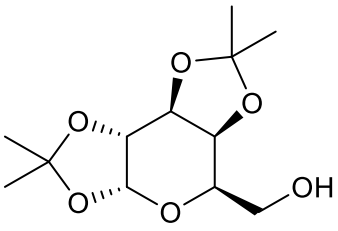

Galactose (1.00 g, 5.55 mmol) was dissolved in dry acetone (30 mL) and followed by 2,2-dimethoxypropane (1 mL, 1.5 eqv, 8.33 mmol) with stirring. A catalytic volume of H_2SO_4 (0.1 mL, 12M) was then added and the reaction mixture was stirred at RT overnight. The crude mixture was then neutralised with solid $NaHCO_3$ until pH 7 and the solution had decolourised.

The slurry was then condensed *in vacuo* and taken up into diethyl ether (30 mL) and filtered, with ether washing (5 x 20 mL). The ether was then removed by rotary evaporation yielding a clear, colourless oil. 1.1 g (76.1%). ^{1}H NMR (400 MHz, $CDCl_3$) δ 5.40 (s, 1H), 4.46 (d, *J* = 7.4 Hz, 1H), 4.31 – 4.03 (m, 2H), 3.89 (ddd, *J* = 16.1, 13.2, 5.8 Hz, 2H), 3.72 – 3.50 (m, 2H), 3.31 (dd, *J* = 31.4, 28.5 Hz, 2H), 3.12 (s, 1H), 2.82 (s, 1H), 1.48 – 1.00 (m, 12H). ^{13}C NMR (101 MHz, $CDCl_3$) δ 109.21, 108.45, 104.93, 103.70, 102.02, 96.04, 88.82 – 87.49, 86.95, 84.58, 81.56, 79.26, 78.22, 77.72, 76.74 – 75.01, 71.07, 70.40, 69.64, 69.29 – 68.72, 68.14, 68.14, 69.29 – 62.36, 61.57, 55.00, 54.53, 27.33 – 26.85, 26.65, 26.71 – 25.16, 24.78, 24.72, 24.12. m/z (ESI, +ve) Observed 283.2 [40%, $M+Na^+$]. Compound previously reported.[15]

Synthesis of methyl 4-((3*R*,5*S*,7*R*,8*R*,9*S*,10*S*,13*R*,14*S*,17*R*)-3,7-dihydroxy-10,13-dimethylhexadecahydro-1*H*-cyclopenta[*a*]phenanthren-17-yl)pentanoate (Chenodeoxycholic acid methyl ester)

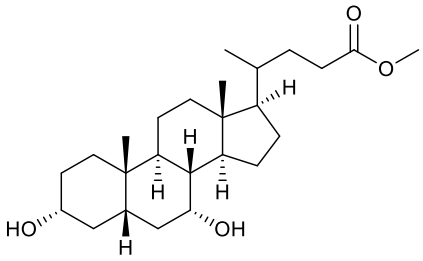

Chenodeoxycholic acid (1.00 g, 2.46 mmol) was dissolved in methanol (25 mL) and 6M HCl (10 mL) added, and the reaction mixture stirred at room temperature for 24 hours. After which, the reaction mixture was condensed *in vacuo*. The dry residue was then redissolved in ethyl acetate and extracted from water (3 x 20 mL), and brine (1 x 30 mL). The combined organic phases were then dried over $MgSO_4$, filtered, and condensed *in vacuo* to give an off-yellow oil. 940 mg (94.5%). ^{1}H NMR (400 MHz, $CDCl_3$) δ 3.73 (s, 1H), 3.56 (s, 3H), 3.24 (d, *J* = 66.7 Hz, 2H), 2.39 (s, 1H), 2.32 – 2.01 (m, 4H), 1.72 (dd, *J* = 57.0, 45.6 Hz, 8H), 1.48 – 0.94 (m, 14H), 0.81 (s, 6H), 0.56 (s, 2H). ^{13}C NMR (101 MHz, $CDCl_3$) δ 174.64 (Ester), 71.69 (**C3**-

OH), 68.14 (**C7**-OH), 55.79, 51.39, 50.34, 42.52, 41.54, 39.63, 39.33, 36.35 – 34.75, 34.70, 32.78, 30.78, 29.38, 28.11, 23.16, 20.56, 18.23, 11.68. m/z (ESI, +ve) Observed 429.4 [100%, $M+Na^+$]. Compound previously reported.[12]

Synthesis of methyl 4-((3*R*,5*S*,8*R*,9*S*,10*S*,13*R*,14*S*,17*R*)-3-hydroxy-10,13-dimethyl-7-oxohexadecahydro-1*H*-cyclopenta[*a*]phenanthren-17-yl)pentanoate (7-ketolithocholic acid methyl ester)

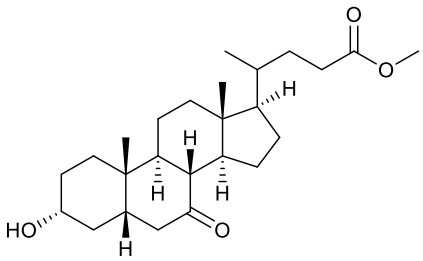

Chenodeoxycholic acid methyl ester (0.44 g, 1.08 mmol) was dissolved in acetone/saturated sodium hydrogen carbonate solution (20 mL, 1:1) and shielded from light. *N*-bromosuccinimide (0.241 g, 1.35 mmol, 1.25 eqv) was added, and the reaction mixture stirred at room temperature for 24 hours. After which, the reaction mixture was quenched with saturated sodium thiosulphate solution (10 mL), and then condensed *in vacuo*. The dry residue was then redissolved in diethyl ether (30 mL) and extracted from saturated sodium hydrogen carbonate solution (3 x 20 mL), and water (1 x 30 mL). The combined organic phases were then dried over $MgSO_4$, filtered, and condensed *in vacuo* to give an off-yellow oil which was loaded onto silica gel and purified by column chromatography ($Et_2O/CHCl_3$, 7:3; R_f = 0.42, Fractions 15 – 23, $KMnO_4$). The condensed fractions yielded a clear crystalline oil (210 mg, 48.1%). ^{1}H NMR (300 MHz, $CDCl_3$) δ 3.56 (s, 3H), 3.54 – 3.41 (m, 1H), 2.76 (dd, *J* = 12.6, 6.1 Hz, 2H), 2.36 – 2.01 (m, 4H), 1.96 – 1.52 (m, 9H), 1.47 – 0.94 (m, 14H), 0.86 (dd, *J* = 17.1, 5.8 Hz, 4H), 0.56 (s, 3H). ^{13}C NMR (75 MHz, $CDCl_3$) δ 212.35 (**C**=O), 174.59 (Ester), 70.52 (**C3**-OH), 54.69, 51.42, 51.03, 49.50, 49.09, 46.05, 45.33, 42.66, 38.04, 38.04, 35.37 – 30.04,

29.75, 28.29, 24.94, 23.56, 21.60, 18.28, 14.02 – 11.05. m/z (ESI, +ve) Observed 427.4 [100%, $M+Na^+$]. Compound previously reported.[12,16]

Stereoselective Reduction of methyl 4-((3*R*,5*S*,8*R*,9*S*,10*S*,13*R*,14*S*,17*R*)-3-hydroxy-10,13-dimethyl-7-oxohexadecahydro-1*H*-cyclopenta[*a*]phenanthren-17-yl)pentanoate (Chenodeoxycholic acid-7-one methyl ester)

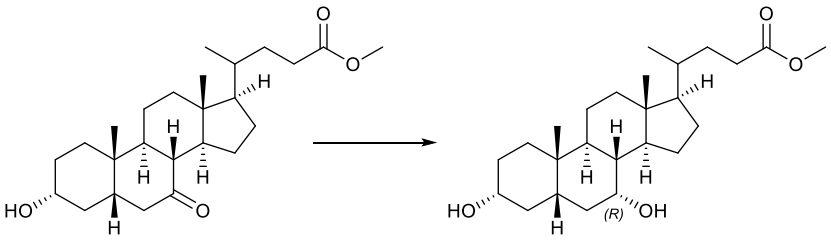

7-ketolithocholic acid methyl ester (0.03 g, 0.074 mmol) was dissolved in methanol (5 mL), and sodium borohydride (0.0056 g, 0.15 mmol, 2 eqv) added, and stirred for 4 hours. Saturated ammonium chloride solution (5 mL) was then added, followed by water (20 mL) and the mixture extracted with diethyl ether (2 x 30 mL). The combined organic phases were then condensed *in vacuo* to give a white solid. 30 mg (99.7%). ^{1}H NMR (400 MHz, $CDCl_3$) δ 4.50 (s, 4H), 3.73 (s, 1H), 3.58 (d, *J* = 8.2 Hz, 3H), 3.43 – 3.09 (m, 1H), 2.62 (s, 1H), 2.50 – 2.00 (m, 4H), 1.98 – 1.49 (m, 10H), 1.20 (dd, *J* = 100.1, 36.4 Hz, 14H), 0.72 (dd, *J* = 97.3, 7.8 Hz, 12H). ^{13}C NMR (101 MHz, $CDCl_3$) δ 174.59 (Ester), 70.96 (**C3**-OH), 67.21 (**C7**-OH), 55.28, 50.54, 49.67, 48.43, 48.18, 48.03 – 47.34, 47.22, 47.00, 41.87, 41.12, 39.09, 38.65, 38.07 – 37.74, 34.81, 34.57, 34.06, 32.12, 30.31, 29.93 – 28.95, 28.69, 27.47, 22.84, 21.93, 19.96, 17.31, 10.76. m/z (ESI, -ve) Observed 441.3 [100%, $M+Cl^-$]. Compound previously reported.[12,17]

Synthesis of methyl 4-((3*R*,5*S*,8*R*,9*S*,10*S*,13*R*,14*S*,17*R*)-3-hydroxy-10,13-dimethyl-7-oxohexadecahydro-1*H*-cyclopenta[*a*]phenanthren-17-yl)pentanoic acid (7-ketolithocholic acid)

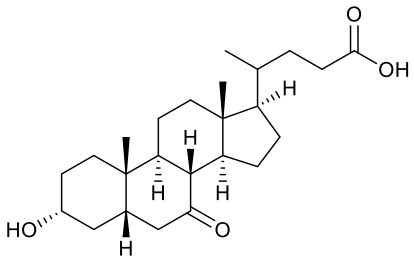

7-Ketolithocholic acid methyl ester (0.21 g, 0.52 mmol) was dissolved in MeOH/water (1:1, 20 mL) and a large excess of sodium hydroxide (0.2 g) added. The mixture was stirred at 60ºC overnight, and then acidified to pH 1 with 6M HCl (30 mL) and extracted with DCM (3 x 30 mL). The combined organic phases were then washed with water (1 x 20 mL), dried over $MgSO_4$, filtered, and condensed *in vacuo* to give a white foam (150 mg, 74.0%). ^{1}H NMR (400 MHz, $CDCl_3$) δ 3.58 (s, 1H), 3.45 (s, 1H), 2.83 (dd, *J* = 12.1, 5.3 Hz, 1H), 2.64 (s, 1H), 2.37 (t, *J* = 11.2 Hz, 3H), 2.28 – 2.18 (m, 2H), 2.03 – 1.73 (m, 8H), 1.68 (s, 3H), 1.53 – 1.05 (m, 18H), 0.94 (t, *J* = 20.6 Hz, 6H), 0.63 (s, 3H). ^{13}C NMR (101 MHz, $CDCl_3$) δ 212.58 (**C**=O), 179.26 (Acid), 70.90 (**C3**-OH), 54.87, 49.63, 48.99, 46.22, 45.47, 42.81, 39.04, 37.26, 35.28, 34.23, 31.81 – 30.27, 29.79, 28.37, 24.91, 23.15, 21.79, 18.45, 12.16, 1.11. m/z (ESI, +ve) Observed 413.4 [100%, $M+Na^+$]. Compound previously reported.[16]

General Procedure for the homo-polymerisation of 7-ketolithocholic acid

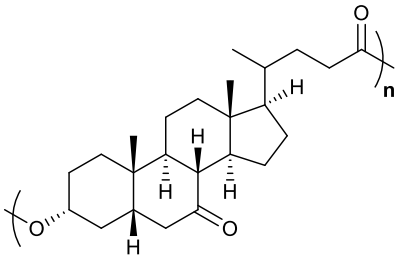

7-Ketolithocholic acid (0.440 g, 1.13 mmol) was dissolved in DCM/DMF (1:1, 20 mL) and EDCI hydrochloride added (0.432 g, 2.26 mmol, 2 eqv), followed by DMAP (5 mg, 0.05 eqv, 0.056 mmol) with stirring. The mixture was heated at 60ºC for 72 hours, and then condensed *in vacuo*. The dry residue was then dissolved in acetone (5 mL) and precipitated from water (45 mL) and centrifuged (20 minutes, 10K RPM), twice over, to give the product – poly(7-ketolithocholic acid) – as an off-beige solid. (240 mg, 54.5%). Polymer weight analysed by SEC.

General Procedure for the glycosylation of poly(7-ketolithocholic acid)

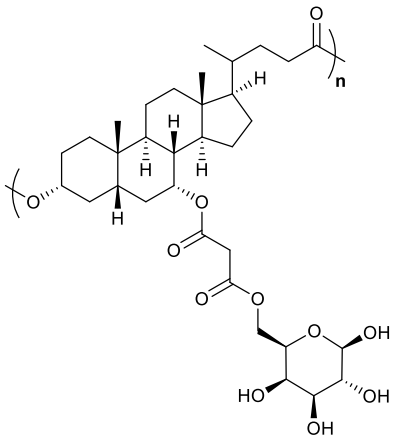

Poly(7-ketolithocholic acid) (240 mg, 0.070 mmol, 3446 g/mol^{-1} Mn) was dissolved in methanol (10 mL) and sodium borohydride (50 mg, 1.32 mmol, 2 eqv) added, and stirred for 2 hours. Saturated ammonium chloride solution (5 mL) was then added, followed by water (20 mL) and the mixture extracted with dichloromethane (2 x 30 mL). The combined organic phases were then condensed *in vacuo* and redissolved in DMF/DCM (1:1, 10 mL). Concurrently, malonic acid (32 mg, 0.31 mmol, 0.5 eqv) was also dissolved in DMF/DCM

(1:1, 10 mL), and EDCI hydrochloride (235.6 mg, 1.23 mmol, 2 eqv) added with stirring, followed by DMAP (1 mg, 8.19 µmol, 0.1 eqv). The DMF/DCM solution of the poly bile acid was then simultaneously introduced *via* syringe to the malonic acid-carbodiimide coupling flask, along with a DMF/DCM (1:1, 5 mL) solution of 1,2:3,4-Di-O-isopropylidene-α-D-galactopyranose (590 mg, 2.27 mmol, 3.7 eqv). The mixture was then stirred for 48 hours at 60ºC. The reaction mixture was then concentrated *in vacuo*, dissolved in acetone (5 mL) and precipitated from water (45 mL) and centrifuged (20 minutes, 10K RPM), twice over, and the precipitate dried under vacuum and redissolved in a solution of MeOH, acidified dropwise with TFA (10 mL, pH 3 – 4), in which it was stirred at RT for 15 minutes. After which, the crude mix was precipitated from water (40 mL) and centrifuged (20 minutes, 10K RPM), twice over, and then dried under vacuum to give the product – poly(chenodeoxycholic acid-7-malonic-6-galactopyranoside) – as a thick orange oil. (130 mg, 33.9%). ^{1}H NMR (400 MHz, $CDCl_3$) δ 4.83 – 4.42 (m, 5H, Gal-**C1**), 3.81 (s, 9H, Gal-**C3,4**), 3.62 (s, 7H, Gal-**C2**) 3.42 – 3.12 (m, 55H, Gal-**C5,6**, Malonic-C**H**$_2$), 2.37 – 2.15 (m, 27H, Bile Acid), 2.02 – 1.59 (m, 97H, Bile Acid), 1.51 – 1.34 (m, 69H, Bile Acid), 1.34 – 1.18 (m, 99H, Bile Acid), 1.18 – 0.79 (m, 136H, Bile Acid), 0.74 (s, 5H, Bile Acid), 0.62 (s, 31H, Bile Acid). ^{13}C NMR (101 MHz, $CDCl_3$) δ 174.86, 174.44 (Polyester **C**=O), 168.89 (Malonic **C**=O), 167.34 (Malonic **C**=O), 124.80, 96.29 (Gal-**C1**), 75.99 (Gal-**C5**), 72.04 – 70.50 (Gal-**C2,3,4**), 68.57 – 68.39 (Polyester **C**-O, **C7**-O), 64.29, 60.27 (Gal-**C6**), 55.88, 53.89, 51.55, 50.47, 42.73 (**C**H_2-Malonic), 41.76, 41.27, 39.68, 39.62, 39.46, 35.40, 35.13 - 34.97, 34.62, 34.40, 32.86, 32.81, 31.37, 31.04, 30.96, 30.55, 29.74, 29.28, 28.20, 26.57, 23.72, 22.84, 22.75, 20.64, 18.33, 14.30, 11.81.

Redundant Procedure for the Synthesis of (3a*R*,5*S*,5a*R*,8a*S*,8b*R*)-5-(iodomethyl)-2,2,7,7-tetramethyltetrahydro-5*H*-bis([1,3]dioxolo)[4,5-b:4',5'-d]pyran (1,2:3,4-Di-O-isopropylidene-6-iodo-α-D-galactopyranose)

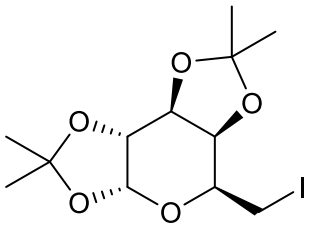

1,2:3,4-Di-O-isopropylidene-α-D-galactopyranose (1.10 g, 4.23 mmol) was dissolved in toluene (75 mL), and iodine (1.65g, 6.50 mmol, 1.54 eqv) added, followed by triphenylphosphine (1.66g, 6.35 mmol, 1.5 eqv) and imidazole (863 mg, 12.69 mmol, 3 eqv). The mixture was then stirred at 70ºC for 24 hours, cooled to RT, and filtered. The filtrate was then extracted with saturated sodium hydrogen carbonate solution (3 x 30 mL), brine (1 x 30 mL), and the organic phase dried over $MgSO_4$, filtered, and then condensed *in vacuo*. The crude mix was then dissolved in chloroform (2 mL) and diethyl ether added (6 mL) with swirling, resulting in near instantaneous precipitation of triphenylphosphine oxide. The slurry was cooled on ice and then filtered through a plug of silica (diethyl ether eluent) and washed with ether. This process was repeated three times (from precipitation onwards), before the combined filtrate was condensed to give a colourless/off-white oil, which crystallised upon cooling. 740 mg (47.3%). ^{1}H NMR (400 MHz, $CDCl_3$) δ 5.44 (d, *J* = 4.7 Hz, 1H), 4.52 (d, *J* = 7.8 Hz, 1H), 4.35 – 4.13 (m, 2H), 3.85 (t, *J* = 6.9 Hz, 1H), 3.37 (t, *J* = 2.9 Hz, 1H), 3.22 (dd, *J* = 9.7, 7.0 Hz, 1H), 3.10 (t, *J* = 8.5 Hz, 1H), 1.51 – 1.06 (m, 15H). ^{13}C NMR (101 MHz, $CDCl_3$) δ 109.35, 108.68, 103.77, 96.55, 71.41, 70.99, 70.53, 68.86, 68.19, 25.93, 24.88, 24.36, 2.31. m/z (ESI, +ve) Observed 393.2 [20%, $M+Na^+$]. Compound previously reported.[15]

Failed Procedure for the Synthesis of methyl 4-((3*R*,5*R*,7*R*,8*R*,9*S*,10*S*,13*R*,14*S*,17*R*)-7-hydroxy-10,13-dimethyl-3-(((3a*R*,5*S*,5a*S*,8a*S*,8b*R*)-2,2,7,7-tetramethyltetrahydro-5*H*-bis([1,3]dioxolo)[4,5-b:4',5'-d]pyran-5-yl)methoxy)hexadecahydro-1*H*-cyclopenta[*a*]phenanthren-17-yl)pentanoate (Chenodeoxycholic acid methyl ester-3-1,2:3,4-Di-O-isopropylidene-α-D-galactopyranose)

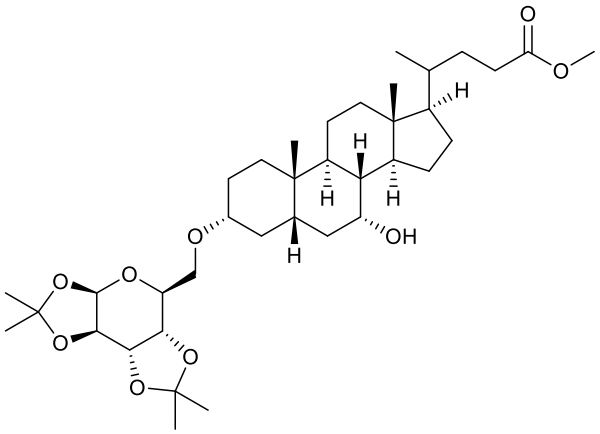

Chenodeoxycholic acid methyl ester (460 mgs, 1.13 mmol) was dissolved into dry THF (5 mL) under a flow of dry nitrogen and sodium hydride (60% dispersion in mineral oil, 83.6 mg, 2.49 mmol, 2.2 eqv) added as a solution in dry THF (5 mL) with stirring. After 15 minutes, 1,2:3,4-Di-O-isopropylidene-6-iodo-α-D-galactopyranose (970 mg, 2.3 eqv, 2.60 mmol) was added as a solution in dry THF (10 mL), dropwise, and the mixture was then stirred under nitrogen at 40ºC for 2.5 hrs, and then cooled to RT, with stirring continued overnight. After which, the flask was opened to air, and saturated ammonium chloride solution (10 mL) was added. The mixture was then extracted from ethyl acetate (3 x 10 mL), and the combined organic phases were then washed with water (1 x 10 mL), dried over $MgSO_4$, filtered, and condensed *in vacuo*. Attempted purification of the resultant oil by loading on to silica gel for column chromatography (100% Et_2O), failed to isolate the desired product.

5.6 – References

1 T. Congdon, R. Notman and M. I. Gibson, *Biomacromolecules*, 2013, **14**, 1578–1586.

2 B. Graham, T. L. Bailey, J. R. J. Healey, M. Marcellini, S. Deville and M. I. Gibson, *Angew. Chemie - Int. Ed.*, 2017, **56**, 15941–15944.

3 S. Liu and R. N. Ben, *Org. Lett.*, 2005, **7**, 2385–2388.

4 M. Leclère, B. K. Kwok, L. K. Wu, D. S. Allan and R. N. Ben, *Bioconjug. Chem.*, 2011, **22**, 1804–1810.

5 C. J. Capicciotti, R. S. Mancini, T. R. Turner, T. Koyama, M. G. Alteen, M. Doshi, T. Inada, J. P. Acker and R. N. Ben, *ACS Omega*, 2016, **1**, 656–662.

6 J. G. Briard, J. S. Poisson, T. R. Turner, C. J. Capicciotti, J. P. Acker and R. N. Ben, *Sci. Rep.*, 2016, **6**, 23619.

7 J. G. Briard, S. Jahan, P. Chandran, D. Allan, N. Pineault and R. N. Ben, *ACS Omega*, 2016, **1**, 1010–1018.

8 D. E. Mitchell, G. Clarkson, D. J. Fox, R. A. Vipond, P. Scott and M. I. Gibson, *J. Am. Chem. Soc.*, 2017, **139**, 9835–9838.

9 R. Drori, C. Li, C. Hu, P. Raiteri, A. L. Rohl, M. D. Ward and B. Kahr, *J. Am. Chem. Soc.*, 2016, **138**, 13396–13401.

10 A. K. Balcerzak, C. J. Capicciotti, J. G. Briard and R. N. Ben, *RSC Adv.*, 2014, **4**, 42682–42696.

11 Merck, *Merck Index, 14th ed., 8539*.

12 H. Xiao, P. Li, X. Li, H. He, J. Wang, F. Guo, J. Zhang, L. Wei, H. Zhang, Y. Shi, L.

Hou, L. Shen, Z. Chen, C. Du, S. Fu, P. Zhang, F. Hao, P. Wang, D. Xu, W. Liang, X. Tian, A. Zhang, X. Cheng, L. Yang, X. Wang, X. Zhang, J. Li and S. Chen, *ACS Med. Chem. Lett.*, 2017, **8**, 1246–1251.

13 K. Kuhajda, S. Kevresan, J. Kandrac, J. P. Fawcett and M. Mikov, *Eur. J. Drug Metab. Pharmacokinet.*, 2006, 31, 179–235.

14 R. Subramanian, X. Fang and T. Prueksaritanont, *Drug Metab. Dispos.*, 2002, **30**, 225–230.

15 G. Sennari, T. Hirose, M. Iwatsuki, S. Omura and T. Sunazuka, *Chem. Commun.*, 2014, **50**, 8715–8718.

16 European Patent Office, CN201710224278, 2017, CN106939030.

17 European Patent Office, CN201710328547, 2017, CN107383137.

CHAPTER 6

Conclusions

This thesis has used synthetic organic, peptide, and polymer chemistries to explore the fundamental design rules for IRI activity. In particular, we have probed the role of amphipathy and have further shown it to be essential in the design of IRI active species.

Poly(proline) was prepared by a variety of methods (including condensation and ring opening of *N*-carboxyanhydrides) and was shown to adopt a similar solution conformation to AFGP – a polyproline type II helix. It is ultimately this conformation, along which exists a fine balance of hydrophilic/phobic groups, which is responsible for poly(proline)'s inherent IRI activity (and the previously assumed activity of poly(L-hydroxy proline). This conformation features an optimal degree of facial amphilicity and domain segregation. It is clear that arbitrary or random introduction of hydroxyl groups will not meaningfully enhance IRI and may well deprecate it, as the additional hydroxyl groups in poly(L-hydroxy proline) distort the surface philicity, and upsets the carefully tuned amphipathic balance. The lack of ice shaping by poly(proline) may further indicate that direct ice face binding by some IRI active AFGP mimetics is not required, and that the energetic disruption of long-range water ordering is sufficient to impart IRI potency.

Similarly, our development of a series of amphipathic monomers and facially amphipathic rigid glycopolymers has added further validity to this hypothesis. Designed to maintain a distinct amphipathic balance and domain segregation, it was found that the hydrophobic poly(Fulvo) derivative, prepared through ROMP, had enhanced IRI activity (of the order of ~ 60 % MGA

at 0.5 μg.mL^{-1}), but required 1 % DMSO for solubilisation. Attempts to sequentially modified this structure by varying the bridgehead (from hydrophobic to hydrophilic), copolymerisation, and alteration of the hydrophilic 'pendant' group, indicated several key observations. Substitution of the dimethylfulvene bridgehead with an oxo-ether indicated the importance of amphipathy, with a loss of activity observed in the wholly hydrophilic derivative, poly(Oxo). Crucially, when assessed in conjunction with the lack of ice shaping and therefore ice face binding by the optimised candidate, poly(Fulvo-*co*-Diol), this implied that hydroxyl group presentation is insufficient to induce IRI activity, as poly(Oxo) was unable to impart IRI even at very high concentration. This would again indicate a mechanism for IRI activity dependent upon the amphipathic disruption of long-range water ordering, that the presence of an (ice orientated) hydrophobic domain is key (which has been heavily asserted previously), and that hydroxyl group presence alone is of no benefit to IRI potency. This study also affirmed the principle of rigidity, in that other 'amphipathic' species – such as flexible glycopolymers featuring sp3 hybridisation – have many degrees of freedom and so the amphipathic balance is distorted, explaining weak activity in candidates of this kind. To this end, the introduction of PEG chains (as a large, flexible hydrophilic domain) in place of the glycosyl motif caused complete loss of activity, due to the large, flexible chains obscuring the domain segregation.

Rigidity, amphipathy, and their careful engineering to give an effective, segregated solution conformation can therefore be mooted as key design motifs in effective IRI design.

However, attempts to advance this further were fundamentally challenged. The synthesis of a series of poly(disperse bile acid derivatives featuring; rigidity, amphipathy, and suspected helicity (giving the segregated domain thought necessary), similar to AFGP, did not impart IRI potency. This shows that the structure produced was not precise enough and suggests that replication of core AFGP structural motifs alone is insufficient to install IRI. On the contrary, this could even suggest an underlying mechanism of inhibition reliant upon some type of ice

binding / interaction (such as hydrophobic binding), for which the prepared candidates were unoptimized.

In Chapter 3, conjugates of antifreeze proteins with dimerizable anthracene units were also prepared, in order to study the possibility of achieving spatio-temporal control over IRI activity and function. This led to the isolation of PC-AFP$_{22}$, featuring a (TAANAAAAAAA)$_2$ repeat unit, representative of wild-type AFP I, conjugated to a dilysine-anthracene motif. This had comparable activity to the hyper potent PVA at DP$_{56}$. Unusually, when irradiated, activity was slightly lost by the conjugate, although it remained statistically similar. This is potentially due to the disruption of supramolecular ordering / pi-pi stacking interactions caused *via* the UV cycloaddition. However, this work represents the first example of its kind, and may represent potential strategies for controlling and tuning IRI activity with a non-invasive photo stimulus.

To summarise, a series of studies have been carried out, which have served to expand our understanding of the structure-activity relationship in IRI design. Acting as blue-print / proof-of-concept work, the observations herein have elucidated several key design rules and properties, and have shown the importance of both amphipathy and rigidity, whilst also demonstrating the potential to tune and exert remote control over activity – providing potential solutions in both biomedicine and cell cryostorage.

APPENDICES

Appendix A – Supplementary Information

APENDIX A: CHAPTER II

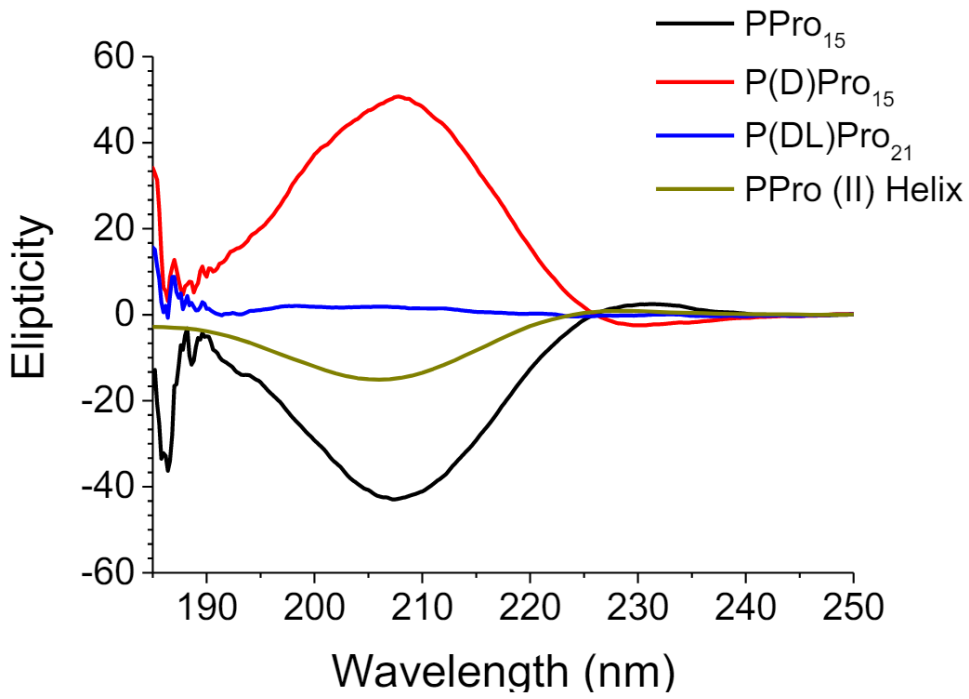

Figure A2.1 – Circular dichroism spectra of the synthesised proline polypeptides compared to a polyproline II helical reference (PPro (II) Helix)[1], not corrected for concentration to enable comparison against reference standard.

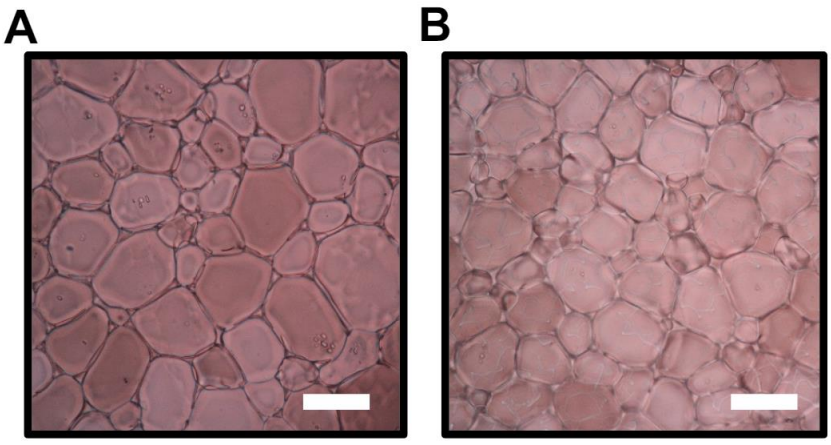

Figure A2.2 – SPLAT assays. A) PBS control; B) L-proline, 20 mg.mL-1. Scale bar = 100 µm

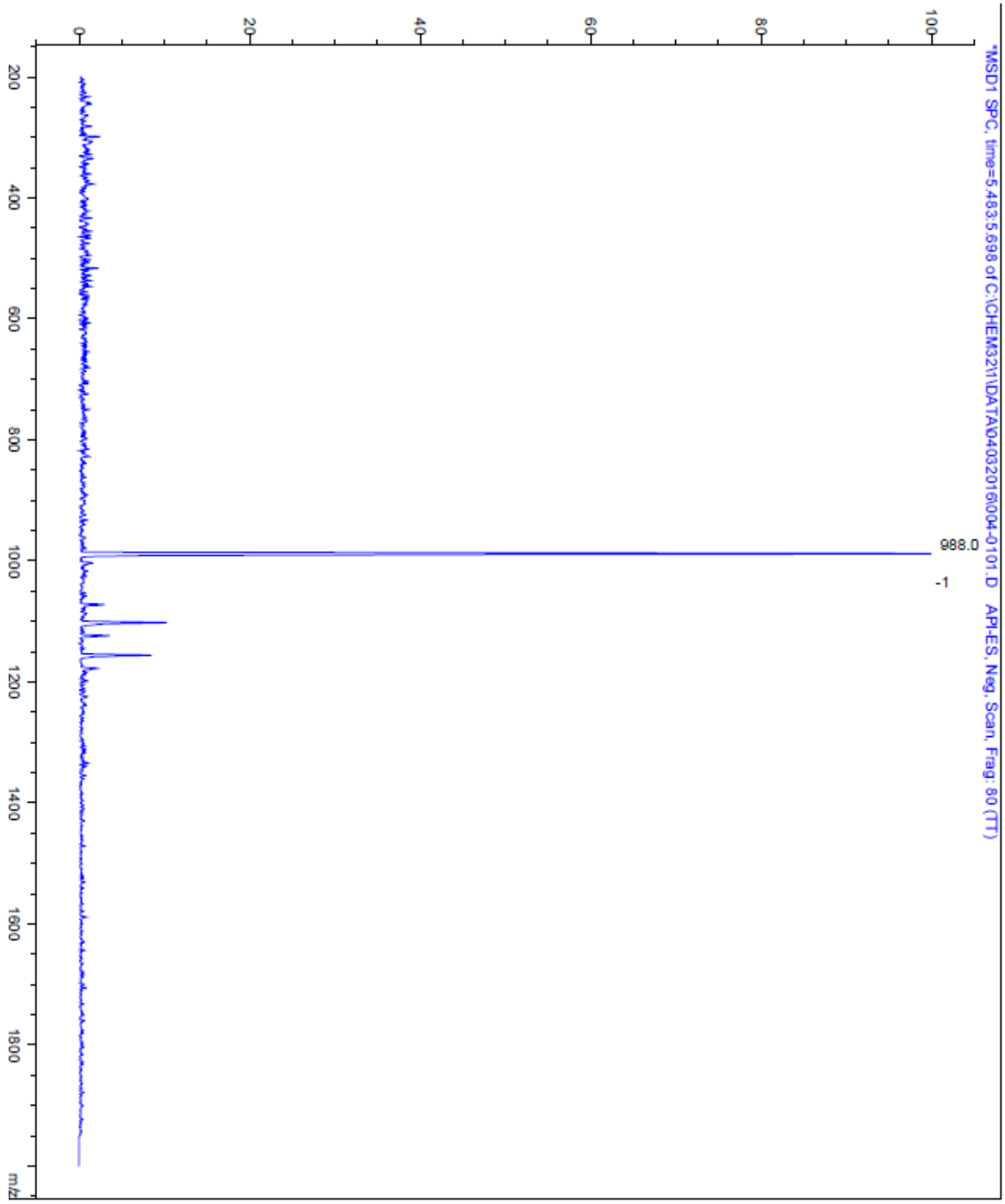

Figure A2.3 – ESI LC-MS of $PPro_{10}$ (Commercial)

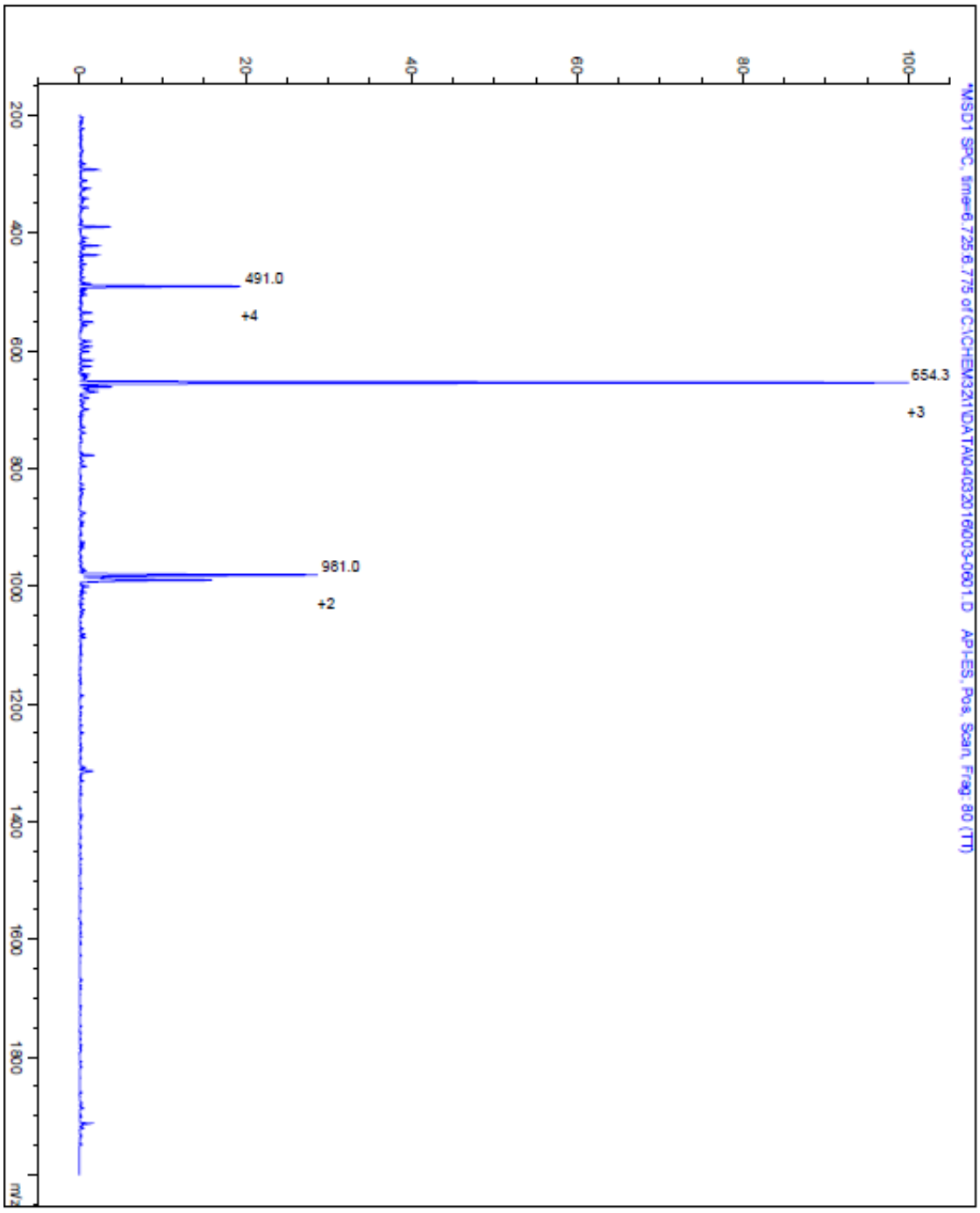

Figure A2.4 – ESI LC-MS of $PPro_{20}$ (Commercial)

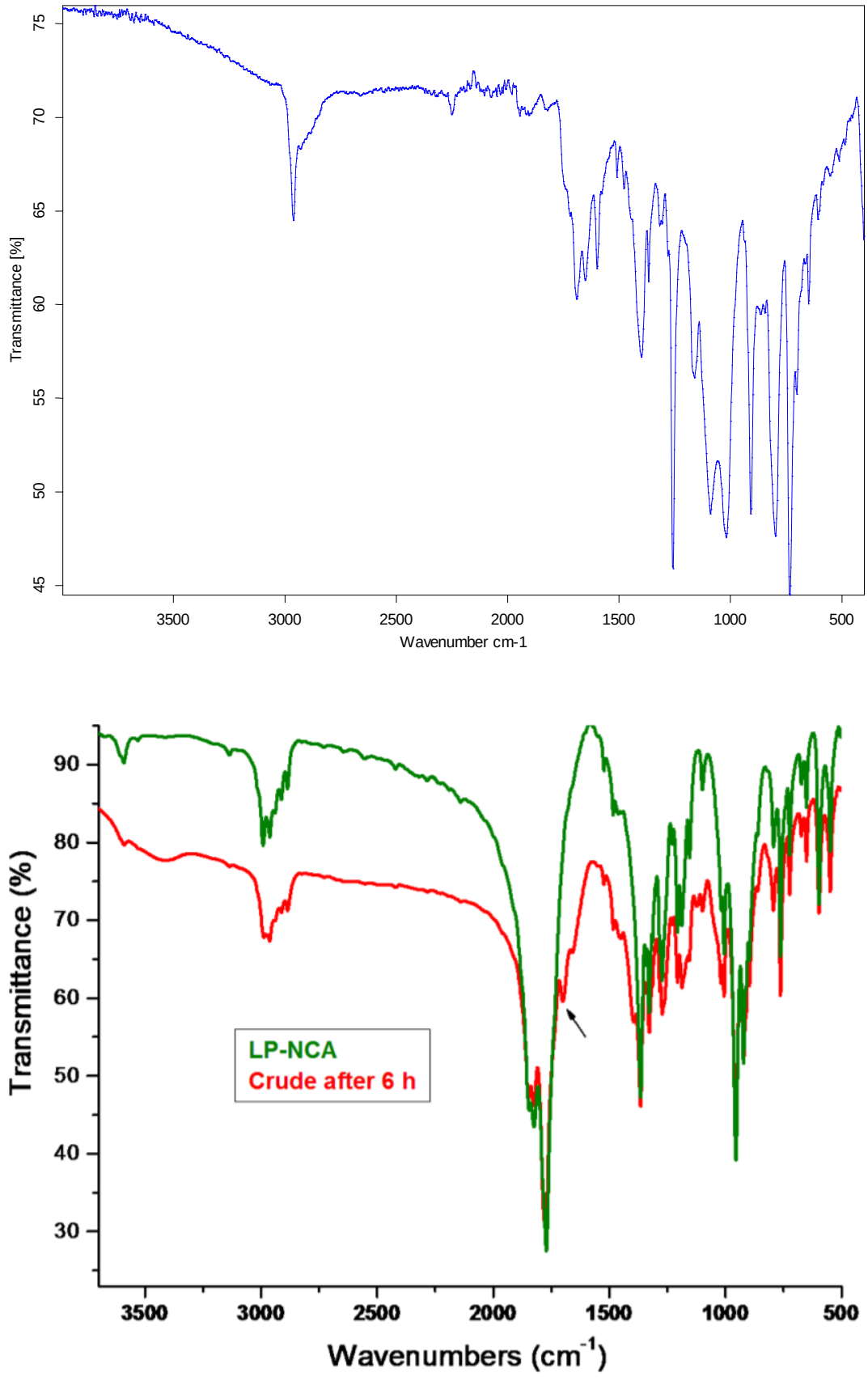

Figure A2.5 – IR Spectra of Pro-NCA (TOP), Compared to previously described preparation (BOTTOM)[2]

APENDIX A: CHAPTER III

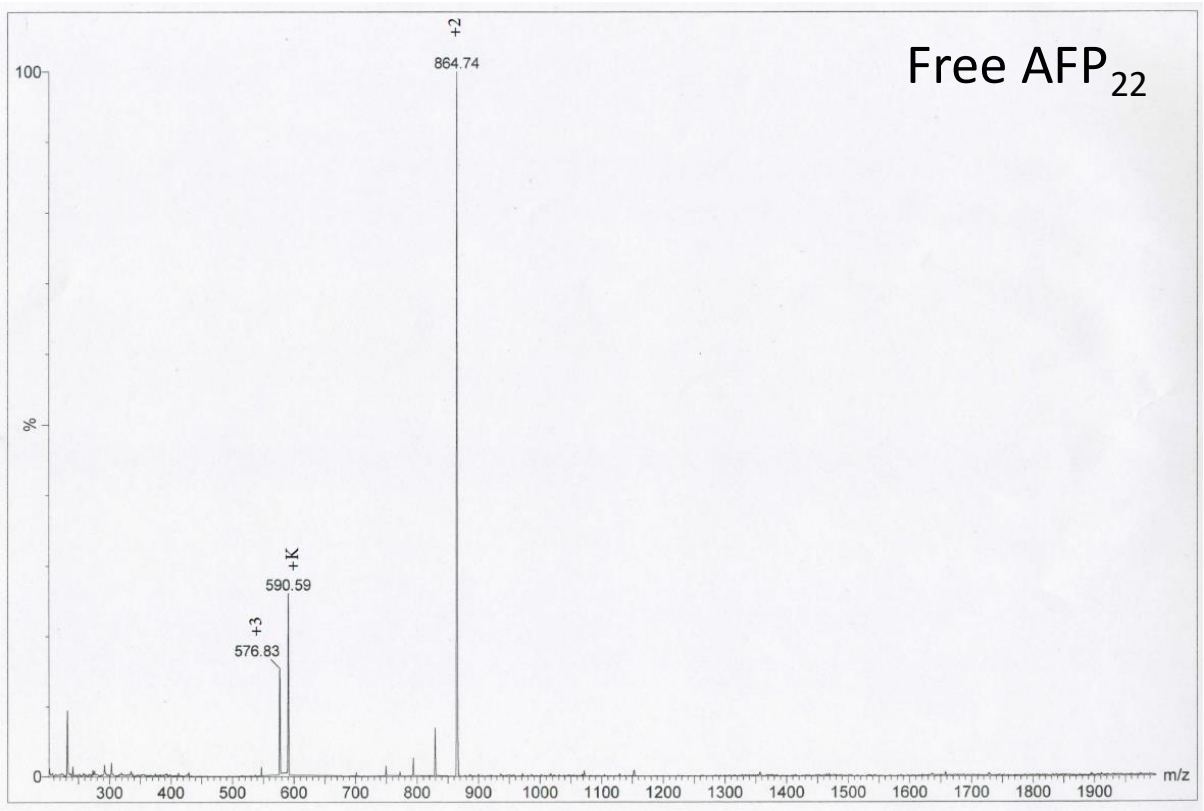

Figure A3.1 – Native AFP_{22} peptide ESI LC/MS from Peptide Protein Research Limited

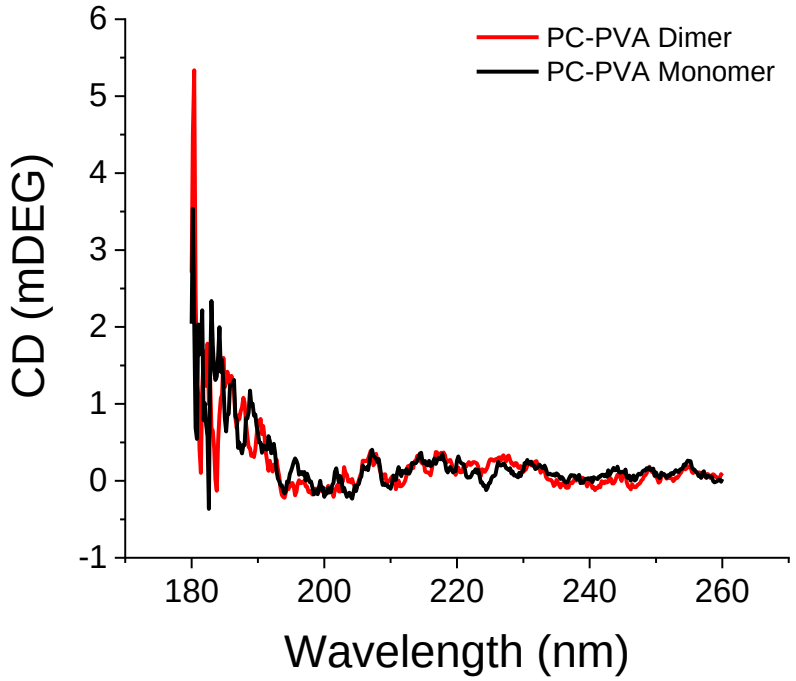

Figure A3.2 – CD Spectra of PC-PVA Dimer and Monomer

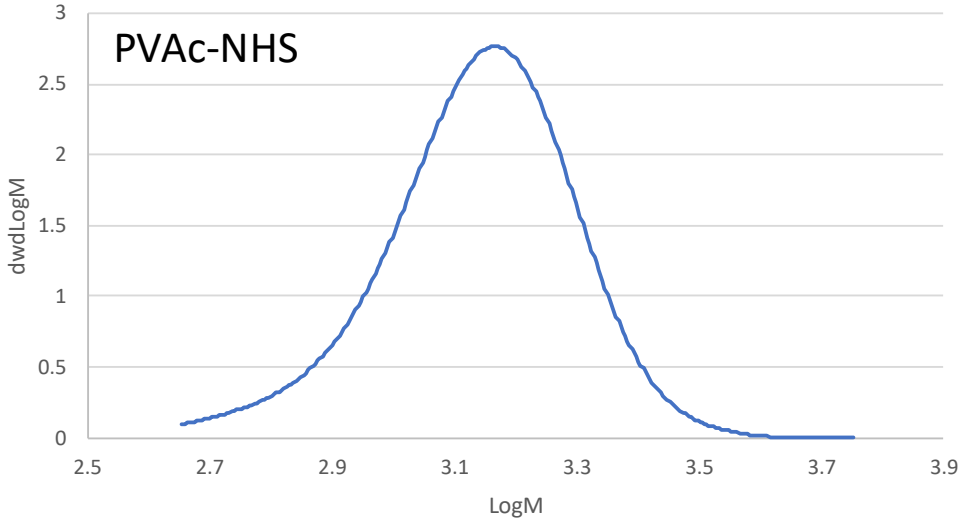

MW Averages							
Peaks	Mp (g/mol)	Mn (g/mol)	Mw (g/mol)	Mz (g/mol)	Mz+1 (g/mol)	Mv (g/mol)	PD
Peak 1	1465	1294	1467	1642	1822	1616	1.133694

Figure A3.3 – SEC/GPC trace of provided PVAc-NHS

APENDIX A: CHAPTER IV

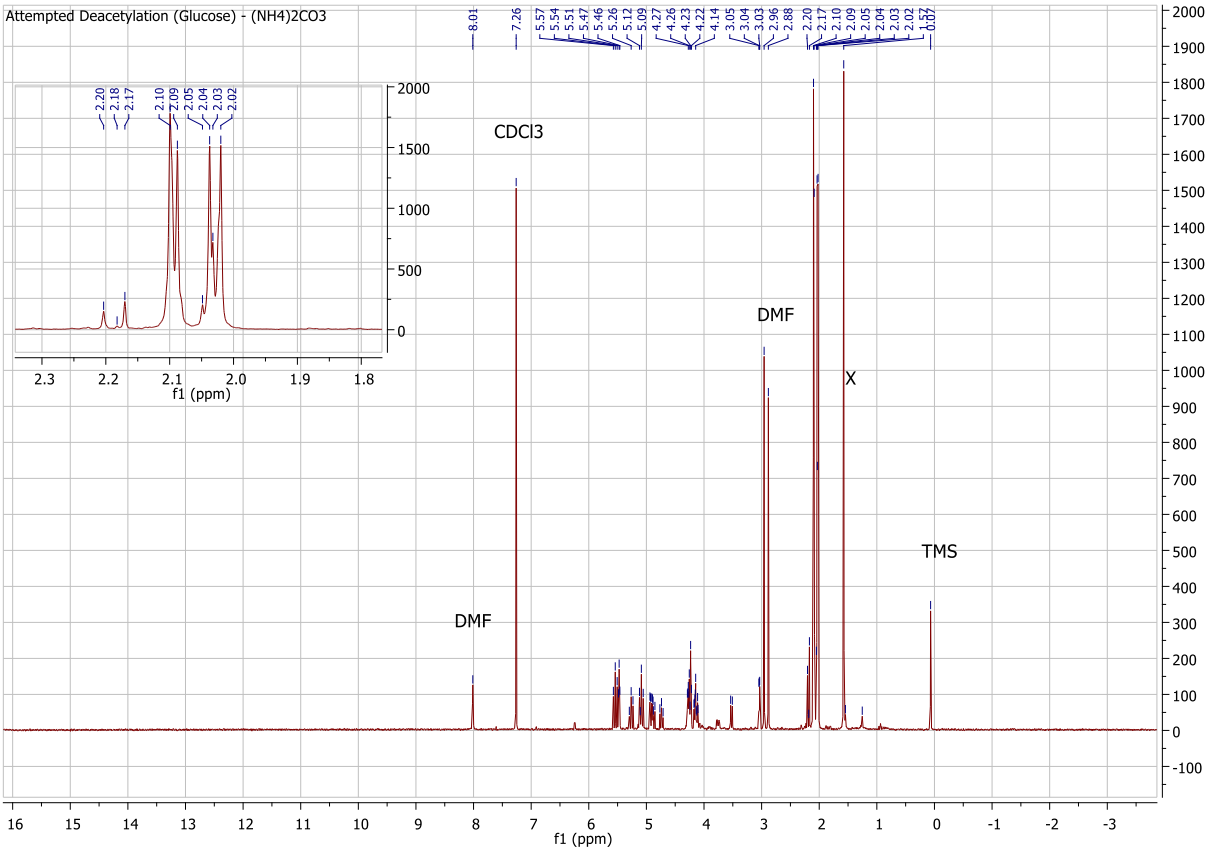

Figure A4.1 – Attempted anomeric deacetylation of glucose pentaacetate using ammonium carbonate in DMF

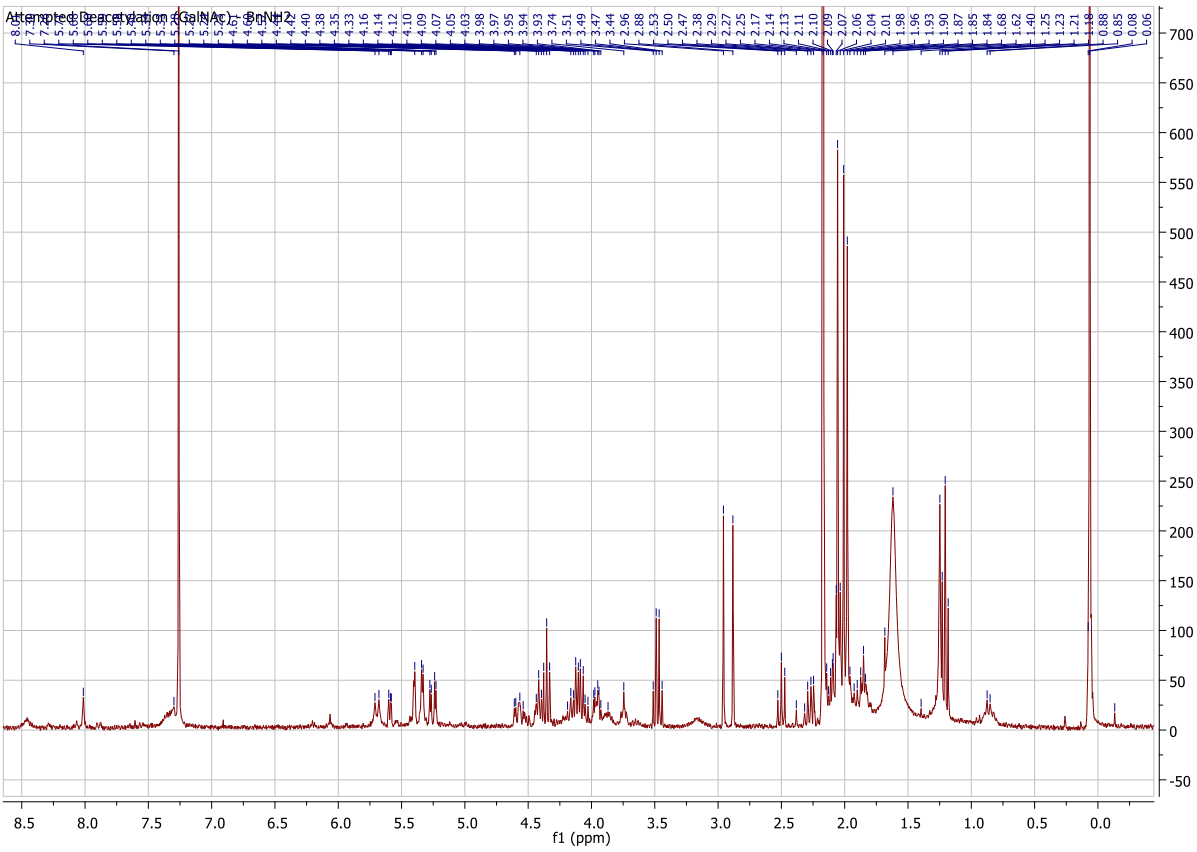

Figure A4.2 – Attempted anomeric deacetylation of *N*-acetyl galactose peracetate using benzylamine in DMF

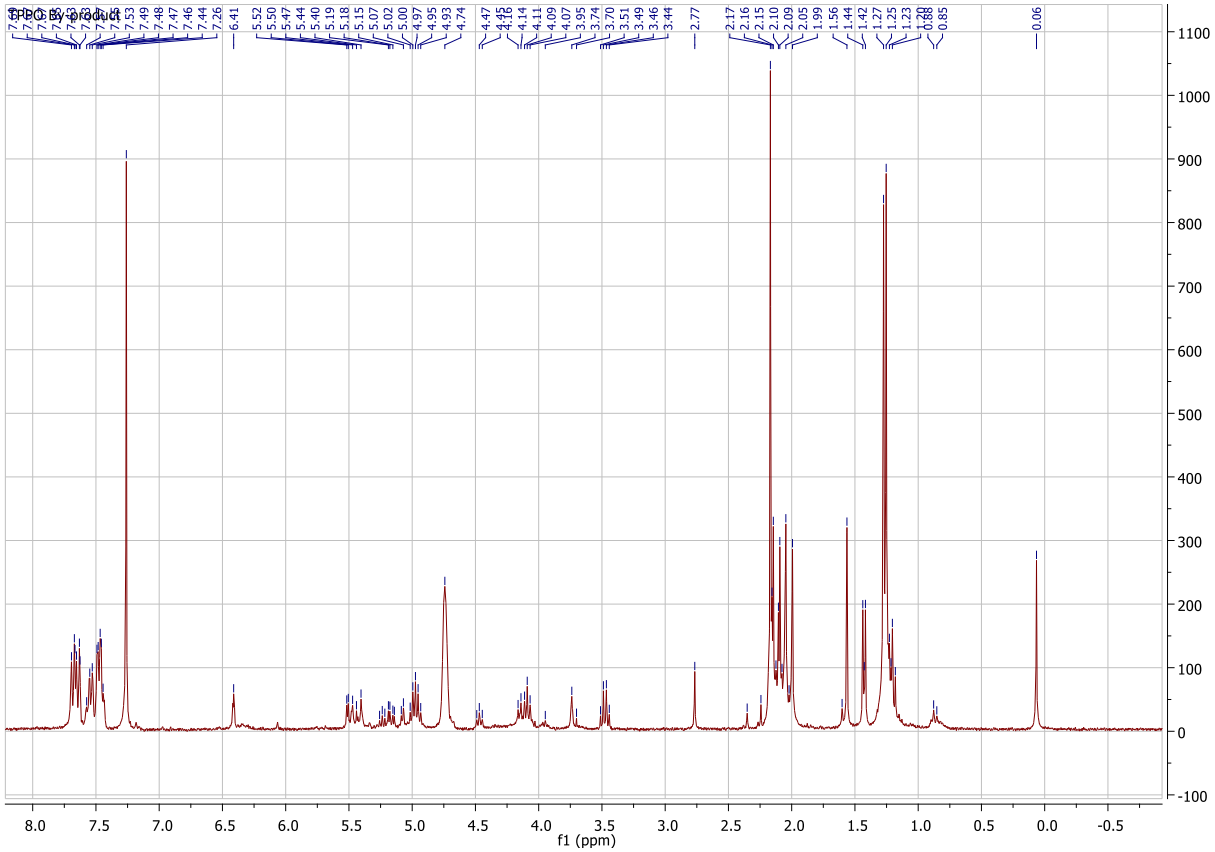

Figure A4.3 – Triphenylphosphine oxide by-product with M1

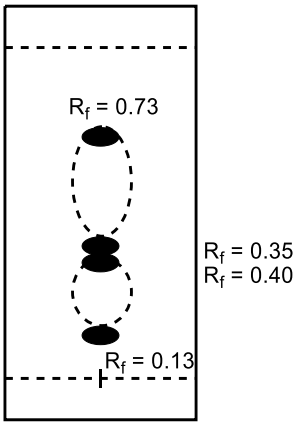

Figure A4.4 – TLC Plate of the Mitsunobu Reaction, Featuring > 4 Spots and Heavy Streaking (Difficult to Isolate) in 4:1 Hexane/Ethyl acetate

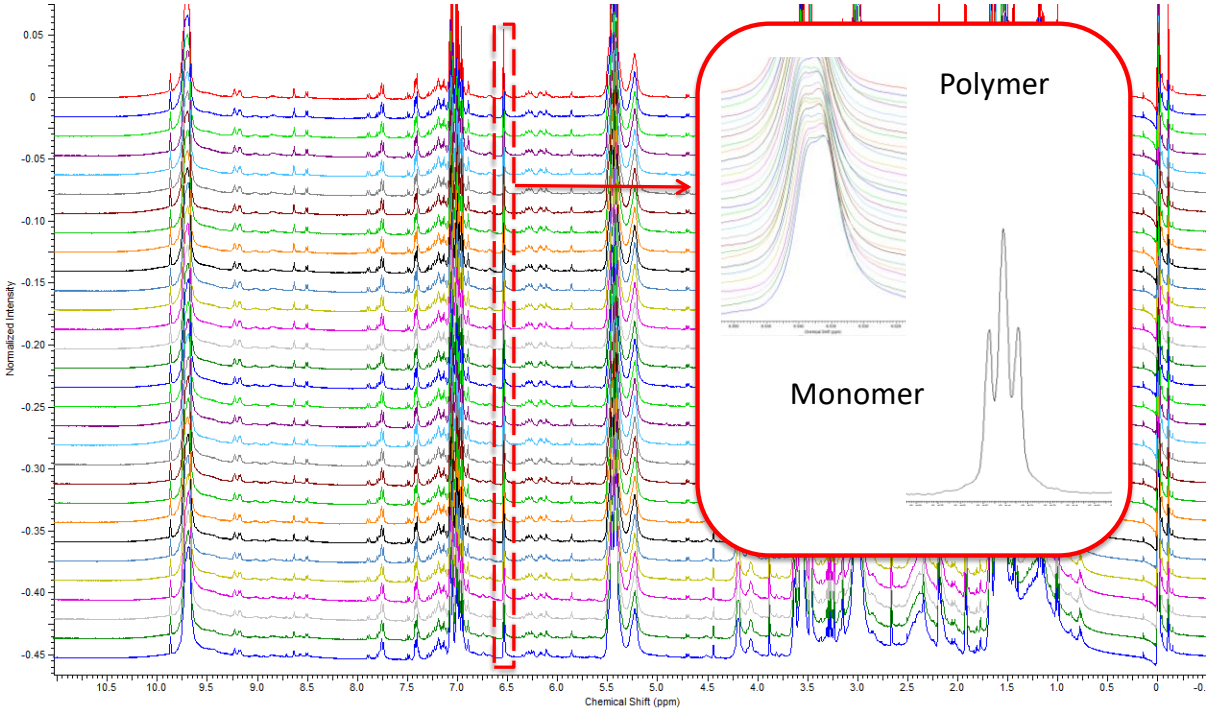

Figure A4.5 – ^{1}H NMR (THF-d_6) Kinetics Study (1 hr Waterfall Plot) of Catalyst and Monomer

Comprehensive small-angle neutron scattering (SANS) data analysis

Contribution from Dr. Rachel C. Evans and Dr. Judith E. Houston: SANS is a popular characterization technique employed to yield structural information at the nanometre length scale. The standard equation for absolute neutron scattering by macromolecules in solution combines form factor, $P(q)$ of the polymer with the interparticle scattering factor, $S(q)$, represented in the equation:

$$I(q) = \frac{1}{V}\frac{d\sigma}{d\Omega} = (\Delta\rho)^2(\Phi_{vol}V_{chain}P(q)\,S(q)) \qquad \textbf{Eq. 1}$$

where $(\Delta\rho)^2 = (\rho_{HA} - \rho_{H2O})^2$ is the contrast factor per unit volume between the polymer and the solvent. V_{chain} is the volume of the N monomers in a chain and Φ_{vol} is the volume fraction of monomer. In a dilute polymer solution, where intermolecular effects should be diminished, the scattering can be assumed to be arising from isolated chains without interactions and without excluded volume (*i.e.* $S(q) \approx 1$ and therefore, $I(q) \approx P(q)$).

A Porod plot ($I(q)$ *vs.* q) yields an exponent that suggests a sub-structural dimensionality from which the overall particle shape can be estimated. The SANS data of *poly*(Fulvo-*co*-Diol)-11 and *poly*(Fulvo-*co*-Diol)-17 (Figure 4.19) displayed Porod exponents in the low q region ($q <$ 0.02 Å^{-1}) of ~$q^{-3.5}$, suggesting the formation of mass fractals.[3] Fractals are self-similar structures that appear analogous at different length scales. Furthermore, *poly*(Fulvo-*co*-Diol)-11 and *poly*(Fulvo-*co*-Diol)-17 exhibit characteristic crossovers in the q dependence of the scattering intensity from that of aggregates (q^{-3}) to that typical for rigid rods (q^{-1}),[4] which is characteristic of polymer associations.[5]

For high molecular weight polymers, such as these, the only pertinent quantity, which can be determined, is the persistence length, b_t, which accounts for the effective rigidity of the uncharged chain. In this case, the b_t is best estimated from the point where the characteristic slopes intersect each other (marked with q^* in Figure 5), using the following equation:[5]

$$b_t = \approx \frac{1.91}{q^*} \qquad \textbf{Eq. 2}$$

Given the transition between the q^{-1} region and q^{-3} (q*) is approximate, this method should be taken with care. However, it still gives our best estimate for b_t. The estimated persistence lengths for *poly*(Fulvo-*co*-Diol)-11 and *poly*(Fulvo-*co*-Diol)-17 are 38.9 and 44.4 Å, respectively. It should be noted that the overlap may actually occur at a lower q region, but is masked by aggregate scattering. Thus, these values should be taken as the minimum persistence lengths for each polymer. Nevertheless, each b_t is much larger than the monomer length (~10 Å), which suggests that the chain backbones are locally stiff.[5] Furthermore, given the approximate contour length, L, of both polymer chains (490 Å and 760 Å for *poly*(Fulvo-*co*-Diol)-11 and *poly*(Fulvo-*co*-Diol)-17, respectively), the large b_t suggests rigid rather than highly flexible aggregates of potentially rod-like structures.

Trial Coupling Reactions and for the Synthesis of the Galactose Fulvonorborneneimides

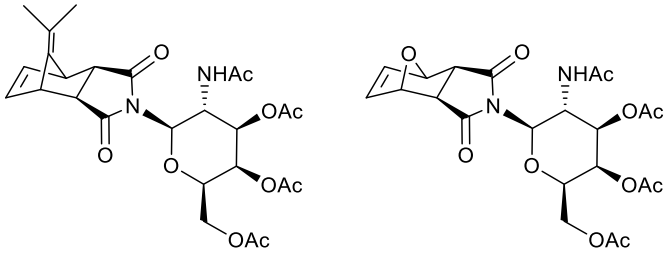

Attempted promoter free synthesis of the *exo,exo*-fulvonorborneneimide:

exo,exo-fulvonorborneneimide (0.599g, 2.947 mmol), acetobromo-α-D-galactose (1.86 eqv), and K_2CO_3 (2.1 eqv) were dissolved into dry, deoxygenated DMF (20 mL) under nitrogen, and stirred at 50ºC and 90ºC for 24 hours, respectively. The crude mixtures were co-evaporated with an excess of toluene (x 3), and the solid residues extracted with DCM/Brine (1:1, 100 mL), which produced emulsions in both instances. Addition of ^{n}Butanol failed to resolve phases, and mixtures were recondensed – characterisation of the solid residue indicated no product, and the fulvene starting material was wholly recovered in each case. m/z (ESI): 202.0 (100%, SM-H^+).

Iodine Catalysed *exo,exo*-fulvonorborneneimide:

Acetobromo-α-D-galactose (91.3 mg), 4Å molecular sieves, and iodine (71 mg) were dissolved into dry, deoxygenated DMF (10 mL) under nitrogen, and stirred at 60ºC for 1 hour. A separate flask was prepared concurrently of *exo,exo*-fulvonorborneneimide (50.4 mg) in dry, deoxygenated DMF (10 mL) with K_2CO_3 (17.1 mg) and was also stirred at RT for 1 hour. Upon elapse, the two mixtures were combined and stirred at 60ºC overnight whilst protected from light. The reaction crude was then neutralised with $Na_2S_2O_4$, condensed *in vacuo* with a large excess of toluene to azeotrope DMF, and redissolved in $CHCl_3$. The mixture was subsequently washed with saturated NaCl solution (2 x 30 mL) and the organic phase dried over Na_2SO_4 and

condensed *in vacuo* to give an orange gum 65.5 mg (55%). Characterisation as fulvene derivative, main text.

Silver Catalysed *exo,exo*-fulvonorborneneimide and *exo,exo*-oxonorborneneimide:

Acetobromo-α-D-galactose (0.1506 g / 0.1424 g), 4Å molecular sieves, *exo,exo*-fulvonorborneneimide (83.9 mg) or *exo,exo*-oxonorborneneimide (63 mg), and Ag_2CO_3 (57 mg / 53.4 mg) were dissolved in dry, deoxygenated DMF (10 mL) and stirred under nitrogen at RT overnight, with protection from light. The dark green reaction crude was then condensed *in vacuo* with a large excess of toluene to azeotrope the DMF, re-dissolved in ethanol and filtered to remove the black silver bromide by-product. The filtrate was subsequently recondensed, dissolved in $CHCl_3$ (30 mL) and extracted with saturated $NaHCO_3$ solution (2 x 30 mL), and the organic phase washed again with saturated NaCl solution (30 mL), dried over Na_2SO_4 and condensed *in vacuo* to give an off-white solid. Fulvene: 20.5 mg (10%), Oxo: 17.6 mg (10%). Characterisation as fulvene and oxo derivatives, main text.

Trial Syntheses of Glucose, Galactose, and N-Acetylgalactosamine Acetates

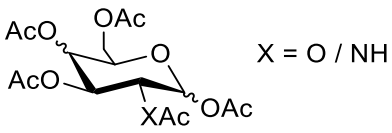

Glucose pentaacetate: Zinc chloride (0.960g, 7.04 mmol) was added quickly to acetic anhydride (20 mL) and the mixture heated to and stirred at 85ºC for five minutes, resulting in a dark brown solution. D-Glucose (4.000g, 22.2 mmol) was added slowly with stirring and the mixture was heated for 1 further hour. The resulting thick black oil which was poured into chilled water (200 mL) and stirred vigorously to give a dark green solution and an off-white precipitate. The solid was recovered at the pump, washed with ice cold water (40 mL), and recrystallised from hot ethanol (20 mL). White crystals were isolated, washed with cold ethanol (10 mL) and dried *in vacuo*. 4.06 g (46.8%). ^{1}H NMR (300 MHz, $CDCl_3$) δ = 6.32 (1H, d, $J_{1,2}$ = 3.7 Hz, Anomeric), 5.47 (1H, t, $J_{3,2}$ = $J_{3,4}$ = 9.9 Hz, H-3), 5.19 – 5.05 (2H, m, H-2,4), 4.26 (1H, dd, $J_{6,6'}$ = 12.5, $J_{6,5}$ = 4.1 Hz, H-6), 4.10 (2H, m, H-5,6'), 2.18 (3H, s, OAc), 2.09 (3H, s, OAc), 2.05 – 1.99 (9H, s, 3 x OAc). m/z (ESI) 413.0 (95%, $M+Na^+$).

Galactose pentaacetate: Zinc chloride (0.998g, 7.32 mmol) was added quickly to acetic anhydride (20 mL) and the mixture stirred and heated to 85ºC for five minutes, resulting in a dark brown solution. D-Galactose (1.005g, 5.55 mmol) was added slowly with stirring and the mixture heated for a further 2 hours, resulting in a dark brown solution, and was poured into chilled water (200 mL). No precipitation was observed with vigorous perturbation. Mixture was condensed *in vacuo* and chilled to 5°C overnight, no crystallisation was observed, and so the crude residue was extracted with dichloromethane (100 mL) and chilled water (100 mL). The aqueous phase was washed twice with dichloromethane (2 x 50 mL), and the combined organic phases washed once with chilled water (50 mL), dried over $MgSO_4$, filtered, and condensed *in vacuo*, yielding an orange/brown oil. m/z (ESI) 413.12 (100%, $M+Na^+$).

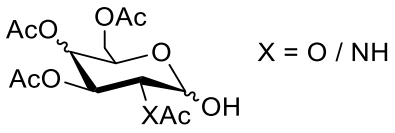

Glucose: Glucose pentaacetate (1.005g) was dissolved in DMF (20 mL) with ammonium carbonate (0.5060g) or benzylamine (2 mL) and stirred at 30ºC for 48 hours. Chloroform (30 mL) was added and the mixture poured into ice cold HCl (1M, 20 mL). The organic phase extracted and the aqueous washed with $CHCl_3$ (3 x 20 mL). The combined organic phases were washed with water (15 mL) and saturated $NaHCO_3$ solution (15 mL), dried over Na_2SO_4 and condensed *in vacuo* with an excess of n-Butanol, resulting in a yellow/brown gum. ^{1}H NMR (300 MHz, CDCl3) δ = 5.51 (2H, dt, *J* = 7.2, 6.7 Hz), 5.26 (1H, t, *J* = 9.5 Hz), 5.00 – 4.65 (2H, m), 4.37 – 4.06 (3H, m, H-5,6$^{',''}$), 2.13 – 1.99 (12H, m, 4 x OAc). m/z (ESI) 371.0 (100%, M+Na^+).

APENDIX A: CHAPTER V

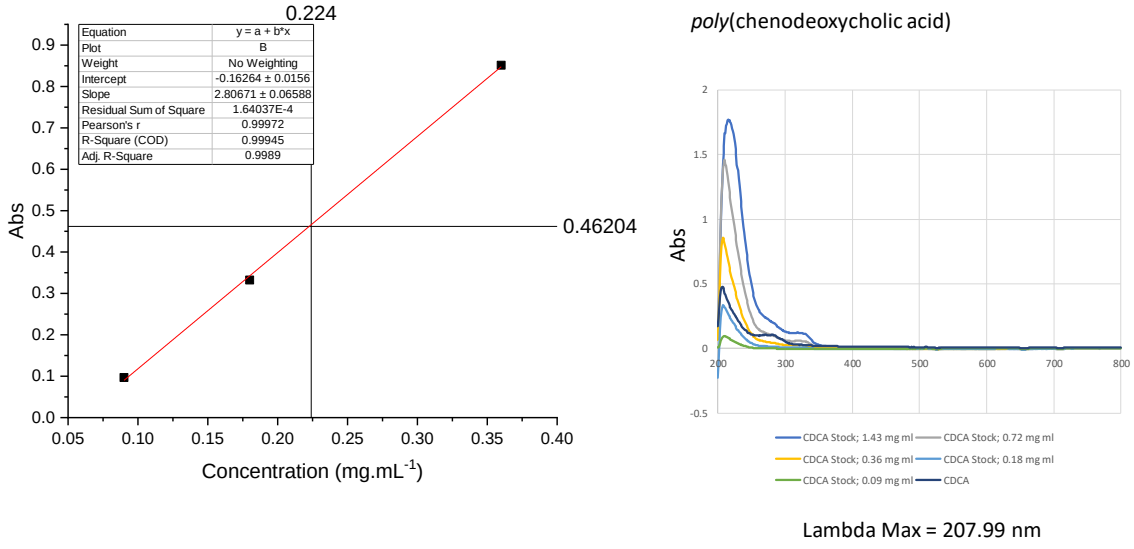

Figure A5.1 – UV/Vis Traces and Beer-Lambert solubility determination of poly(chenodeoxycholic acid)

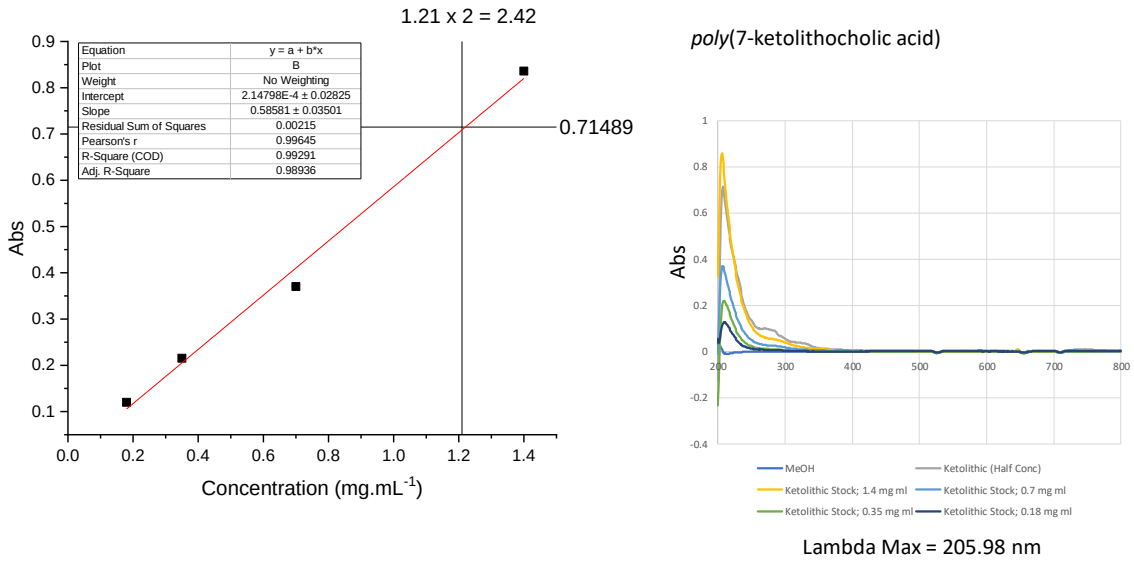

Figure A5.2 – UV/Vis Traces and Beer-Lambert solubility determination of poly(7-ketolithocholic acid)

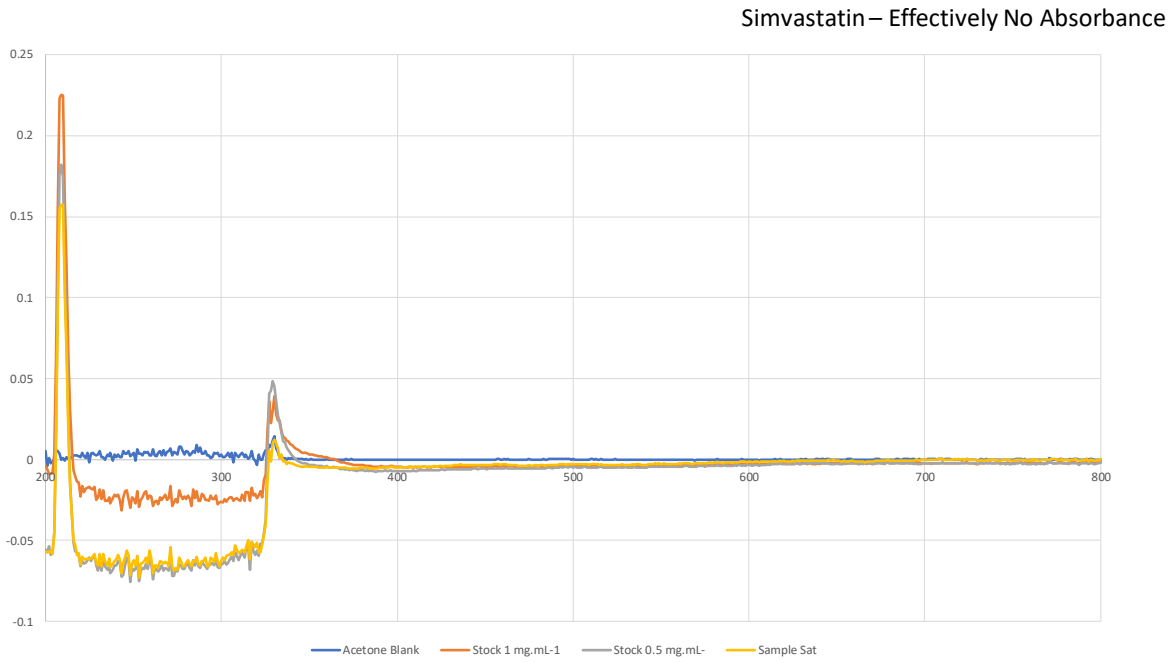

Figure A5.3 – UV/Vis Trace of Simvastatin

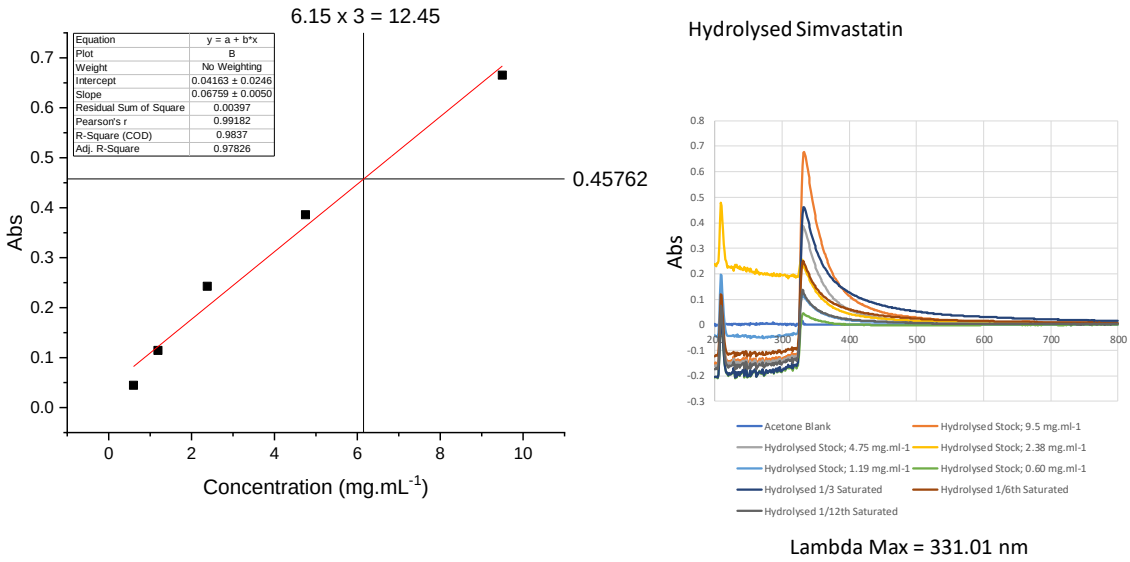

Figure A5.4 – UV/Vis Trace and Beer-Lambert solubility determination of Hydrolysed Simvastatin

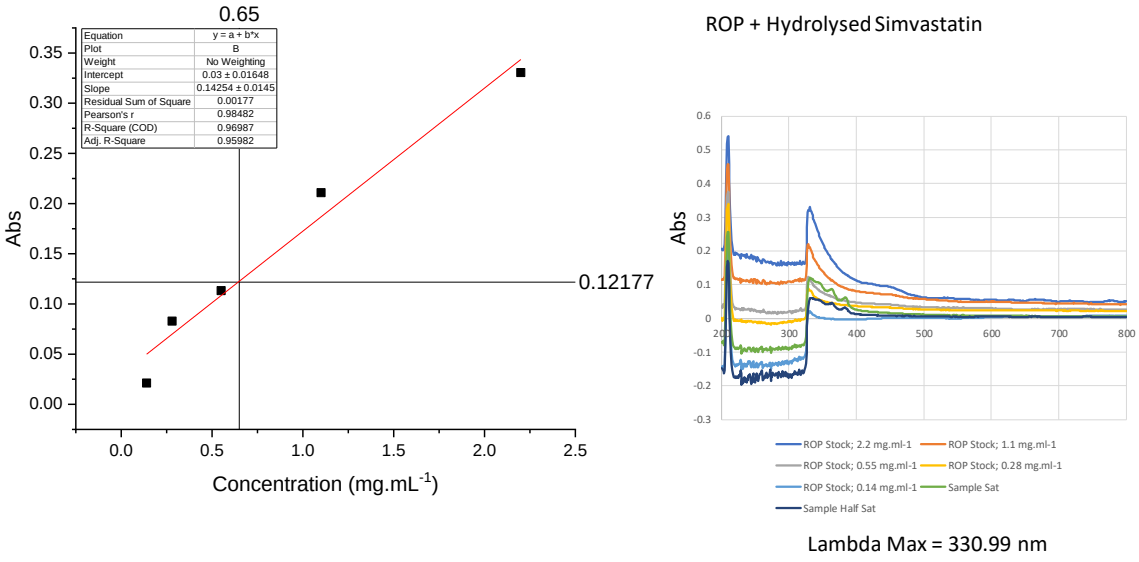

Figure A5.5 – UV/Vis Trace and Beer-Lambert solubility determination of Ring Opened and Hydrolysed Simvastatin

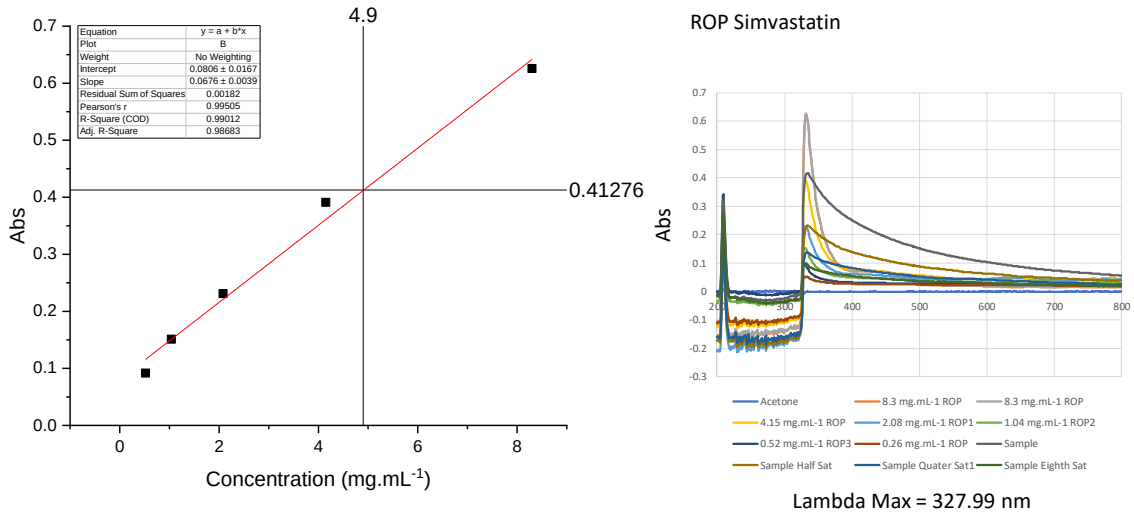

Figure A5.6 – UV/Vis Trace and Beer-Lambert solubility determination of Ring Opened Simvastatin

REFERENCES

1 Protein Circular Dichroism Data Bank, 2016, CD0004553000.

2 M. Gkikas, R. K. Avery and B. D. Olsen, *Biomacromolecules*, 2016, **17**, 399–406.

3 G. Beaucage, *J. Appl. Crystallogr.*, 1996, **29**, 134–146.

4 A. Guinier and G. Fournet, *Small-angle scattering of X-rays*, John Wiley & sons, New York, 1955.

5 E. Buhler and F. Boué, *Macromolecules*, 2004, **37**, 1600–1610.

APPENDICES

Appendix B – Additional Experimental Data

Optimised procedure for the synthesis of *p*-azido-L-phenylalanine (Fmoc Protected)

Step 1:

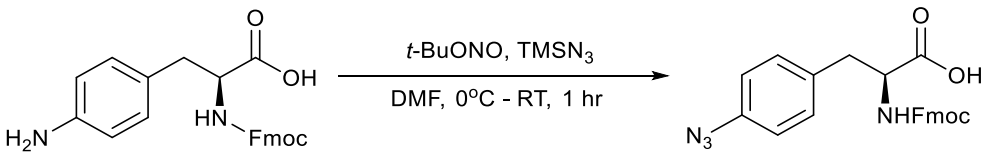

N-Fmoc-4-amino-L-phenylalanine (9.4 g, 23.36 mmol) was suspended in DMF (300 mL), with stirring and cooling to 0°C. *t*-BuONO (4 mL, 33.63 mmol, 1.43 eqv) was subsequently added, followed by TMS azide (3.3 mL, 25.01 mmol, 1.07 eqv). The ice bath was removed, and the mixture allowed to warm to RT, and stirring continued for 60 minutes. The reaction mixture was concentrated under vacuum (65°C, 50 mbar) until dry, to yield the Fmoc-protected-product as an orange-brown solid. 10 g (100%). ^{1}H NMR (400 MHz, DMSO-d_6) δ 7.88 (d, J = 7.5 Hz, 2H), 7.73 – 7.46 (m, 3H), 7.45 – 7.24 (m, 4H), 7.05 – 6.85 (m, 2H), 6.47 (d, J = 8.1 Hz, 2H), 4.29 – 4.11 (m, 3H), 4.12 – 4.00 (m, 1H), 2.87 – 2.81 (m, 1H), 2.68 (dd, J = 13.9, 10.1 Hz, 1H). ^{13}C NMR (101 MHz, DMSO-d_6) δ 174.06 (**C**=O), 156.37 (NH**C**=O), 147.49 – 141.12 (Aromatics), 129.97 –114.24 (Aromatics), 66.07 (**C**H2, Ala), 56.53 (**C**H, Ala), 47.05. m/z (ESI, –ve) Expected 427.1, Observed 427.2 [100%, M–H^{+}]. Analytical RP-HPLC: 98%, 7.08 min, t_R = 60 min (Water/Acetonitrile 0 : 100 for 5 minutes, to 70 : 30 by 15 min, to 100 : 0 by 55 min, λ = 315 nm).

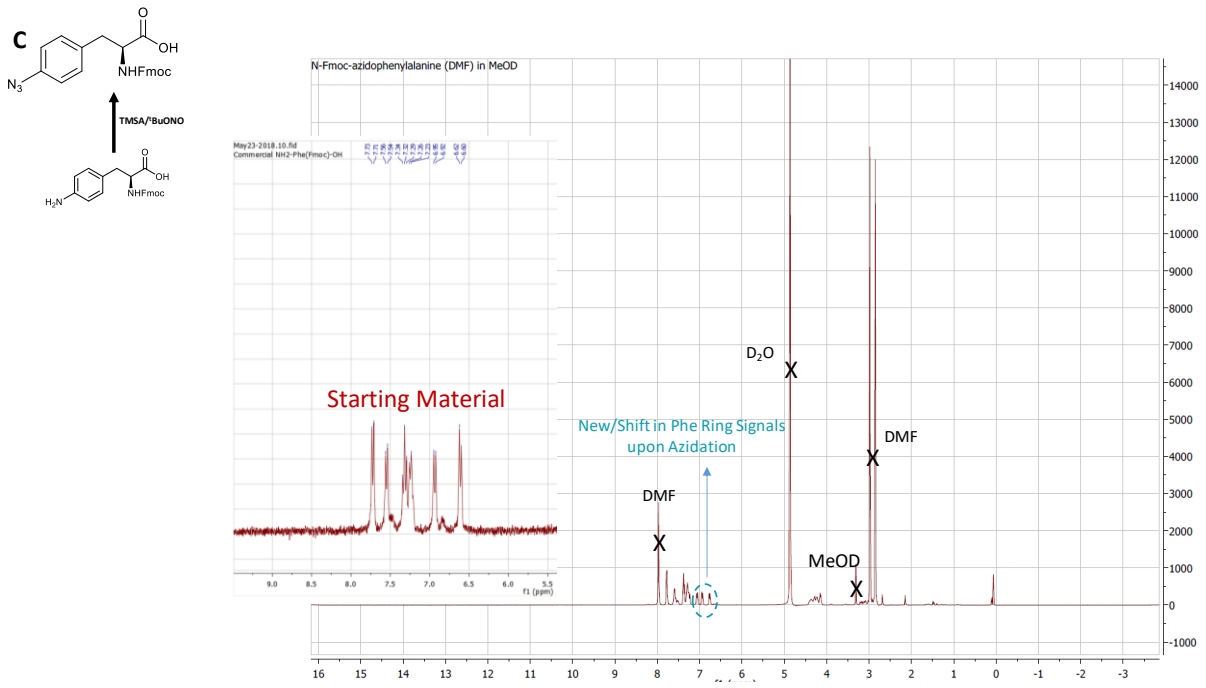

Figure B1 – NMR of *N*-Fmoc-4-azidophenylalanine hydrochloride from protected azidation

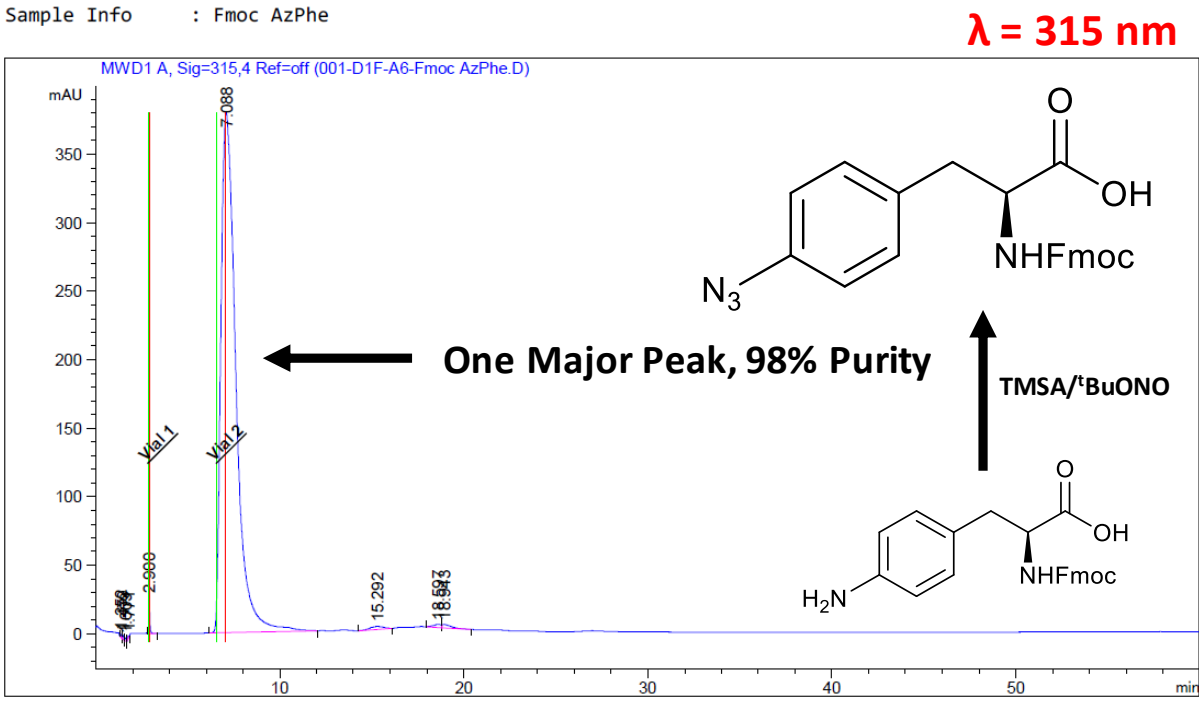

Figure B2 – HPLC of *N*-Fmoc-4-azidophenylalanine hydrochloride from protected azidation

Step 2:

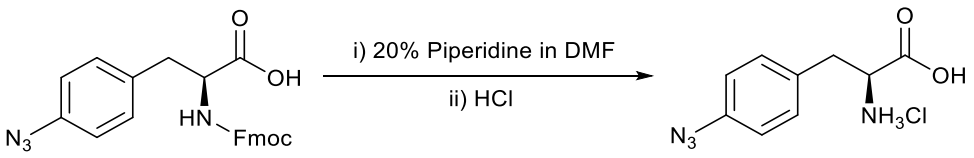

To the ring azidated *N*-Fmoc-4-azido-L-phenylalanine (80 mg, 0.187 mmol), 20% 4-methyl piperidine/DMF was added (10 mL) with stirring and protection from light. After one hour, the reaction mixture was condensed *in vacuo* (80°C, 50 mbar) until dry, dissolved in H_3O^+ (pH 2, 10 mL) and the acidified mixture extracted with hexane (4 x 30 mL), and the aqueous phase condensed again *in vacuo*, to give the product as a pale-yellow solid, the hydrochloride salt. 70 mg (Quant %). Analytical RP-HPLC (Slow): t_R = 30 min (Water/Acetonitrile 100 : 0 to 70 : 30 by 2 min to 0 : 100 by 25 min, λ = 324 nm). Analytical RP-HPLC (Fast): 98%, 7.08 min, t_R = 60 min (Water/Acetonitrile 0 : 100 for 5 minutes, to 70 : 30 by 15 min, to 100 : 0 by 55 min, λ = 324 nm). ^{1}H NMR (300 MHz, D_2O) δ 7.33 (d, J = 8.2 Hz, 2H), 7.12 (d, J = 8.1 Hz, 2H), 3.97 (t, J = 6.4 Hz, 1H), 3.32 – 3.03 (m, 2H). ^{13}C NMR (101 MHz, D_2O) δ 171.54 (C=O), 164.87, 139.42 (Aromatic), 135.53 (Aromatic), 131.06 (Aromatic), 123.63 –119.51, 54.23 (CH_2, Ala), 36.90 (CH, Ala), 35.18, 31.81 – 30.31, 23.79. m/z (ESI, +ve) Expected 279.1, Observed 278.3 [100%, M+MeOH+$^{41}K^+$].

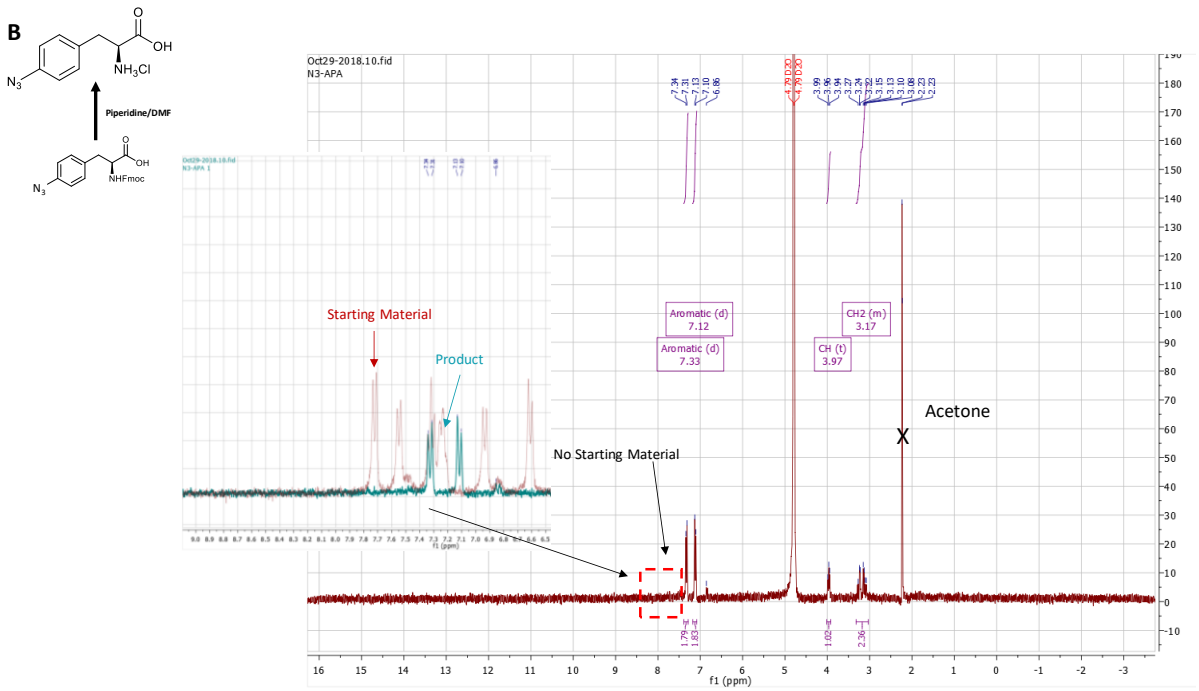

Figure B3 – NMR of *para*-azidophenylalanine hydrochloride from protected azidation

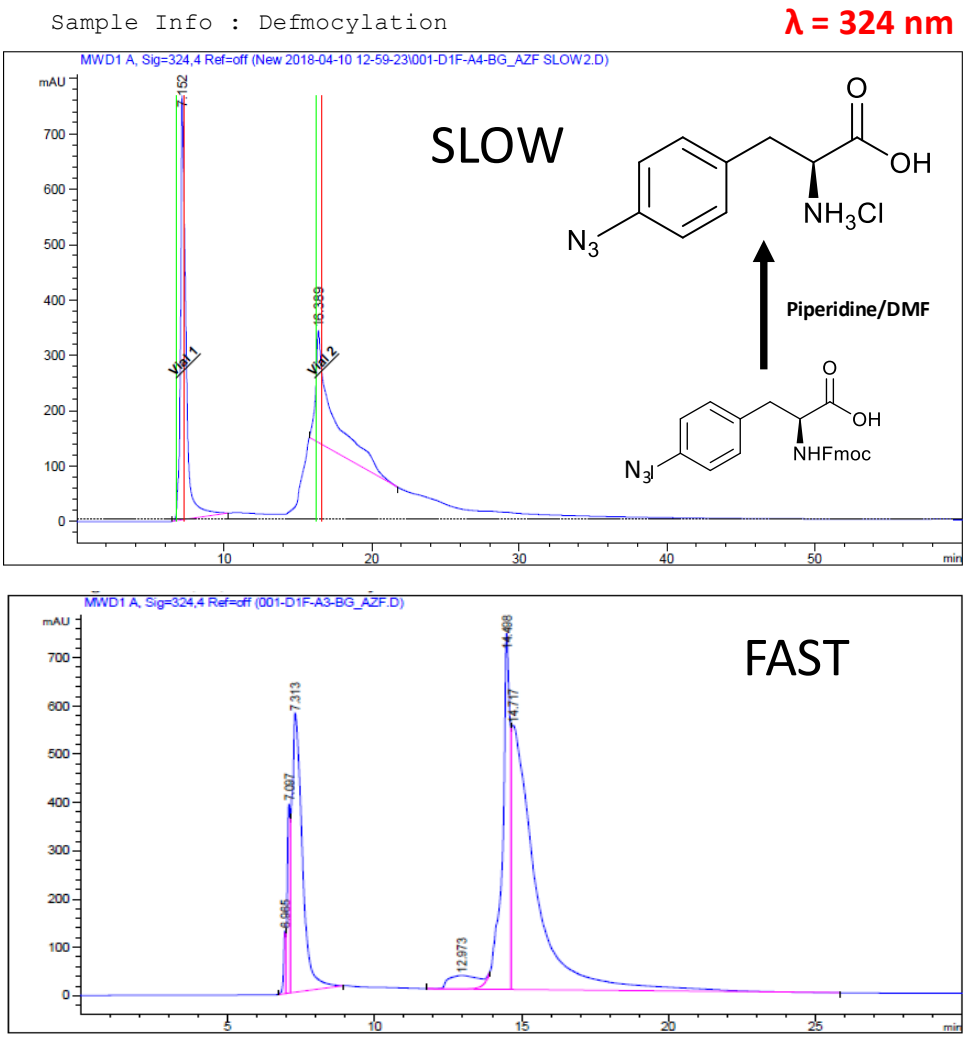

Figure B4 – HPLC of *para*-azidophenylalanine hydrochloride from protected azidation (slow and fast solvent rates)

Optimised procedure for the synthesis of *p*-azido-L-phenylalanine (No Fmoc Protection)

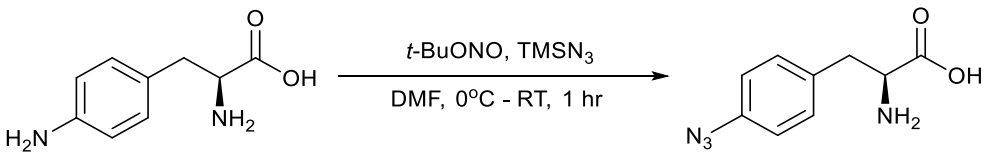

4-Amino-L-phenylalanine (50 mg, 0.278 mmol) was dissolved in DMSO with sonication (25 mL), with stirring and cooling to 0°C. The flask was protected from light, and *t*-BuONO (50 µL, 0.416 mmol, 1.5 eqv) was subsequently added, followed by timethylsilyl azide (42 µL, 0.306 mmol, 1.1 eqv), and equilibrated for 60 minutes. The reaction mixture was concentrated under vacuum (65°C, 50 mbar) and precipitated from ethyl acetate, to give an off-white/orange solid, which was isolated by centrifugation (10K RPM, 10 minutes). 40 mg (60%). Analytical RP-HPLC: t_R = 30 min (Water/Acetonitrile 100 : 0 to 70 : 30 by 2 min to 0 : 100 by 25 min λ = 324 nm). ^{1}H NMR (400 MHz, D_2O) δ 7.12 (d, J = 7.8 Hz, 2H), 6.84 (d, J = 7.8 Hz, 2H), 3.92 (dd, J = 8.1, 5.0 Hz, 1H), 3.19 – 3.12 (m, 1H), 3.02 (dd, J = 14.8, 7.8 Hz, 1H). ^{13}C NMR (101 MHz, D_2O) δ 176.56, 174.03 (C=O), 145.35, 130.28, 125.63 (Aromatic), 116.85 (Aromatic), 66.46, 59.43, 56.09, 41.55, 38.71, 35.51. m/z (ESI, +ve) Expected 495.2, Observed 495.4 [100%, 2M+Acetonitrile+N_3^+].

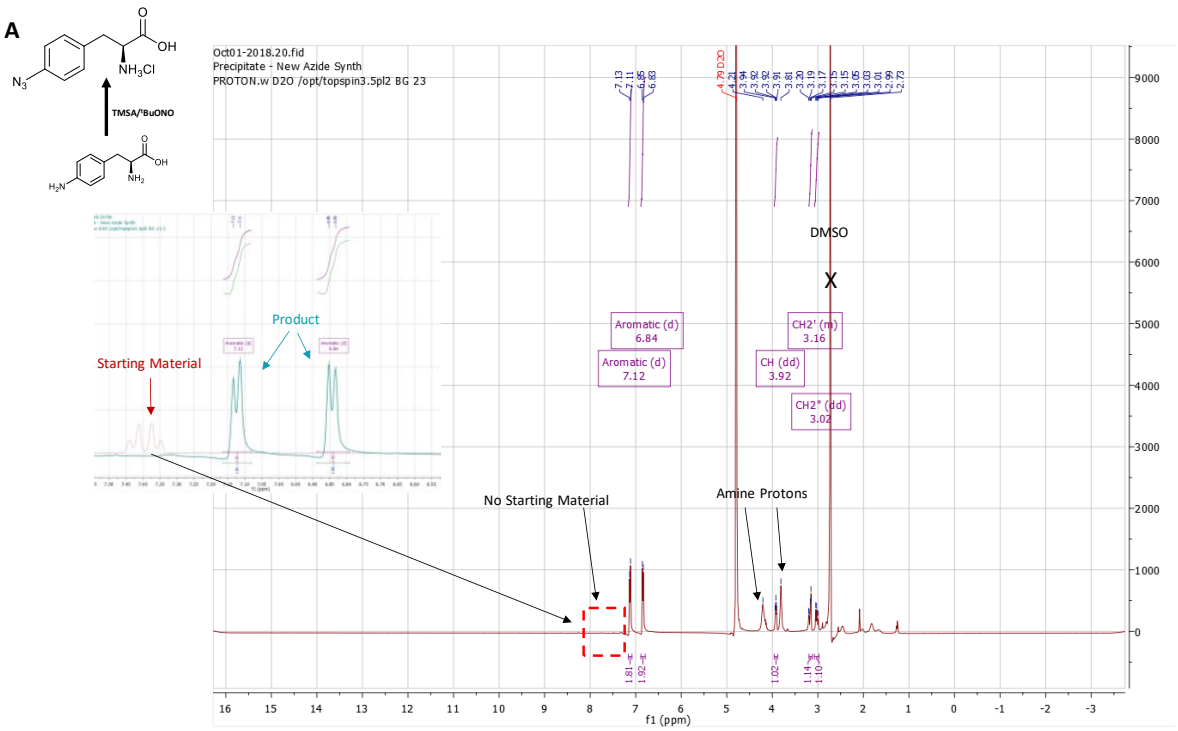

Figure B5 – NMR of *para*-azidophenylalanine hydrochloride from direct azidation

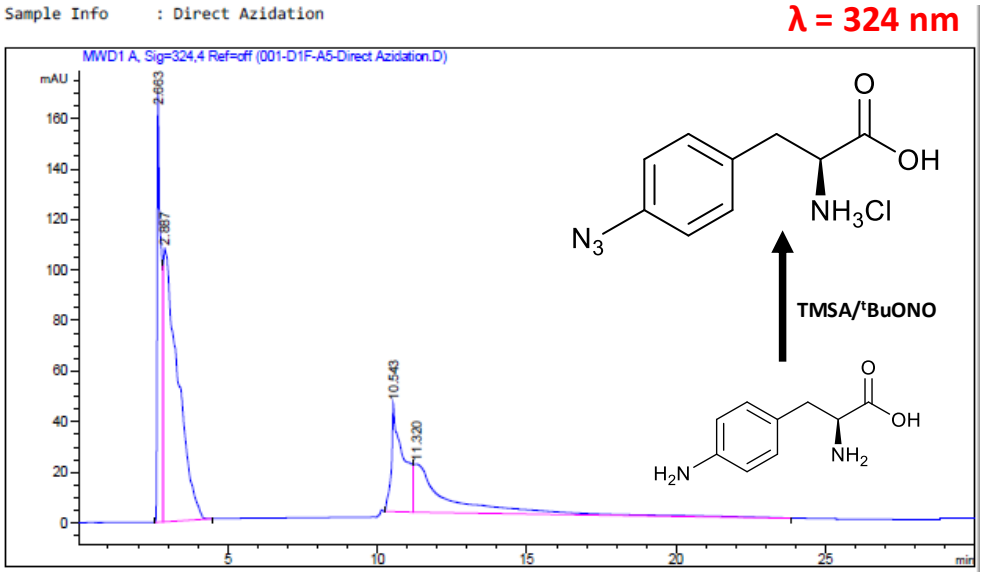

Figure B6 – HPLC of *para*-azidophenylalanine hydrochloride from direct azidation

APPENDICES

Appendix C – Publications

Biomaterials

Deutsche Ausgabe: DOI: 10.1002/ange.201706703
Internationale Ausgabe: DOI: 10.1002/anie.201706703

Polyproline as a Minimal Antifreeze Protein Mimic That Enhances the Cryopreservation of Cell Monolayers

*Ben Graham, Trisha L. Bailey, Joseph R. J. Healey, Moreno Marcellini, Sylvain Deville, and Matthew I. Gibson**

Abstract: *Tissue engineering, gene therapy, drug screening, and emerging regenerative medicine therapies are fundamentally reliant on high-quality adherent cell culture, but current methods to cryopreserve cells in this format can give low cell yields and require large volumes of solvent "antifreezes". Herein, we report polyproline as a minimum (bio)synthetic mimic of antifreeze proteins that is accessible by solution, solid-phase, and recombinant methods. We demonstrate that polyproline has ice recrystallisation inhibition activity linked to its amphipathic helix and that it enhances the DMSO cryopreservation of adherent cell lines. Polyproline may be a versatile additive in the emerging field of macromolecular cryoprotectants.*

Tissue engineering, gene therapy, therapeutic protein production, and transplantation rely on the successful storage and transport of donor cells.[1] For example, in the production of therapeutic proteins, a specific cell line must be developed for each protein.[2] Given that any in vitro culture will undergo phenotypic and genotypic changes when propagated for long periods of time, it is neither possible nor practical to maintain a continuous culture of cells.[3] The only solution to this is the cryopreservation of cells using significant volumes of cryoprotectants, such as DMSO (dimethyl sulfoxide), which are intrinsically toxic.[4] The repeated use of DMSO has an impact on the epigenetic profile of cells, specifically the alteration of DNA methylation profiles, which results in phenotypic changes.[5,6] There is a real need for robust methods to cryopreserve cells in monolayer (adhered to tissue culture scaffolds) format to provide phenotypically identical cells for assays, obviating the need for replating between freeze–thaw cycles. Formulations containing 5–10% DMSO reduce cryoinjury by moderating the increase in solute concentration during freezing[7–9] but for adhered embryonic stem cells, their use results in just 5% cell recovery.[10,11] A key contributor to cell death during cryopreservation is ice recrystallisation (growth) and additives that can inhibit recrystallisation have the potential to redefine cell storage and hence biomedicine.

Antifreeze (glyco)proteins (AF(G)Ps) are potent ice recrystallisation inhibitors (IRIs), but are unsuitable for cryopreservation applications owing to their potential toxicity/immunogenicity and their secondary effect of dynamic ice shaping (DIS), which leads to needle-like ice crystals that pierce cell membranes.[12] Synthetic polymers that are potent IRIs have emerged as new tools for controlling ice growth.[13] The most studied one is poly(vinyl alcohol) (PVA), which can inhibit ice growth at concentrations below 0.1 mg mL^{-1} and enhances the cryopreservation of cells in suspension.[14–16] It is hypothesized that the activity of PVA is related to its regularly spaced hydroxyl groups.[17] Matsumura and Hyon have developed polyampholytes[18] that are cryoprotective but have moderate IRI activity.[19,20] Wang and co-workers have demonstrated the significant IRI activity of graphene oxide.[21] Ben and co-workers have developed low-molecular-weight surfactants that also inhibit ice growth.[22] A major setback is that the above synthetic IRIs are neither biodegradable nor bioresorbable and have not been applied to the significant challenge of cell monolayer storage.

There are no crystal structures for AFGPs but solution-state NMR and circular dichroism (CD) spectroscopy suggest a polyproline II (PP II)-type helix.[23] Polyproline is unique amongst the canonical amino acids in that it has no amide N–H, meaning that it cannot form intramolecular hydrogen bonds. Therefore, it is water-soluble and quite hydrophobic at the same time, as is the case for AFP I, which contains 70% alanine (a hydrophobic amino acid). We thus hypothesised that polyproline could be a minimal AF(G)P mimic owing to its amphiphilicity.[24] Homopolypeptides are appealing targets compared to vinyl polymers as they can be prepared by solid-phase synthesis,[25] solution-phase polymerisation,[26] or recombinant methods,[27] proving vast (bio)synthetic space.

Herein, we introduce polyproline as a minimum (bio)-synthetic antifreeze protein mimic. We demonstrate that polyproline has ice recrystallisation inhibition activity, which is linked to its amphipathic PP II helix structure. Polyproline was found to improve the post-cryopreservation recovery of cell monolayers compared to DMSO alone, demonstrating

[*] B. Graham, T. L. Bailey, Prof. M. I. Gibson
Department of Chemistry, University of Warwick
Gibbet Hill Road, Coventry, CV47 AL (UK)
E-mail: m.i.gibson@warwick.ac.uk
J. R. J. Healey, Prof. M. I. Gibson
Warwick Medical School, University of Warwick
Coventry, CV4 7AL (UK)
Dr. M. Marcellini, Dr. S. Deville
Ceramics Synthesis and Functionalization Lab
UMR3080 CNRS/Saint-Gobain
550 Avenue Alphonse Jauffret, 84306 Cavaillon (France)
Supporting information and the ORCID identification number(s) for the author(s) of this article can be found under: https://doi.org/10.1002/anie.201706703.

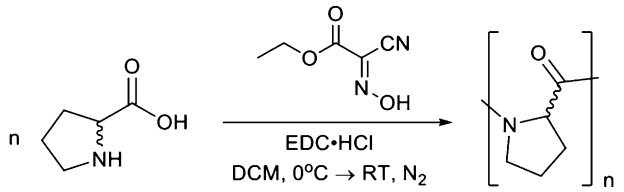

Scheme 1. Condensation polymerisation of proline. The materials were used in stereopure form but both the L- and D-isomers were used, hence no stereocentres are shown.

a new macromolecular approach for the storage of complex cells to enable next-generation therapies.

L-, D-, and (racemic) D/L-polyproline were synthesised by condensation polymerisation using 1-ethyl-3-(3-dimethylaminopropyl) carbodiimide (EDC, Scheme 1), alongside several commercial samples. Following dialysis, the polymers were characterised by size exclusion chromatography (SEC; Table 1). The polymers were less disperse than expected owing to fractionation during dialysis.

Table 1: Polyproline characterisation.

	M_n [g mol^{-1}]	$Đ^{SEC}$[a]	DP	Secondary structure
$PPro_{11}$	1300[a]	1.03	11	
$PPro_{15}$	1700[a]	2.12	15	PP II
$PPro_{19}$	2100[a]	1.50	19	
$P(D\text{-}Pro)_{15}$	1700[a]	1.01	15	enantiomeric PP II
$P(D/L\text{-}Pro)_{21}$	2400[a]	1.01	21	random coil
$PPro_{10\text{-}100}$	1–10 000[b]	–	10–100	PP II[e]
$PPro_{10}$	900[c]	[d]	10	PP II[e]
$PPro_{10\text{-}25}$	1–3000	1.01–1.03	10–25	PP II[e]
$PPro_{20}$	2000[c]	[d]	20	PP II[e]

[a] Determined by SEC. [b] Value from supplier. [c] Determined by mass spectrometry. [d] Single species. [e] From Ref. [28–30].

CD spectroscopy confirmed that $PPro_{15}$ adopted a PP II helix (Figure 1 A; see also the Supporting Information, Figure S1)[31] with characteristic signals present at 207 and 228 nm, whilst a random coil would exhibit slight peak shifting, with signals absent in the 220 nm region.[32] $P(D\text{-}Pro)_{15}$ gave the mirror spectrum whilst the D/L racemic mixture showed no secondary structure. This series of peptides were subsequently tested for IRI activity using a splat assay.[33] This involved seeding a large number of small ice crystals, which were annealed for 30 min at −8 °C before being photographed. The average crystal size was measured relative to a PBS control, with smaller values indicating more IRI activity (Figure 1 B, C).

All polyproline variants were found to display dose-dependent activity but weak molecular-weight dependence in the range tested (Figure 1 B). The shortest peptide ($PPro_{10}$) lost activity below 10 mg mL^{-1}, but the longer ones retained activity at 5 mg mL^{-1}. The magnitude of activity was significantly smaller than for AF(G)Ps, which function at concentrations as low as 0.14 μg mL^{-1},[34] but comparable to that of polyampholytes.[19,20] Knight and co-workers have observed that poly(hydroxyproline) has IRI activity, which was assumed to be due to the regularly spaced hydroxyl groups along the backbone.[35] However, the observations made here suggest that the PP II helix, rather than (or in addition to) the

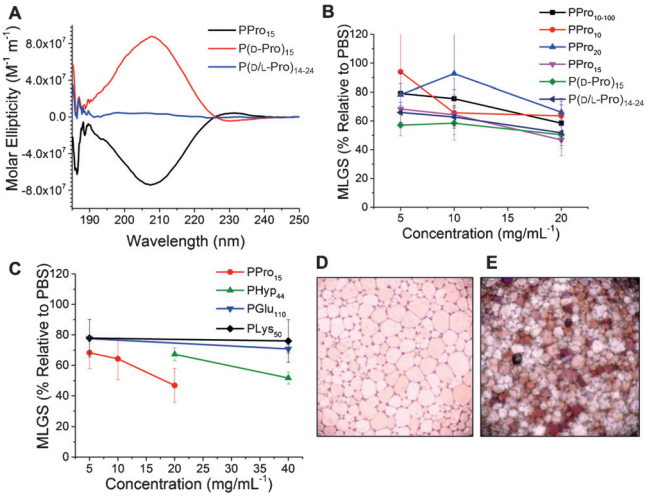

Figure 1. A) Circular dichroism spectra. B) IRI activity of the polyproline series. C) IRI activity compared to other homopolypeptides. D) Cryomicrograph of a PBS negative control. E) Cryomicrograph of 20 mg mL^{-1} polyproline. Photographs taken after 30 min at −8 °C. Error bars represent ± standard deviation from a minimum of three replicates. Images shown are 1.2 mm across. MLGS = mean largest grain size.

hydroxyl groups, gives rise to the observed activity. Figure 1 C compares the IRI activity of poly(hydroxyproline) with those of $PPro_{15}$ and two α-helical poly(amino acid)s.[36] Polylysine ($PLys_{50}$) and poly(glutamic acid) ($PGlu_{110}$) showed no IRI activity. $PPro_{15}$ was found to be more active than poly(hydroxyproline) of higher molecular weight. This finding confirmed that hydroxyl groups are not essential for activity in IRI-active compounds. $P(D\text{-}Pro_{15})$ and $P(D/L\text{-}Pro_{21})$ had statistically identical activity to $PPro_{15}$, suggesting that local rather than long-range order is crucial for activity.

We hypothesise that IRI activity requires segregated hydrophilic and hydrophobic domains (amphipathy).[37,22,24] $PPro_{10}$ was compared to a non-glycosylated type I sculpin AFP[38] and also to $PGlu_{10}$ by mapping their hydrophobic/hydrophilic domains (Figure 2). The type I sculpin AFP (Figure 2 A) possesses "patches" of hydrophobic/hydrophilic groups. $PPro_{10}$ (Figure 2 B) also possesses this facial amphi-

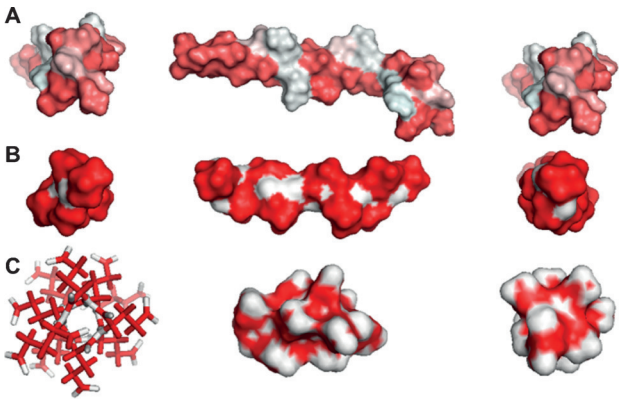

Figure 2. Hydrophobic surface mapping of A) recombinant type I sculpin AFP, B) $PPro_{10}$, and C) $PGlu_{10}$, showing charged hydrophilic surfaces. Hydrophobic regions (red), hydrophilic regions (white).

philicity. In comparison, $PGlu_{10}$ (no IRI activity) has charged groups around the core of the helix, which prevents the presentation of hydrophobic domains. This agrees with our previous study on nisin A, which has IRI activity associated with segregated domains,[37] and also the results obtained with amphiphiles developed by Ben et al., which only function below the critical micelle concentration.[22]

Aside from IRI activity, AF(G)Ps display unwanted ice shaping, which promotes the formation of needle-like ice crystals, which damage cell membranes.[12] Cryo-confocal microcapillary microscopy has emerged as a tool for monitoring ice crystal shaping,[39] and was also employed here (Figure 3). A non-IRI-active dye, sulforhodamine B, provided

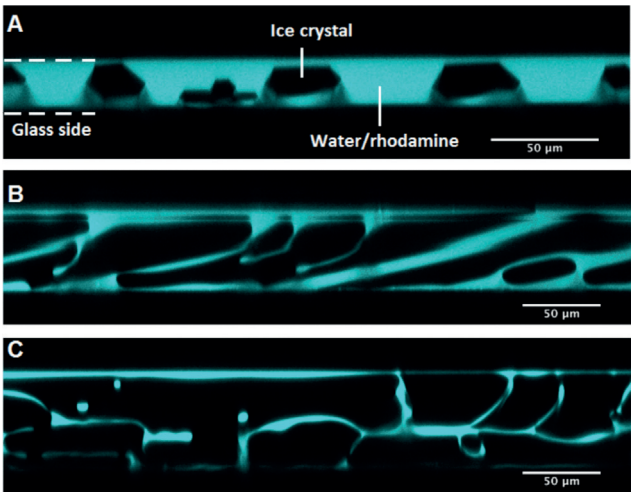

Figure 3. Cross-section of ice crystals perpendicular to the temperature gradient: A) ZrAc (positive control), B) $PPro_{19}$, C) PBS (negative control). The ice crystals expel the dye while growing, appearing in black, while the remaining liquid fluoresces.

contrast against the ice (which appears dark). A control using pure PBS showed no shaping whilst zirconium acetate (ZrAc), which is a strong ice shaper, produced hexagonal crystals.[39] $PPro_{19}$ did not induce shaping, supporting the concept that polyproline inhibits ice crystal growth without inhibiting the formation of a specific plane of ice; however, as these are relatively weak IRIs, the concentrations needed for ice shaping would be very high.

To explore polyproline as a macromolecular cryopreservative, A549 cells were employed as a prototypical adherent cell line.[40] The protective osmolyte proline (which has no IRI activity; see the Supporting Information) was used as a secondary cryoprotectant. A549 cells were incubated with 200 mM (23 $mg\,mL^{-1}$) proline (blue bars; Figure 4) or medium alone (red bars; Figure 4) for 24 h. The medium was then removed and replaced with a medium containing 10% DMSO with varying concentrations of $PPro_{11}$ (1250 $g\,mol^{-1}$, $Đ = 1.03$). After 10 min exposure to this solution, all excess solvent was removed, and the cells were subjected to controlled-rate freezing at 1 °C min^{-1} to −80 °C. Following storage at −80 °C, the cells were thawed by addition of warm medium (37 °C), and the total number of viable cells was determined by trypan blue staining 24 h after thawing.

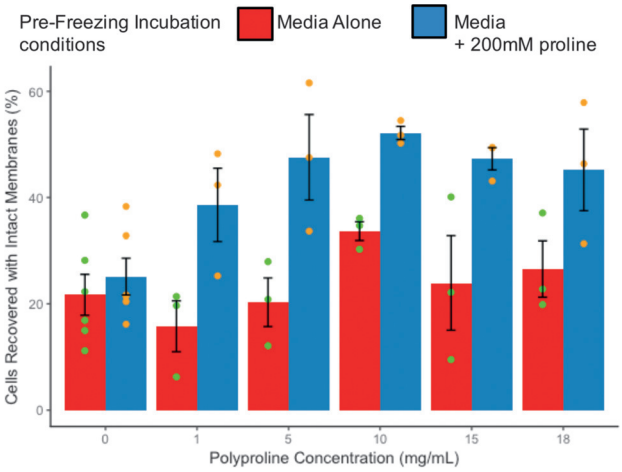

Figure 4. A549 cryopreservation. Cell recovery determined by trypan blue assays. Cells were first incubated either in the medium alone or with 200 mM proline for 24 h. They were subsequently cryopreserved by addition of 10% DMSO with the indicated $PPro_{11}$ concentration. Error bars ± S.E.M. from $n = 3$ with two nested replicates. # $P < 0.05$ compared to 10% DMSO treatment; * $P < 0.05$ compared to 200 mM proline exposure with 10% DMSO treatment.

Figure 4 shows that the use of DMSO alone led to 27% cell recovery. Addition of polyproline alone to 10% DMSO failed to give any additional protection. However, for cells that had been preconditioned with 200 mM proline for 24 h before treatment with 10 $mg\,mL^{-1}$ $PPro_{11}$/10% DMSO, the cell recovery doubled to 53%. Increasing the concentration of polyproline beyond 10 $mg\,mL^{-1}$ did not increase recovery further, suggesting that the additive benefits plateau at 10 $mg\,mL^{-1}$.[14] It should be highlighted that the cell viability assays measure intact cells, and that detailed functional analysis will be needed in the future for demonstration of complex function. For comparison with other macromolecular cryopreservatives, Matsumura and co-workers have reported poly(ampholyte)-enhanced monolayer storage using vitrification solutions, giving near-quantitative cell recovery.[41] However, this required very high DMSO concentrations of 6.5 M (> 500 $mg\,mL^{-1}$) plus 10 wt% (ca. 100 $mg\,mL^{-1}$) of the polymer, and there was a reduction in the post-thaw proliferation rate associated with the large solvent volumes, which may limit practical applications. In our PPro system introduced here, the total recovery levels were less, but far lower concentrations of DMSO were employed (10 wt%/ca. 100 $mg\,mL^{-1}$), and the total exposure time to this potentially toxic component was only 10 min. To critically compare PPro, another batch ($PPro_{10-25}$) was synthesised and tested for cytotoxicity and heamocompatibility. A549 monolayers were exposed to PPro for 24 h, and the cell viability was assessed (see the Supporting Information). This extended exposure period led to a reduction in alamar blue to 60% for 5 $mg\,mL^{-1}$ PPro, suggesting some cytotoxicity if exposed to elevated concentrations for long periods of time. It is important to note that in this cryopreservation procedure, PPro is only in contact with the cells for 10 min before the excess is removed and the cells are frozen. Red blood cell heamolysis experiments (see the Supporting Information)

showed this was not due to any inherent membrane activity of the (amphipathic) PPro.

In summary, we have demonstrated that polyproline is a potent additive for cell-monolayer cryopreservation when appropriate freezing conditions are employed. Polyproline has moderate ice recrystallisation inhibition activity, which was hypothesised to be due to its "patchy" amphipathic structure associated with its PP II helix. Addition of polyproline to adherent cell cultures led to an increase from 20% to >50% in total cell recovery post-cryopreservation, which is significantly better than for the use of DMSO alone. This increase in recovery is thought to be associated with the inhibition of ice recrystallisation. Short exposure times of just 10 min to the polyproline/DMSO solution, followed by removal of the excess solvent, reduced the cytotoxicity associated with long-term (24 h) exposure to elevated levels of polyproline. The minimal solvent exposure times may give benefits in downstream processing and biomedical applications compared to current high-solvent-concentration methods using vitrification. Polyproline is appealing compared to other macromolecular cryoprotectants as it only comprises native amino acids and can be obtained by chemical and biochemical methods.

Acknowledgements

This study has received funding from ERC grants (CRYOMAT 638661, 278004 FreeCo), the BBSRC (BB/F011199/1), and the Royal Society. The University of Warwick WCPRS partially supports T.L.B. J.R.J.H. thanks the EPSRC for funding via MOAC DTC EP/F500378/1. M. Menze is thanked for providing the Biocision CoolCell to enable controlled-rate freezing.

Conflict of interest

The authors declare no conflict of interest.

Keywords: biomaterials · cryopreservation · ice recrystallization inhibitors · monolayers · polymers

How to cite: *Angew. Chem. Int. Ed.* **2017**, *56*, 15941–15944
Angew. Chem. **2017**, *129*, 16157–16160

[1] A. Fowler, M. Toner, *Ann. N. Y. Acad. Sci.* **2005**, *1066*, 119–135.
[2] G. Walsh, *Nat. Biotechnol.* **2014**, *32*, 992–1000.
[3] G. Seth, *Methods* **2012**, *56*, 424–431.
[4] K. Brockbank, M. Taylor, *Adv. Biopreserv.* **2007**, *5*, 157–196.
[5] M. Iwatani, K. Ikegami, Y. Kremenska, N. Hattori, S. Tanaka, S. Yagi, K. Shiota, *Stem Cells* **2006**, *24*, 2549–2556.
[6] K. Kawai, Y.-S. Li, M.-F. Song, H. Kasai, *Bioorg. Med. Chem. Lett.* **2010**, *20*, 260–265.
[7] P. Mazur, *Science* **1970**, *168*, 939–949.
[8] P. Mazur, J. Farrant, S. P. Leibo, E. H. Chu, *Cryobiology* **1969**, *6*, 1–9.
[9] X. Stéphenne, M. Najimi, E. M. Sokal, *World J. Gastroenterol.* **2010**, *16*, 1–14.
[10] C. H. Boon, P. Y. Chao, H. Liu, S. T. Wei, A. J. Rufaihah, Z. Yang, H. B. Boon, Z. Ge, W. O. Hog, H. L. Eng, T. Cao, *J. Biomed. Sci.* **2006**, *13*, 433–445.
[11] Q. Xu, W. J. Brecht, K. H. Weisgraber, R. W. Mahley, Y. Huang, *J. Biol. Chem.* **2004**, *279*, 25511–25516.
[12] H. Chao, P. L. Davies, J. F. Carpenter, *J. Exp. Biol.* **1996**, *199*, 2071–2076.
[13] M. I. Gibson, *Polym. Chem.* **2010**, *1*, 1141–1152.
[14] R. C. Deller, M. Vatish, D. A. Mitchell, M. I. Gibson, *Nat. Commun.* **2014**, *5*, 3244.
[15] B. Wowk, E. Leitl, C. M. Rasch, N. Mesbah-Karimi, S. B. Harris, G. M. Fahy, *Cryobiology* **2000**, *40*, 228–236.
[16] R. C. Deller, J. E. Pessin, M. Vatish, D. A. Mitchell, M. I. Gibson, *Biomater. Sci.* **2016**, *47*, 935–945.
[17] C. Budke, T. Koop, *ChemPhysChem* **2006**, *7*, 2601–2606.
[18] K. Matsumura, S. H. Hyon, *Biomaterials* **2009**, *30*, 4842–4849.
[19] D. E. Mitchell, M. Lilliman, S. G. Spain, M. I. Gibson, *Biomater. Sci.* **2014**, *2*, 1787–1795.
[20] D. E. Mitchell, N. R. Cameron, M. I. Gibson, *Chem. Commun.* **2015**, *51*, 12977–12980.
[21] H. Geng, X. Liu, G. Shi, G. Bai, J. Ma, J. Chen, Z. Wu, Y. Song, H. Fang, J. Wang, *Angew. Chem. Int. Ed.* **2017**, *56*, 997–1001; *Angew. Chem.* **2017**, *129*, 1017–1021.
[22] C. J. Capicciotti, M. Leclere, F. A. Perras, D. L. Bryce, H. Paulin, J. Harden, Y. Liu, R. N. Ben, *Chem. Sci.* **2012**, *3*, 1408–1416.
[23] D. H. Nguyen, M. E. Colvin, Y. Yeh, R. E. Feeney, W. H. Fink, *Biophys. J.* **2002**, *82*, 2892–2905.
[24] D. E. Mitchell, G. Clarkson, D. J. Fox, R. A. Vipond, P. Scott, M. I. Gibson, *J. Am. Chem. Soc.* **2017**, *139*, 9835–9838.
[25] R. B. Merrifield, *J. Am. Chem. Soc.* **1963**, *85*, 2149.
[26] M. I. Gibson, N. R. Cameron, *J. Polym. Sci. Part A* **2009**, *47*, 2882–2891.
[27] E. Gutierrez, B. S. Shin, C. J. Woolstenhulme, J. R. Kim, P. Saini, A. R. Buskirk, T. E. Dever, *Mol. Cell* **2013**, *51*, 35–45.
[28] A. A. Adzhubei, M. J. E. Sternberg, A. A. Makarov, *J. Mol. Biol.* **2013**, *425*, 2100–2132.
[29] P. Wilhelm, B. Lewandowski, N. Trapp, H. Wennemers, *J. Am. Chem. Soc.* **2014**, *136*, 15829–15832.
[30] A. V. Mikhonin, N. S. Myshakina, S. V. Bykov, S. A. Asher, V. Pennsyl, *J. Am. Chem. Soc.* **2005**, *127*, 7712–7720.
[31] Protein Circular Dichroism Data Bank **2016**, pCD0004553000.
[32] J. L. S. Lopes, A. J. Miles, L. Whitmore, B. A. Wallace, *Protein Sci.* **2014**, *23*, 1765–1772.
[33] T. Congdon, R. Notman, M. I. Gibson, *Biomacromolecules* **2013**, *14*, 1578–1586.
[34] S. Lui, W. Wang, E. von Moos, J. Jackman, G. Mealing, R. Monette, R. N. Ben, *Biomacromolecules* **2007**, *8*, 1456–1462.
[35] C. A. Knight, D. Wen, R. A. Laursen, *Cryobiology* **1995**, *32*, 23–34.
[36] M. I. Gibson, C. A. Barker, S. G. Spain, L. Albertin, N. R. Cameron, *Biomacromolecules* **2009**, *10*, 328–333.
[37] D. E. Mitchell, M. I. Gibson, *Biomacromolecules* **2015**, *16*, 3411–3416.
[38] A. H. Kwan, K. Fairley, P. I. Anderberg, C. W. Liew, M. M. Harding, J. P. Mackay, *Biochemistry* **2005**, *44*, 1980–1988.
[39] M. Marcellini, C. Noirjean, D. Dedovets, J. Maria, S. Deville, *ACS Omega* **2016**, *1*, 1019–1026.
[40] B. Stokich, Q. Osgood, D. Grimm, S. Moorthy, N. Chakraborty, M. A. Menze, *Cryobiology* **2014**, *69*, 281–290.
[41] K. Matsumura, K. Kawamoto, M. Takeuchi, S. Yoshimura, D. Tanaka, S.-H. Hyon, *ACS Biomater. Sci. Eng.* **2016**, *2*, 1023–1029.

Manuscript received: July 4, 2017
Revised manuscript received: September 27, 2017
Accepted manuscript online: October 18, 2017
Version of record online: November 22, 2017

JACS JOURNAL OF THE AMERICAN CHEMICAL SOCIETY

Communication

Cite This: J. Am. Chem. Soc. 2018, 140, 5682−5685

pubs.acs.org/JACS

Facially Amphipathic Glycopolymers Inhibit Ice Recrystallization

Ben Graham,[†] Alice E. R. Fayter,[†] Judith E. Houston,[§] Rachel C. Evans,[∥] and Matthew I. Gibson*[,†,‡]

[†]Department of Chemistry, University of Warwick, Coventry CV4 7AL, U.K.

[‡]Warwick Medical School, University of Warwick, Coventry CV4 7AL, U.K.

[§]Jülich Centre for Neutron Science, Forschungszentrum Jülich GmbH, Garching 85747, Germany

[∥]Department of Materials Science & Metallurgy, University of Cambridge, Cambridge CB3 0FS, U.K.

Supporting Information

ABSTRACT: Antifreeze glycoproteins (AFGPs) from polar fish are the most potent ice recrystallization (growth) inhibitors known, and synthetic mimics are required for low-temperature applications such as cell cryopreservation. Here we introduce facially amphipathic glycopolymers that mimic the three-dimensional structure of AFGPs. Glycopolymers featuring segregated hydrophilic and hydrophobic faces were prepared by ring-opening metathesis polymerization, and their rigid conformation was confirmed by small-angle neutron scattering. Ice recrystallization inhibition (IRI) activity was reduced when a hydrophilic oxo-ether was installed on the glycan-opposing face, but significant activity was restored by incorporating a hydrophobic dimethylfulvene residue. This biomimetic strategy demonstrates that segregated domains of distinct hydrophilicity/hydrophobicity are a crucial motif to introduce IRI activity, which increases our understanding of the complex ice crystal inhibition processes.

Antifreeze glycoproteins (AFGPs) are found in the tissues and blood serum of extremophile fish species and act to modulate the growth of extracellular ice.[1] A key property of AFGPs is ice recrystallization inhibition (IRI), which slows ice crystal growth (distinct from nucleation[2]).[3] Ice recrystallization is a major cause of cell death during the freezing of cells and tissue for transfusion, fundamental biomedicine, and cell biology. Hence, AFGPs (or their mimics) have many potential applications.[4] Cryopreservation with AFGPs (and non-glycosylated antifreeze proteins, AFPs)[5] is limited, however, by their secondary property of dynamic ice shaping, whereby the AFGPs shape the ice into needle-like (spicular) morphologies, which can pierce cell membranes.[3] AFGPs are also challenging to synthesize, requiring multistep procedures.[6,7] Gibson and co-workers have developed synthetic polymers[8,9] based upon poly(vinyl alcohol) and poly(ampholytes) which have been found to enhance the cryopreservation of blood[10−12] and nucleated cells.[4,13]

In the case of AFPs, defined ice-binding faces have been identified using structural biology methods.[14] Conversely, there is no crystal structure available for AFGPs, and the exact structural motifs required for IRI are unknown, although the glycan unit is essential for ice shaping.[7] Solution NMR studies suggest that AFGPs form a polyproline II type of helix, with the glycans on one face and peptides on the opposite, forming a facially amphipathic structure.[15] It is emerging that this segregated display of hydrophobic/hydrophilic groups, rather than a "binding site", is the essential feature for IRI activity.[8,16,17] Molecular modeling recently revealed that the hydrophobic face, not the glycans, of AFGPs interacts with the ice, and that the spatial segregation along the polyproline II helix is essential.[18] Gibson and co-workers have shown that homopolyproline has a weak IRI,[4] and that self-assembled metallohelicities with "patchy" amphipathy are potent IRIs,[19] which supports a hypothesis that well-defined ice-binding domains are not essential for IRI.[20] Amphipathy has also been seen to be important in ice nucleation.[21] This evidence suggests that IRI, but not ice shaping,[22] could be selectively introduced into new and emerging (bio)materials, if precise control over hydrophilic/hydrophobic domains is possible.

The design of polymers with solvent-exposed hydrophobic domains is, however, nontrivial. Block copolymeric amphiphiles spontaneously self-assemble into micelles/vesicles to reduce the hydrophobic domain's contact with water, and hence only "water-loving" surfaces are exposed.[23] Tew and co-workers have developed facially amphipathic cationic polymers, with opposing positive charges and lipophilic domains to mimic the function of antimicrobial peptides.[24,25] A crucial design step was the use of ring-opening metathesis polymerization (ROMP), which introduces rigid alkene backbones, while balancing the hydrophobicity/hydrophilicity to maintain both solubility and the presentation of hydrophobic faces. These have shown particular potency as potential antimicrobials.[26]

Considering the above, we designed and synthesized locally rigid, facially amphipathic glycopolymers. A combination of ice binding assays, modeling, and small-angle neutron scattering (SANS) provides compelling evidence that local amphipathy is an essential motif for introducing IRI activity, providing design rules for new materials to mimic AFGP function.

Figure 1A shows the solution-state structure of AFGP,[7] with the disaccharide units spatially segregated from the hydrophobic peptide backbone. Our approach was to use ROMP to introduce local rigidity,[27] in contrast to flexible backbones obtained from radical polymerization. Four monomers were synthesized to give a range of amphipathies: **M1** was prepared

Received: February 23, 2018
Published: April 16, 2018

DOI: 10.1021/jacs.8b02066
J. Am. Chem. Soc. 2018, 140, 5682−5685

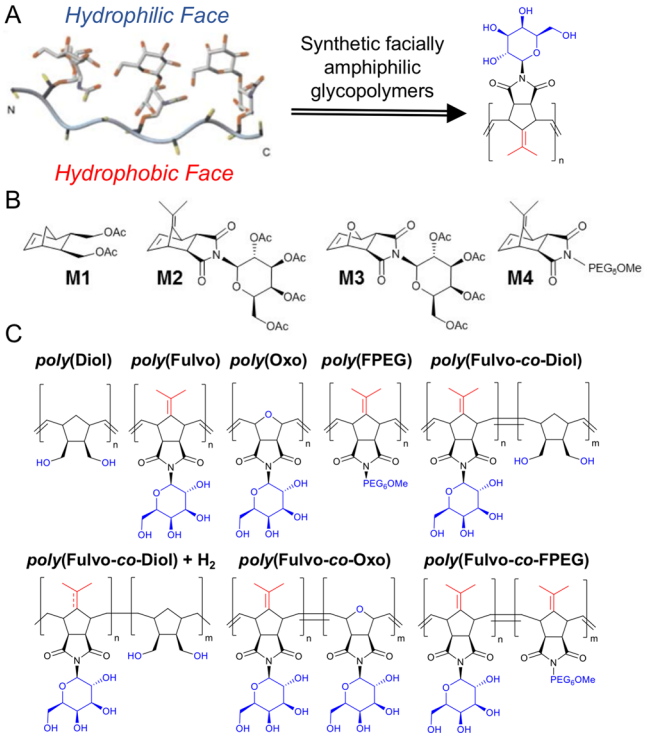

Figure 1. (A) Concept of facially amphipathic ROMP polymers to mimic AFGP. Adapted from ref 7. (B,C) Monomers and polymers synthesized here; hydrophilic groups are indicated in blue, and hydrophobic in red.

by acetylation of a commercial norbornenediol; **M2** and **M3** were synthesized by Koenigs–Knorr coupling of acetobromo-α-D-galactose with *exo,exo*-[oxo/fulvene]norborneneimide; and **M4** was synthesized by substitution of monomethoxyhexaethylene glycol monotosylate (Figure 1B). The hydrophilic galactose and hydrophobic fulvene motifs were selected in particular due to their intrinsic rigidities, giving monomers with structurally distinct domains of opposing polarity. These monomers were polymerized using Grubbs's third-generation catalyst, and acetate protecting groups were subsequently removed by treatment with sodium methoxide followed by ion exchange (Figure 1C). The panel of amphipathic polymers was characterized by size-exclusion chromatography (SEC; Đ < 1.4) and NMR (nuclear magnetic resonance) and IR (infrared) spectroscopy (see Supporting Information (SI) and Table 1).

The polymer library was assessed for IRI activity using a "splat" assay, where ice crystals are nucleated and their growth after 30 min at −8 °C was recorded. Activity is expressed as the mean grain area (MGA) relative to a phosphate-buffered saline (PBS) control, with smaller values representing more activity. Polymers derived from **M2** containing the "fulvo" motif were significantly less soluble than those derived from **M3** containing the "oxo"-ether units. Their solution concentrations were therefore determined by UV–vis absorption spectroscopy (see SI for Beer–Lambert plots) at saturation. In the case of poly(Fulvo), 1% v/v dimethylsulfoxide was required, and controls were adjusted to account for this.

Poly(Oxo) was found to inhibit ice crystal growth by ∼50% MGA at concentrations above 5 mg·mL^{-1} (Figure 2A), which makes it more active than many previously reported IRI-active polymers.[28,29] The poly(Fulvo) derivative featuring the hydrophobic face, however, was considerably more active, inhibiting by ∼50% MGA at just 0.5 mg·mL^{-1} (solubility limit), supporting the facially amphipathic hypothesis for IRI. Molecular models corroborate this (Figure 2B) and illustrate the relative increase in hydrophobicity across the poly(Oxo) and poly(Fulvo) homopolymers. To improve the solubility, a 1:1 statistical copolymer of **M2**/**M3**, poly(Fulvo-*co*-Oxo), was prepared. This co-polymer had significantly improved solubility and comparable overall IRI activity to poly(Fulvo), showing that some co-monomer incorporation is tolerated, unlike PVA,[30] and example ice wafers are shown in Figure 2C. However, the non-ideal copolymerization kinetics of the oxo (**M2**) and fulvo (**M3**) co-monomers led to a blocky rather than statistical copolymerization.[31,32] Infrared analysis confirmed incomplete acetate removal (in contrast to the homopolymers), suggesting an internalized domain structure and/or aggregation, with some (hydrophobic) surfaces being solvent inaccessible and hence limiting the total activity of poly(Fulvo-*co*-Oxo). The monomers alone also had no activity (SI), confirming that a macromolecular architecture is essential.

To improve solubility, a norbornenediol monomer, **M1**, with a non-hydrophilic bridgehead was investigated. De-acetylated homopolymers of **M1**, poly(Diol), were found to have surprisingly low solubility and no activity at their solubility limit of 0.5 mg·mL^{-1}. However, when **M1** was incorporated as a co-monomer with the (IRI-active) "fulvo" monomer **M2** to give

Table 1. Polymer Characterization

	M_n (g mol^{-1})				
	theor	exptl[a]	Đ (−)[a]	DP (−)[a]	conv (%)[b]
poly(Diol)[c]	10 000	2 200	1.01	14	100
		5 300	1.01	34	
		8 400	1.02	54	
poly(Fulvo)	25 000	10 300	1.21	28	100
poly(Oxo)	10 000	7 300	1.18	22	100
poly(FPEG)	10 000	35 900	1.38	133	100
poly(Fulvo-*co*-Diol)-11	5 000	10 700	1.12	14, 35	94/97
poly(Fulvo-*co*-Diol)-17	10 000	16 800	1.10	22, 54	100
poly(Fulvo-*co*-Diol)-35	25 000	34 600	1.26	47, 112	100
poly(Fulvo-*co*-Oxo)	10 000	7 700	1.35	11, 11	100/96
poly(Fulvo-*co*-FPEG)	10 000	55 600	1.47	76, 58	71

[a] M_n = molar mass, Đ = dispersity, and DP = degree of polymerization, determined by SEC. [b] Conversion, determined by ^{1}H NMR. [c] Single species.

DOI: 10.1021/jacs.8b02066
J. Am. Chem. Soc. 2018, 140, 5682−5685

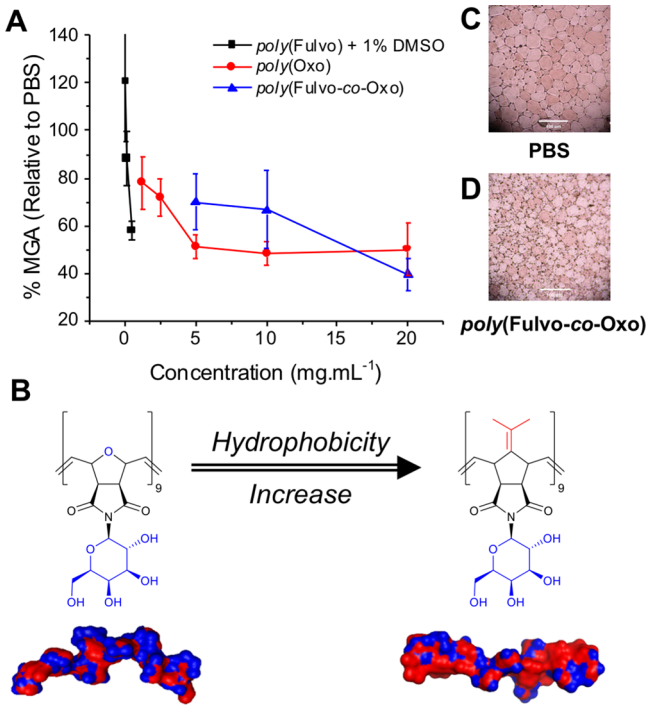

Figure 2. (A) IRI activities of the poly(Fulvo), poly(Oxo), and copolymer series. (B) Hydrophobic surface map of poly(Fulvo) and poly(Oxo). (C,D) Optical microscopy of ice crystal wafers of PBS and poly(Fulvo-*co*-Oxo).

poly(Fulvo-*co*-Diol), an overall increase in solubility was achieved. Poly(Fulvo-*co*-Diol)-17 had remarkable IRI activity: 40% MGA at just 1.3 mg·mL^{-1} (Figure 3). This polymer

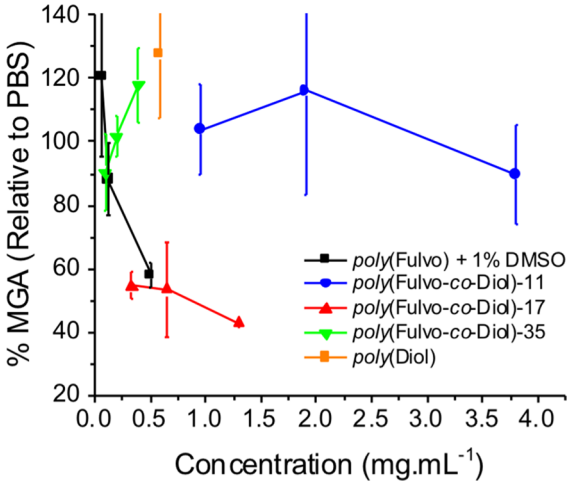

Figure 3. IRI activities of the poly(Fulvo-*co*-Diol) molecular weight series.

showed some molecular weight dependence on activity, with 17 kDa being more active than 11 kDa (and far more than the monomer, indicating the need for a macromolecular architecture). Increasing the molecular weight further to 35 kDa lowered the solubility of the copolymer, and hence the activity, highlighting a "sweet spot". Work undertaken by Inada et al. described the molecular weight dependence on IRI of PVA.[33] Similarly, a previous study by Deswal et al. reported on the IRI activity of proteins extracted from the leaves of the freeze-tolerant plant Seabuckthorn, of which superior antifreeze activity was observed only for polypeptides of elevated molecular weights.[34] Replacing the glycan with a short oligo(ethylene glycol) PEG chain, to give both poly(Fulvo-*co*-FPEG) and poly(FPEG), decreased activity, as the (flexible) PEG can access numerous conformations, reducing the overall amphipathy (see SI). Hydrogenation of the alkene backbone to increase flexibility resulted in a wholly insoluble polymer (see SI). These observations demonstrate that precise macromolecular engineering is essential to achieve a potent IRI mimetic.

AF(G)Ps bind to specific ice crystal faces,[35,36] leading to dynamic ice shaping (unwanted in cryopreservation[3]). Control ice crystals (Figure 4A) showed no dynamic ice shaping, but

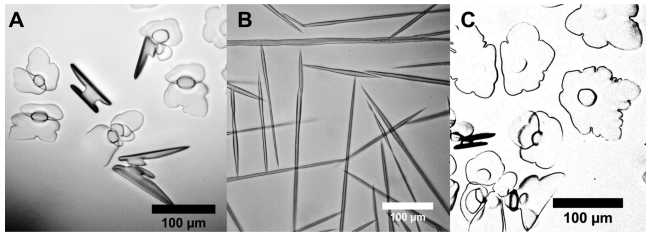

Figure 4. Optical microscopy ice morphology analysis: (A) water, −6 °C; (B) AFGP-8, −5 °C; (C) poly(Fulvo-*co*-Diol)-17 (0.72 mg·mL^{-1}), −8 °C.

addition of AFGPs (Figure 4B) produced distinctive spicular (needle-like) crystals. Poly(Fulvo-*co*-Diol) (Figure 4C) did not lead to ice shaping, ruling out strong and specific ice face recognition and showing that these effects can be separated by macromolecular design.

SANS was employed to evaluate the solution conformation and rigidity of the poly(Fulvo-*co*-Diol) series (Figure 5 and SI).

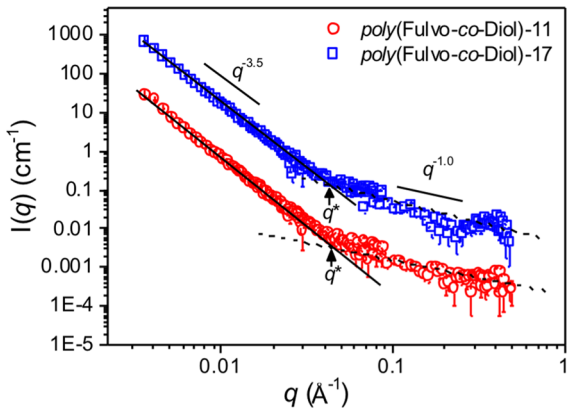

Figure 5. SANS data for poly(Fulvo-*co*-Diol)-11 (1 mg.mL^{-1}, red) and poly(Fulvo-*co*-Diol)-17 (1 mg.mL^{-1}, blue) in D_2O at 25 °C. Straight lines show −3.5 and −1 decays for comparison.

The persistence lengths, b_t, were estimated from the position of the characteristic crossover between the scattering profile typical for fractal aggregates ($q^{-3.5}$) and that of rigid rods (q^{-1}) (see SI).[37,38] The estimated b_t values for poly(Fulvo-*co*-Diol)-11 and poly(Fulvo-*co*-Diol)-17 are 38.9 and 44.4 Å, respectively. It should be noted that the overlap may actually occur at a lower q region, but is masked by aggregate scattering. Thus, these values should be taken as the minimum persistence length for each polymer. Nevertheless, each b_t is much larger

DOI: 10.1021/jacs.8b02066
J. Am. Chem. Soc. 2018, 140, 5682−5685

than the monomer length (~10 Å), which suggests that the chain backbones are locally stiff.[38] Furthermore, given the approximate contour length, L, of both polymer chains (490 and 760 Å for poly(Fulvo-*co*-Diol)-11 and poly(Fulvo-*co*-Diol)-17, respectively), the large b_t suggests rigid rather than highly flexible aggregates of potentially rod-like structures. This rigidity, coupled with the intrinsic amphipathy of the polymers, is aligned with the hypothesized semi-rigid (and generally amphipathic) ice binding faces of AFPs,[14,39] and the flexible hydrophilic "glycan face" of AFGPs, providing evidence that facial amphipathy is a key motif for introducing IRI activity into a diverse range of polymers.

To conclude, we have designed and synthesized facially amphipathic glycopolymers to mimic the solution confirmation and selective functions of antifreeze glycoproteins. It was found that the addition of hydrophobic faces, opposing the glycan units, introduced potent IRI activity, but that substitution with a more hydrophilic ether unit removed activity. These results support a mechanism for IRI activity which is dependent upon local water ordering rather than an essential ice binding unit, and there was no evidence of dynamic ice shaping. Small-angle neutron scattering supports a locally rigid confirmation, as seen for AF(G)Ps, supporting the hypothesis of amphipathy as the driver for activity.

■ ASSOCIATED CONTENT

Supporting Information

The Supporting Information is available free of charge on the ACS Publications website at DOI: 10.1021/jacs.8b02066.

Full experimental details, including synthesis/characterization, additional IRI data, and SANS analysis (PDF)

■ AUTHOR INFORMATION

Corresponding Author

*m.i.gibson@warwick.ac.uk

ORCID

Ben Graham: 0000-0003-1313-6874
Alice E. R. Fayter: 0000-0001-9470-9560
Judith E. Houston: 0000-0001-5205-3620
Rachel C. Evans: 0000-0003-2956-4857
Matthew I. Gibson: 0000-0002-8297-1278

Notes

The authors declare no competing financial interest.

■ ACKNOWLEDGMENTS

M.I.G. holds an ERC Starter Grant (CRYOMAT 638661). Thanks to A. L. DeVries for supplying the antifreeze glycoprotein AFGP-8. The SANS portion of this work is based upon experiments performed at the KWS-2 instrument operated at the Heinz Maier-Leibnitz Zentrum(MLZ), Garching, Germany.

■ REFERENCES

(1) Harding, M. M.; Anderberg, P. I.; Haymet, A. D. J. *Eur. J. Biochem.* **2003**, *270* (7), 1381.
(2) Congdon, T.; Dean, B. T.; Kasperczak-Wright, J.; Biggs, C. I.; Notman, R.; Gibson, M. I. *Biomacromolecules* **2015**, *16* (9), 2820.
(3) Chao, H.; Davies, P. L.; Carpenter, J. F. *J. Exp. Biol.* **1996**, *199* (Pt 9), 2071.
(4) Graham, B.; Bailey, T. L.; Healey, J. R. J.; Marcellini, M.; Deville, S.; Gibson, M. I. *Angew. Chem., Int. Ed.* **2017**, *56*, 15941.
(5) Davies, P. L. *Trends Biochem. Sci.* **2014**, *39*, 548−555.
(6) Wilkinson, B. L.; Stone, R. S.; Capicciotti, C. J.; Thaysen-Andersen, M.; Matthews, J. M.; Packer, N. H.; Ben, R. N.; Payne, R. J. *Angew. Chem., Int. Ed.* **2012**, *51* (15), 3606.
(7) Tachibana, Y.; Fletcher, G. L.; Fujitani, N.; Tsuda, S.; Monde, K.; Nishimura, S. I. *Angew. Chem., Int. Ed.* **2004**, *43* (7), 856.
(8) Biggs, C. I.; Bailey, T. L.; Ben Graham; Stubbs, C.; Fayter, A.; Gibson, M. I. *Nat. Commun.* **2017**, *8* (1), 1546.
(9) Gibson, M. I. *Polym. Chem.* **2010**, *1* (8), 1141.
(10) Deller, R. C.; Vatish, M.; Mitchell, D. A.; Gibson, M. I. *Nat. Commun.* **2014**, *5*, 3244.
(11) Mitchell, D. E.; Cameron, N. R.; Gibson, M. I. *Chem. Commun.* **2015**, *51* (65), 12977.
(12) Mitchell, D. E.; Lovett, J. R.; Armes, S. P.; Gibson, M. I. *Angew. Chem., Int. Ed.* **2016**, *55* (8), 2801.
(13) Deller, R. C.; Pessin, J. E.; Vatish, M.; Mitchell, D. A.; Gibson, M. I. *Biomater. Sci.* **2016**, *4*, 1079.
(14) Strom, C. S.; Liu, X. Y.; Jia, Z. *J. Biol. Chem.* **2004**, *279* (31), 32407.
(15) Nguyen, D. H.; Colvin, M. E.; Yeh, Y.; Feeney, R. E.; Fink, W. H. *Biophys. J.* **2002**, *82* (6), 2892.
(16) Capicciotti, C. J.; Leclere, M.; Perras, F. A.; Bryce, D. L.; Paulin, H.; Harden, J.; Liu, Y.; Ben, R. N. *Chem. Sci.* **2012**, *3* (5), 1408.
(17) Capicciotti, C. J.; Kurach, J. D. R.; Turner, T. R.; Mancini, R. S.; Acker, J. P.; Ben, R. N. *Sci. Rep.* **2015**, *5*, 9692.
(18) Mochizuki, K.; Molinero, V. *J. Am. Chem. Soc.* **2018**, *140*, 4803.
(19) Mitchell, D. E.; Clarkson, G.; Fox, D. J.; Vipond, R. A.; Scott, P.; Gibson, M. I. *J. Am. Chem. Soc.* **2017**, *139* (29), 9835.
(20) Geng, H.; Liu, X.; Shi, G.; Bai, G.; Ma, J.; Chen, J.; Wu, Z.; Song, Y.; Fang, H.; Wang, J. *Angew. Chem., Int. Ed.* **2017**, *56* (4), 997.
(21) Liu, K.; Wang, C.; Ma, J.; Shi, G.; Yao, X.; Fang, H.; Song, Y.; Wang, J. *Proc. Natl. Acad. Sci. U. S. A.* **2016**, *113* (51), 14739.
(22) Leclère, M.; Kwok, B. K.; Wu, L. K.; Allan, D. S.; Ben, R. N. *Bioconjugate Chem.* **2011**, *22* (9), 1804.
(23) Mai, Y.; Eisenberg, A. *Chem. Soc. Rev.* **2012**, *41* (18), 5969.
(24) Ilker, M. F.; Nüsslein, K.; Tew, G. N.; Coughlin, E. B. *J. Am. Chem. Soc.* **2004**, *126* (48), 15870.
(25) Arnt, L.; Tew, G. N. *J. Am. Chem. Soc.* **2002**, *124* (26), 7664.
(26) Lienkamp, K.; Madkour, A. E.; Musante, A.; Nelson, C. F.; Nüsslein, K.; Tew, G. N. *J. Am. Chem. Soc.* **2008**, *130* (30), 9836.
(27) Colak, S.; Nelson, C. F.; Nusslein, K.; Tew, G. N. *Biomacromolecules* **2009**, *10* (2), 353.
(28) Stubbs, C.; Lipecki, J.; Gibson, M. I. *Biomacromolecules* **2017**, *18* (1), 295.
(29) Capicciotti, C. J.; Trant, J. F.; Leclère, M.; Ben, R. N. *Bioconjugate Chem.* **2011**, *22* (4), 605.
(30) Congdon, T.; Notman, R.; Gibson, M. I. *Biomacromolecules* **2013**, *14* (5), 1578.
(31) Kiessling, L. L.; Strong, L. E. In *Alkene Metathesis in Organic Synthesis*; Fuerstner, A., Ed.; Springer-Verlag: Berlin/eidelberg, 2013; pp 219−220.
(32) Tallon, M. A. In *Handbook of Maleic Anhydride Based Materials*; Musa, O. M., Ed.; Springer International Publishing: Cham, Switzerland, 2016; pp 387−388.
(33) Inada, T.; Lu, S. S. *Cryst. Growth Des.* **2003**, *3* (5), 747.
(34) Deswal, R.; Gupta, R.; Sharma, B. *J. Proteins Proteomics* **2016**, *7* (3), 199.
(35) Raymond, J. A.; Wilson, P.; DeVries, A. L. *Proc. Natl. Acad. Sci. U. S. A.* **1989**, *86* (3), 881.
(36) Knight, C. A.; Driggers, E.; DeVries, A. L. *Biophys. J.* **1993**, *64* (1), 252.
(37) Schmidt, M.; Paradossi, G.; Burchard, W. *Makromol. Chem., Rapid Commun.* **1985**, *6* (11), 767.
(38) Buhler, E.; Boué, F. *Macromolecules* **2004**, *37* (4), 1600.
(39) Howard, E. I.; Blakeley, M. P.; Haertlein, M.; Haertlein, I. P.; Mitschler, A.; Fisher, S. J.; Siah, A. C.; Salvay, A. G.; Popov, A.; Dieckmann, C. M.; Petrova, T.; Podjarny, A. *J. Mol. Recognit.* **2011**, *24* (4), 724.

DOI: 10.1021/jacs.8b02066
J. Am. Chem. Soc. 2018, 140, 5682−5685